UNIVERSITY OF SOUTHAMPTON

FACULTY OF NATURAL AND ENVIRONMENTAL SCIENCES

Centre for Biological Sciences

Interaction of fatty acids and phospholipids with multiple binding sites on the potassium channel KcsA

by

Juan Hernando Bolívar González

Thesis for the degree of Doctor of Philosophy

September 2011

UNIVERSITY OF SOUTHAMPTON

ABSTRACT

FACULTY OF NATURAL AND ENVIRONMENTAL SCIENCES

CENTRE FOR BIOLOGICAL SCIENCES

Doctor of Philosophy

INTERACTION OF FATTY ACIDS AND PHOSPHOLIPIDS WITH MULTIPLE BINDING SITES ON THE POTASSIUM CHANNEL KcsA

by Juan Hernando Bolívar González

The majority of lipids that interact with a transmembrane protein act as a solvent for the protein, forming a shell around it; these lipids are called annular or boundary lipids. However, some lipids interact in a more specific way, binding between transmembrane α-helices or at protein-protein interfaces, and these lipids are referred to as non-annular lipids. The crystal structure of the bacterial potassium channel KcsA shows a non-annular lipid molecule bound at the subunit interfaces in the homotetrameric structure, and binding of this non-annular lipid has been shown to be essential for channel function, making KcsA an ideal candidate for the study of lipid-protein interactions. Recently, a third type of binding site at the hydrophobic inner cavity of the pore of potassium channels has been proposed for fatty acid molecules, where binding was suggested to cause block of ion flux. Fatty acids are known to affect ion channel activity, but it is not yet certain how they act. Here, fluorescence spectroscopy and electron spin resonance (ESR) are combined to analyse the interaction of fatty acids with the annular and non-annular sites, and with the hydrophobic inner cavity of the pore on KcsA.

To study fatty acid binding by fluorescence spectroscopy, KcsA was reconstituted in bilayers of phosphatidylcholine (PC) containing brominated fatty acid. Quenching of the Trp fluorescence of wild type KcsA by brominated fatty acids allows an analysis of their interaction with annular sites on the channel and interaction at non-annular sites was studied using a Trp mutant of KcsA. The results shown that fatty acids can bind with an affinity rather similar to that of PC to both annular and non-annular sites, but uncharged fatty acid analogues show limited binding, emphasising the importance of charged interactions in these systems. In ESR studies KcsA was reconstituted in PC membranes containing a small amount of spin labelled fatty acid. Spin labelled lipids in contact with the protein show a different ESR spectrum from those in the bulk lipid due to the different mobilities of their acyl chains. The ESR spectra show that the spin labelled fatty acid bound to KcsA is strongly immobilised and binds with high affinity. It is proposed that the fatty acid binds to the hydrophobic cavity with a dissociation constant of ca. 0.22 μM. The studies show that fatty acids can bind to the channel at a variety of sites, suggesting that ion channel function could be modulated directly by interactions with fatty acids.

Other studies here presented focused on the influence of the annular lipids on the aggregation of KcsA. Protein-protein contacts are important for membrane protein association and activity, but little is known about the influence that the lipid bilayer can have on protein-protein association. ESR experiments with spin labelled phospholipids show that at lipid:channel molar ratios of ca. 100:1 or higher, KcsA is solvated by ca. 31 annular phospholipid molecules, as expected from its crystal structure, but that, at lower lipid content, protein-protein contacts become favourable and KcsA aggregates. The ESR data also show that aggregation is reduced in bilayers of anionic phosphatidylglycerol (PG) in comparison to bilayers of zwitterionic PC, as confirmed by quenching experiments where brominated PG was able to quench wild type KcsA more efficiently than brominated PC at the low lipid:channel molar ratios. The results highlight the importance that the lipid bilayer composition can have on membrane protein association.

List of Contents

Declaration of authorship

I, Juan Hernando Bolívar González, declare that the thesis entitled "Interaction of fatty acids and phospholipids with multiple binding sites in the potassium channel KcsA" and the work presented in the thesis are both my own, and have been generated by me as the result of my own original research. I confirm that:

- this work was done wholly or mainly while in candidature for a research degree at this University;
- where any part of this thesis has previously been submitted for a degree or any other qualification at this University or any other institution, this has been clearly stated;
- where I have consulted the published work of others, this is always clearly attributed;
- where I have quoted from the work of others, the source is always given. With the exception of such quotations, this thesis is entirely my own work;
- I have acknowledged all main sources of help;
- where the thesis is based on work done by myself jointly with others, I have made clear exactly what was done by others and what I have contributed myself;
- none of this work has been published before submission,

Signed: ……..

Date:…….

Acknowledgements

I am really glad I had the opportunity to do my PhD with Professor Tony Lee before his retirement. He is not only a great researcher in the field of membrane proteins, but also a fantastic mentor. He has been at all moments supportive, always having time to carefully explain, discuss and think about science. Thanks to him I have not only learnt but also enjoyed from my PhD.

I have been lucky enough to be also supervised by another world known membrane protein researcher, Dr. Derek Marsh, and would like to thank him for his great guidance and help during my stay in Germany. I would also like to thank his lovely group: Gitta and Birgit who showed me the lab-work secrets for ESR, and Inge who arranged all my stay; they all made my time in Germany fantastic.

It was great to also have Dr. Malcolm East here in Southampton, as everyone knows, he is the Molecular Biology master, and despite my PhD drifting to a more biophysical area, it was always reassuring to know that I had someone like him to ask for help with any kind of problem. With Neville Wright also in the School, who knows all the Chemistry you may need, I never felt without guidance.

A huge thank you also goes to Phedra for teaching me all the secrets about KcsA, always so kind, she will find the time to help you and talk about any problems you may have. Andy, Jeab and John were the very first ones introducing me to the lab routines and with my other PhD companions: Helen, Nik, and the rest of members of the lab/office, always helped me along the way and made me feel so welcomed in Southampton. They have all become invaluable friends.

I must also mention my housemates and many other friends, from whom Marc deserves a special thank you. And, of course, my parents and my sister, who have been always there for me and to whom I owe everything I have achieved.

Finally I would like to thank the E.U. Marie Curie program for fantastic economic support and the labs involved in it for the organization of great meetings and courses from which I have been able to learn and enjoy so much.

Abbreviations

14-PASL	1-palmitoyl-2-[14-(4,4-dimethyloxazolidinyl-*N*-oxyl)stearoyl]-*sn*-glycero-3-phosphate
14-PCSL	1-palmitoyl-2-[14-(4,4-dimethyloxazolidinyl-*N*-oxyl)stearoyl]-*sn*-glycero-3-phosphocholine
14-PESL	1-palmitoyl-2-[14-(4,4-dimethyloxazolidinyl-*N*-oxyl)stearoyl]-*sn*-glycero-3-phosphoethanolamine
14-PGSL	1-palmitoyl-2-[14-(4,4-dimethyloxazolidinyl-*N*-oxyl)stearoyl]-*sn*-glycero-3-phosphoglycerol
14-SASL	14-(4,4-dimethyloxazolidinyl-*N*-oxyl)stearic acid
AR	Analytical reagent
AEA	N-arachidonylethanolamide
BrPC	1,2-di(9,10-dibromostearoyl)-*sn*-glycero-3-phosphocholine
BrPG	1,2-di(9,10-dibromostearoyl)-*sn*-glycero-3-phospho-(1'-*rac*-glycerol)
BSA	Bovine serum albumin
CMC	Critical micelle concentration
DDM	n-dodecyl-β-D-maltopyranoside
DHA	Docosahexaenoic acid
DMPC	1,2-dimyristoyl-*sn*-glycero-3-phosphocholine
DOPC	1,2-dioleoyl-*sn*-glycero-3-phosphocholine
DOPG	1,2-dioleoyl-*sn*-glycero-3-phospho-(1'-*rac*-glycerol)
DOXYL	4,4-dimethyloxazolidine-*N*-oxyl
EGTA	Ethylene glycol tetraacetic acid
HEPES	4-(2-hydroxyethyl)-1-piperazineethanesulphonic acid

IPTG	Isopropyl-β,D-thiogalactoside
LB Broth	Luria-Bertani Broth
NPTH	*N*-palmitoyl-L-tryptophan *n*-hexyl ester
PA	Phosphatidic acid
PAGE	Polyacrylamide gel electrophoresis
PBS	Phosphate buffered saline
PC	Phosphatidylcholine
PE	Phosphatidylethanolamine
PG	Phosphatidylglycerol
PI	Phosphatidylinositol
PS	Phosphatidylserine
rPE	1,2-dioleoyl-*sn*-glycero-3-phosphoethanolamine-N-(lissamine rhodamine B sulphonil)
SDS	Sodium dodecyl sulphate
TBA	Tetrabutylammonium
TEA	Tetraethylammonium
TEMED	N,N,N',N'-tetramethylethylenediamine
Tris	Tris(hydroxylmethyl)aminomethane
WT	Wild type

Chapter 1: General introduction.

1.1 Biological membranes: an overview

Membranes represent one of the key elements of cellular regulation. They do not just limit the cell and its compartments. Through the plasma membrane the cell interacts with its environment and communicates with other cells, and it is also the site of action of many drugs. Biological membranes have turned out to be very complex and dynamic structures that have intimate interactions between their components: lipids and proteins.

1.1.1 Membrane lipids

Lipids constitute the membrane building blocks, forming a matrix to which proteins can associate in many different ways. The basis of the formation of membranes is primarily the amphipathic nature of the lipids that compose them, and their cylindrical shape[1].

Types of membrane lipids

Phospholipids, glycolipids and sterols are the most abundant lipids in biological membranes. The hydrophobic region of a phospholipid molecule is composed of fatty acyl chains anchored to a backbone that links the molecule to the hydrophilic region, which, in phospholipids, consists of a phosphate attached to an alcohol through an ester group[1,2].

There are two main types of phospholipids: glycerophospholipids (also called phosphoglycerides) and sphingophospholipids (Figure 1.1). In phosphoglycerides the backbone is glycerol and different alcohol groups give rise to some of the main classes of phospholipids found in membranes, such as phosphatidylglycerol (PG), phosphatidylserine (PS), phosphatidylcholine (PC), phosphatidylethanolamine (PE) and phosphatidylinositol (PI) (Figure 1.2). The simplest phospholipid lacks the alcohol group, and is called phosphatidic acid (PA). In the phosphoglycerides found

in most biological membranes the phosphate group is attached to carbon 3, with the two fatty acyl chains attached to carbons 1 and 2, respectively (because glycerol possesses a chiral carbon, the carbon atoms of glycerol derivatives are numbered stereospecifically: the prefix '*sn*' for 'stereospecifically numbered' is used in this nomenclature to differentiate it from conventional numbering). The acyl chains normally contain an even number of carbon atoms and their lengths vary between 14 and 24 carbon atoms. Many phosphoglycerides have their acyl chain at position 1 saturated, and their acyl chain at position 2 unsaturated, the latter often being longer.

In sphingophospholipids the backbone is sphingosine (Figure 1.1), a long chain amino alcohol that itself contains one of the hydrophobic chains of the molecule. In addition, in these lipids a fatty acyl chain binds through an amide linkage to the sphingosine backbone. The compound formed by the sphingosine and a fatty acyl chain is called a ceramide. In the lipid head group, when the alcohol group incorporated is choline, the resulting molecule is another important component of membranes: sphingomyelin.

Glycolipids are characterised by containing one or more monosaccharide residues. Many glycolipids have a very similar structure to that of phospholipids, but their head group consists of an oligosaccharide, instead of the phosphate group bound to an alcohol. Thus, the main types of glycolipids found in membranes can be classified as glycoglycerolipids and glycosphingolipids.

These membrane lipids can be named in different ways: the term "sphingolipids" can be used to refer to all lipids that contain sphingosine in their structure, including both sphingophospholipids and glycosphingolipids; glycolipids can include phospholipids with monosaccharide residues, like glycophosphatidylinositols; also, the term "phospholipid" is commonly used to primarily refer to glycerophospholipids.

Sterols are a type of isoprenoid, molecules constituted by repeating isoprene units, a branched five carbon hydrocarbon. Sterols belong to a subgroup of isoprenoids called steroids, which are complex derivatives of three isoprene units cyclised to form a fused four ring molecule. Different steroids contain carbon double

bonds at different positions, and different substituents. Sterols are characterised by possessing a hydroxyl group attached to carbon 3 in their structure, which provides the molecule with a polar region. An important sterol present in practically all animal plasma membranes is cholesterol[1,2].

The lipid phase

When membrane lipids are placed in an aqueous medium, the hydrophilic region (lipid head group) permits the lipids to interact with the water molecules, while the long hydrophobic chains tend to aggregate to escape from unfavourable interactions with water.

The aggregation of the lipid monomers into complex structures like bilayers depends on several factors, including lipid concentration, hydration, temperature and the ionic strength of the water phase. However, the most important factor in determining the lipid organization adopted is the molecular shape, which is determined by the size and polarity of the lipid head group relative to the size and saturation state of the hydrophobic acyl chains[1,3].

Roughly speaking, lipids with a cylindrical shape tend to organize in bilayers, as for example phosphatidylcholine. At high concentrations the lipid bilayers can pile up to form a lamellar phase (Figure 1.3). Some lipids have an inverted conical shape and aggregate to form micelles; at higher concentration these lipids can also adopt a hexagonal I phase, in which the lipids form hexagonally arranged cylinders, with the hydrophobic tails pointing towards the axis of the cylinders and the hydrophilic head groups being in contact with the water between the cylinders (positive curvature). Other lipids have a conical shape and tend to aggregate in a hexagonal II phase, in which the lipids form hexagonally arranged cylinders, in this case, with the hydrophobic tails facing the outside of the cylinders (negative curvature), and with the lipid head groups pointing towards the axis, where the water is trapped; similarly, at low concentrations, conical shape lipids can also form inverted micelles when placed in a hydrophobic medium (Figure 1.3). However, conical and inverted conical shaped lipids can form bilayers when mixed with a sufficient quantity of a cylindrically shaped lipid, as in the case of phosphatidylethanolamine, which has a conical shape but is abundant in biological membranes. Another lipid phase, structurally more

complex, is the cubic phase, a phase with a three dimensional cubic symmetry. These cubic phases can also have a positive or a negative curvature, and they can form a great variety of different three dimensional structures[1].

A full analysis of why lipids adopt a bilayer or some other phase is, however, more complicated than the concept of lipid shape might suggest. The main factor that keeps lipid molecules packed together is the hydrophobic effect, which tends to reduce as much as possible the contact between the lipid acyl chains and the water molecules, by decreasing the interfacial area, generating an attractive force at the polar-apolar interface (Figure 1.4). This attractive force creates a negative pressure that keeps the lipids together. However, as the lipid molecules get closer, other forces arise with a net repulsive effect. In the hydrocarbon region there are attractive van der Waals interactions between the acyl chains, but these are opposed by the thermal motions of the chains, and the balance is a net repulsive effect that tends to separate the lipids (a positive lateral pressure). Similarly, in the lipid head group region, steric, hydrational and electrostatic repulsions create a net positive pressure despite attractive contributions such as those due to hydrogen bonding. The balance of all these forces will depend on the structure of the lipid and will vary with temperature, lipid concentration, hydration and ionic strength, and, depending on these, the lipids will adopt different phases in order to reduce as much as possible their free energy[1,4] (Figure 1.4).

Aggregation of the lipid molecules gives them physical properties different from those found in other phases of matter; they are referred to as liquid crystals. The characteristic of a liquid crystal is that even though the molecules do not have a positional order, they have an oriented disposition: the molecules are free to move as long as they maintain their hydrophobic regions and hydrophilic regions aligned with their neighbours[3]; the lipid molecules can diffuse in the plane of the bilayer or other phase, and can rotate around their own axis; the fatty acyl chains are disordered, with free rotational movement around the C-C bonds that allow the lipid molecules to continuously change their acyl chains conformation (Gauche isomers)[1,5]. As a result, liquid crystals are oriented fluid systems.

However, lipid bilayers are not always in a liquid crystalline phase. At low temperatures the molecules are highly packed and organized, with the maximum number of van der Waals interactions between the fatty acyl chains; the lipids can no longer diffuse in the plane of the membrane. This phase is called the gel phase (L_{β}, Figure 1.5). Sometimes, depending mainly on the structure of the lipid head group, the acyl chains are tilted with respect to the bilayer normal, in which case the gel phase is symbolised as $L_{\beta'}$. Above a critical temperature, called the transition temperature (which varies depending on the lipid), the lipid bilayer transforms into the liquid-crystalline state (L_{α}). Lipids with short fatty acyl chains present less van der Waals interactions, and lipids with *cis* double bonds in the acyl chains have kinks that impede efficient van der Waals interactions, so that these lipids tend to have lower transition temperatures, needing less energy to reach a liquid-crystalline state[3,5] (Figure 1.5).

Because of its shape and its rigid ring system, cholesterol can affect the fluidity and other physical properties of lipid bilayers. Bilayers containing the appropriate amounts of cholesterol and a phospholipid with a high transition temperature can form an intermediate phase called the liquid-ordered phase (L_o). In this phase, the cholesterol molecules prevent intimate interactions between the phospholipid fatty acyl chains, inhibiting formation of the gel state at temperatures below the transition temperature, making the bilayer adopt a liquid-ordered phase. In the liquid-ordered phase the acyl chains are relatively extended and packed, but the lipids have rapid lateral mobility[5,6].

Biological membranes generally exist in a liquid-crystalline state, with a complex mixture of lipids. However, detergent resistant membrane domains can be isolated from a variety of eukaryotic cells and are thought to exist in a liquid-ordered state because they are mostly composed of sphingolipids (which have a high transition temperature and hence tend to be in a gel state at physiological temperatures) and cholesterol[6].

1.1.2 Membrane proteins

Although the lipid bilayer provides the basic structure of biological membranes, the membrane proteins are the elements that perform most of the specific functions of the membrane. Proteins can associate with the lipid bilayer in many different ways, although they can be generally classified as peripheral or integral (Figure 1.6). Peripheral membrane proteins interact only with the lipid head groups or the hydrophilic regions of other membrane proteins, mainly through electrostatic interactions and hydrogen bonds, and can usually be dissociated easily from the bilayer by varying the pH or increasing the ionic strength of the medium. In contrast, integral membrane proteins penetrate the hydrophobic region and can also interact with the hydrophilic groups of the lipids; this makes their association more intimate and strong, and therefore, their solubilisation usually requires the use of detergents or organic solvents[2].

Some proteins are covalently linked to lipid molecules; the lipid moiety inserts into the membrane acting as an anchor for the protein. In some cases the lipid permits the protein to associate with the membrane permanently (e.g. GPI anchored proteins). In other cases, the association with the membrane can be temporary (e.g. some palmitoylated proteins) and can be important for modulating the activity of the protein. There are some cases of integral membrane proteins that contain lipid moieties, but their presence is not necessary for the protein to stay in the membrane (e.g. G-protein coupled receptors with palmitoyl anchors)[7].

Integral proteins that cross the lipid bilayer from one side to another are called transmembrane proteins. Because the peptide bonds themselves are polar, they tend to form hydrogen bonds with one another in the hydrophobic regions of these proteins. When the polypeptide chain forms a regular α-helix, the hydrogen bonding between peptide bonds is maximized and therefore, most transmembrane regions adopt this structure. An alternative way to satisfy the hydrogen bonding between the peptide bonds is to arrange the multiple transmembrane strands as a β-sheet in the form of a closed barrel[8].

The transmembrane region of an integral protein is embedded in the lipid bilayer, and the lipids surrounding this region of a membrane protein influence the

conformational state of the membrane protein, affecting its activity[9]. Studying the interactions that take place between the lipids and proteins that compose biological membranes was the main objective of the study presented here. Fluorescence and electron spin resonance (ESR) studies were carried out on the potassium channel KcsA for this purpose.

1.1.3 Organization of biological membranes

In 1972 Singer and Nicolson[10] proposed a model for biological membranes in which the proteins were embedded in a two dimensional fluid lipid bilayer, and moved freely along its plane. More than thirty years later, this basic idea of a fluid membrane with proteins floating free in a "sea of lipids" is still accepted, but has evolved to show an image of biological membranes much more complex, with a high degree of regulation and organization. The majority of biological membranes are asymmetric, with a different lipid and protein composition on each side of the bilayer. A lateral asymmetry also exists, which in part results from the poor miscibility of certain types of lipids that generate specialized microdomains. Moreover, membrane proteins associated with the cytoskeleton can create barriers defining different membrane regions that will have different specialisations in the cell[11]. Biological membranes have turned out to be very complex systems whose complexity seems indeed justified given the broad critical functions in which they are involved for the survival of the cell.

1.2 Interactions of lipids with transmembrane proteins.

The structure and activity of membrane proteins can be strongly influenced by their lipid environment. This influence in structure and activity can be explained by two main types of effects of the lipid bilayer on the protein[9,12]. One such type of effects refers to the influence of the bulk physical properties of the lipid bilayer, such as its fluidity, tension and curvature stress. A classic example of a membrane protein affected by the bilayer in this way is the mechanosensitive channel of large conductance MscL, which opens upon increase of membrane tension due to excess influx of water in bacterial cells when they are placed in a hyposmotic medium[4]. The other type of effects follow directly from interactions at the molecular level between the lipids and the protein, and will depend on the chemical structures of the lipids

(acyl chain length and unsaturation, hydrogen bonding groups, charge, etc.) and the protein. A good example is the potassium channel KcsA, whose open probability depends on the presence of negatively charged phospholipids that interact with specific sites on the channel[13] (see below). Effects caused by the bulk physical properties of the lipid bilayer will tend to be less specific, being able to affect different proteins at the same time, while effects arising from direct lipid-protein interactions will tend to be more specific, affecting only proteins sensitive to particular interactions with particular types of lipid molecule. However, both effects are interconnected, as obviously the physical properties of the bilayer will finally translate into how the lipid molecules are able to interact with the proteins embedded in the bilayer[4,9,12].

The studies presented here will focus on lipid-protein interactions. There are two main ways in which a lipid molecule can interact with a transmembrane protein in the lipid bilayer. The majority of lipid molecules that interact with a transmembrane protein act as a solvent for the protein, forming a shell around it; these lipids are called annular or boundary lipids[4] (Figure 1.7A). The interactions of annular lipids with transmembrane proteins are relatively non-specific (although there may be hot-spots that prefer a certain kind of lipid interaction[14]), and the exchange rate between the annular lipids and the bulk of the lipids that are not in contact with the protein is fast, in the nanosecond to microsecond range, indicating that this type of interaction is a non-sticky one. For this reason annular lipids do not generally appear in the crystal structures of membrane proteins, as they are easily displaced by detergent molecules or are disorganised in the crystal[9]. Nevertheless, this annular shell of lipids around membrane proteins can be essential for maintaining their structure, oligomeric state and function. For example, the activity of the Ca^{2+}-ATPase from sarcoplasmic reticulum is influenced by the annular lipids around it: the activity is maximum in phosphatidylcholine bilayers of monounsaturated acyl chains of 18 carbon atoms length, and decreases in bilayers of shorter or longer chain lengths or in membranes composed of negatively charged phospholipids[9]. Annular lipids could also influence oligomerisation of complex proteins, which can be an important mechanism for regulating their activity. Some G-couple coupled receptors are known to be activated upon dimerization[15,16]; ion channels like the inwardly rectifying potassium channel Kir4.1[17] and the voltage gated potassium channel Kv2.1[18] have been reported to form

large clusters in cell cultures and *in vivo*, respectively. Further, ryanodine receptors (calcium ion channels in the sarcoplasmic reticulum of cardiac and skeletal muscle cells, and in the endoplasmic reticulum of other excitable cells) have been shown to be arranged in regular arrays forming clusters of 100-300 receptors, and have been proposed to undergo concerted opening due to conformational spread between neighbouring channels, i.e. channel-channel physical coupling[19,20]. However little is known about the driving forces that trigger or influence oligomerisation or about its biological relevance.

An important feature of the lipid-protein interaction is hydrophobic matching between a transmembrane protein and a lipid bilayer[4,21,22]. The hydrophobic core of a phospholipid bilayer corresponds to the segment between the glycerol backbones on the two sides of the bilayer, and so the hydrophobic thickness of a bilayer is determined by the acyl chain length and degree of unsaturation. The exposure of hydrophobic acyl chains or peptide residues to water has a very high energetic cost, hence hydrophobic mismatch tends to be compensated with changes in the lipid bilayer and/or the protein. Lipids surrounding a transmembrane protein could stretch or compress in order to match the hydrophobic region of the protein. The other possibility is for the transmembrane α-helices in a transmembrane protein to change their tilt, resulting in changes in the overall structure of the protein (Figure 1.8). When the energetic cost of these changes is high, it can be minimised by aggregation of the protein, reducing the area of contact between the lipids and the protein; if the energetic costs are still too high, the protein could be excluded from the membrane altogether.

Although the interactions of annular lipids with transmembrane proteins generally have a low specificity, the lipid head group can have important effects on the structure and function of transmembrane proteins. The –NH and C=O groups at the ends of a transmembrane α-helix cannot hydrogen bond with the other groups in the α-helix itself because they are the ending amino acids of the helix. These groups can, however, hydrogen bond with the glycerol backbone and the lipid head group of the bilayer. Changes in the lipid head group could change this pattern of hydrogen bonding and alter the structure of the protein and hence its activity. The presence of charged lipid head groups can also have important effects on the structure of a

membrane protein when the protein contains charged amino acids capable of interacting with the lipid head groups. Additionally, interactions with the lipid headgroup could also affect the oligomeric or aggregation state of membrane proteins, which can also be important for protein function. Finally, a more indirect way in which charged lipid head groups could affect the activity of a membrane protein would be by modifying the concentration of important charged molecules or ions (that could be implicated in the activity of the protein) in proximity to the surface of the bilayer[4,22].

Some lipid molecules interact with membrane proteins in a more specific way, binding between the transmembrane α-helices or at protein-protein interfaces in multi-subunit proteins. These lipids are referred to as non-annular lipids, and non-annular lipid binding sites on a protein are sometimes accessible to only certain types of lipid molecule. The number of lipids that interact with a protein in this way is much smaller than the number of those interacting with annular sites, and these lipids may be essential for maintaining the structure of the protein or for the activity of the protein, acting like co-factors[4,9,22] (Figure 1.7B). Several multimeric complexes contain non-annular lipid molecules buried at intersubunit interfaces, which have been suggested to be necessary to keep the subunits together[22]. For example, the crystal structure of cytochrome bc1 from yeast (a homodimer involved in the electron transport chain in mitochondria) shows a PE molecule at the dimer interface which interacts with both monomers, which has been suggested to be important for dimer formation. The activity of the Ca^{2+}-ATPase from sarcoplasmic reticulum is low in PE membranes, and its crystal structure shows a PE molecule bound at a cavity that opens between two transmembrane α-helices in the Ca^{2+}-free conformation. This cavity closes in the Ca^{2+}-bound conformation, and it has been proposed that the activity of the Ca^{2+}-ATPase in PE membranes could be reduced due to occupancy of the cavity by PE, making the binding of Ca^{2+} less favourable[12]. Another good example of a protein influenced by binding of non-annular lipid molecules was already mentioned above, the potassium channel KcsA, which will be discussed later in detail. In many cases, non-annular lipid molecules are resolved in crystal structures, but their function, if any, is unknown, like in the cytochrome c oxidase from the bacteria *Paracoccus denitrificans* where two phosphatidylcholine molecules, one on each side of the membrane, are bound in deep clefts in the protein surface[22] (Figure 1.7B).

1.3 Studying the interactions of lipids with transmembrane proteins.

There are four main ways of studying lipid-protein interactions: molecular dynamics simulations, x-ray crystallography, electron spin resonance and fluorescence spectroscopy.

1.3.1 Molecular dynamic simulations

Computer simulations can create models that provide a view of the dynamics of membranes that experimental techniques cannot provide. However, several problems need to be considered when using these models. Both the time and space scales of the simulations need to be considered. Rotations of the C-C bonds take place on a picosecond timescale, while the observation of lipid diffusion in the plane of the membrane requires up to the order of microseconds. Similarly, the extent of motions go from the range of Å for rotations about C-C bonds, to the range of micrometers for collective motions of groups of lipids involved in undulations of the bilayer. Another important feature to consider is the positioning of the membrane protein into the bilayer, since this will be crucial in describing the interactions between the lipids and the protein in the membrane[9].

1.3.2 X-ray crystallography

Although x-ray crystallography is the most direct method for observing lipid-protein interactions, it is not possible to prepare samples of proteins for x-ray crystallography embedded in lipid bilayers. In fact, the intrinsic basis of the technique, the formation of crystals, which are static structures, oppose the basic characteristic of biological membranes: their dynamism. Membrane proteins must be solubilised in detergent in order to form crystals, and most of the lipid molecules will be either lost or insufficiently ordered to be resolved in the resulting crystal. This fact is consistent with the suggested low specificity in the binding of the lipid annular shell to the transmembrane region of a membrane protein, which should make it easy for the lipids to be lost in the solubilisation process. Bacteriorhodopsin, a trimeric proton pump that uses light as its source of energy in the archaebacteria *Halobacterium*

halobium, is one of the few cases in which a considerable amount of annular lipid has been resolved bound to the surface of the protein (Figure 1.7A). This was possible thanks to the disposition of the protein in the membrane, where only one annular shell of lipids separates the different trimmers from each other, meaning that the motion of the annular lipid molecules is more restricted than usual. In the structure, the fatty acyl chains seem to bind into grooves on the surface of the protein, but the lipid head groups are not resolved, probably due to a considerable disorder in the head group region. Usually only a few, if any, lipid molecules are resolved in protein crystal structures, and normally these correspond to non-annular lipids that bind more tightly to the protein (Figure 1.7B). These structures show how specific and intimate the interactions with these lipids can be[4,9,22,23].

1.3.3 Electron spin resonance (ESR)

Electron spin resonance, like fluorescence spectroscopy (see below), has the advantage of reporting information on the protein in its native lipid bilayer environment. ESR uses probes with an unpaired electron (spin labels), normally involving a nitroxide group, attached to chosen positions in the phospholipid fatty acyl chains (find examples in Chapter 2, Figure 2.2)[24,25]. The spin label absorbs microwave radiation when placed in a magnetic field, and this absorption varies as the magnetic field is increased, giving an absorption spectrum (see examples of absorption spectra in Chapter 2, Figures 2.3 and 2.5). The way this is detected in the ESR spectrophotometer gives the first derivative of the absorption spectrum, resulting in the characteristic ESR spectrum normally observed (Figure 1.9). The resulting spectrum is highly sensitive to rotation around the axis of the lipid molecule; as a result, lipid molecules in the bulk liquid crystalline bilayer, where their acyl chains are able to rotate quickly, have a characteristic narrow and intense spectrum, while lipid molecules in contact with the rough surface of a membrane protein are less mobile, giving a broader and less intense spectrum. The distance separation between the outer peaks of the spectrum is called the maximum splitting of the spectrum and is a good indicator of the degree of mobility of the spin labelled lipid, so that the greater the maximum splitting, the lower the mobility of the lipid (Figure 1.9). Because the time a lipid molecule resides on the surface of a membrane protein is just on the range of ESR sensitivity it is possible to distinguish between spin label lipids in contact with a

membrane protein and spin label lipids in the bulk lipid bilayer, due to their different mobilities. The result is that samples of spin label lipids in bilayers containing membrane proteins give rise to a composite ESR spectrum (Figure 1.9), i.e. a spectrum formed by the addition of two different spectra: one coming from the population of spin label lipid in the bulk bilayer (mobile or fluid component) and the other coming from the population of spin label lipid in contact with the proteins (immobile or restricted component). Deconvolution of the composite spectrum into its single component spectra allows determination of the fraction of lipid in contact with the protein. Thanks to this, ESR studies allow an estimate to be made of the number of lipid molecules that surround a membrane protein (which provides information about the oligomeric state of a protein, see Chapter 3) and lipid affinities for the protein (see Chapter 5). Because the time a lipid molecule is bound to the protein is on the borderline of ESR sensitivity, the spectra can also give information on the length of time a lipid molecule stays bound to the transmembrane region of a protein (generally 50-100 ns), lipid-protein interactions being only slightly more favourable than lipid-lipid interactions (generally lasting ca. 10 ns), indicating a non-sticky interaction between the lipid and the protein[9,25].

Other ESR approaches where spin labels are attached to cysteine residues in the protein are also possible and can be used to probe the environment of membrane proteins and even determine structural features[26].

1.3.4 Fluorescence spectroscopy

Like ESR, fluorescence spectroscopy can report on membrane proteins embedded in their lipid environment. In this case, a fluorophore is the reporter molecule, characterised by its ability to absorb light of a certain wavelength and then emit light (fluorescence) of a larger wavelength that is detected in a spectrofluorimeter[27]. With the use of site directed mutagenesis it is possible to position a reporting fluorophore in the desired position in the sequence of the protein that is being studied[28]. The three aromatic amino acids tryptophan, tyrosine and phenylalanine have intrinsic fluorescence, tryptophan being the dominant fluorophore and being normally used as a natural fluorescence reporter. Tryptophan fluorescence is environmentally sensitive, and similarly to spin labels attached to cysteine residues

in proteins in ESR, a tryptophan residue in a protein can report information about the environment of the protein and reveal some features about its structure. A tryptophan residue located within the lipid bilayer will have different emission spectra from one facing the aqueous medium, thus it is possible to estimate the relative positions of protein residues with respect to the lipid bilayer[28,29].

For the study of lipid-protein interactions in particular, quenching of tryptophan fluorescence with brominated lipid molecules is a powerful tool[28]. A pair of bromine atoms attached at the *cis* double bond positions in mono-unsaturated fatty acyl chains of phospholipids act as powerful quenchers of tryptophan fluorescence[30]. For quenching of tryptophan fluorescence it is necessary for the pair of bromine atoms to be very close to the tryptophan residue, so that only lipids interacting with the protein will be able to quench the fluorescence of a tryptophan residue in the hydrophobic core of the lipid bilayer. Mixtures of brominated and non-brominated lipids can be used to study binding constants of the respective lipids to certain regions of a membrane protein[28,31]. The fluorescence lifetime of tryptophan[27] (i.e. the time lapse from the moment exciting light is absorbed until light is emitted as fluorescence) is ca. 3 ns, significantly shorter than the time a lipid molecule resides bound to the surface of a transmembrane protein (generally 50-100 ns)[9,25], and so fluorescence measurements give a static picture of the lipid-protein interactions occurring in the membrane. The method, however, differs significantly from that of ESR with spin labelled lipids. In the ESR method the information is reported by a probe attached to a lipid molecule, generally giving an average picture of the lipid molecules interacting at all the lipid binding sites on the protein. On the fluorescence method the information is reported by a particular tryptophan residue in a defined region of a protein, giving information about particular lipid binding sites[28].

1.3.5 ESR and fluorescence spectroscopy can be used to estimate lipid binding constants

As described above, both ESR and fluorescence spectroscopy can be used to measure the affinities of lipids for a protein. In the present study, both techniques will be used to analyse interactions of lipids with annular and non-annular sites on KcsA[13,32]. The interaction of lipid molecules with the annular sites of a

transmembrane protein can be described in terms of an exchange equilibrium between the lipid bound to the protein and the bulk lipid (Figure 1.10). In this way a binding constant for a lipid *A* relative to a lipid *B* can be determined, as will be explained in detail in the following chapters. For lipid molecules binding at non-annular sites, an exchange equilibrium model can also be used, when both lipid *A* and lipid *B* can bind at the site, or alternatively, a simple binding model may apply when only lipid *A*, for example, can bind at the non-annular site (Figure 1.10). The potassium channel KcsA has been chosen for these studies for its convenience for studying lipid-protein interactions with both annular and non-annular sites, and for the importance of the interactions with lipids for potassium channel function (see below).

1.4 Potassium channels

Numerous potassium channels have been identified in a wide range of species from archaeal, bacterial and eukaryotic cells, and all of them are related members of a single protein family. These channels are all characterised by containing a highly conserved amino acid sequence called the K^+ channel signature sequence. This sequence forms part of the pore of the channels and is essential for them to discriminate between K^+ and Na^+ ions. In fact, all potassium channels show very similar ion permeability properties. Their permeability to K^+ is very similar to that of Rb^+, but they also show a lower permeability for Cs^+. Their permeability to the smallest alkali metal ions, Na^+ and Li^+, is extremely low, K^+ being 10,000 times more permeant than Na^+. Potassium channels are also characterized by having a multi-ion conduction mechanism, in which several ions queue in a single file inside a long and narrow pore to cross to the other side of the membrane[33,34].

In most cases, the functional potassium channel protein is a tetramer, generally composed of four identical subunits; the subunits generally contain two or six transmembrane α-helices[34]. In the case of "two pore domain" potassium channels, the functional channel is a dimer in which each monomer consists of two fused subunits of the type initially described, so that only two monomers need to come together to form a channel. These are the basic subunits that form the channels, and are called primary (α) subunits. Additionally, in some cases, other subunits, called accessory (β) subunits, may associate with the α-subunits modifying the channel characteristics,

such as ion selectivity, kinetics and pharmacology. Some of these β-subunits are located in the cytoplasm, whilst others are associated with the membrane. Finally, in some cases there are also special types of α-subunits, called silent α-subunits, which cannot form functional channels on their own, but can combine with other functional α-subunits to form heterotetramers with altered properties[35].

1.4.1 Potassium channel regulation

As described above, all potassium channels share very similar ion permeability properties due to the conserved sequence in the pore. However, they show many different modes of regulation, and so the variety of potassium channels in nature is immense. Potassium channels can be regulated by ligands, voltage or mechanical stimuli[33,36]. It is hard to produce a classification of all potassium channels because in many cases different regulatory domains combine in different groups. Voltage-gated potassium channels contain six transmembrane α-helices, named S1 to S6 from the N-terminus to the C-terminus. The last two transmembrane helices, S5 and S6, constitute the core of the channel, and are present in all potassium channels. The first four helices, S1 to S4, form the voltage sensor of these channels, where the S4 helix is characterised by containing positively charged residues essential for voltage sensing. Ligand binding potassium channels normally have the two core S5 and S6 transmembrane α-helices and cytoplasmic domains that are the ligand binding domains that regulate their activity. The diversity of ligands described is immense, from ions and small organic molecules to proteins. Numerous channels combine voltage and ligand regulation, having complex structures. Additionally, potassium channels can have extra domains involved in tetramerization and the binding of β-subunits[35,37]. All these properties permit potassium channels to be tightly regulated, letting cells control numerous physiological processes. In prokaryotes it is thought that they are necessary to maintain the membrane potential[38], while in eukaryotes they are further known to be necessary for complex processes such as neuronal integration, heart rate, K^+ reabsorption in the kidney, vascular tone and insulin release[8].

Potassium channels can be influenced by their lipid environment.

Potassium channel structure and function can also be influenced by lipids. For example, the conformation and functionality of the voltage sensor of voltage-gated

potassium channels is greatly influenced by its lipid environment: the phosphodiester group in phospholipids has been shown to be essential for the functionality of the voltage sensor. However, it is not yet certain how phospholipids mediate their influence on the voltage sensor. First it was proposed that specific interactions of the phosphodiester groups with two Arg residues in the S4 helix were responsible for maintaining the voltage sensor in the correct conformation in the membrane[39]. However, a recent study has shown that this is not the case, as mutation of those Arg residues to Cys does not disrupt the conformation and functionality of the voltage-sensor[40]. Instead, it was proposed that the interactions providing stability for the voltage sensor in the membrane corresponded to the sum of many weak interactions between the voltage sensor and the annular lipid molecules surrounding it, the annular lipids and voltage sensor acting as a functional unit[40].

Another group of potassium channels known as inwardly rectifying potassium channels or Kir channels (channels formed by subunits with two transmembrane α-helices that preferentially conduct potassium ions towards the inside of the cell) are also influenced by the lipid bilayer composition. Kir channels require the presence of highly negatively charged phosphoinositides (two to four negative charged groups) to be active[41], and it has been proposed, on the basis of mutagenesis studies, that the highly negatively charged headgroups interact with a cluster of conserved positively charged residues located in cytoplasmic domains in a region close to the membrane interface[42].

Another type of lipid molecule that has been shown to affect the activity of numerous different types of potassium channels (and numerous other ion channels) are (unesterified) fatty acids[43,44]. Fatty acids can be particularly useful as messenger molecules for activity regulation because in resting conditions their concentrations in the membrane are very low, but in response to a particular stimulus they can be quickly released from phospholipid molecules in the membrane. Moreover, their significant water solubility allows them to also leave the lipid bilayer and interact with other regions of a membrane protein apart from those embedded in the lipid bilayer. Numerous studies have reported that fatty acids affect potassium channel function, and it is likely that there is more than one mechanism of action. Two reports, based on mutagenesis studies, have provided strong evidence that inhibition of some

potassium channels by fatty acids occurs by binding of fatty acid molecules to the hydrophobic inner cavity of the pore, blocking ion flux[45,46] (see below for the structure of potassium channels and Chapter 5 for more details about fatty acids binding in the cavity).

Some of the experiments presented in this thesis will focus on the study of interactions of fatty acids with potassium channels. In particular, the potassium channel KcsA was chosen as a model because its particular characteristics (see below) allow an analysis of lipid-protein interactions at the annular and non-annular sites separately with the use of fluorescence spectroscopy (Chapter 4). Further, combined with ESR studies, binding of fatty acids at the hydrophobic inner cavity can also be explored (Chapter 5), allowing a thorough analysis of interactions with all binding sites potentially involved in channel function regulation.

1.5 The potassium channel KcsA

1.5.1 Structure of KcsA

The potassium channel of the Gram-positive soil bacteria *Streptomyces lividans* was named KcsA. It was identified by Schrempf *et al.*[47] in 1995, and its amino acid sequence (160 amino acids) and structure is closely related to that of other potassium channels, including eukaryotic potassium channels[34,48,49]. It was first crystallized by Doyle *et al.*[34] in 1998, being the first potassium channel ever crystallised. Their results revealed a channel with the form of an inverted cone composed of four identical subunits (Figure 1.11). Each subunit has only two transmembrane α-helices, one facing the central pore (inner helix) and the other the lipid bilayer (outer helix). These transmembrane α-helices are connected by 30 amino acids that constitute the *P*-loop region, which consists of the turret, a short helix (pore helix) and the selectivity filter (which contains the channel signature sequence TTVGYG). Both the extracellular and intracellular entry ways for K^+ ions are marked by acidic amino acids. The overall length of the pore is 45 Å, and the polar selectivity filter for K^+ ions (which is very narrow) is found near the extracellular surface of the membrane. Towards the middle of the bilayer, the pore opens into a wide hydrophobic cavity (called the central cavity) and narrows again at the intracellular side of the

membrane where the inner transmembrane helices of adjacent subunits cross, forming a bundle that occludes the pore. Thus, the crystal structure of KcsA obtained by Doyle *et al.*[34] shows, at least at the intracellular side of the membrane, a channel in its closed state. Since then, numerous other crystal structures of the KcsA channel have been resolved, some of them in the open state, with the helical bundle wide open[50].

To obtain crystals for X-ray analysis Doyle removed the C-terminus from KcsA, and the N-terminus residues were unresolved[34]. None of the crystal structures determined at present show the N-terminus of KcsA, however, ESR studies carried out by Cortes *et al.* in 2001[51] with reconstituted KcsA channels revealed for the first time the molecular architecture of the N and C-termini (Figure 1.12). Both termini contain a significant number of charged residues, specially the C-terminus. The N-terminus forms an interfacial α-helix up to position 20 to 21, with some residues facing the lipid bilayer, and others facing the cytoplasm. It is then connected to the outer transmembrane helix by two to three residues. This interfacial helix expands about 30 to 40 Å away from the transmembrane core and it is not completely parallel to the membrane, showing an insertion angle of about 14˚ relative to the membrane plane. The C-terminus was, more recently, revealed by X-ray crystallography[52] which gave a rather different picture to that suggested by the ESR study; although both studies suggested that the C-terminus was a highly α-helical domain extending towards the cytoplasm perpendicularly to the lipid bilayer (Figure 1.12).

1.5.2 Potassium conductance

Given that K^+ concentrations are high inside the cell and low outside, K^+ ions will generally move through the channel from the inside to the outside, although, ion flux is possible in both directions. Before ions enter the channel, negatively charged residues in the extracellular and intracellular sides of the protein are thought to increase the local concentration of cations compared to anions, in order to favour cation conductance (Figure 1.13A). The reason why KcsA conducts K^+ much better than Na^+ relies mainly on the structure of the selectivity filter[34,53]. Outside the selectivity filter, the ions are hydrated, interacting with water molecules. The selectivity filter is too narrow for either Na^+ or K^+ to enter hydrated, and so, before entering, they must lose their bound water molecules. The energetic cost of

dehydration is balanced for K^+ ions by interaction with the selectivity filter. In detail, the signature sequence residues in the selectivity filter are arranged with their polar carbonyl oxygen main chain atoms pointing towards the pore. Dehydration of K^+ is balanced by optimal interaction of the ion with the carbonyl oxygen atoms from the four subunits, but Na^+ is too small to interact well with the carbonyl oxygen atoms in the selectivity filter, and so the activation energy for Na^+ binding to the filter is very high (Figure 1.13B).

There are four sites where K^+ ions could bind in the selectivity filter, but only two ions are present at a time, occupying alternate positions. This is because if all the binding sites in the selectivity filter were occupied with ions, there would be unfavourable electrostatic repulsions between them. Thus, the conductive selectivity filter exists in two ion configurations: K^+-water-K^+-water (1, 3 configuration) and water-K^+-water-K^+ (2, 4 configuration). The structure of the selectivity filter might suggest that a K^+ ion would be held very tightly in the filter. However, the multi ion conduction system provides a mechanism to avoid ion retention, because as a new ion enters, the previous ion in the filter becomes destabilized by electrostatic repulsion, helping its release into solution[34,53].

The selectivity filter is located on the extracellular side of the membrane and to cross the lipid bilayer, the ions must pass through the region of the channel that is held in the hydrophobic core of the bilayer. The hydrophobic core of the lipid bilayer constitutes a great impediment for ion passage because of the low electrical polarizability of the hydrocarbon chains, meaning that they hardly interact with the ion. The crystal structure of KcsA has revealed the mechanism by which the structure of the channel creates an environment that stabilizes the ions in the middle of the bilayer, allowing them to cross it. Two structures are involved: the pore helices (Figure 1.13C and D) and the inner cavity (Figure 1.13D) [34,53,54].

The hydrophobic central cavity is located right at the hydrophobic core of the bilayer. It is large enough to contain around 50 water molecules, creating a polar environment that reduces the free energy cost for transferring an ion into the bilayer core (Figure 1.13D). In addition, the pore helices act as dipoles stabilising cations crossing the bilayer. The C=O and N-H groups in the peptide bonds of an α-helix are

all disposed in the same orientation, acting together as a dipole along the axis of the helix. The result is a more negatively charged C-terminus and a more positively charged N-terminus (Figure 1.13C). Together the four pore helices point their C-termini towards the central cavity, and this provides a negatively charged environment that helps stabilise K^+ ions in the central cavity. At the same time, the hydrophobicity of the inner cavity means that K^+ ions do not bind tightly to the channel on their passage through the pore, allowing very fast flux.

1.5.3 Gating of KcsA

The gating mechanism of KcsA is complex and is not yet fully understood. It is clear that the channel is gated by binding intracellular protons, needing a pH <5.5 on the intracellular side of the membrane for opening[55], although it seems unlikely that protons are physiological ligands of KcsA, since intracellular pH is normally tightly regulated and would not be expected to reach a value of 5; the mechanism by which KcsA gating occurs *in vivo* remains unknown. Recently, a group of three residues at the cytoplasmic ends of the transmembrane helices (E118, E120 and H25) have been shown to be the pH sensors in KcsA; it has been proposed that these residues form a complex network of inter and intrasubunit interactions at the cytoplasmic ends of the two transmembrane helices (Figure 1.14). At neutral pH this network would keep together the ends of the inner transmembrane α-helices, creating a crossed bundle that impedes the flow of ions. At acidic pH, the network would be disrupted and as a consequence the inner helices could separate, opening the channel[56].

The movement apart of the inner helices had already been related to channel opening at acidic pH by several groups[57-61]. Recently, the crystal structure of a constitutively open KcsA mutant has shown that the helix bundle indeed opens widely, the inner helix undergoing a hinge-bending and rotational motion, the hinge point being located somewhere above Gly-104[50] (Figure 1.15).

The movement of the inner transmembrane helices is not the only process that governs channel gating. Even at acidic pH, the channel shows a very low open probability, which does not correlate with the helix movement[62]. In order to explain

this apparent contradiction, it was suggested that the proton dependent activation is followed by an inactivation process. This inactivation process has been shown to take place in the selectivity filter, and is referred to as C-type inactivation. In the closed state, at neutral pH, a hydrogen bond network in the selectivity filter holds it in a conductive state. When the channel is activated at acidic pH, the movements of the inner helices partially destabilise this hydrogen bond network, and the selectivity filter is then able to fluctuate between its conductive and non-conductive conformations[63-65]. C-type inactivation also happens in other potassium channels, where involvement of the selectivity filter has also been shown[66].

As described previously, gating of KcsA is further influenced by the lipid bilayer. Negatively charged phospholipid molecules are required to bind at the non-annular sites located at the intersubunit junctions to increase the open probability of the channel[13], as will be described in more detail below.

Other potassium channels have other mechanisms to regulate ion flux. One important mechanism is called N-type inactivation. This inactivation mechanism takes advantage of the wide hydrophobic inner cavity present in the potassium channel family, which, as described above, is necessary for ions to cross the hydrophobic core of the bilayer. In N-type inactivation, the N-terminus of the channel (or in some cases a β-subunit) acts as a blocking arm that penetrates the inner cavity after the channel has opened, impeding ion flow through the pore[67,68]. KcsA lacks N-type inactivation, but, because it has a wide hydrophobic inner cavity, it is susceptible to pore blockage by hydrophobic cations like tetraethylammonium (TEA)[69] or tetrabutylammonium (TBA)[67,70,71] that bind to the inner cavity, the positive charge on these ions helping to maintain them within the cavity due to the stabilising effect of the polarised pore helices that normally stabilise potassium ions in the cavity, as explained above. Thus KcsA is a good model for studying potassium channel regulation by pore blocking molecules[67], including, potentially, fatty acids.

1.5.4 Lipid interactions with KcsA

Interaction with annular lipids

Tryptophan and tyrosine residues are often observed at the lipid-water interfaces in transmembrane proteins. Because of their amphipathic nature, these residues are thought to act as floats that help anchor the proteins into the membrane. KcsA possess two girdles of Trp residues, one at each membrane-water interface, with a distribution almost parallel to the bilayer. Also, at the extracellular side, it has another band of Tyr residues, just above the band of Trp residues (Figure 1.16).

The particularly clear distribution of Trp residues in KcsA is very convenient for fluorescence studies aimed at analysing lipid-protein interactions. Due to the environmentally sensitive fluorescence of tryptophan, major changes in the location of the Trp residues with respect to the lipid bilayer will result in major changes in fluorescence emission spectra. In fact, it has been shown that reconstituting KcsA into lipid bilayers of different thickness does not result in any change in fluorescence emission[72]. This implies that either the lipid or the channel, or both, distort in order to achieve hydrophobic matching, maintaining the Trp residues at the lipid protein interface.

The distribution of tryptophan residues around KcsA also allows a determination of the relative affinities of different types of phospholipid molecule for the annular sites of the channel using fluorescence spectroscopy and brominated phospholipids (see below). Using this methodology, it has been shown that, like in many other proteins, binding of lipids at the annular sites of KcsA shows little specificity, although negatively charged phospholipids show a clear slightly higher affinity (ca. 1.5 to 3 fold) than zwitterionic phospholipids[73,74].

Despite the low specificity that the annular shell of lipids generally shows for membrane proteins, the annular lipids are important because they provide a suitable environment for the protein, shielding its hydrophobic surface from water. KcsA is a particularly stable protein, which is easily reconstituted in artificial bilayers, where single channel activity recordings can be performed[47,55]. Its tetrameric structure is largely maintained in sodium dodecyl sulphate (SDS) detergent micelles[75,76], resisting

temperatures of up to 100 ˚C in the presence of 100 mM KCl[77]. However, numerous studies have reported aggregates of KcsA: from channel dimers in detergent micelles[78], to large aggregates in reconstituted systems[79,80]. It is not clear what triggers this aggregation behaviour and if it has any biological relevance, but these observations make KcsA an attractive model to analyse protein-protein contacts and the influence that annular lipids have on these protein-protein interactions. Part of the studies presented here will therefore focus on studying the lipid-channel stoichiometry (i.e. number of annular lipids around KcsA) in bilayers of different composition using both ESR and fluorescence spectroscopy (see Chapter 3).

Interaction with non-annular lipids

Crystallization of KcsA in complex with a Fab antibody fragment provided a higher resolution structure for KcsA than that first obtained by Doyle *et al.*[34]. The newer structure revealed a non-annular lipid molecule bound at each interface between the monomers[53]. The lipid molecule is not completely resolved, but biochemical assays have shown this lipid to be the negatively charged phospholipid phosphatidylglycerol (PG)[81]. The partial PG molecule seen in the crystal structure of KcsA indicates that the negatively charged lipid head group is located near the extracellular surface, close to two positively charged residues (R64 and R89) which could provide favourable electrostatic interactions for binding the lipid. The lipid acyl chains project into the lipid bilayer; one of them is located in a groove between the inner and the pore helices, while the other seems to interact less intimately with the protein (Figure 1.17).

It has been shown that the presence of negatively charged phospholipids is needed for the channel to be opened[81,82] and recently it has been found that at least three of the four non-annular sites need to be occupied by a negatively charged lipid molecule for the channel to open[13]. However, the molecular mechanism by which the binding of negatively charged phospholipids to the non-annular sites permit opening of the channel remains unknown.

1.5.5 Studying lipid-protein interactions in KcsA using fluorescence spectroscopy

Fluorescence quenching of KcsA reconstituted into membranes containing brominated lipid molecules allows an analysis of the interactions of lipid molecules with the annular and non-annular sites on the channel, separately. Binding of a brominated lipid molecule to a site close to a Trp residue in KcsA will result in quenching of tryptophan fluorescence. The mechanism by which the pair of bromine atoms on a lipid fatty acyl chain quench tryptophan fluorescence is not clear[28], but it has been shown that quenching efficiency depends on the sixth power of the distance of separation between the Trp residue and the dibromo group[30], as in Föster energy transfer theory:

$$E = \frac{R_o^6}{R_o^6 + d^6} \qquad (1.1)$$

where E is the quenching efficiency, d is the distance between the Trp residue and the dibromo group, and R_o is the distance at which the quenching efficiency is 50 %. For quenching of Trp by dibrominated fatty acyl chains, R_o has been shown to be approximately 8 Å[83,84], and this means that only brominated lipid molecules in contact with KcsA will be able to quench effectively the fluorescence of the Trp residues in the channel[28].

KcsA contains five Trp residues per monomer, three of which, W23, W87 and W113, are on the outer surface of the protein, facing the lipid bilayer (Figure 1.16). These Trp residues would be expected to be quenched by brominated lipid molecules binding to the annular sites around the KcsA tetramer. In the brominated lipid molecule di(9,10-dibromostearoyl) phosphatidylcholine (BrPC), derived from dioleoylphosphatidylcholine (DOPC) the bromine atoms will be at the 9 and 10 positions in the chain, about 7 Å from the glycerol backbone region of the bilayer since the hydrophobic thickness of a bilayer of BrPC is about 30 Å. The surface exposed Trp residues in KcsA are close to the glycerol backbone region of the bilayer. The distance between one of the surface exposed Trp residues and a brominated chain of the nearest lipid molecule in the annulus will then be ca. 7 Å, giving rise to efficient quenching[72]. It is possible that more than one dibromo group will be close

enough to the Trp to result in quenching. The efficiency of transfer to multiple quenchers can be calculated. The efficiency of transfer from a donor to a single acceptor is

$$E = \frac{k_T}{\tau_D^{-1} + k_T} \tag{1.2}$$

where k_T is the rate of energy transfer and τ_D is the lifetime of the donor in the absence of acceptor[27]. In the presence of two acceptors this would become:

$$E = \frac{k_{T1} + k_{T2}}{\tau_D^{-1} + k_{T1} + k_{T2}} \tag{1.3}$$

where k_{T1} and k_{T2} are the rates of energy transfer to the two acceptors. Generalising this to x acceptors all the same distance from the donor this becomes:

$$E = \frac{xk_T}{\tau_D^{-1} + xk_T} \tag{1.4}$$

Since:

$$k_T = \tau_D^{-1}\left(\frac{R_o}{d}\right)^6 \tag{1.5}$$

this becomes:

$$E = \frac{xR_o^6}{d^6 + xR_o^6} \tag{1.6}$$

If, for example, there are three brominated chains 7 Å from a Trp residue, then the efficiency of quenching would be 87 %. If the Trp residues W23, W87 and W113 are slightly buried below the protein surface, then the effective distance d would be greater than 7 Å. In fact it is not obvious exactly from where on the Trp group

distances should be measured. In studies with MscL, Carney *et al.*[85] found that the best agreement between experiment and theory was obtained measuring distances to the α-carbon of the Trp residue. This would increase the Br-Trp distance for the surface exposed residues from 7 to about 8 Å, decreasing the efficiency of quenching to 50 % for quenching by a single chain, and to 75 % for three chains. Importantly, however, quenching of these surface exposed Trp will be predominantly by the annular lipids and not the bulk lipids. With a lipid diameter of ca. 9.4 Å, the Trp-Br distance between a surface exposed Trp and a next nearest second shell lipid molecule will be ca. 12 Å, giving an efficiency of quenching of 8 % if quenching is dominated by a single chain or of 20 % if quenching is caused by three chains.

Of the remaining two Trp residues, W67 is close to one of the chains of the anionic lipid molecule bound at the protein-protein interface (non-annular lipid) in the crystal structure of KcsA (PDB 1K4C, Figure 1.18) and so would be expected to be quenched by a brominated lipid molecule binding to the protein-protein interface[74]. The distance between W67 and the nearest chain of the bound non-annular lipid is ca. 7.4 Å, giving an efficiency of quenching of 61 %. In contrast, the distance between W67 and the closest fatty acyl chain of an annular lipid molecule is ca. 12 Å, for which the efficiency of quenching would be ca. 8 %. The final Trp residue, W68, is distant from both the annular and non-annular sites. The expected level of quenching of W68 from the non-annular site is ca. 7 % and ca. 1 % from the closest annular sites. Binding of a brominated lipid molecule to the non-annular site will result in ca. 7 % quenching of the fluorescence of the lipid-exposed W87. In conclusion, W23, W87 and W113 will be quenched by annular lipid but only slightly by non-annular lipid, W67 will be quenched by non-annular lipid but only slightly by annular lipid and W68 will be quenched by neither annular nor non-annular lipid. Therefore quenching of the Trp fluorescence of wild type KcsA by brominated lipid will result from binding at either the annular or the non-annular sites, while quenching of the Trp fluorescence of a KcsA mutant lacking the three lipid-exposed Trp residues, W26, W87 and W113 will only result from binding to the non-annular site. As a result, comparing fluorescence quenching in wild type KcsA and the mutant lacking W26, W87 and W113, allows an analysis of binding of annular and non-annular lipids (see Chapter 4).

1.6 Objectives

The aim of the studies presented in this thesis is to characterise lipid-protein interactions in the model potassium channel KcsA using fluorescence spectroscopy and ESR methods. As described in the introduction, lipid-protein interactions are important for regulating membrane protein function, and there is much interest in understanding how lipids exert their effects on membrane proteins. KcsA has been shown to be a representative model of the potassium channel family and as discussed above, it is also a good model to study lipid-protein interactions. Fatty acid molecules have been shown to affect ion channel function, but little is known about their mechanism of action. A part of the studies here presented will focus on the interaction of fatty acids with their potential sites of action: annular and non-annular sites (Chapter 4) and the hydrophobic inner cavity (Chapter 5). There is also interest on understanding the factors that influence protein-protein contacts of membrane proteins, as oligomerisation of proteins in the membrane can influence their function. Several studies have reported aggregation of KcsA, but little is known about the mechanisms that trigger aggregation of the channel. Chapter 3 will focus on analysing the influence of annular lipids on aggregation of KcsA.

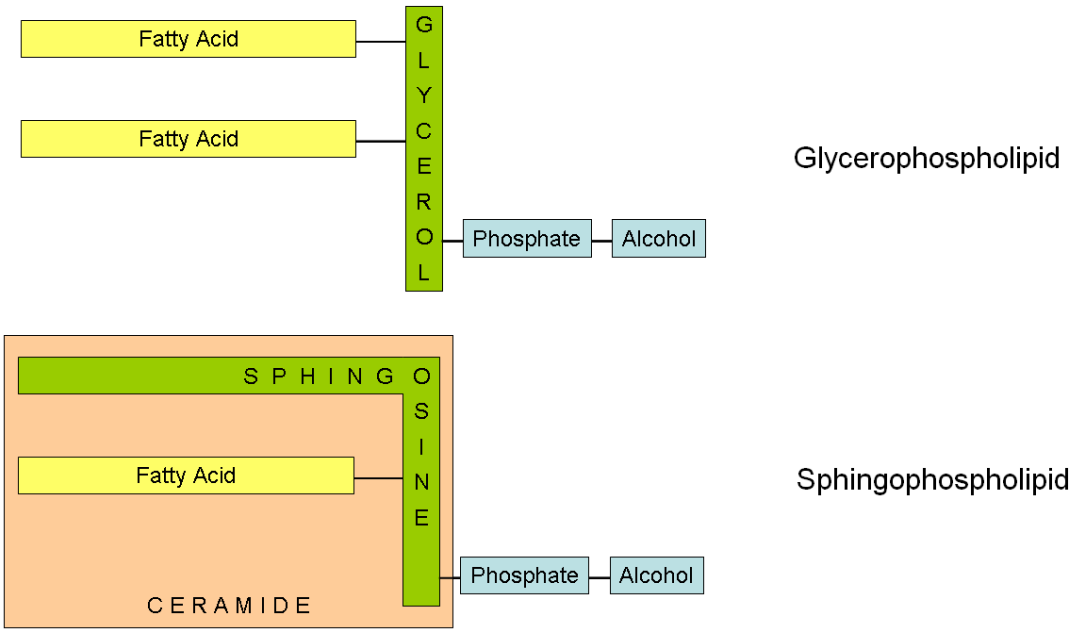

Figure 1.1 Schematic structures of phospholipids: glycerophospholipids and sphingophospholipids. In glycerophospholipids, the glycerol backbone is attached to two fatty acyl groups through ester bonds, while in sphingophospholipids the sphingosine backbone contributes one of the acyl chains and a fatty acyl chain is attached through an amide bond.

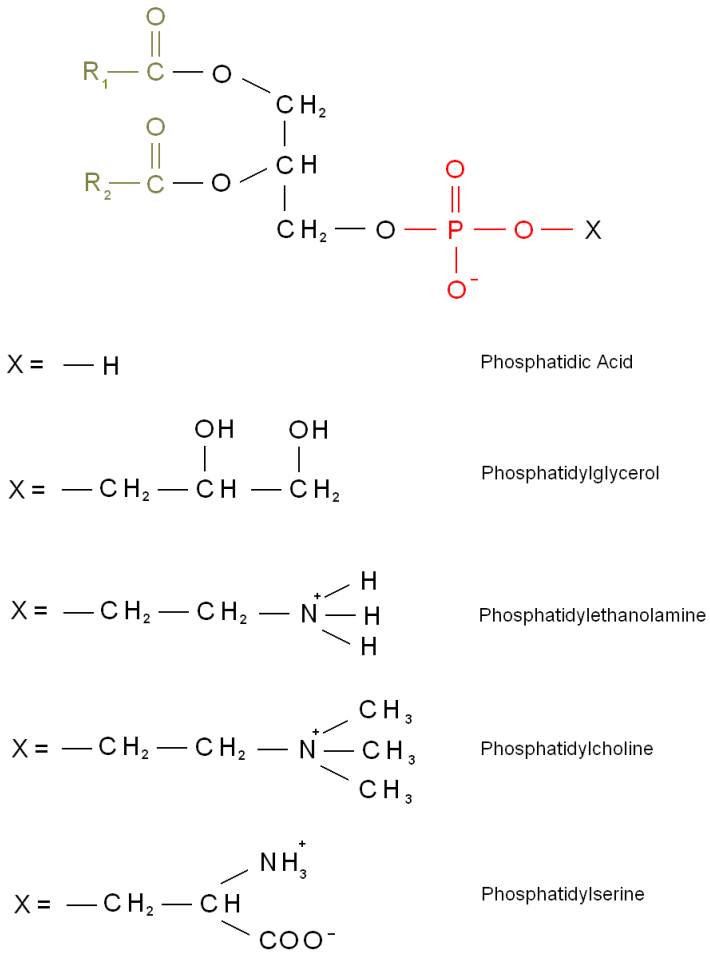

Figure 1.2 Structures of some common glycerophospholipids. The basic structure common to all glycerophospholipids is shown at the top. In black is the glycerol backbone. In pale green are the two fatty acyl chains, which may have different lengths and number of double bonds (R1 and R2), and are linked through ester bonds to the glycerol backbone. In red is the phosphate group, which binds to the alcohol group (X). Some of the most common alcohol group structures are shown below the general structure.

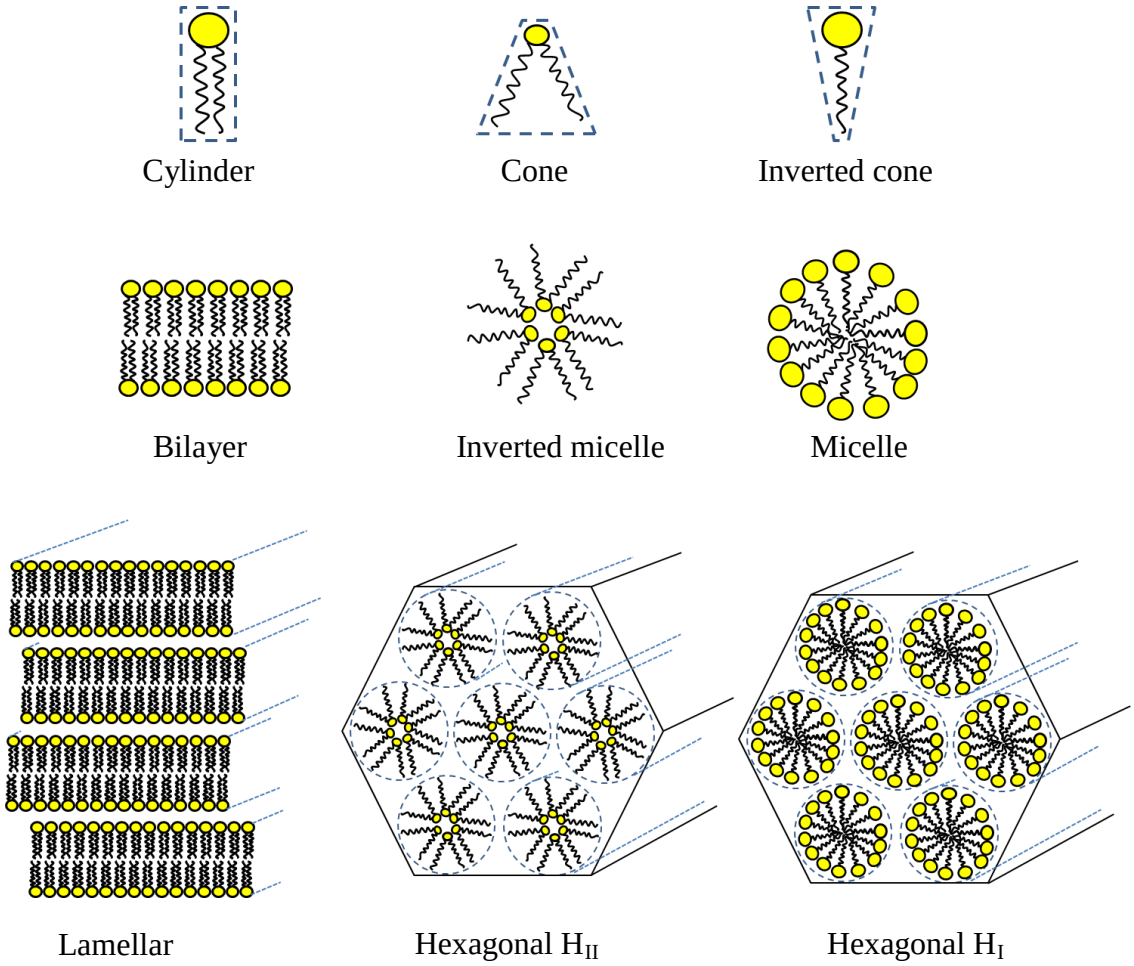

Figure 1.3 Lipid phases. The shape of the lipid molecule is important for determining the type of aggregation in water. Lipids with a cylindrical shape tend to form bilayers that at high concentrations can pile up in a lamellar fashion; cone shaped lipid molecules tend to form the (hexagonal) H_{II} phase (negative curvature) at high concentrations, while at low concentrations can form inverted micelles when placed in a hydrophobic medium; inverted cone shaped lipid molecules tend to form micelles, and at high concentrations arrange in the (hexagonal) H_I phase (positive curvature).

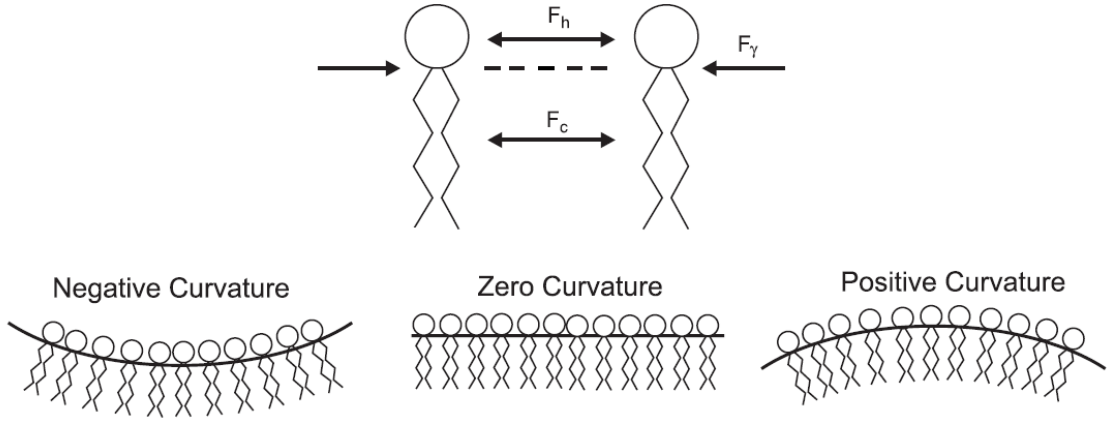

Figure 1.4 Lateral forces acting in a lipid bilayer. A net attractive force (F_γ) due to the hydrophobic effect keeps the membrane assembled, acting at the polar-apolar interface (dashed line). Net repulsive forces act at the hydrophobic core (F_c) and the lipid head groups (F_h). When F_c and F_h are balanced an ideal bilayer is formed. When F_c or F_h are not balanced, the membrane tends to adopt a negative or positive curvature. Symmetrical bilayers (bilayers with the same lipid composition on both sides of the membrane) will not be able to bend and would be under a curvature stress, which could disrupt the membrane if the repulsive forces are stronger than the attractive forces. Adapted from Lee, 2004[4].

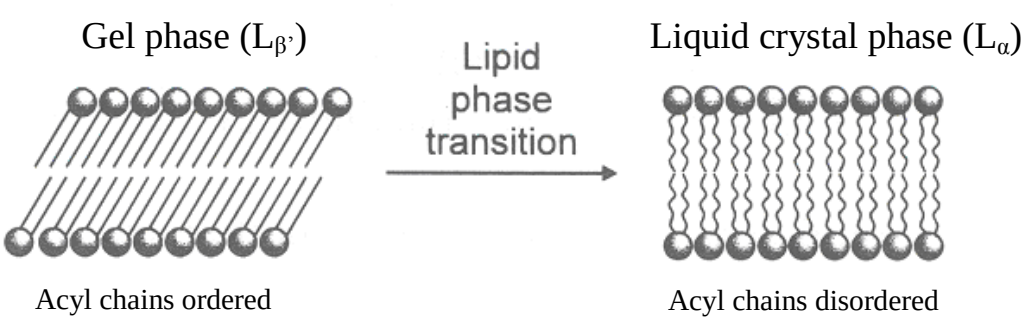

Figure 1.5 The gel and liquid crystal phases. Below their phase transition temperature, lipid bilayers are in a gel phase, with their lipid molecules tightly packed, not being able to diffuse along the membrane plane. Above the transition temperature lipid bilayers go into the liquid crystal phase, with their acyl chains disordered, the membrane is fluid and the lipid molecules can diffuse along the membrane plane. Taken from Vance, 1996[5].

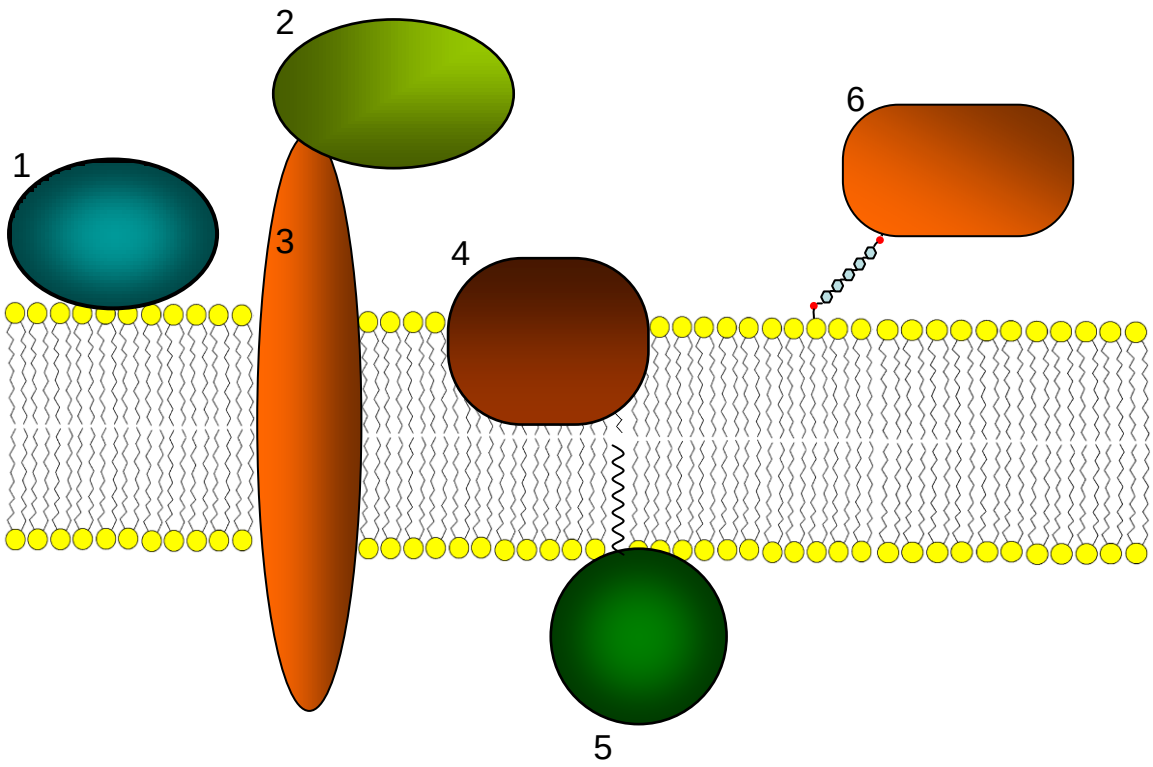

Figure 1.6 Types of membrane proteins. Peripheral membrane proteins: 1 associates with the bilayer interacting with the lipid head groups; 2 associates with the membrane by interacting with an integral membrane protein. Integral membrane proteins: 3 is a transmembrane protein because it crosses the lipid bilayer interacting with the lipid head groups and acyl chains; 4 is not a transmembrane protein because it does not cross the bilayer, but interacts both with the hydrophobic core and the lipid head groups. Proteins that associate through covalently bound lipids: 5 has a lipid moiety covalently bound to its structure which lets the protein associate with the bilayer by inserting the lipid tail in the hydrophobic core; 6 is a GPI anchored protein, bound to a phospholipid through a conserved phosphate-oligosaccharide group (this type of association is always extracellular).

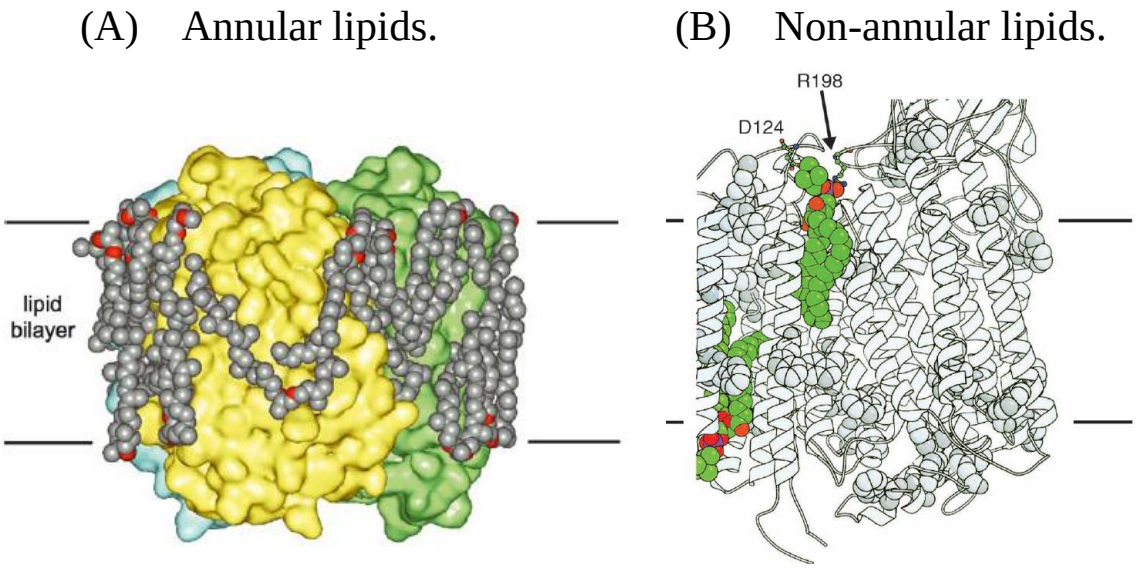

Figure 1.7 Two main types of lipid-protein interactions. (A) The crystal structure of the bacteriorhodopsin trimer from *Halobacterium salinarum*. Numerous annular lipid molecules were resolved; the lipids have been modelled as 2,3-di-O-phytanlyl-*sn*-propane. Each monomer is in a different colour. Taken from Lee, 2005[9]. (B) Crystal structure of cytochrome c oxidase from *Paracoccus denitrificans*; detail of the transmembrane region: two non-annular lipid molecules are intimately bound in grooves between the transmembrane α-helices of the protein; D124 from subunit III and R198 from subunit II, in ball and stick representation, form salt bridges with the lipid head group of one of the lipids. Taken from Lee, 2002[22].

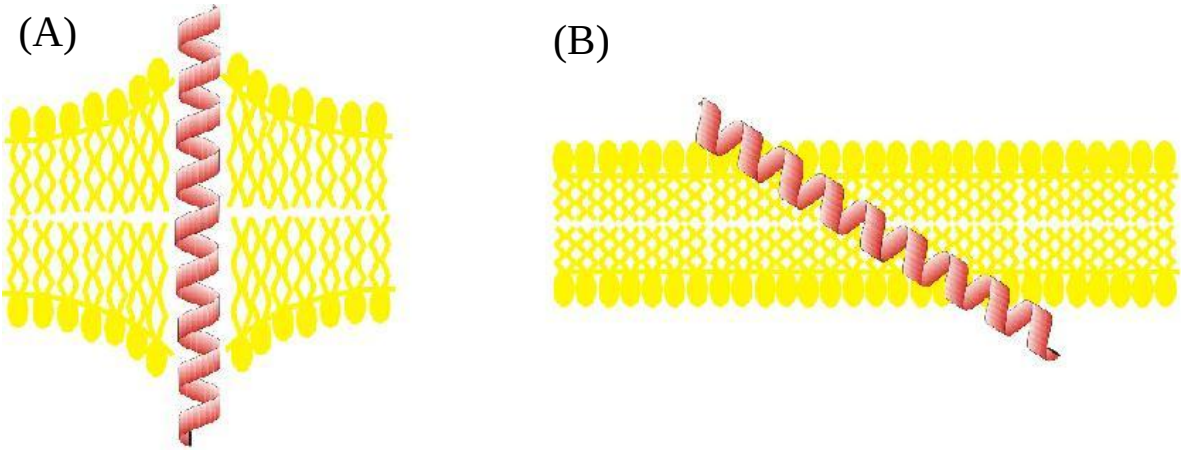

Figure 1.8 Compensation of hydrophobic mismatch. In these examples, the hydrophobic region of the transmembrane α-helix of a protein is thicker than the hydrophobic region of the lipid bilayer. In (A) the lipid bilayer adapts by stretching around the α-helix. In (B) the α-helix adapts by tilting with respect to the bilayer normal. Picture kindly provided by Dr. A Powl.

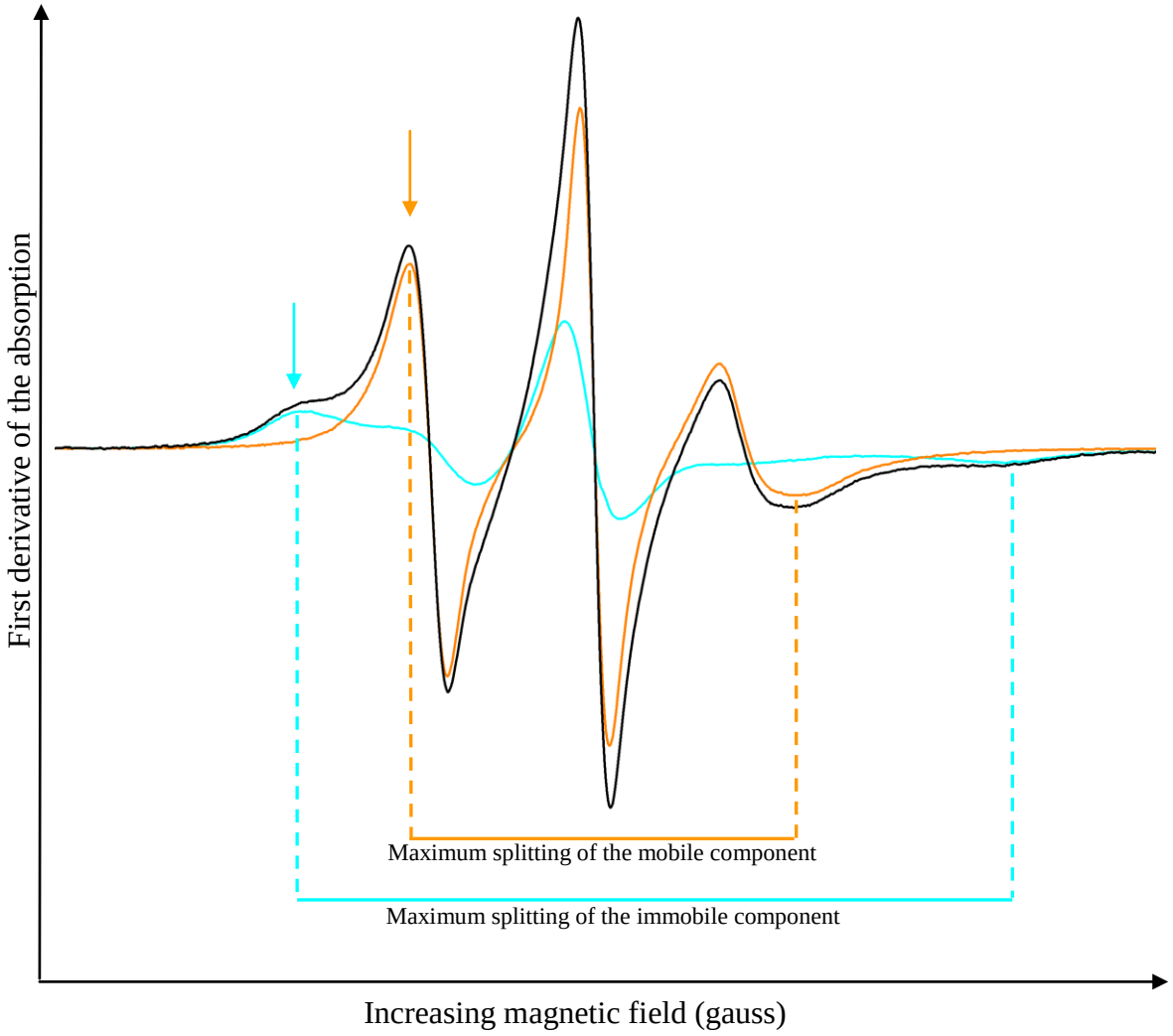

Figure 1.9 Example of a spin labelled phospholipid ESR spectra. In black is the two component spectrum arising from addition of two single component spectra: in cyan is the restricted component (wide and of low intensity), in orange is the mobile component (narrow and of high intensity). Note that the single component spectra differ most in the low magnetic field peaks (left), as highlighted by the cyan (immobile component) and orange (mobile component) arrows. The maximum splitting for each component is also indicated in the respective colours. (Magnetic field increases from left to right.)

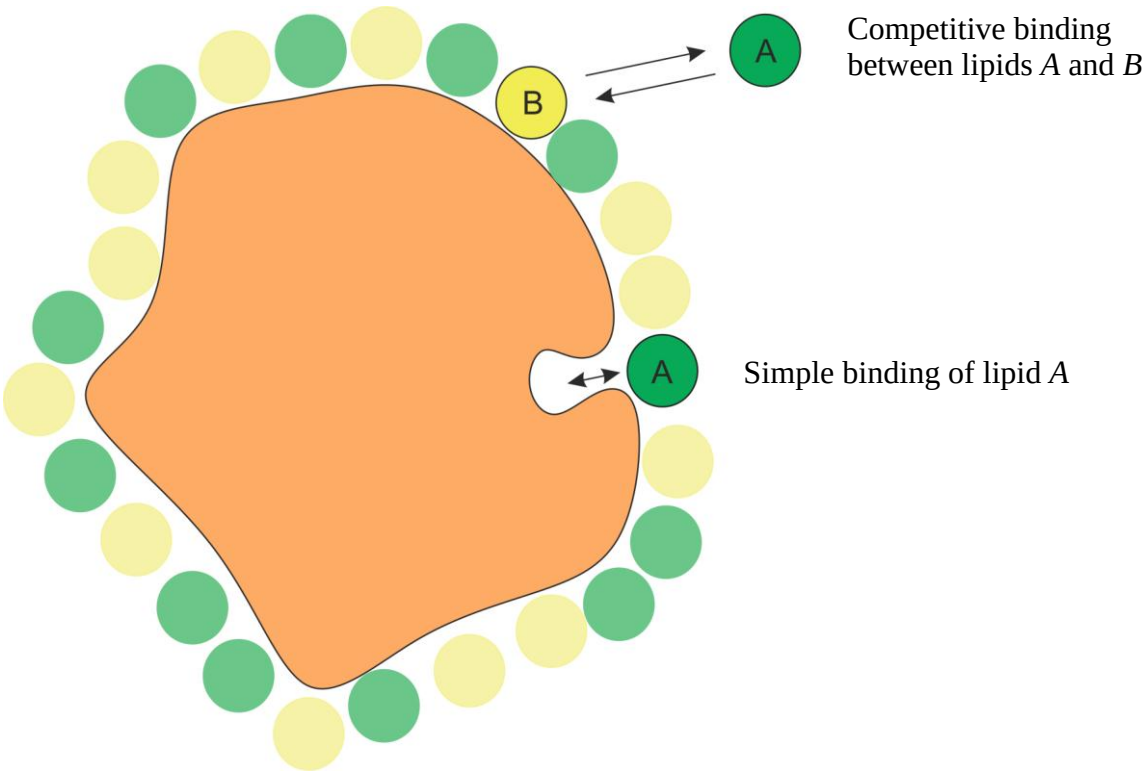

Figure 1.10 Interaction of lipids at annular and non-annular sites on a protein. The cartoon represents a membrane protein (orange) in a bilayer containing two species of lipid molecule (green and yellow circles, respectively), viewed from outside the membrane. The annular lipids solvate the protein, and so a particular annular site is always occupied either by lipid *A* or *B*, so that the lipids compete for binding at the site (see bright green and yellow lipids *A* and *B*, respectively, in exchange equilibrium). A less accessible grove constitutes a non-annular site to which, in this example, only lipid *A* can bind, the site otherwise remaining empty; lipid *A* establishes a simple binding equilibrium. However, a competitive model would describe binding if lipid *B* were also able to bind to the site.

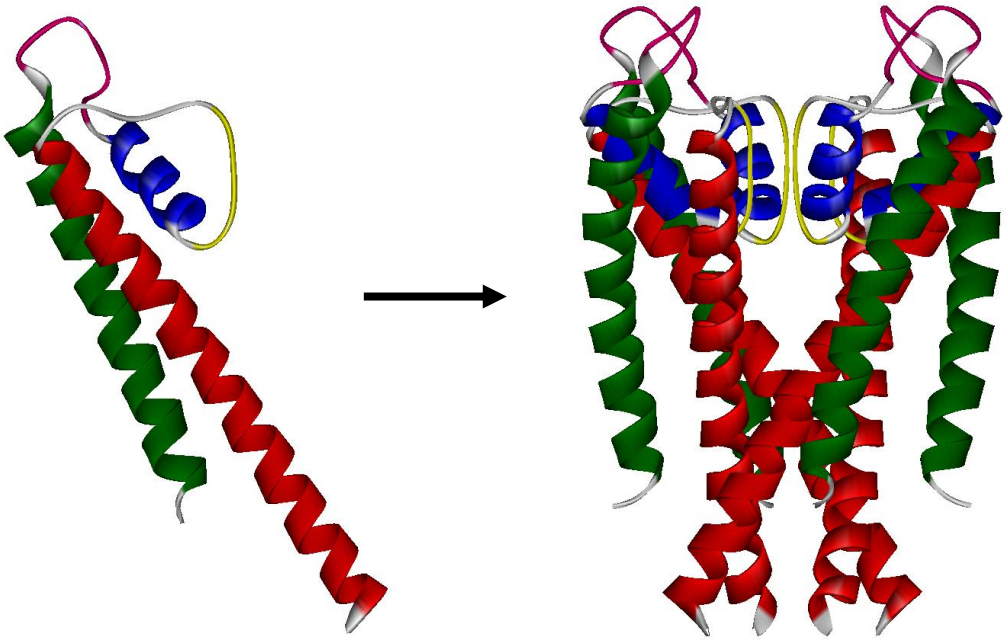

Figure 1.11 Crystal structure of KcsA. A single monomer (left) and the tetrameric structure (right) are shown. In green, outer transmembrane α-helix; in red, inner transmembrane α-helix; in blue, pore helix; in yellow, selectivity filter; in pink, turret. (PDB file 1K4C)

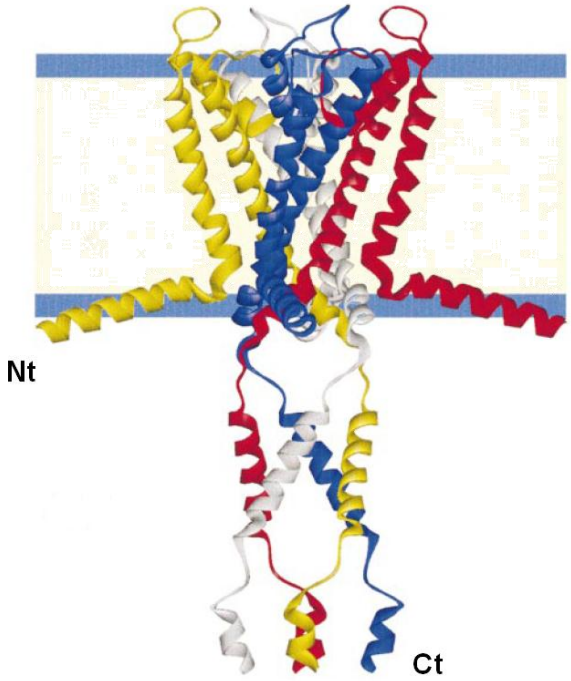

Figure 1.12 Molecular architecture of full length KcsA. Each subunit is represented with a different colour. The X-ray structure of KcsA obtained by Zhou *et al.* in 2001[53] only shows residues 22 to 124 (the first X-ray structure obtained by Doyle *et al.* in 1998[34] showed residues 23 to 119); ESR studies carried out by Cortes *et al.*[51] revealed the structure of the N (residues 5-24) and C (residues 121-160) termini; the N-terminus consists of an interfacial α-helix that does not interact with other parts of the protein, while the C-terminus expands into the cytoplasm where α-helices from the different subunits cross to form two right handed bundles. Taken from Cortes *et al.*, 2001[51].

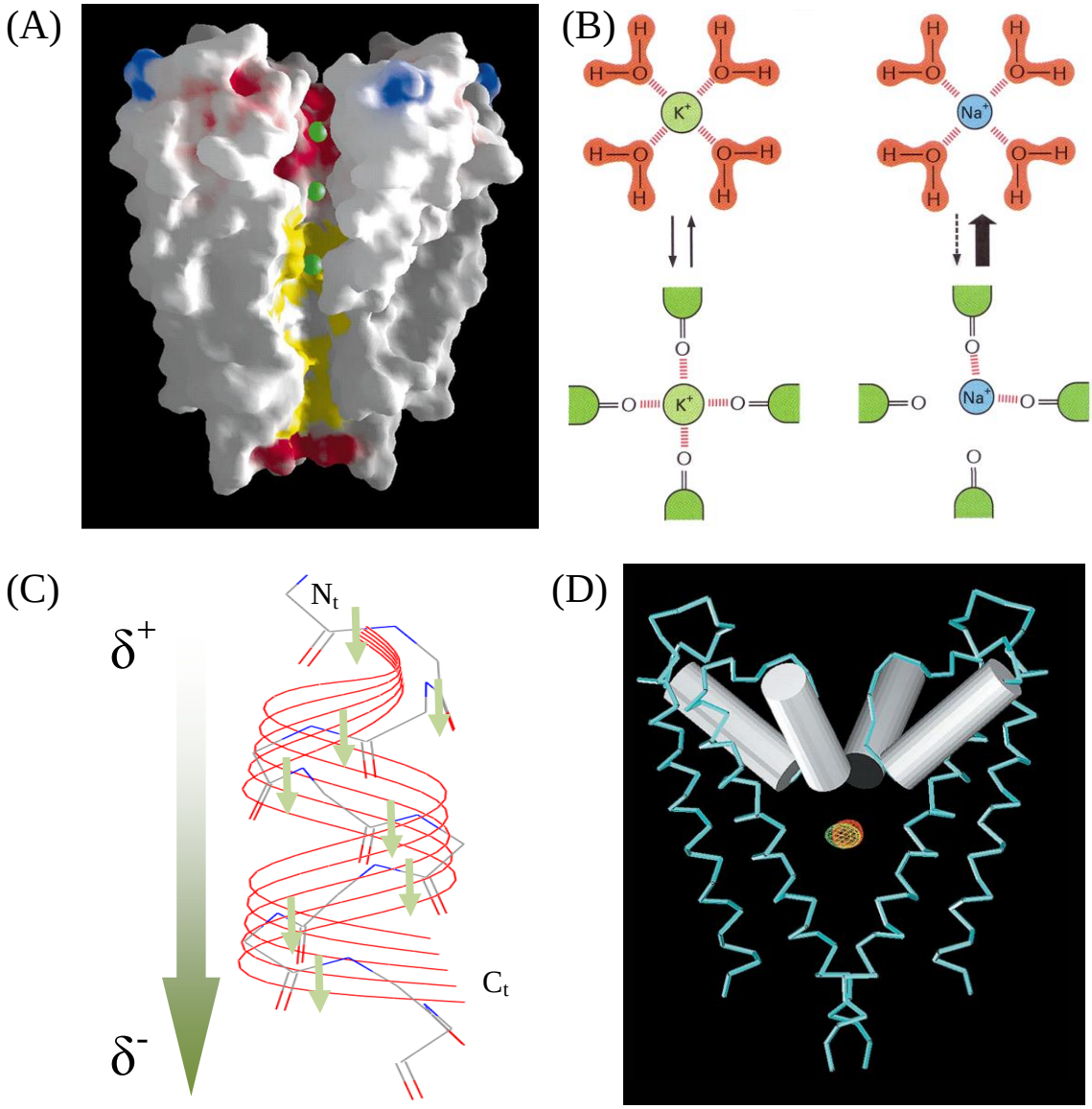

Figure 1.13 Potassium conductance. (A) Longitudinal section of the solvent accessible surface of KcsA, where the pore can be observed in the centre with K^+ ions shown as CPK spheres. The surface is coloured according to the charge potential: from blue in highly positively charged regions through white (neutral) to red in highly negatively charged regions. In yellow are hydrophobic regions from semi-conserved residues in the inner cavity. Taken from Doyle *et al.*, 1998[34]. (B) A schematic representation of the favourable interaction of the K^+ ion with the selectivity filter. Na^+ ions cannot interact optimally with the selectivity filter and therefore cannot enter the selectivity filter. Taken from Alberts, 2002[8]. (C) Polarization of the pore helix due to the addition of the dipole moments of the peptide bonds. The peptide backbone of the pore helix of KcsA is shown in line representation with N and O atoms in blue and red, respectively (PDB 1K4C). The small green arrows represent the dipole moments of each individual peptide bond. In (D) the four pore helices in KcsA point their C termini towards the central cavity, stabilizing the K^+ ions (or other cations) in the bilayer. (D) Crystal structure of KcsA with the electron density of a Rb^+ ion (red mesh) and a Na^+ ion (green mesh, where superposition with the red mesh gives yellow) in the central cavity. Only two monomers are shown (wire representation) illustrating the wide dimensions of the central cavity, which creates a polar environment for the cation in its centre; the four polarised pore helices pointing their partially negatively charged C-termini towards the centre of the cavity are shown in schematic representation. Taken from Roux *et al.*, 1999[54].

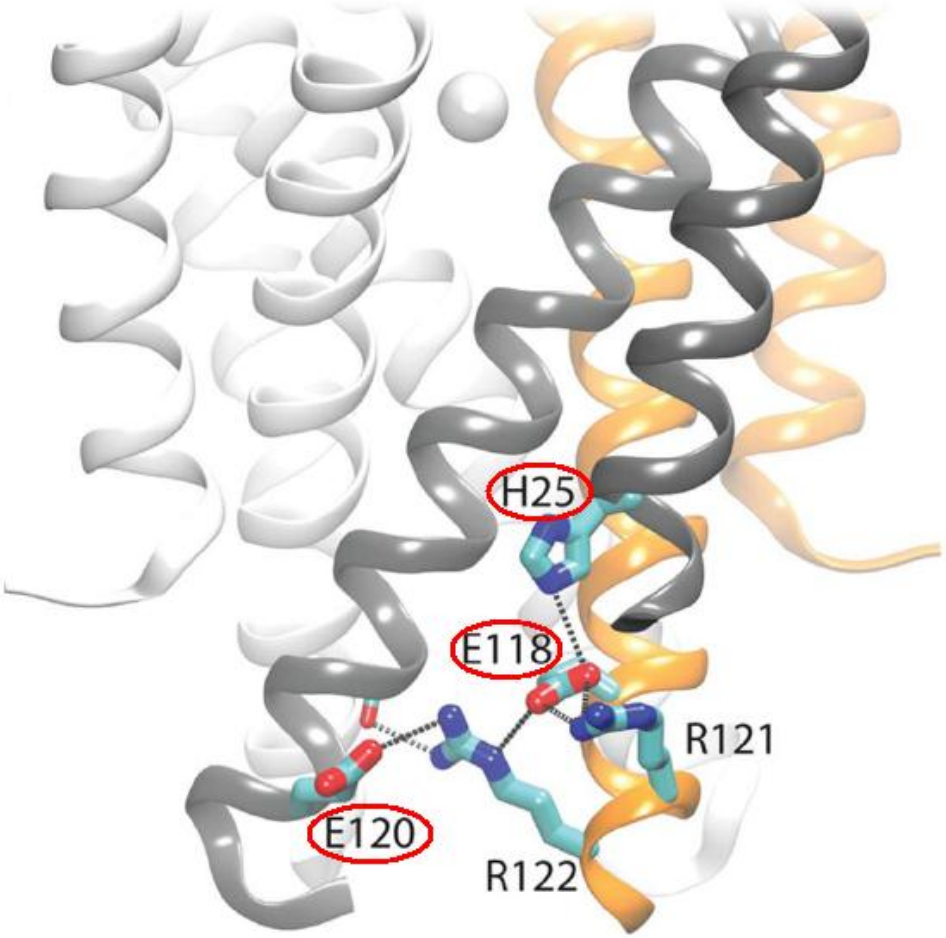

Figure 1.14 The pH sensor of KcsA, showing the proposed network interactions. The transmembrane helices of two adjacent subunits are highlighted in dark grey and orange, respectively. Residues that form part of the network are shown with carbon atoms in light blue, nitrogen atoms in dark blue, and oxygen atoms in red. Residues that sense the pH change are circled in red. Intersubunit interactions are proposed between E120, G116 (only backbone carbonyl shown) and R122; and between H25 and E118. Intrasubunit interactions are proposed between E118, R121 and R122. Taken from Thompson *et al.*, 2008[56].

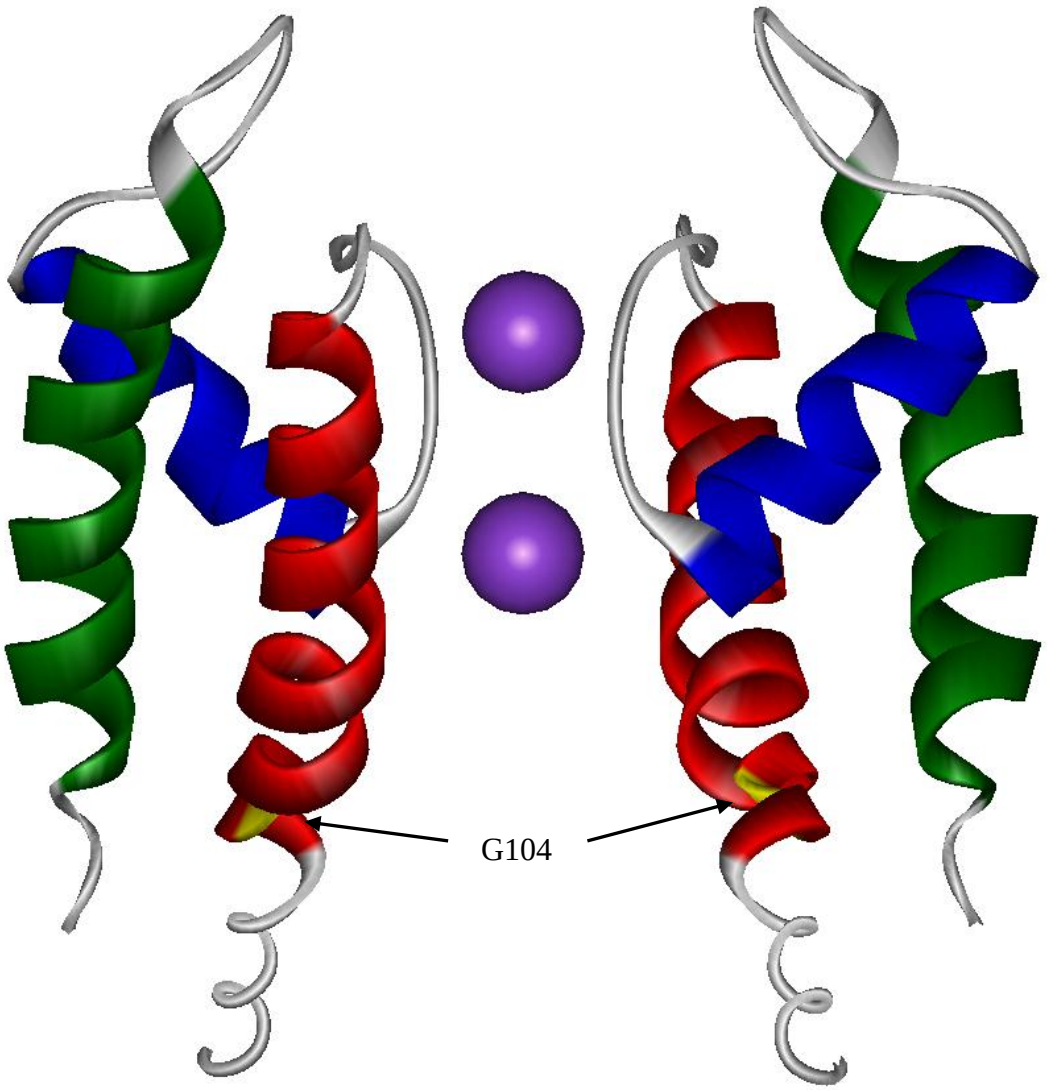

Figure 1.15 Open structure of KcsA. Only two monomers (solid ribbon representation) are shown for clarity. The outer transmembrane α-helices, inner transmembrane α-helices and pore helices are coloured in green, red and blue, respectively. Gly-104, which is just below the hinge point in the inner helices, is highlighted in yellow. Two potassium ions were also revealed in the structure, shown in purple CPK representation in a 1,4 configuration, which was suggested to represent the occupancy of ions in the inactivated selectivity filter state (C-type inactivated state); hence, the structure was proposed to represent the open-inactivated state of KcsA[50]. (PDB 3F5W)

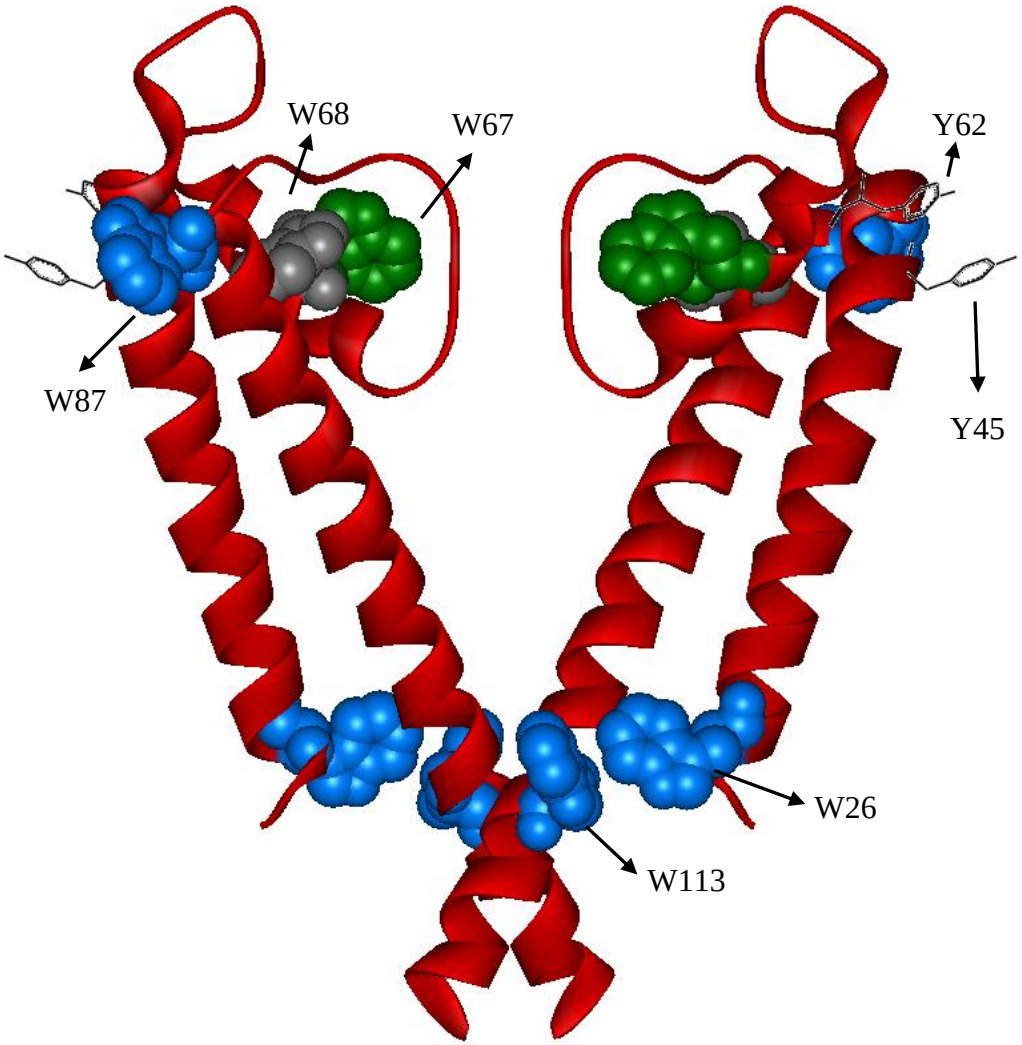

Figure 1.16 Girdles of aromatic residues in the crystal structure of KcsA. Only two monomers are shown for clarity with the aromatic residues at the lipid-water interface in blue, CPK (tryptophans) and black, stick (tyrosines) representations; W26, W113 are located on the intracellular side of the bilayer, and W87, Y45 and Y62 on the extracellular side. Because these tryptophan residues are facing the lipid bilayer they are quenched by brominated lipid molecules binding at the annular sites on KcsA. Tryptophan residues pointing towards the pore are also shown: W67 (which can be quenched by brominated lipid molecules binding at the non-annular sites, see Figure 1.18) in green, and W68 in grey. (PDB 1K4C)

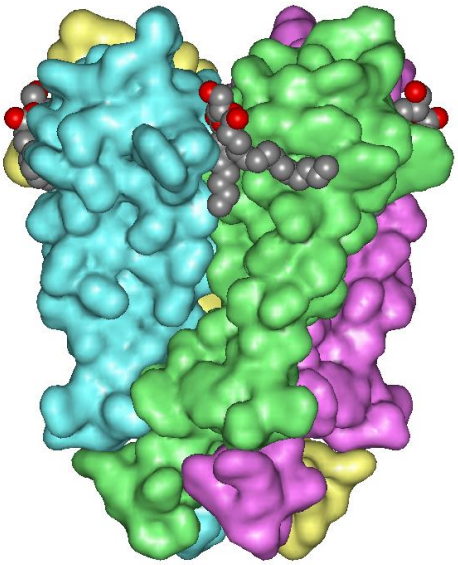

Figure 1.17 Surface plot of KcsA showing the non-annular lipid molecules. Each subunit is shown in a different colour. The lipid molecule is shown in CPK representation; one of the acyl chains (*sn*-1) is deeply bound in a groove between the subunits, while the other acyl chain (*sn*-2) seems to interact less intimately with the protein. (PDB 1K4C)

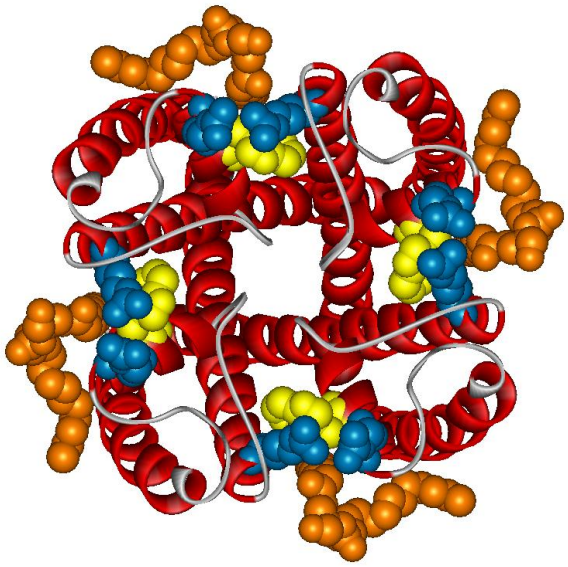

Figure 1.18 Extracellular side view of the crystal structure of KcsA. The non-annular lipid molecule and key residues are highlighted in CPK representation. In orange, the non-annular lipid molecule. In blue, R64 and R89, which are thought to contribute to binding of the anionic head group of the non-annular lipid molecule. In yellow, W67 whose fluorescence can only be quenched by the non-annular lipid thanks to its proximity to that lipid. (PDB 1K4C)

Chapter 2: General materials and methods.

2.1 Materials

2.2.1 Chemicals of general use

-Analytical reagent grade water (AR water) was obtained from Fisher Scientific.

-Organic solvents: methanol, chloroform, acetone and diethyl ether were obtained from Fisher Scientific.

-Salts, acids and basis were obtained from Fisher Scientific or Sigma. HEPES was obtained from Calbiochem at an ultrol grade to avoid the presence of any fluorescent impurities.

2.1.2 Bacteria growth

-Luria-Bertani Broth EZ Mix Powder (LB Broth) medium (Sigma): 20.6 g were dissolved in 1 l of distilled water. Media were autoclaved at 120 ˚C and 15 lbs of pressure for 20 min. Ampicillin was added to a final concentration of 0.1 mg/ml after cooling the media and immediately prior to be used.

-Luria-Bertani Broth-agar plates: 3 g of granulated agar (Sigma) were dissolved in 300 ml of LB Broth media, followed by autoclaving at 120 ˚C and 15 lbs of pressure for 20 min. After cooling below 50˚C ampicillin was added to a final concentration of 0.1 mg/ml and the plates were kept at 4 ˚C until use.

-Ampicillin (Formedium or Sigma): stock solutions were prepared dissolving the ampicillin in analytical range water to a concentration of 100 mg/ml, aliquoted and stored at -20˚C until use.

-Isopropyl-β,D-thiogalactoside (IPTG) (Melford): stock solutions were prepared at 1 M in AR water and stored at -20 ˚C until use.

-Vector: pQE-32 (Qiagen); a diagram of the vector and a description of its properties are shown in section 2.2.1.

-Host cells: *Escherichia coli* XL1Blue (Stratagene), containing the mutated lacIq gene for control of protein expression.

2.1.3 Protein purification

-PBS (pH 7.4)

Na_2HPO_4	10 mM
KH_2PO_4	1.8 mM
NaCl	140 mM
KCl	2.7 mM

-n-dodecyl-β-D-maltopyranoside (DDM) (Anatrace): anagrade, greater than 99 % pure by HPLC analysis.

-Ni-NTA agarose (Qiagen): composed of Ni^{2+} nitrilotriacetic acid coupled to Sepharose® CL-6B.

-Imidazole (Calbiochem): ultrol grade to avoid fluorescent impurities.

2.1.4 SDS-PAGE analysis

-Running buffer (pH 8.3): prepared 5x concentrated as follows

Tris	123.82 mM
Glycine	959.1 mM
SDS	0.5 %
Distilled water	

-Loading buffer: prepared as follows

Tris (pH 6.8, HCl)	62.5 mM
Glycerol	10 %
SDS	2 %
β-mercaptoethanol	715 mM
Bromophenol blue	0.05 %
AR water	

-Stain solution:

Coomassie brilliant blue	0.25 %
Acetic acid glacial	9 %
Methanol	45 %
Distilled water	46 %

-Destain solution:

Acetic acid glacial	7.5 %
Methanol	20 %
Distilled water	72.5 %

2.1.5 Reconstitution

-Lipids: 1,2-dioleoyl-*sn*-glycero-3-phosphocholine (DOPC), 1,2-dioleoyl-*sn*-glycero-3-phospho-(1'-*rac*-glycerol) (DOPG) and 1,2-dioleoyl-*sn*-glycero-3-phosphoethanolamine-N-(lissamine rhodamine B sulfonil) (rPE) were obtained from Avanti Polar Lipids; fatty acids and fatty acid analogues were obtained from Sigma. Brominated lipids where prepared as described below from the purchased non-brominated stocks. Lipids spin labelled at the C-14 position were synthesised by Brigitta Angerstein at the Max Plank Institute of Biophysical Chemistry (Göttingen, Germany), as described by Derek Marsh, 2008[24]. The chemical structures and names of the spin labelled lipids used are shown in Figure 2.2.

-Potassium cholate was prepared from cholic acid and potassium hydroxide as described in section 2.2.3

-Reconstitution buffer (pH 7.2):

HEPES	20 mM
KCl	100 mM
EGTA (Fluorescence only)	1 mM

2.2 Methods

2.2.1 KcsA expression

Vector containing the KcsA gene.

The pQE-32 expression plasmid (Figure 2.1, Qiagen) containing the KcsA gene[47] was kindly given by Professor Schrempf. The protein had been inserted between the restriction sites SphI and PstI. As a result, a short sequence of thirteen amino acids containing a six histidine tag is added to the N-terminus of the protein when it is expressed. Thus, the recombinant KcsA protein (Figure 2.1) is 173 amino acids long, with a theoretical molecular weight of 19,274.3 Da (molecular weight calculated with the ExPasy pI/MW tool available on the website http://us.expasy.org/tools/pi_tool.html).

KcsA mutant W67,68

The KcsA mutant with the lipid-exposed Trp residues (W26, W87 and W113) mutated to Leu was prepared by Dr. Phedra Marius[13] and will be referred here as mutant W67,68.

Storage

Escherichia coli XL1Blue cells containing the pQE-32 plasmid containing the KcsA gene (wild type or W67,68) were kept in glycerol stocks at -80 ˚C. The stocks were prepared in autoclaved cryotubes containing 0.5 ml glycerol; 1 ml aliquots from bacterial cultures grown over night were inoculated into the cryotubes and then kept at -80 ˚C.

Overnight cultures

The overnight cultures were grown from single colonies streaked on LB Broth-agar plates containing 0.1 mg/ml ampicillin. The cells were grown overnight in 200 ml of LB Broth-ampicillin (0.1 mg/ml), at 37 ˚C, shaking at 200 rpm.

Expression

For expression, overnight cultures were prepared from glycerol stocks as described above. Conical flasks with 1 l of LB Broth-ampicillin (0.1 mg/ml) were inoculated with 10 ml of overnight culture. The cultures were then incubated at 37 ˚C, shaking at 220 rpm until an optical density of 0.6 at 600 nm was reached. Protein expression was then induced adding isopropyl-β,D-thiogalactoside (IPTG) to a final concentration of 0.5 mM; the cells were then grown for another 2 h under the same conditions to allow protein synthesis, and finally cell pellets were harvested by centrifugation at 8,983 g (6,000 rpm, Avanti J20 series centrifuge), for 20 min. Cell pellets were immediately frozen at -20 ˚C and stored until use.

2.2.2 KcsA purification

From 12 litres of culture of either wild type (WT) or mutated KcsA, approximately 15 to 20 g of wet cell pellet was obtained and used for purification. The cell pellet was resuspended in approximately 60 ml of PBS and the cells were lysed by sonication (XL-2020 Misonix sonicator) with 18 cycles of 20 s on pulses and 15 s off pulses (a total of 6 min of sonication). The membrane fraction was isolated from the lysed cells by ultracentrifugation (Beckman L7-65 ultracentrifuge) at 100,000 g for 40 mins at 4 ˚C. The membrane pellet was then homogenised in 150 ml of PBS containing 15 mM n-dodecyl-β-D-maltopyranoside (DDM) and left to solubilise the membrane proteins by stirring at room temperature for 1-2 h. The sample was then spun at 8,000 g (Beckman J2-21 centrifuge) for 20 min at 4 ˚C to eliminate the insoluble fraction; imidazole was then added to the supernatant up to a concentration 20 mM to avoid non specific binding of proteins to the Ni-NTA resin when added. Four millilitres of Ni-NTA resin were first washed twice with 20 ml PBS and then added to the sample to bind the His tagged KcsA, stirring at 4 ˚C for at least 1 h. After binding, the resin was loaded into a column and washed with 15 ml of PBS containing 1 mM DDM and 20 mM imidazole to eliminate non specifically bound proteins. Finally, KcsA was eluted with 7 ml of PBS containing 1 mM DDM and 300 mM imidazole (carefully corrected to pH 7.4), collecting 0.5 to 1.5 ml fractions.

SDS PAGE analysis

The collected fractions from the purification process were analysed by SDS-PAGE to confirm the size and purity of the protein. The gels were prepared as follows:

15% acrylamide resolving gel:

AR water	1,565 µl
Tris 1.5 M pH 8.8	850 µl
Protogel	2,475 µl
SDS 10%	50 µl
Amonium persulfate (APS) 25%	60 µl
TEMED	2.5 µl

4.5% acrylamide stacking gel

AR water	850 µl
Tris 3.6 M pH 9.3	800 µl
Protogel	300 µl
SDS 10%	20 µl
Amonium persulfate 25%	10 µl
TEMED	2 µl

For the analysis, 2.5 µl of each collected fraction were mixed with 5 µl of loading buffer and loaded onto the gel without boiling the samples. Electrophoresis was run at a constant voltage of 120 V (and a current set at 65 mA) for 1 h. The gels were then stained with Coomassie brilliant blue, followed by destaining several times with destaining solution until the protein bands were revealed.

Determination of the protein concentration

The protein concentration was determined by measuring the absorbance at 280 nm and applying the Beer-Lambert Law:

$$A = \varepsilon \cdot l \cdot c$$

where A is absorbance, ε is the molar extinction coefficient of the absorber ($M^{-1} \cdot cm^{-1}$), l is the path length (cm) and *c* is the concentration of the absorber (M). The molar extinction coefficient of WT and mutated KcsA were calculated considering that at 280 nm:

Tryptophan $\varepsilon = 5{,}690\ M^{-1}\cdot cm^{-1}$

Tyrosine $\varepsilon = 1{,}280\ M^{-1}\cdot cm^{-1}$

Cystine (disulfide bond) $\varepsilon = 120\ M^{-1}\cdot cm^{-1}$

Therefore, given the number of Trp and Tyr residues present in a wild type or mutated KcsA monomer, the molar extinction coefficients were calculated as follows: ε = (number of Trp) x 5690 + (number of Tyr) x 1280 + (number of cystines) x 120, giving:

WT KcsA (monomer) $\varepsilon = 34{,}850\ M^{-1}\cdot cm^{-1}$

KcsA mutant W67,68 (monomer) $\varepsilon = 17{,}780\ M^{-1}\cdot cm^{-1}$

First, the purity and approximate concentrations of the eluted fractions were checked by SDS-PAGE. Fractions containing a high concentration of pure KcsA were pooled. The exact concentration was then determined by absorbance, diluting 50 to 150 µl of sample in 800 µl of a 1 % SDS solution, and adding A. R. water up to 1 ml. The yield of purified KcsA was typically 0.6-1.5 mg per litre of culture (see Appendix 1). The purified samples were aliquoted, snap frozen in liquid N_2 and kept at -80˚C, typically at 4-9 mg/ml.

2.2.3 Reconstitution for fluorescence and ESR studies

Lipid preparation

Solutions of non-spin labelled lipids were prepared by dissolving the lipids in chloroform to a concentration of 10 to 40 mg/ml. Spin labelled lipids were kept in ethanol or methanol at a concentration of 1 mg/ml. The working solutions were kept at -20 ˚C to avoid oxidation and evaporation of the solvent.

Lipid bromination

Brominated lipids were prepared from the purchased stocks by adding small aliquots of bromine to the resuspended lipid in chloroform (kept on ice) until a very pale yellow colour was obtained. The sample was then left on ice for 30 min, and free bromine was finally eliminated by evaporation of the solvent first under a stream of

N_2 and then by application of vacuum. The brominated lipid was then resuspended in chloroform to a concentration of 10 to 40 mg/ml and kept -20 ˚C protected from light. The respective brominated phospholipids will be abbreviated as follows: BrPC for di(9,10-dibromostearoyl) phosphatidylcholine and BrPG for di(9,10-dibromostearoyl) phosphatidylglycerol.

Preparation of potassium cholate

For preparation of potassium cholate 48.9 mmols of cholic acid were dissolved in 250 ml of methanol by warming and stirring. An equimolar amount of potassium hydroxide was slowly added and dissolved. Heating was continued to evaporate as much methanol as possible without precipitation of the potassium cholate produced. Excess diethyl ether (2-3 litres) was then added to precipitate the potassium cholate. The potassium cholate was collected by filtration and dried for several days, protected from light until the smell of diethyl ether disappeared.

Reconstitution

The required amount of lipid was dried from chloroform solution onto the side of a glass vial under a stream of N_2 and then in a vacuum desiccator. At least 500 µl of 20 mM HEPES buffer containing 100 mM KCl, and 20 – 75 mM potassium cholate [as required to maintain potassium cholate above its critical micelle concentration (12.5 mM) after later addition of the protein], pH 7.2 was then added. The samples were then sealed under N_2 to protect them from oxidation, heated to 60 ˚C for 2-6 min, vortexed and sonicated for at least 6 min in a bath sonicator until optically clear. If needed, more buffer was added after sonication to give the required concentration of lipid (sonication is normally optimum in smaller volumes, here 20 ml glass vials containing 0.5 to 1.5 ml were used). Then, 110 - 120 µl aliquots were taken from the vial and added to Eppedorf tubes to which the protein (solubilised in 1 mM DDM) was then added to give the required molar ratio of lipid:KcsA tetramer.

The samples for fluorescence were incubated at a final potassium cholate concentration of 20 mM at room temperature for at least 15 min and then reconstitution of the protein into lipid bilayers was achieved by dilution of 50 µl of the detergent-lipid-protein mixture into 2.45 ml of 20 mM HEPES, pH 7.2, containing 100 mM KCl, in order to decrease the concentration of cholate below its critical

micelle concentration. Lipid samples were also prepared in the absence of protein to be used as blanks for light scattering correction.

For the fluorescence experiments with the fatty acid, in most cases the fatty acid was dried together with the phospholipid at the start of the process as described above. However, in some cases, for convenience, the fatty acid in a small volume of methanol (always less than 4 % of the final volume) was added directly into the fluorescence cuvette after the membrane had been reconstituted by dilution. This allowed simple titration of fatty acid into the sample: to minimise accumulated error during the titration process, two separate samples were used to generate one complete titration curve.

The samples for ESR were incubated at a final potassium cholate concentration of 13.5 mM (just above its critical micelle concentration, 12.5 mM) at room temperature for at least 15 min and reconstitution was achieved by dilution of the entire detergent-lipid-protein sample, in this case, into a volume of 20 mM HEPES, 100 mM KCl (pH 7.2) enough to decrease the concentration of potassium cholate to 1.47 mM. [Note that this also resulted in dilution of DDM below its CMC (ca. 0.12 mM) which is important because the large size of its micelles could impede its adequate elimination by dialysis, as follows]. The samples were then dialysed against 100x their volume (at least) of 20 mM HEPES (pH 7.2), containing the necessary amount of KCl to reach a concentration of 100 mM after processing the samples as described below. Dialysis was carried out at 4 ˚C for at least 24 h, changing the dialysis buffer three times. Once dialysed, the samples were aliquoted as required, freeze-dried, sealed under a N_2 atmosphere, and kept at 4 ˚C. Before use, the samples, typically containing 0.5 mg of lipid and the corresponding amount of protein, were resuspended in 1 ml water (so that the concentration of HEPES and KCl were 20 mM and 100 mM respectively, pH 7.2) and centrifuged in a standard bench top centrifuge at 14,000 r.p.m for 20 min (samples with a high protein content would pellet in less than 20 min due to their higher density, but the samples with a low protein content required always the full 20 min centrifugation). The membrane pellets were resuspended in 100 µl of the reconstitution buffer (20 mM HEPES, 100 mM KCl, pH 7.2) and the spin labelled lipid was added directly in a small volume (1-5 µl) of ethanol, followed by vigorous vortexing. Spin labelled phospholipids were added to

give a final concentration of 1 mol % with respect to the total lipid in the sample, and the samples were incubated overnight to allow fusion of the small spin labelled phospholipid vesicles with the sample membranes. The next day samples were washed twice by centrifugation in a standard bench top centrifuge at 14,000 r.p.m. for 20 min followed by resuspension in 100 μl of the same buffer (this is to eliminate small vesicles of spin labelled phospholipid not incorporated into the sample membranes). For experiments with spin labelled stearic acid, the spin labelled stearic acid was added to give a final concentration of only 0.5 % mol with respect to the total lipid in the sample, and no washing steps were required (this is because the stearic acid partitions into the bilayers). All samples with the spin labelled lipids incorporated were finally spun again and the membrane pellets were loaded into glass capillaries. The capillaries were also spun and most of the supernatant was removed, leaving approximately 2 mm of the latter to prevent dehydration of the samples; the capillaries were then flamed-sealed. All samples contained a fixed amount of lipid (DOPC or DOPG): 636 nmol, equivalent to ca. 0.5 g of lipid, to ensure a strong ESR signal after addition of 1 mol % of spin labelled phospholipid or 0.5 % spin labelled stearic acid, with varying amounts of KcsA to achieve the desired lipid:channel molar ratio.

Fluorescence measurements

Fluorescence was recorded on an SLM 8100C spectrofluorometer (Urbana, IL) at 25 ˚C with excitation at 290 nm, fluorescence emission intensities being read at 333 nm. Fluorescence was corrected for light scatter by subtraction of a blank containing only the lipid in buffer.

ESR measurements

ESR spectra were recorded on a continuous-wave (9GHz) ESR spectrometer using the following settings: scan range, 100 G; time of scan, 2 min; modulation amplitude, 1.25 G; incident power, 5 mW; time constant, 250 ms. The spectra were averaged from 4 to 20 measures (depending on the quality of the signal) recorded at 15 ˚C, 20 ˚C, 25 ˚C, 30 ˚C and 35 ˚C. The flame-sealed capillaries containing the samples were placed in a standard 4 mm quartz sample tube containing silicone oil for thermal stability.

2.2.4 ESR spectra processing

Analogue recorded spectra were digitised to give 1000 points where each point along the x-axis was equivalent to an increase in the magnetic field of 0.1 G; the graphs were saved as .txt files.

Some of the recorded ESR spectra revealed a small but significant background signal attributable to the glass capillaries and quartz cooling system. This background signal was revealed on calculation of the first integral of the spectra (ESR spectra are first-derivative displays of the energy absorption spectra), where the absorption on the high magnetic field side of the spectra does not return to zero, due to this background noise (Figure 2.3, red). A standard background spectrum was therefore subtracted on a computer from the experimental spectra by an iterative process so that the first integral began and ended at zero (Figure 2.3, blue). Before subtraction all spectra were aligned as described below to ensure comparable correction for all spectra.

2.2.5 ESR spectral comparisons

To allow proper comparison of the different ESR spectra, the spectra were aligned on the basis of the point at which the high-field side of the central peak crossed the base line (Figure 2.4, vertical red dotted line). Spectral simulations have suggested that this point only shifts by ca. 0.6 G from mobile to restricted components[86]. The resulting shift among different composite spectra will therefore be very similar, and use of this crossing point to align composite spectra is a good way to compare the different spectra.

The amount of microwave energy absorbed by the different samples will vary from one sample to another due to small differences among the samples, such as in the concentration of spin label, so that the signal intensity measured will vary from one sample to another. ESR spectra are recorded as the first derivative of the absorption spectra and so, in order to normalise the amount of absorbed energy in different samples, the areas of the absorption spectra for the different samples have to be made equal. After alignment and background correction (see above), the areas under the absorption spectra (i.e. the second integrals of each ESR spectra) were determined with Microsoft Excel and scaling factors were then calculated to make the

areas equal. The ESR spectra were then normalised by multiplying each point in each ESR spectrum by the respective scaling factor: Figure 2.5 illustrates this with an example of two different spectra.

2.2.6 Deconvolution of the ESR spectra

The composite spectra obtained in the ESR experiments arise from the combination of two different components (Figure 1.9). One component comes from a population of spin labelled lipid in the membrane, not in contact with the channel, where the acyl chains have fast motion (the fluid or mobile component). The other component comes from a population of spin labelled lipid in contact with the channel, where the acyl chains have a slower motion due to the interactions established with the protein (the restricted or immobile component).

To determine the proportions of mobile and immobile component in a composite spectrum it is necessary to find single component spectra that are similar to those forming the composite spectrum. These single component spectra are normally obtained from libraries of spin labelled lipid spectra recorded under conditions that are likely to generate single spectra similar to those in the composite spectrum. Here, the mobile components for deconvolution of all ESR spectra were chosen from a library of 14-PCSL in DOPC recorded at 1 ˚C intervals, from 0 ˚C to 40 ˚C. The immobile components were chosen from two different libraries. For samples containing spin labelled phospholipid, the immobile components were chosen from a library of 14-PCSL in sonicated, small, unilamellar vesicles of dimyristoylphosphatidylcholine (DMPC) recorded at 1 ˚C intervals, from 0 ˚C to 40 ˚C. For samples containing spin labelled fatty acid (14-SASL), immobile components were chosen from a library of 14-SASL bound to bovine serum albumin (BSA) recorded at 3 or 4 ˚C intervals, from 1 ˚C to 37 ˚C.

To estimate the relative proportions of mobile and restricted components in the composite spectra, all the spectra were first aligned (Figure 2.4) and corrected for background signal (Figure 2.3), as described above. As mentioned in the previous section, spectral simulations have suggested that the alignment point shifts by ca. 0.6 G from mobile to restricted components[86], and so a facility to introduce a relative shift

of the spectra during the analysis in the computer software was introduced. For each experimental spectrum a mobile and a restricted component spectra chosen from the libraries were normalised to equal areas and combined to fit the experimental spectrum with the help of computer software; the procedure was then repeated for other pairs of single component spectra, and the pair giving the best fit was then chosen[86]. The central peak was found to make a relatively large contribution to the goodness of fit because the peak is sharp so that small differences in peak width and peak position became important. The best fit was therefore determined for the low field region of the spectra, as this is the region where the two components differ the most, allowing a better quantification of each component (Figure 2.4), whilst checking that the fitted composite spectrum reproduced correctly all the other key features of the experimental spectrum. Figure 2.4 shows an example of a spectrum analysed this way, with the experimental spectrum in black and the resulting fitted spectrum in blue. In addition, to give an indication of the goodness of the fit, the line resulting from the subtraction of the fitted spectrum from the experimental spectrum is shown in green, which for a 'perfect' fit would be zero; also a 'noise' value is calculated corresponding to the sum of the absolute values of the differences between the experimental and calculated spectra over the chosen region. Small differences between the fitted and the experimental spectra are normally seen in the region of steep slope in the experimental spectrum due to small differences in peak position and width.

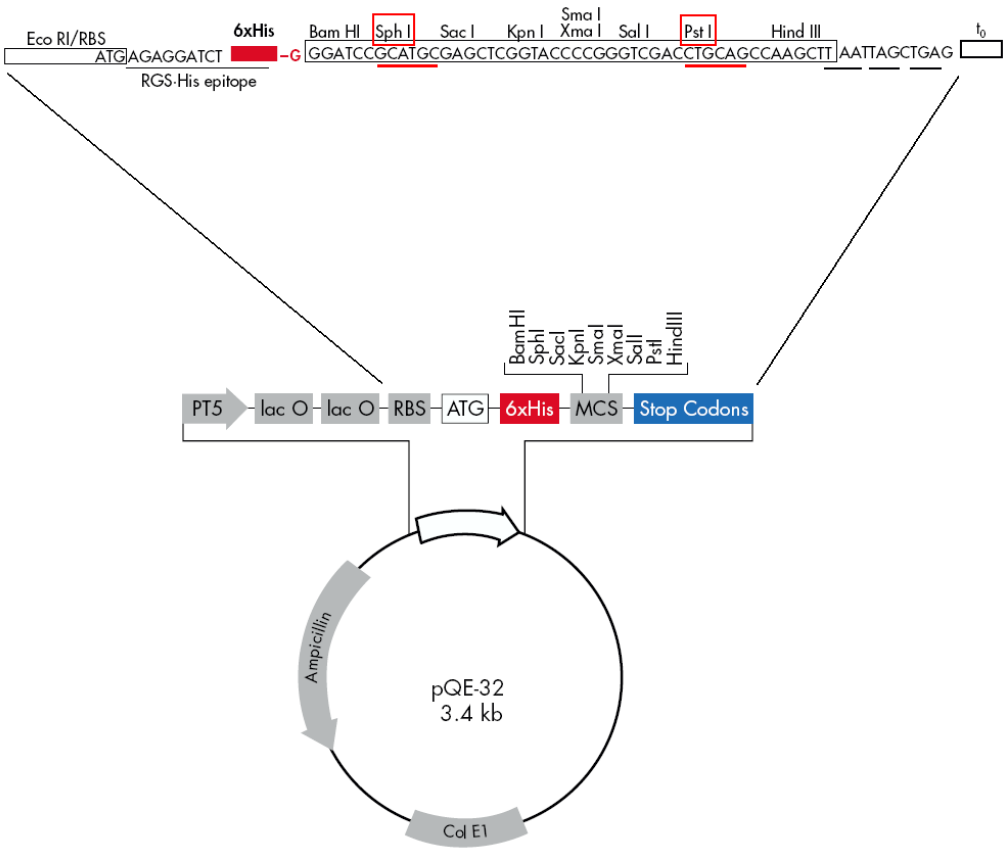

MRGSHHHHHH GIRMPPMLSG LLARLVKLLL GRHGSALHWR AAGAATVLLV
IVLLAGSYLA VLAERGAPGA QLITYPRALW WSVETATTVG YGDLYPVTLW
GRLVAVVVMV AGITSFGLVT AALATWFVGR EQERRGHFVR HSEKAAEEAY
TRTTRALHER FDRLERMLDD NRR

Figure 2.1 Plasmid pQE-32 from Qiagen and sequence of the recombinant KcsA protein. The vector confers ampicillin resistance for selection. Protein expression is inhibited by binding of the lac repressor protein (coded by the mutated laqIq gene in the genome of the *E .coli* XL1Blue cells) to the lacO sequences. Expression is only induced with the addition of IPTG, which binds and inhibits the repressor protein. The KcsA gene is inserted between restriction sites SphI and PstI (marked in red). As a result the recombinant protein has an extra 13 amino acids at the N-terminus, including six consecutive histidine residues for purification. In green is highlighted the original starting methionine of the KcsA sequence. In red are highlighted the five tryptophan residues.

14-PASL	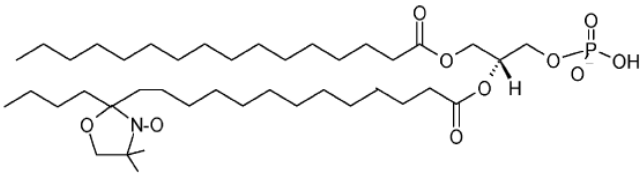
14-PCSL	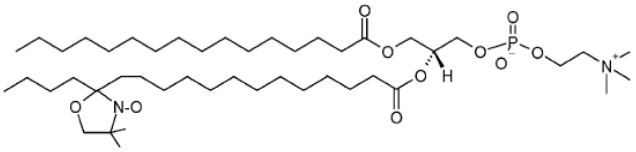
14-PESL	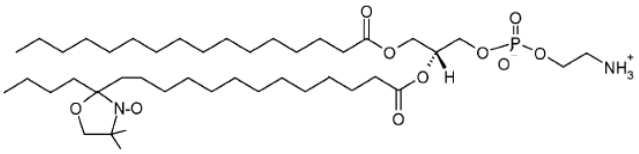
14-PGSL	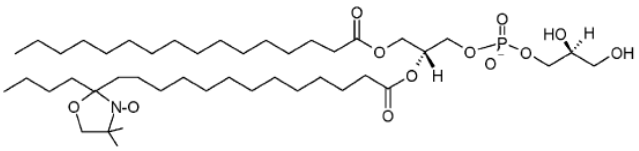
14-PSSL	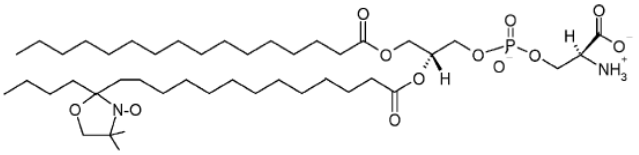
14-SASL	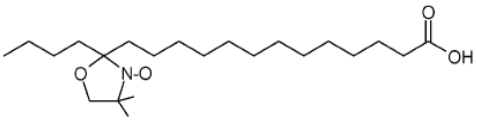

Figure 2.2 Chemical structures of the spin labelled lipids used for the ESR studies. A spin-label nitroxyl ring (DOXYL: 4,4-dimethyloxazolidine-*N*-oxyl) is rigidly attached to the C14-position of the lipids. Lipids labelled at the C14-position are ideal for studying lipid-protein interactions because the mobility of the nitroxyl group in this region allows detection of differences in the ESR spectra when the lipid is immobilised due to interaction with the protein, as opposed to when it is highly mobile when it is not interacting with the protein. 14-SASL is 14-(4,4-dimethyloxazolidinyl-*N*-oxyl)stearic acid; 14-PASL, -PCSL, -PESL, -PGSL and –PSSL are 1-palmityl-2-[14-(4,4-dimethyloxazolidinyl-*N*-oxyl)stearoyl]-*sn*-glycero-3-phosphate, -phosphocholine, -phosphoethanolamine, -phophoglycerol and –phosphoserine, respectively.

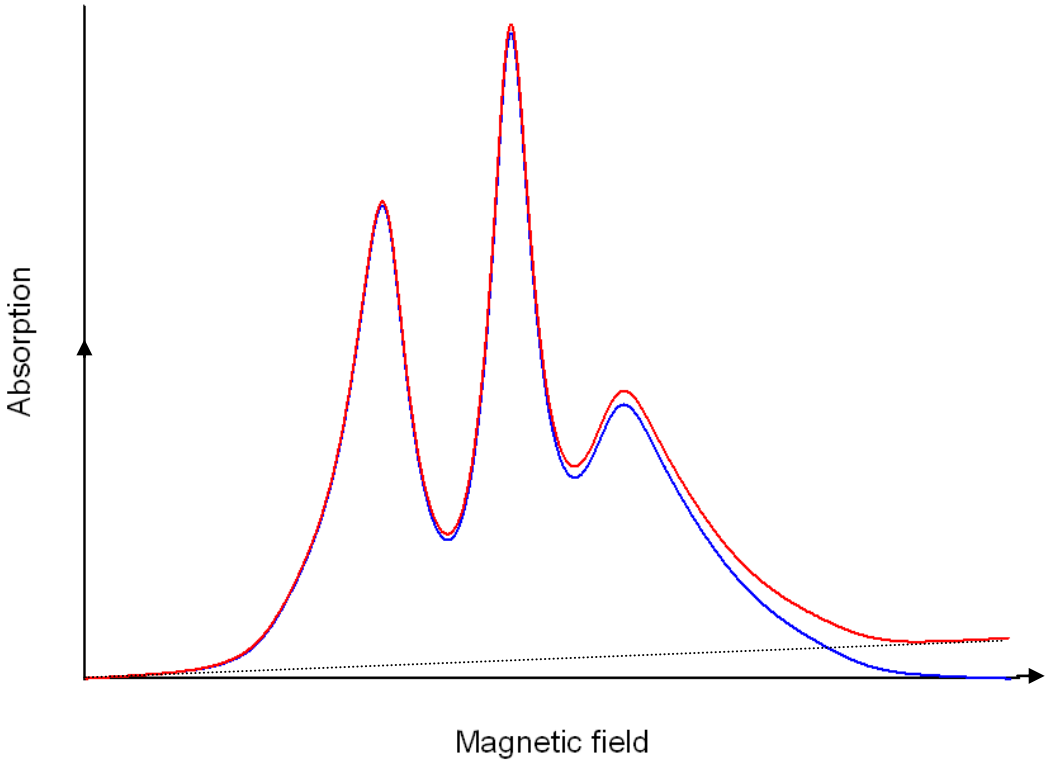

Figure 2.3 ESR background signal. Shown are an ESR absorption spectrum before (red) and after (blue) background signal subtraction. Before the correction, the background signal increases slowly and linearly (dotted line), so that in the high magnetic field region the spectrum does not return to zero. After subtraction of the background signal (blue) absorption comes back to zero at high magnetic field. The opposite can happen (not shown): the ESR measurement can start with a background noise that decreases slowly and linearly as the scanning progresses. In that case, the intensity becomes negative at high magnetic field, and correction is carried out by subtraction of a background signal of negative values. The noise in this example has been exaggerated for illustrative purposes and generally the background noise was much smaller.

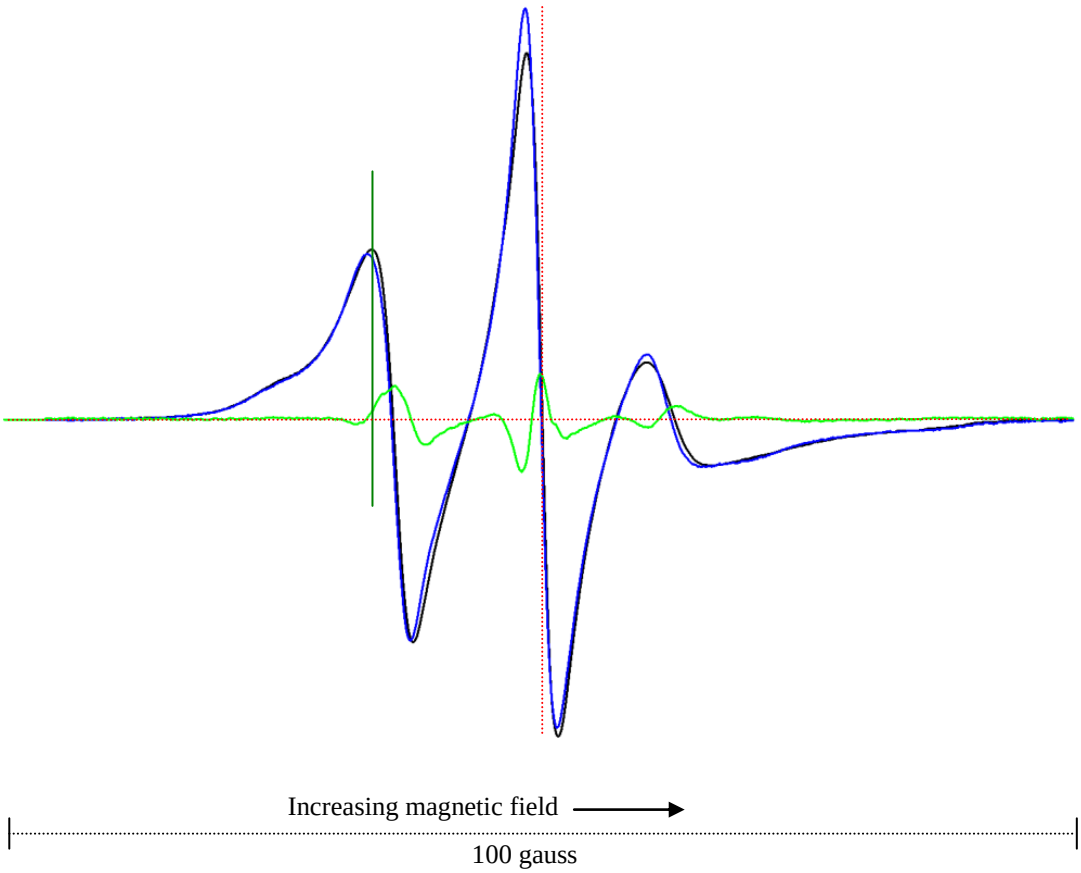

Figure 2.4 ESR spectral analysis. Spectra were analysed by combining single component spectra chosen from the corresponding libraries. The chosen spectra were fitted to the experimental spectrum in the region of the low field peaks (the region to the left of the dark green line). In black is the experimental spectrum; in blue is the resulting fitted spectrum; in light green is the result of the subtraction of the fitted spectrum from the experimental spectrum. The vertical red line shows the point to which all the spectra were initially aligned, as explained in the text; during fitting of the spectra, the single spectra where allowed to shift slightly with respect to the composite spectrum to give the best fit. The example shows the spectrum of 14-PCSL in bilayers containing DOPC and KcsA at a lipid:channel molar ratio of 60:1, measured at 25 ˚C.

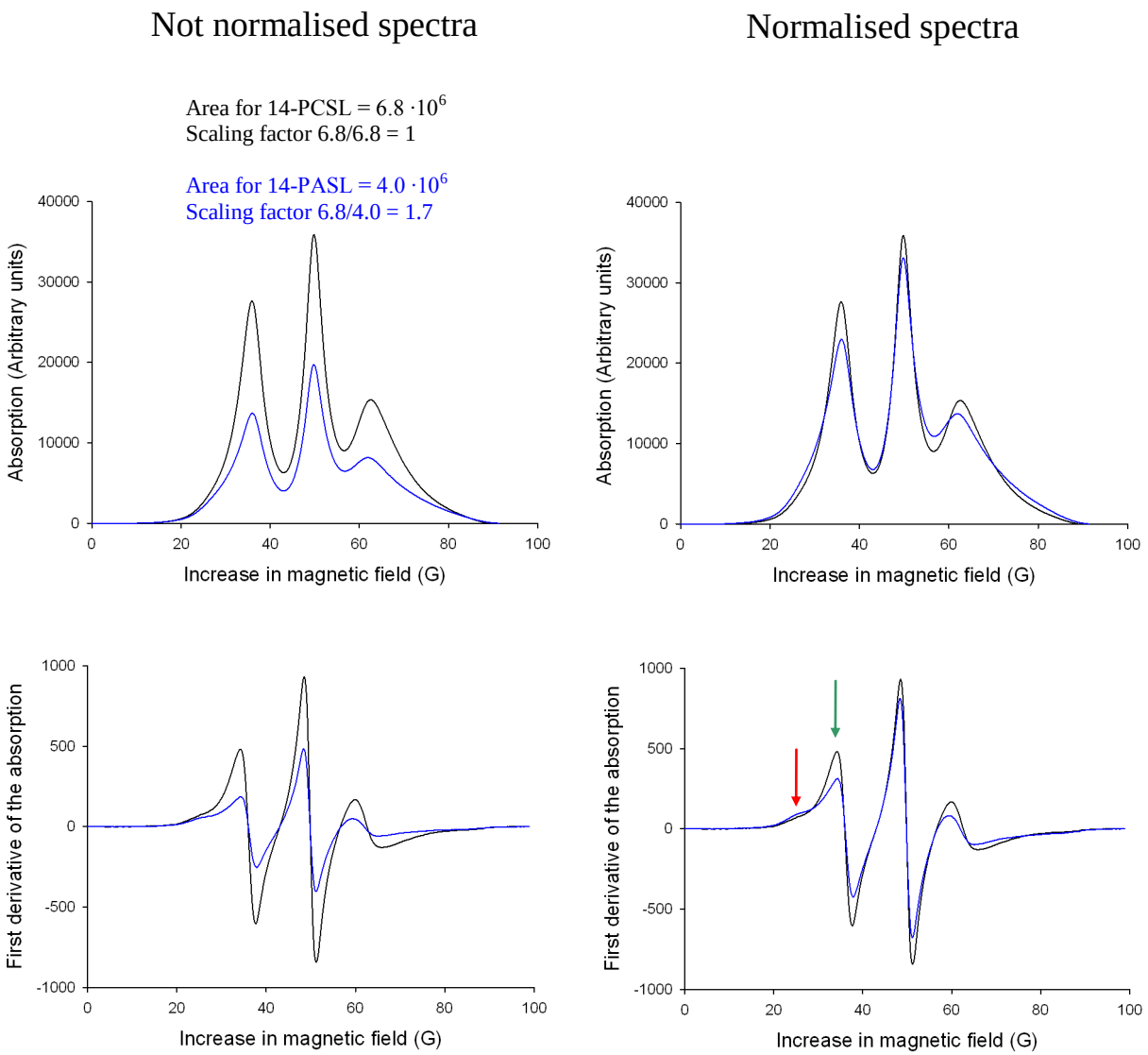

Figure 2.5 Normalisation of ESR spectra. The ESR spectra of 14-PCSL (black) and 14-PASL (blue) in DOPC bilayers with KcsA at a lipid to channel molar ratio of 60:1 measured at 30 ˚C are compared before (left) and after (right) being normalised to equal areas. In the spectra before normalisation it can be seen that the ESR spectra signal intensity (first derivative) is much weaker for 14-PASL than for 14-PCSL; the same is observed when the spectra are integrated to obtain the absorption spectra, the area under the 14-PCSL absorption spectrum being 1.7 times larger than the area under the 14-PASL absorption spectrum. To correct this difference each point on the ESR spectrum (first derivative) of 14-PASL was multiplied by 1.7 (scaling factor). The normalised spectra of the two samples can now be easily compared, the 14-PASL sample having a larger immobile component (red arrow) and a smaller immobile component (green arrow) than the 14-PCSL sample.

*Note: the 14-PASL spectrum was here intentionally changed to show a weaker signal to better illustrate the normalisation procedure, as the difference in ESR signal among the different samples was generally rather smaller.

Chapter 3: Effect of the annular shell of lipids on the aggregation of KcsA.

3.1 Introduction

The first layer of lipid molecules surrounding the transmembrane region of a membrane protein are referred to as annular or boundary lipids[4,22]. These lipids interact directly with a membrane protein, and are essential in maintaining the structure and function of the protein. Annular lipids act as a solvent keeping membrane proteins embedded in the lipid bilayer and maintaining any oligomeric state of the protein. The number of annular lipid molecules around a membrane protein depends on the size of its transmembrane region and on its oligomeric state; the lipid-protein stoichiometry provides information about these characteristics of a membrane protein in a lipid bilayer[87,88].

The annular lipids provide an effective seal at the lipid-protein interface to maintain the permeability barrier properties of the membrane. The atomic structures revealed by electron and x-ray crystallography of numerous membrane proteins show that the surface of the transmembrane region of a membrane protein is rough, containing many shallow grooves and protuberances. The annular lipid molecules adapt their conformations to interact with the rough surface of the protein and show reduced motional fluctuations, efficiently solvating the protein and sealing the lipid-protein interface[4,22,89] (Figure 1.7A). This reduction in the motional fluctuations of the lipid molecules interacting with membrane proteins can be detected by ESR with the use of spin labelled lipids[24,25]. The basic principles of the study of lipid-protein interactions with ESR and spin labelled lipids were described in Chapter 1.

The potassium channel KcsA is known to be active as an isolated tetramer in the lipid bilayer, but several studies have reported aggregation of KcsA channels[78-80]. In this chapter, the influence of the annular lipids on channel aggregation is explored. ESR is used to determine the number of phospholipid molecules necessary to solvate KcsA when the channel is reconstituted into bilayers at different molar ratios of lipid to channel. The solvation state is compared in membranes of the zwitterionic

phospholipid phosphatidylcholine (PC) and in membranes of the anionic phosphatidylglycerol (PG), which has been shown to have a greater affinity for KcsA than PC. Fluorescence quenching of KcsA with the use of brominated phospholipids is also used to confirm the information obtained with ESR. Basic principles of fluorescence quenching of Trp with brominated lipid molecules are described in Chapter 1.

3.2 Methods

Chapter 2 includes all the materials and describes all general methods used in this chapter (lipid handling, KcsA expression, purification, and reconstitution into lipid bilayers for both ESR and fluorescence studies).

3.2.1 Samples for determination of phospholipid-KcsA stoichiometry

The detailed protocol for reconstitution of the samples can be found in Chapter 2, Section 2.2.3. For the analysis of lipid-channel stoichiometry three sets of samples were prepared. Two of these sets had KcsA reconstituted in dioleoylphosphatidylcholine (DOPC); the other set had KcsA reconstituted in dioleoylphosphatidylglycerol (DOPG). Each set consisted of duplicate samples of KcsA reconstituted at lipid:channel molar ratios ranging from 30:1 to 100:1. The three sets were prepared on different days. For the DOPC sets, one of the duplicates was labelled with spin labelled phospholipid for the study discussed in this chapter, while the other was labelled with spin labelled stearic acid, as discussed in Chapter 5, Section 5.2.4. This allows direct comparison of the samples labelled with spin labelled phosphatidylcholine (14-PCSL) and the corresponding samples labelled with spin labelled stearic acid (14-SASL), as each originated from the same preparation, only differing in the spin labelled lipid incorporated.

3.2.2 Sucrose density gradient analysis

Discontinuous sucrose density gradients were used to determine the homogeneity and confirm the lipid:protein molar ratios of two samples prepared for the ESR studies, as described in Chapter 2, Section 2.2.3. The gradient was prepared

by layering 5 ml samples of aqueous solutions of sucrose of increasing concentrations in 35 ml ultracentrifuge tubes. Loading of the sucrose layers was carried out carefully on ice with a glass Pasteur pipette with the end curved into a hook to avoid disruption of the bottom layers. The sucrose solutions were prepared in 20 mM HEPES and 100 mM KCl (pH 7.2), and the following w/w percentages of sucrose were used: 70%, 60%, 50%, 40%, 30% and 2.5%.

Two reconstituted samples were prepared for sucrose density gradient analysis, one at a DOPC:KcsA tetramer molar ratio of 30:1 and another at a molar ratio of 100:1. The samples were treated as described in Chapter 2, Section 2.2.3, except for the incorporation of a small proportion of lissamine rhodamine B labelled dioleoylphosphatidylethanolamine (rPE), (ca. 3 % total lipid). Two control samples, one containing KcsA in 1 mM DDM and one containing DOPC alone, were also prepared for comparison with the reconstituted samples. The lissamine rhodamine B sulphonil moiety is a fluorescent probe attached to the head group of DOPE (Figure 3.1); it allows visualization of lipid molecules in the sucrose gradient and quantification of the amount of lipid by absorbance spectroscopy. The molar extinction coefficient of lissamine rhodamine B sulphonil chloride is 88,000 $M^{-1}cm^{-1}$ in methanol at 568 nm (Molecular Probes Handbook, www.invitrogen.com). The latter value was used for rPE in these experiments because the exact molar extinction coefficient was not important as rPE was being used simply as a marker for lipid content.

For the analysis of the reconstituted membrane systems in the sucrose gradient, absorption spectra were recorded in 1 % SDS to reduce light scatter. A sample of DOPC containing ca. 5 % rPE was dissolved in 1 % SDS and the spectrum recorded (Figure 3.1). Maximum absorption occurred at 573 nm. Absorption was also seen at 280 nm. This was important as protein absorbance at 280 nm is used to determine protein concentrations; absorption at 280 nm for protein was therefore corrected in samples also showing absorption for rPE using the empirical relationship for rPE derived from Figure 3.1 that $OD_{573nm} / OD_{280nm} = 5.54$.

The sample at a DOPC:channel molar ratio of 30:1 was prepared with a KcsA tetramer:rPE molar ratio of 1:1, and the sample at a DOPC:channel molar ratio 100:1

was prepared with a KcsA tetramer:rPE molar ratio of 1:1.5; the lipid content of rPE in the lipid bilayers were 3.2 % and 1.5 %, respectively. These KcsA:rPE molar ratios were chosen to allow adequate absorbance measurements of KcsA at 280 nm and rPE at 573 nm: with these ratios the absorbance of rPE at 280 nm was very small relative to that of KcsA, and the absorbances of KcsA at 280 nm and of rPE at 573 nm were similar. The content of rPE was kept low to avoid any distortion of the bilayer.

After rehydration and resuspension of the samples, a washing step was performed to reproduce the steps involved in the preparation of the samples for ESR (Chapter 2, Section 2.2.3). Finally, the spun samples were resuspended in buffer (1.6 ml; 20 mM HEPES and 100 mM KCl, pH 7.2) and loaded on top of the sucrose density gradient. Centrifugation was carried out at 104,000 g (Beckman SW28 ultracentrifuge swing rotor at 24,000 r.p.m), over night (18 h) at 4˚C.

After centrifugation, 1.5 ml fractions were carefully collected from the top of the centrifuge tube. The absorbances of all fractions were then analysed at 573 nm and 280 nm to determine the locations of the lipids and proteins in the gradient, and to determine the lipid to protein ratio. Absorbances were determined by diluting 100 – 150 µl of each fraction into a final volume of 1 ml of 1 % SDS (a minimum 6.7 fold dilution was required as smaller dilutions resulted in SDS precipitates due to the KCl content of the sample; at this dilution sucrose had no significant absorption at 280 nm or 573 nm).

3.2.3 Sample preparation for fluorescence quenching

To compare with the information obtained from the ESR analysis, samples were also prepared for fluorescence quenching with brominated phospholipids. KcsA was reconstituted in DOPC, di(9,10-dibromostearoyl) phosphatidylcholine (BrPC), DOPG and di(9,10-dibromostearoyl) phosphatidylglycerol (BrPG) at increasing lipid:channel molar ratios as described in Chapter 2, Section 2.2.3. For these experiments, the final phospholipid concentration in the fluorescence cuvette was always 30 µM.

3.2.4 Analysis of ESR experiments: determination of phospholipid-KcsA stoichiometry

KcsA was reconstituted in DOPC or DOPG bilayers at lipid-channel molar ratios ranging from 30:1 to 100:1. Addition of 1 mol % spin labelled phospholipid to each sample allowed the measurement of the fraction of spin labelled phospholipid interacting with the protein.

The fraction of an ESR spectrum arising from the population of spin labelled lipid in contact with the protein yields information on the stoichiometry of the lipid-protein complex. Provided the spin labelled lipid and the non labelled lipid bind to the same sites on the protein, the number of lipid molecules associated with the protein can be deduced from the equation for equilibrium lipid exchange (Eq. 3.1)[24,90], where *P* is a lipid binding site on the protein, *A* is the spin labelled phospholipid and *B* is the non labelled phospholipid, also referred to as the background or the host lipid:

$$PB + A \rightleftharpoons PA + B \tag{3.1}$$

A binding constant *K* for the spin labelled phospholipid relative to that of the background lipid can be written as follows:

$$K = \frac{[PA][B]}{[PB][A]} \tag{3.2}$$

where the brackets indicate concentrations. This equation can be modified to determine the number of phospholipid binding sites on the protein (hence the lipid-protein stoichiometry) by using the following relations[90]:

$$[PB] + [PA] = n[P] \tag{3.3}$$

$$[A_t] = [PA] + [A] \tag{3.4}$$

$$[B_t] = [PB] + [B] \tag{3.5}$$

$$[A] + [B] = [A_t] + [B_t] - n[P] \tag{3.6}$$

where n is the total number of phospholipid binding sites per protein, $[A_t]$ is the concentration of total spin labelled phospholipid (bound plus free) and $[B_t]$ is the concentration of total background lipid (bound plus free). The term $[PB]$ can be eliminated from Eq. 3.2 by substituting it with $n[P] - [PA]$ (from Eq. 3.3); rearranging the terms then gives:

$$[PA] = \frac{nK[P]\{[A]/[B]\}}{1 + K\{[A]/[B]\}} \tag{3.7}$$

The term $[PA]$ can be then replaced in Eq. 3.7 by $[A_t] - [A]$ (from Eq. 3.4) and the terms can be rearranged to give:

$$\frac{[A_t] - [A]}{[P]} = \frac{nK\{[A]/[B]\}}{1 + K\{[A]/[B]\}} \tag{3.8}$$

Dividing numerator and denominator on the right side of Eq. 3.8 by $[A]/[B]$ gives:

$$\frac{[A_t] - [A]}{[P]} = \frac{nK}{\{[B]/[A]\} + K} \tag{3.9}$$

Next, the term $[B]$ in Eq. 3.9 can be substituted by $[A_t] + [B_t] - n[P] - [A]$ (from Eq. 3.6), and because in ESR experiments the concentration of spin labelled phospholipid is always about 100 times smaller than the background lipid, i.e. $[B_t] >>> [A_t]$, $[B]$ can be approximated by $[B] \approx [B_t] - n[P]$, giving:

$$\frac{[A_t] - [A]}{[P]} = \frac{nK}{\frac{\{[B_t] - n[P]\}}{[A]} + K} \tag{3.10}$$

Rearranging the terms by multiplying numerator and denominator on the right hand side of Eq. 3.10 by $[A]$ gives:

$$\frac{[A_t] - [A]}{[P]} = \frac{nK[A]}{\{[B_t] - n[P]) + K[A]} \tag{3.11}$$

Again, because in the ESR samples $[B_t]$ >>> $[A_t]$, the term $K[A]$ can be ignored in the denominator of the right hand side of Eq. 3.11, as $[B_t] - n[P]$ >>> $K[A]$

$$\frac{[A]}{[A_t]-[A]} = \frac{1}{K}\left(\frac{[B_t]}{n[P]} - 1\right) \tag{3.12}$$

This linear equation can be used to determine the number of lipid binding sites per channel (n) and the average relative affinity (K) of the lipid A (spin labelled lipid) with respect the lipid B (background lipid) for the binding sites[24,90]. The term on the left hand side of Eq. 3.12 represents the ratio of free spin labelled lipid over bound spin labelled lipid; it is not necessary to know the exact concentration of spin labelled lipid loaded into the sample (which can vary from one sample to another) since all that is required is the ratio of free to bound, which can be deduced from the ESR spectrum. The fraction of spin label bound to the protein is usually written as f with the fraction unbound as (1-f). The term $[B_t]/[P]$ corresponds to the DOPC/channel molar ratio and is normally written as N_t. The number of binding sites n is normally written as N_b. The equation then is normally written as:

$$\left(\frac{1-f}{f}\right) = \frac{1}{K}\left(\frac{N_t}{N_b} - 1\right) \tag{3.13}$$

Data are usually plotted with (1-f)/f (which is obtained from the ESR spectra) as the y axis, with N_t (the lipid:channel molar ratio of a given sample) as the x axis. This gives a straight line where the y intercept is $-1/K$ and the x intercept is N_b. For such an analysis it is important that the lipid:protein molar ratios are greater than the number of sites available ($N_t > N_b$) in order to avoid protein-protein contacts.

In the present experiments, the spin labelled lipid used is the same as the background lipid species, the only difference being that the spin labelled lipid has an attached nitroxide group. If the affinities of the spin labelled lipid and its non spin labelled form are assumed to be the same, so that, for example, for 14-PCSL in DOPC, K = 1, the number of lipid binding sites is then given directly by:

$$N_b = f \cdot N_t \tag{3.14}$$

This way, the solvation state of the channel can be investigated at different lipid:channel molar ratios (N_t).

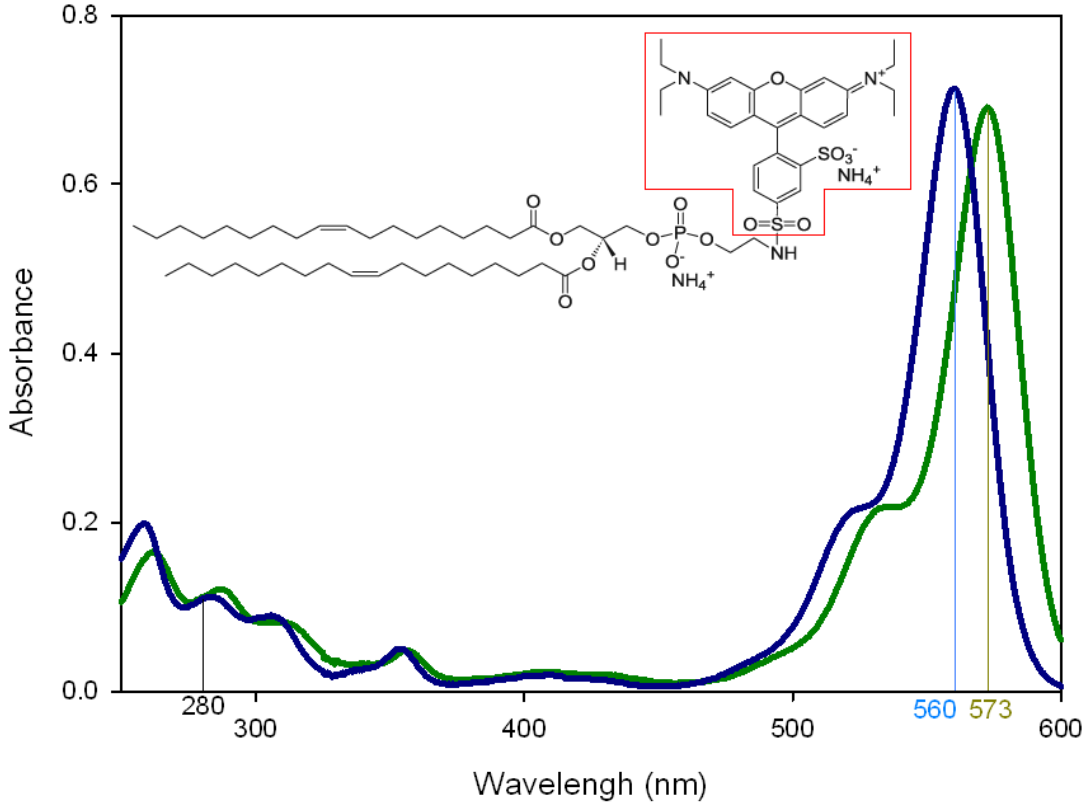

Figure 3.1 Absorption spectrum of lissamine rhodamine B labelled DOPE. The lissamine rhodamine B sulphonil moiety is enclosed in the red box. In blue is the spectrum of rPE in methanol showing maximum absorption at 560 nm; in green is the spectrum in 1 % SDS in the presence of DOPC, showing a maximum absorption at 573 nm. In both cases the same concentration of rPE was present, showing that there is a shift in the wavelength of maximum absorption but almost no change in the molar extinction coefficient at the emission maximum.

3.3 Results

3.3.1 Sucrose density gradient analysis

Figure 3.2 shows discontinuous sucrose density gradients of KcsA reconstituted in DOPC at lipid:channel molar ratios of 30:1 and 100:1, and compares them with DOPC in the absence of KcsA, and KcsA in 1 mM DDM in the absence of DOPC. All samples containing lipid also contained rPE to allow the location of the lipid to be determined. It can be seen that the DOPC sample remains at the top of the gradient. For unreconstituted KcsA in 1 mM DDM it can be seen that the majority of the protein remains towards the top of the gradient (light yellow band between the 30% and 40% sucrose bands), presumably in detergent micelles (fractions 7 to 11, see absorbance measurements in Figure 3.3) and only a small amount is seen at the bottom of the gradient, presumably present in the form of aggregates. In contrast, the reconstituted samples show single sharp bands within the gradient that indicate that the reconstituted samples are homogeneous with a density higher than that of DOPC alone. Absorbances were determined at 280 nm and 575 nm for each 1.5 ml fraction from the gradients (Figure 3.3). These confirm that lipid and protein co-localize in the reconstituted system. The concentrations of lipid and KcsA in the reconstituted samples confirm the lipid:channel molar ratios are maintained within ca. 10 % of the initial lipid:protein ratios (Table 3.2).

As expected, the sample at a DOPC:channel molar ratio of 30:1 (located at the top of the band of 60 % sucrose) has a higher density than that of the sample at a DOPC:channel molar ratio of 100:1 (located between the 30 and 40 % sucrose bands). It is possible to estimate the density of the reconstituted samples by adding the densities of the lipids and proteins weighted by their mass fractions in the sample. Taking a density for DOPC[91] of 1.01189 g/cm^3 and an average protein density[92] of 1.35 g/cm^3, the resulting densities of the samples with DOPC:channel molar ratios of 30:1 and 100:1 are 1.2707 and 1.1792 g/cm^3, respectively. These values are in close agreement with the location of the bands in the sucrose density gradients at 60 % and 40 % sucrose[93], respectively (Table 3.1).

These results indicate that processing of the samples as described in Chapter 2 generates homogeneous, reconstituted samples and that the lipid:protein molar ratios are maintained during the process of sample preparation.

3.3.2 ESR experiments: determination of phospholipid-KcsA stoichiometry

Three sets of samples were prepared containing spin labelled lipid, each with phospholipid:channel molar ratios ranging from 30:1 to 100:1. Two sets were of KcsA reconstituted in DOPC bilayers while the third set was KcsA reconstituted in DOPG. Figure 3.4 shows the ESR spectra of the first set of samples normalised to equal areas, which contained 1 mol % 14-PCSL in reconstituted membranes of DOPC and KcsA. In each sample the ESR spectrum arises from the absorption of microwave radiation by two different populations of spin labelled lipid (bound and unbound), generating a composite or two component spectrum. One component of the spectrum comes from a population of 14-PCSL in the membrane, not in contact with KcsA, where the acyl chains have a fast motion (known as the fluid or mobile component), and the other component comes from a population of 14-PCSL in contact with the channel, where the motion of the acyl chains is restricted (known as the restricted or immobile component). Deconvolution of each spectrum into their two components reveals the fraction of 14-PCSL free and bound to the protein.

Spectra were deconvoluted as described in Chapter 2, Section 2.2.6, and Appendix 2 shows details of the deconvolution of each spectrum. Table 3.3 shows the proportions of the restricted component deduced from the deconvolution analysis. Generally, the proportion of lipid interacting with a membrane protein is seen to increase as the lipid:protein ratio decreases[24]. However, for the data shown in Table 3.3 the fraction of 14-PCSL in contact with the protein remains relatively constant from a lipid:channel molar ratio of 30:1 to 75:1; only at molar ratios of 88:1 and 100:1 is there a more significant change in the mole fraction of immobilised 14-PCSL. The N_b values (lipid binding sites per channel) calculated using Eq. 3.14 are also shown in Table 3.3. From a molar ratio of lipid:KcsA tetramer of 30:1 to 75:1 the estimated number of lipids associated with the protein is not constant and, as it will be described later, it increases linearly as the molar ratio increases (see Figure 3.9C). In

contrast, for molar ratios of lipid:KcsA tetramer of 88:1 and 100:1 the number of lipid binding sites is constant (32.5 ± 3.9 and 31.9 ± 3.7, respectively). From the circumference of the KcsA tetramer, taken from the crystal structure, and with a diameter for a lipid molecule of about 9.6 Å, it can be estimated that ca. 33 lipid molecules will be required to form a complete annular shell around the tetramer [88]. The N_b values obtained for lipid:protein molar ratios 88:1 and 100:1 are therefore in close agreement with that expected from the crystal structure of the channel. The fact that lipid:protein molar ratios lower than 88:1 show a fraction of lipid in contact with the protein lower than expected (resulting in low N_b values when applying Eq. 3.14) suggests that at these molar ratios KcsA tends to aggregate reducing the surface of protein exposed to the lipid molecules.

There is also an unexpected change in the maximum splitting of the immobile component of the spectra when the lipid:channel molar ratio changes from 67.5:1 to 60:1 (Figure 3.4). A change in the maximum splitting normally reflects a change in the degree of mobility of the acyl chains of the spin labelled lipid: a narrower splitting at molar ratios of lipid:channel lower than 67.5:1 would indicate a higher mobility of the acyl chains. Unfortunately, the outer peak in the high magnetic field of the spectra is not resolved well enough to accurately measure the small change in maximum splitting detected in the low field outer peak.

A second set of samples of KcsA reconstituted in DOPC with 1 mol % 14-PCSL was prepared separately to assess reproducibility. The normalised ESR spectra of the latter are shown in Figure 3.5 and the fraction of immobile component and N_b values deduced from the analysis are presented in Table 3.3. The results are similar to those obtained with the previous set of samples: with lipid:channel molar ratios from 30:1 to 75:1 the fraction of the immobile component is approximately constant and lower than expected, resulting in very low N_b values that increase linearly as the lipid:channel molar ratio increases (see Figure 3.9C). The low fraction of immobile component again suggests KcsA is aggregating in the membrane at these molar ratios while with a lipid:channel molar ratio 100:1 the resulting number of lipid binding sites (32.5 ± 3.1) is in close agreement with that expected from the crystal structure of the channel, suggesting the channel is fully solvated by lipid molecules at this molar ratio. As observed in the first set of samples, this second set of samples also shows a

change in the maximum splitting of the immobile component in the samples of lipid:channel molar ratios from 30:1 to 67.5:1 (Figure 3.5).

Finally, a set of samples of KcsA reconstituted in the anionic phospholipid DOPG with 1 mol % of spin labelled phosphatidylglycerol (14-PGSL) were also studied. Figure 3.6 shows the normalised ESR spectra of the different lipid:channel molar ratios. The spectra were also deconvoluted as indicated in Chapter 2 and the details of the deconvolution can be seen in Appendix 2. The fraction of the immobile component deduced from the analysis is summarised along with the N_b values in Table 3.3. The fraction of immobile component in samples of lipid:channel molar ratios ranging from 30:1 to 75:1 are again lower than expected, indicating that aggregation of the protein occurs in bilayers of DOPG as well as in bilayers of DOPC. As for the DOPC samples, the N_b values increase linearly up to a lipid:channel molar ratio of 75:1 as discussed later (see Figure 3.9C). For molar ratios 88:1 and 100:1 the N_b values are 29.1 ± 2.2 and 28.5 ± 3.5, respectively, which are very similar to the values obtained with the samples in DOPC at those molar ratios. However, the fraction of immobile component in the 30:1 to 75:1 range for samples of 14-PGSL in DOPG is higher than that of the two sets of samples with 14-PCSL in DOPC (Table 3.3). The average value of the immobile fraction over this molar ratio range for the two sets of samples in DOPC is 0.272 ± 0.027, while for the samples in DOPG it is 0.362 ± 0.036, which is also reflected in the higher N_b values obtained for samples in DOPG (see also Figure 3.9C). This suggests that protein aggregates less in DOPG than in DOPC.

Unlike the samples reconstituted in DOPC, the spectra from the samples in DOPG do not show a change in the maximum splitting of the immobile component in any of the samples (Figure 3.6). However, the maximum splitting of 14-PGSL in the DOPG samples is slightly different from both the maximum splittings observed for 14-PCSL in the DOPC samples (Figure 3.7). Again, the outer peaks at high magnetic field are not resolved well enough to accurately measure the differences in maximum splitting, but clearly the outer peaks at low magnetic field are in different positions. The position of the low magnetic field outer peaks in the different spectra rank, from higher to lower magnetic field, as follows: 14-PCSL with DOPC:channel molar ratios

30:1 to 60:1 or 67.5:1, 14-PGSL in all DOPG:channel molar ratios studied and 14-PCSL with DOPC:channel molar ratios from 67.5:1 or 75:1 to 100:1.

3.3.3 Fluorescence quenching of KcsA as a function of lipid-channel molar ratio

Fluorescence quenching studies were carried out to compare with the results obtained with ESR. KcsA contains a belt of Trp residues at each side of the lipid bilayer (Figure 1.16) whose fluorescence will report on lipid binding around the transmembrane region of the channel. Figure 3.8A shows the fluorescence intensity of KcsA reconstituted in bilayers of either DOPC or BrPC, as a function of lipid:protein molar ratio. At a molar ratio of lipid:channel of 400:1, the fluorescence intensity of KcsA in DOPC has reached a maximum, and quenching of fluorescence by BrPC has also reached a maximum, reducing the fluorescence intensity to 50 % of that in DOPC. Decreasing the molar ratios of lipid:protein to 200:1 or 100:1 results in little change in fluorescence intensity in either DOPC or BrPC, but at lower molar ratios the fluorescence intensity in BrPC starts to increase and the fluorescence intensity in DOPC starts to decrease. When KcsA is reconstituted in BrPC, the level of quenching depends on the extent of binding of BrPC to KcsA, and a decrease in the level of quenching therefore implies protein aggregation, decreasing the proportion of the surface of KcsA occupied by BrPC. The decrease of quenching observed in BrPC is most apparent at molar ratios of lipid:channel lower than 100:1, consistent with the ESR results that also suggest aggregation at low lipid:protein molar ratios. The fluorescence intensity for KcsA in DOPC is also seen to decrease at low molar ratios of lipid:protein, either reflecting a change in Trp environment due to aggregation or caused by quenching of Trp fluorescence as a result of Trp-Trp contact/proximity at low molar ratios of lipid to protein. If the decrease in fluorescence intensity with decreasing molar ratios of DOPC:channel are due to Trp-Trp proximity effect then the observed change in fluorescence intensity would not necessarily imply aggregation. The important observation is a decrease in fluorescence quenching in BrPC below a molar ratio of lipid:protein of ca. 100:1, in agreement with the ESR results.

The change in fluorescence intensity over the range of lipid:protein molar ratios from 30:1 to 75:1 can be fitted to a straight line (Figure 3.9A), as the N_b values obtained from the ESR experiments listed in Table 3.3 (Figure 3.9C). This is

consistent with the proposal that aggregation affects both the fluorescence and the ESR experiments in the same way, through a decrease in the number of lipid molecules bound to the KcsA surface.

Fluorescence emission for KcsA reconstituted in DOPG or BrPG was also studied (Figure 3.8B). As in DOPC and BrPC, at a lipid:channel molar ratio of 400:1 the fluorescence emission and fluorescence quenching, are at a maximum in DOPG and BrPG respectively. However, unlike in BrPC, fluorescence quenching in BrPG only starts to decrease at molar ratios below ca. 30:1. This suggests that BrPG is better able to prevent aggregation of KcsA than is BrPC and would be consistent with stronger binding of BrPG than BrPC (see Chapter 4). The ESR results also show that PG is better able to prevent aggregation of KcsA than PC (Table 3.3 and Figure 3.9C). The changes in fluorescence observed for KcsA in DOPG and in BrPG fit to a straight line at molar ratios of lipid:channel below ca. 75:1 (Figure 3.9B), as described above for KcsA in DOPC or in BrPC.

Although the effects of lipid:channel molar ratio on quenching by BrPG and BrPC are different, the effects of lipid:channel molar ratio on fluorescence intensities are very similar in DOPG and DOPC (Figure 3.8): as in DOPC, fluorescence intensities in DOPG start to decrease at molar ratios of lipid:channel below about 100:1. This suggests that the effects of lipid:channel molar ratio on fluorescence intensity of DOPG and DOPC are not the result of aggregation, but follow simply from the decrease in distance between Trp residues that will occur with increasing KcsA concentration in the membrane, as previously described. To allow a clear comparison of the fluorescence results described above, Figure 3.8C also shows the effects of lipid:protein molar ratio on the observed changes in fluorescence intensity expressed as a fractional change.

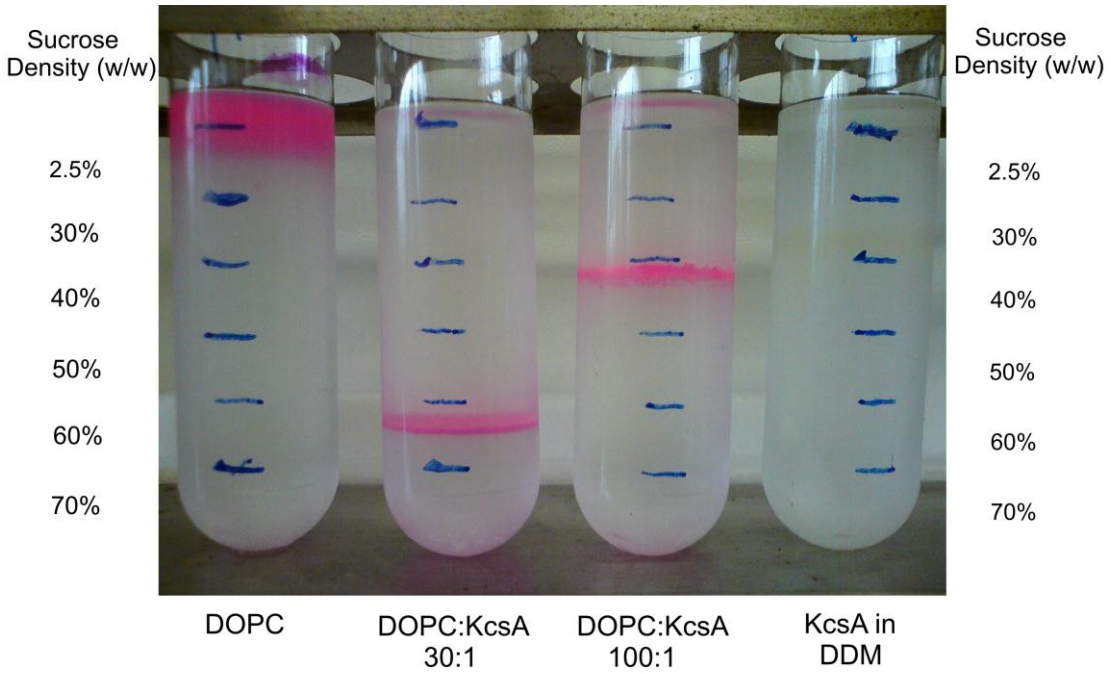

Figure 3.2 Discontinuous sucrose density gradients of KcsA reconstituted in DOPC at a lipid:channel molar ratio of 30:1 and 100:1, DOPC alone and KcsA in 1 mM DDM. The lipid-containing samples also contained rPE as a marker. The faint pink colour observed in this picture at the top and bottom of the tubes of the DOPC:KcsA samples and at the bottom of the DOPC sample is due to reflection along the tube from the bands containing rPE.

Sucrose % (w/w)	Sucrose density (g/cm^3)	Estimated density of the sample (g/cm^3)	Lipid:channel molar ratio
2	1.0060		
3	1.0099	1.0118	DOPC only
30	1.1270		
40	1.1764	1.1792	100:1
50	1.2296		
60	1.2865	1.2794	30:1

Table 3.1 Sucrose densities and estimated densities of the samples. The densities of the samples were estimated as described in the text from the initial lipid:channel molar ratios. The estimated values for the sample densities agree well with the densities of the sucrose solutions[93] where the samples were observed on the gradients.

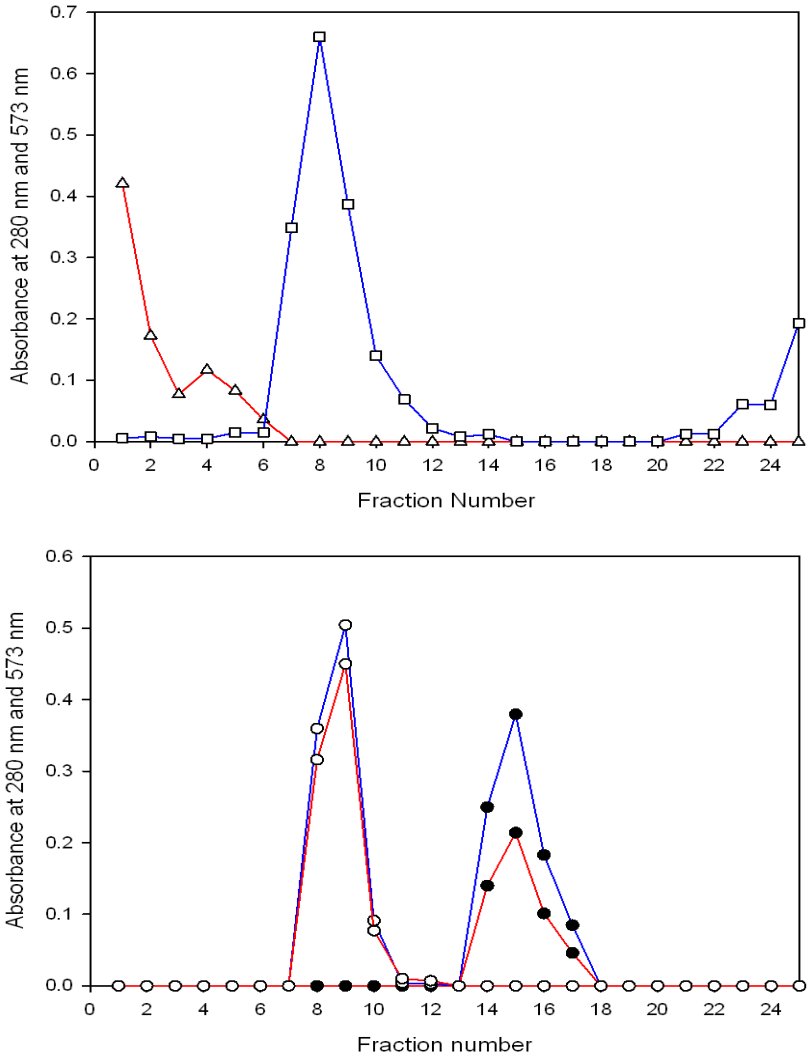

Figure 3.3 Absorbance at 280 nm and 573 nm for 1.5 ml fractions taken from the sucrose density gradients. Upper graph: (△) absorbance at 573 nm for DOPC alone; (□) absorbance at 280 nm for KcsA in 1 mM DDM. Bottom graph: absorbance at 573 nm (red) and at 280 nm (blue) for KcsA reconstituted in DOPC at a lipid:channel molar ratio of 100:1 (○) and 30:1 (●). The absorbance of KcsA at 280 nm is corrected for the absorbance of rPE at 280 nm as described Section 3.2.2.

	Sample of lipid:KcsA tetramer molar ratio 100:1			Sample of lipid:KcsA tetramer molar ratio 30:1			
Fraction	**8**	**9**	**10**	**14**	**15**	**16**	**17**
DOPC (μM)	1596	3409	389	477	730	230	105
KcsA tetramer (μM)	17.2	36.2	4.4	17.9	27.2	8.7	4.1
Lipid:KcsA tetramer molar ratio	93	94	89	27	27	26	26

Table 3.2 Concentrations and lipid:channel molar ratios determined from the absorbance measurements of the samples analysed by sucrose density centrifugation.

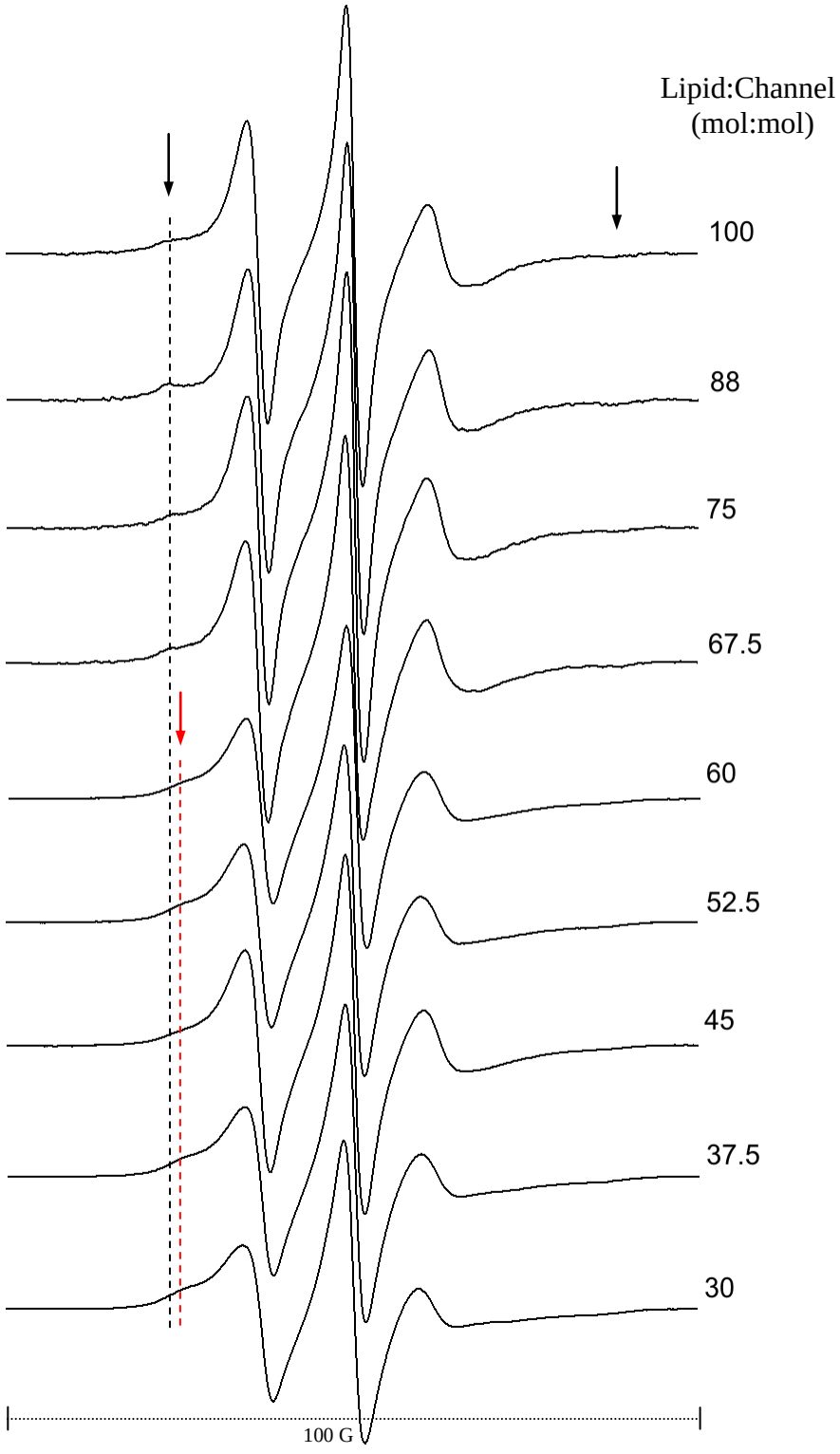

Figure 3.4 Normalised ESR spectra for 14-PCSL in DOPC membranes containing KcsA as a function of DOPC:channel molar ratio, recorded at 25˚C. The outer peaks (maximum splitting) of the component arising from spin labelled lipid in contact with KcsA (restricted component) are indicated by the black arrows. The maximum splitting is constant for samples of lipid:channel molar ratios from 100:1 to 67.5:1, as indicated by the black dashed line. Samples with molar ratios from 60:1 to 30:1 have a narrower maximum splitting, as indicated by the red arrow and red dashed line. Total scan width is 100 gauss.

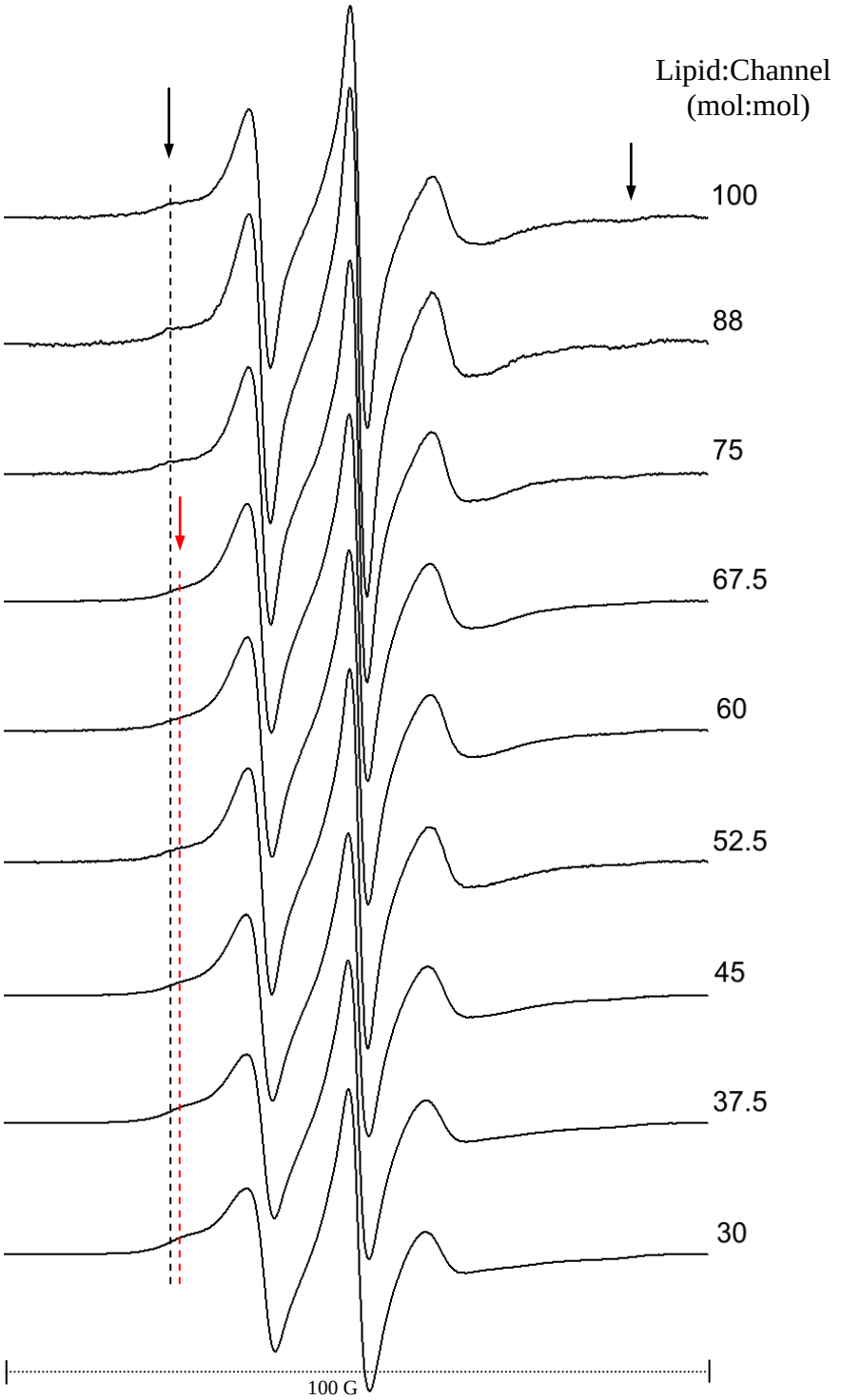

Figure 3.5 Normalised ESR spectra of a second set of samples of 14-PCSL in DOPC membranes containing KcsA as a function of DOPC:channel molar ratios, recorded at 25˚C. Details as in the legend of Figure 3.4.

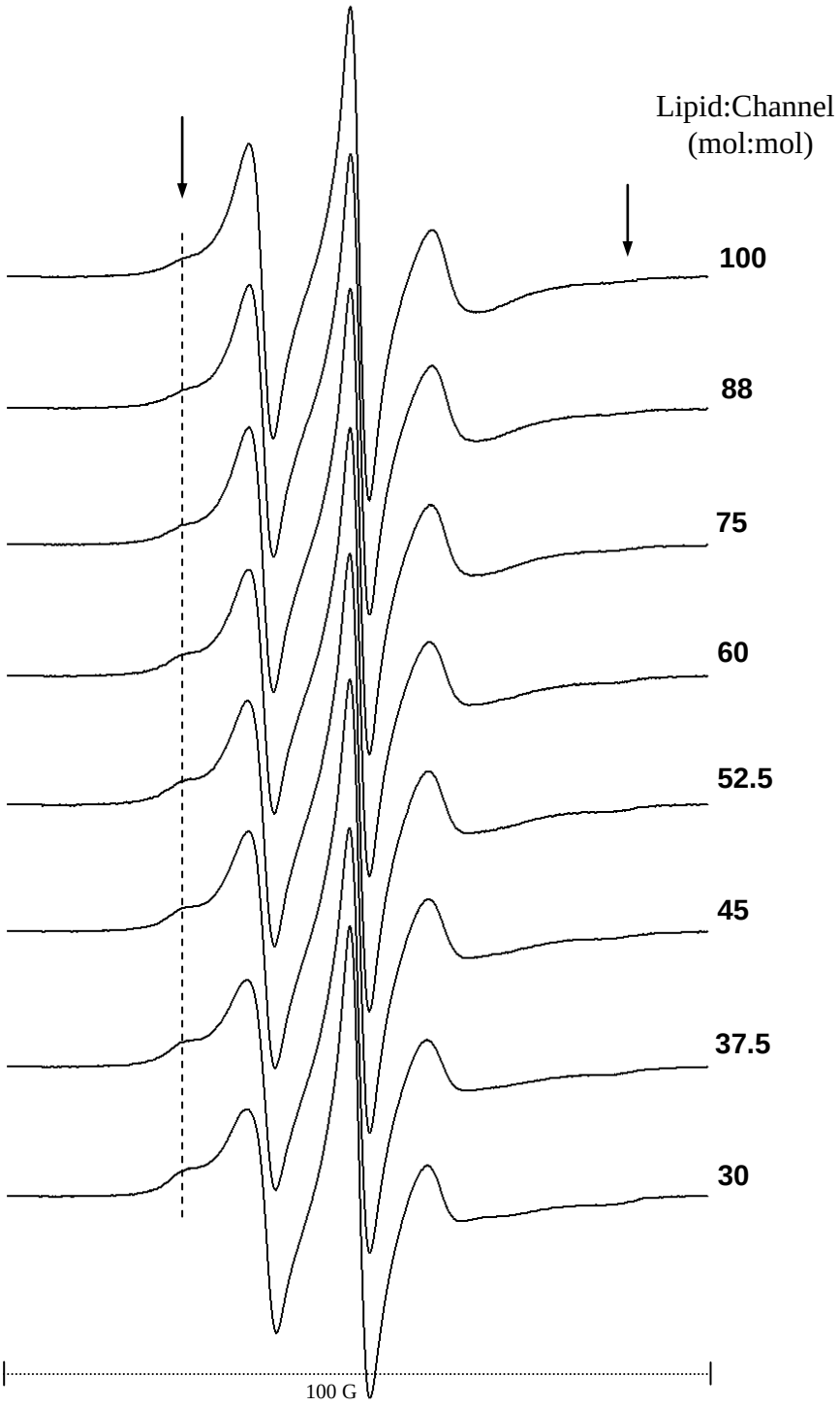

Figure 3.6 Normalised ESR spectra for 14-PGSL in DOPG membranes containing KcsA as a function of DOPG:channel molar ratios, recorded at 25˚C. As in Figures 3.4 and 3.5, the outer peaks (maximum splitting) of the component arising from the spin labelled lipid in contact with KcsA (restricted component) are marked by the black arrows and black dashed line. No change in the maximum splitting is observed in these samples. Total scan width is 100 gauss.

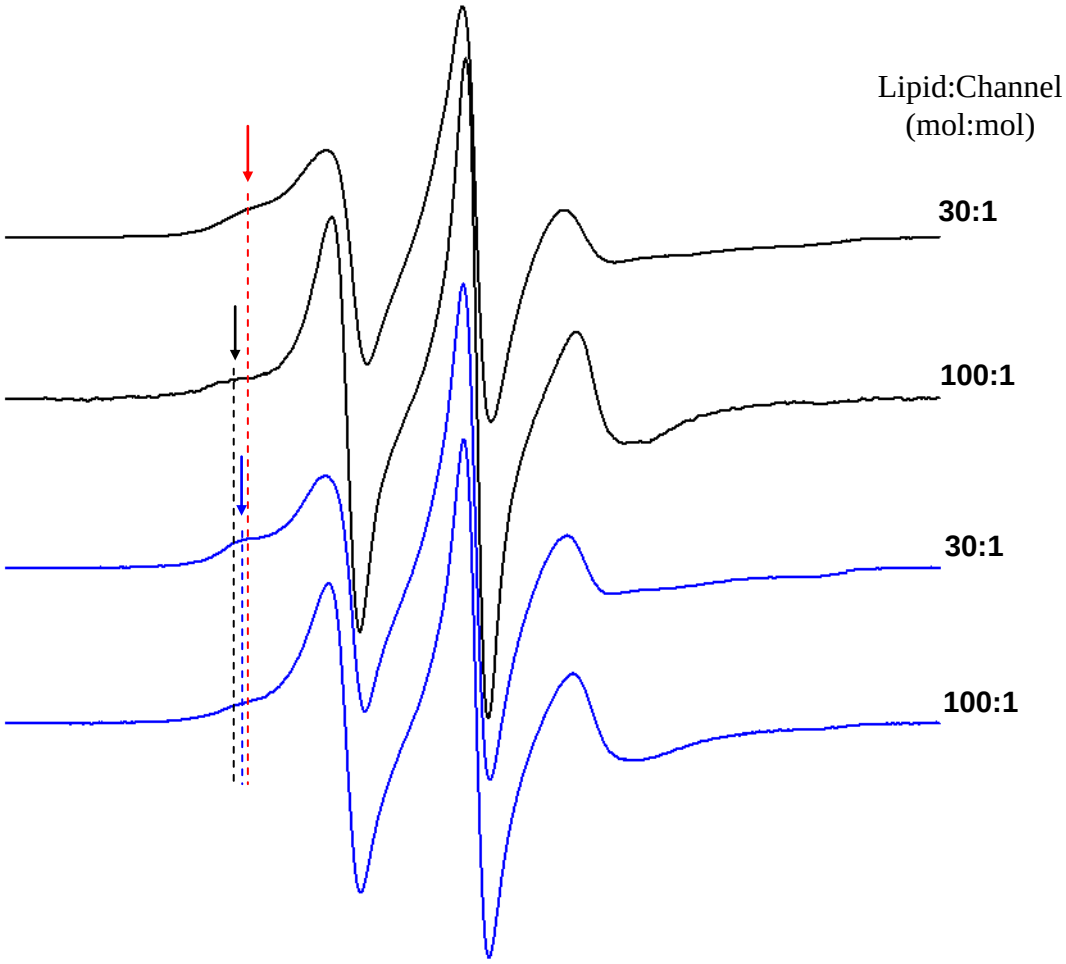

Figure 3.7 Difference in the maximum splitting for 14-PCSL in samples with KcsA reconstituted in DOPC (black spectra) and for 14-PGSL in samples with KcsA reconstituted in DOPG. The shown spectra are those from Figures 3.4, 3.5 and 3.6, and have been normalised to equal areas. The outer peaks at low magnetic field are indicated by the arrows and their position is further indicated by the dashed lines as follows: red, 14-PCSL with a DOPC:channel molar ratio 30:1; black, 14-PCSL with a DOPC:channel molar ratio 100:1; blue, 14-PGSL with DOPG:channel molar ratios of 30:1 and 100:1. The outer peaks at high magnetic field are not resolved well enough to accurately determine their positions in the spectra.

	DOPC (first set)		DOPC (second set)		DOPG	
Lipid/channel molar ratio	Fraction of immobile component	N_b value	Fraction of immobile component	N_b value	Fraction of immobile component	N_b value
30	0.278 ± 0.022	8.3 ± 0.7	0.294 ± 0.037	8.8 ± 1.1	0.413 ± 0.038	12.4 ± 1.1
37.5	0.300 ± 0.019	11.3 ± 0.7	0.286 ± 0.042	10.7 ± 1.6	0.384 ± 0.003	14.4 ± 0.2
45	0.225 ± 0.012	10.1 ± 0.5	0.262 ± 0.007	11.8 ± 0.3	0.369 ± 0.006	16.6 ± 0.3
52.5	0.281 ± 0.006	14.8 ± 0.2	0.275 ± 0.025	14.4 ± 1.3	0.363 ± 0.007	19.1 ± 0.4
60	0.278 ± 0.009	16.7 ± 0.5	0.240 ± 0.010	14.4 ± 0.6	0.335 ± 0.004	20.1 ± 0.2
67.5	0.275 ± 0.038	18.6 ± 2.6	0.231 ± 0.044	15.6 ± 3.0	--	--
75	0.263 ± 0.019	19.7 ± 1.4	0.325 ±0.019	24.4 ± 1.4	0.310 ± 0.041	23.3 ± 3.1
88	0.369 ± 0.044	32.5 ± 3.9	--	--	0.331 ± 0.025	29.1 ± 2.2
100	0.319 ± 0.037	31.9 ± 3.7	0.325 ± 0.031	32.5 ± 3.1	0.285 ± 0.035	28.5 ± 3.5

Table 3.3 Fraction of the immobile component and the number of lipid molecules associated with the KcsA tetramer (N_b value) derived from deconvolution of the ESR spectra of 14-PCSL and 14-PGSL in DOPC and DOPG membranes, respectively, containing KcsA at the given lipid:channel molar ratios. Details of the deconvolution analysis can be found in Appendix 2; The N_b values were calculated using Eq. 3.14.

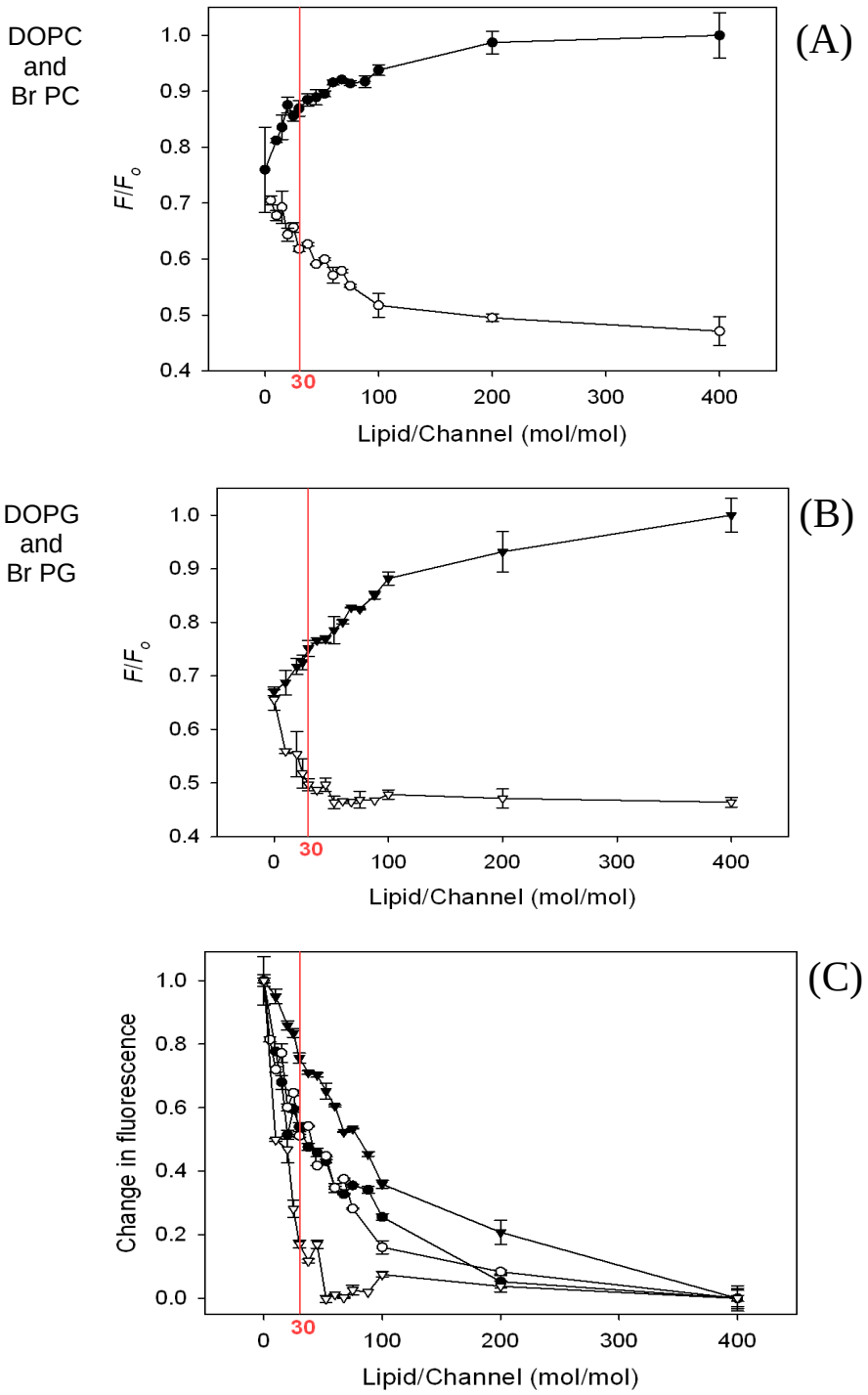

Figure 3.8 Fluorescence emission intensities for KcsA in brominated and non-brominated lipid as a function of lipid:channel molar ratio. (A) Fluorescence intensities in (●) DOPC or (○) BrPC. (B) Fluorescence intensities in (▼) DOPG or (▽) BrPG. In (A) and (B) fluorescence intensities are expressed as F/F_o where F is the fluorescence intensity observed at the given molar ratio of lipid:channel and F_o is the fluorescence intensity observed in DOPC (A) or (DOPG) (B) at a molar ratio of lipid:channel of 400:1. (C) Changes in fluorescence intensity plotted as $(F-F'_{min})/(F'_o-F'_{min})$, where F'_o and F'_{min} are the maximum and minimum fluorescence intensities observed for KcsA reconstituted with DOPC or DOPG and BrPC or BrPG, respectively. Changes in fluorescence intensity correspond to increases in intensity for BrPC and BrPG, and a decrease in intensity for DOPC and DOPG. The red line marks the lipid:channel molar ratio of 30:1. Excitation was at 290 nm and fluorescence intensities were measured at 333 nm.

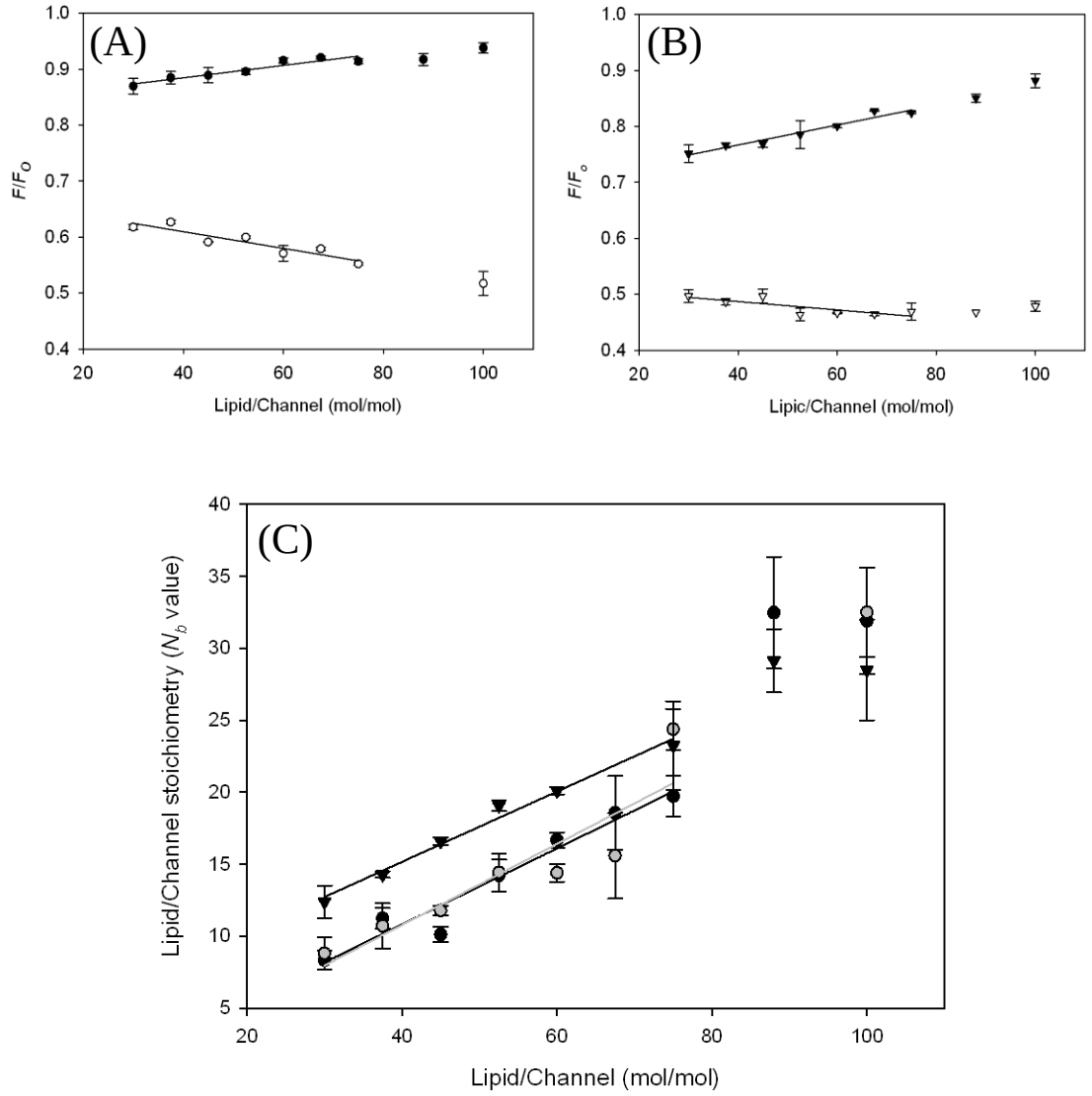

Figure 3.9 Straight line plots of changes in fluorescence intensity (A, B) and in N_b values obtained from ESR experiments as a function of lipid:channel molar ratio. (A) Fluorescence intensities for KcsA reconstituted in DOPC (●) or BrPC (○) as a function of lipid:channel molar ratio. (B) Fluorescence intensities for KcsA reconstituted in DOPG (▼) or BrPG (▽) as a function of lipid:channel molar ratio. (C) Calculated phospholipid:channel stoichiometries (N_b values) (see Table 3.3) as a function of lipid:channel molar ratios for KcsA reconstituted in DOPC (●, ◍; first and second set of samples in Table 3.3, respectively) or DOPG (▼). The lines show best fits to a straight line on the 30:1 to 75:1 lipid:channel molar ratio range.

3.4 Discussion

The crystal structure of KcsA[53] reveals a channel whose transmembrane region could accommodate ca. 33 annular phospholipid molecules[88]. The ESR results reported here show that at lipid-channel molar ratios of 88:1-100:1 the average number of lipid molecules interacting with KcsA obtained from reconstitutions in DOPC or DOPG (Table 3.3) is 31 ± 3, in agreement with the number deduced from the crystal structure. However, at lipid:channel molar ratios below 88:1 the number of lipid molecules interacting with KcsA does not remain constant as it does with most membrane proteins [24,88], but gradually decreases with decreasing lipid:channel molar ratio (Table 3.3). This suggests that the extent of the surface of the channel exposed to the lipid bilayer decreases as the lipid:channel molar ratio decreases, in a linear fashion (Figure 3.9C). The fluorescence studies of KcsA reconstituted in BrPC as a function of lipid:channel molar ratio (Figure 3.8) support the data obtained from ESR, as the level of quenching caused by BrPC decreases with decreasing lipid:channel molar ratio, again consistent with a decreased exposure of the channel surface to the lipid bilayer.

As the concentration of KcsA in the membrane increases, the number of protein-protein contacts would be expected to increase. If these contacts involve the transmembrane domains, they will result in a decrease in the number of immobilised lipids, as observed. The reason why such an effect has not been observed with many other membrane proteins[24,88] could be that other membrane proteins contain large extra-membranous domains and these would prevent contact between trans-membrane domains even at high protein concentrations; KcsA does not contain large extra-membranous domains that would prevent contact between transmembrane regions of adjacent channels, although see the discussion later.

It is possible to make some estimates for the likelihood of random protein-protein contacts for a membrane protein if the protein has a simple cylindrical shape, which is a reasonable initial approximation for the KcsA channel. East *et al.*[86] calculated the probability for the occurrence of random protein-protein contacts for a simplified bilayer system in which the lipids and protein molecules were represented

as small and large discs, respectively (Figure 3.10). The calculations assumed a ratio of lipid to protein radii of 4, which corresponds to a system in which 32 lipid molecules would be required to form a complete shell around a protein molecule. This size ratio corresponds well to the KcsA channel in bilayers of DOPC or DOPG. The random arrangements of disks were divided into a group of four different types of triangles that result from connecting each disk centre with the centre of its neighbouring disks, as illustrated in Figure 3.10. In this way, the triangles were classified as LLL, PLL, PPL and PPP, where L and P represented the lipid and protein molecules connecting each type of triangle, respectively. This representation allows the calculation of the probability of the appearance of these triangles in membranes of different lipid to protein molar ratios as shown in Figure 3.10. The calculations show that the frequencies of PPP and PPL triangles are low at lipid to protein molar ratios greater that ca. 30:1, showing that the probability of random protein-protein contacts is vanishingly small at molar ratios of lipid:protein greater than 30:1. Unfortunately with this model it is not possible to quantify the number of protein-protein contacts, because the triangles share their sides so that a single type of contact (protein-protein, protein-lipid or lipid-lipid) will be counted in more than one triangle.

The calculations described by East *et al.*[86] suggest that the reduction of lipid-protein contacts observed in DOPC at lipid:KcsA tetramer molar ratios below 88:1 cannot be attributed to random contacts between DOPC and the KcsA channel but, instead, suggest that KcsA-KcsA contacts are more favourable than KcsA-DOPC contacts. From these experiments it is not possible to describe the nature of any aggregates formed, but it is certain that the aggregates remain embedded in the lipid bilayers, as shown by the sucrose gradient analysis of a sample at a DOPC:channel molar ratio of 30:1 (Figure 3.2).

The ESR results for KcsA in DOPG show that the number of immobilized lipids in DOPG is higher than the number of immobilised lipids in DOPC, at molar ratios of lipid:channel less than 88:1 (Figure 3.9C). This suggests that DOPG binds more strongly to KcsA than does DOPC and is thus better able to prevent KcsA-KcsA contacts. It is possible that the stronger binding of DOPG to KcsA follows from its negative charge; ESR determinations of the strength of lipid binding (Chapter 5, Section 5.3.1) indeed show that PG binds more strongly to KcsA than PC.

The fluorescence studies for KcsA reconstituted in BrPC or BrPG (Figure 3.8) support the data obtained from ESR. A key observation from these fluorescence experiments is that whereas quenching by BrPC decreases at molar ratios of lipid:channel below ca. 100:1, large decreases in quenching by BrPG only appear at molar ratios below about 30:1. This again suggests that BrPG is better able to prevent KcsA-KcsA contacts than is BrPC.

The crystal structure of KcsA shows that its transmembrane region on the intracellular side of the membrane contains several charged residues. It has been proposed that, in particular, Arg-27 could favour interaction with DOPG molecules[74]. Arg-27 forms a belt of positively charged residues around KcsA, very close to the belt of Trp residues (Trp-26 and Trp-113) on the narrower side of the channel (the side that normally faces the intracellular side of the bacterial membrane) (Figure 3.11) which marks the location of the glycerol backbone region of the lipid bilayer around KcsA[72]. Because the negative charge present in DOPG is located in the lipid phosphate group, right next to the glycerol backbone region, and the Arg-27 side chain is snorkelling towards this region, it is likely that Arg-27 can easily interact with the negatively charged phosphate group of DOPG. This favourable interaction between DOPG and Arg-27, and interactions with other positively charged residues, could result in BrPG being able to better prevent KcsA-KcsA contacts than BrPC.

From the experiments presented here, it is not possible to determine the factors that trigger the aggregation of KcsA at low lipid:channel molar ratios. However, it is worth noting some features of the full length channel that could be involved. Because the first crystal structures of KcsA only showed the transmembrane region of the protein[34,53], it has become common to represent this region of the channel alone. However, as mentioned in Chapter 1, Cortes *et al.*[51], in 2001 described the N-terminal and C-terminal architecture of the channel using ESR methods, and more recently, the crystal structure of KcsA with its C-terminal region (but lacking the N-terminus) was determined by Uysal *et al.*[52] The ESR structure obtained by Cortes *et al.*[51,75] was determined for KcsA reconstituted in bilayers of soybean asolectin (which comprises a mixture of PC, PE and phosphatidylinositol) at a lipid:channel molar ratio of 500:1; the study suggested that the N-terminus consists of an amphipathic α-helix located at

the interface between water and the intracellular face of the bilayer, extending away from the core of the channel (Figures 1.12 and 3.12) at a 14˚ angle relative to the plane of the membrane. Detection of the N-terminus by x-ray diffraction studies has not yet been achieved.

It seems reasonable then to suggest that the N-terminus must be affected by aggregation of the channel at low lipid:protein molar ratios, where the reduced number of lipid molecules will force the channels closer together. The N-terminal domain comprises residues from Met-1 to Ser-22, and the distance between Met-1 and Ala-23 where the first transmembrane helix starts, is 33.0 Å (Figure 3.12). As the N-terminus is tilted ca. 14˚ with respect to the plane of lipid bilayer, by simple trigonometry it can be deduced that it extends about 31.9 Å away from the core of the channel (Figure 3.12). This distance is equivalent to three adjacent phospholipid molecules since the diameter of an all-*trans* acyl chain is 4.8 Å[25] giving an approximate diameter of a phospholipid molecule of 9.6 Å; this means that three aligned phospholipid molecules will cover a distance of about 28.8 Å. As a result, if KcsA channels are reconstituted in bilayers with a lipid content lower than that needed to achieve three shells of lipid between the different channels, the N-termini of each protein will be forced to come into contact with the transmembrane region of its neighbouring channels, unless the N-termini distort.

A simple geometrical model can be used to illustrate the minimum space required in the membrane for undistorted N-termini not to come into contact with the transmembrane region of a neighbouring channel. As in the model described by East *et al.*[86], the lipids and proteins viewed from the top of the membrane can be represented as discs of the appropriate sizes. But in the model presented here, to provide a better representation of the KcsA channel, the channel was modelled as an inverted, truncated cone, with the diameter of the transmembrane region of the channel being smaller on one side than on the other (Figure 3.13). As mentioned above and in Chapter 1, KcsA possesses two belts of Trp residues facing the lipid bilayer which are located at the membrane-water interfaces at each side of the membrane (Figure 1.16), and so the distance between two Trp residues in opposite monomers in each of the belts in the tetrameric structure, measured as the greatest distance between C atoms in the side chains, gives a good estimate of the diameter of

KcsA on each side of the membrane. Figure 3.13 shows these distances measured on the crystal structure of KcsA[53] (PDB identification number 1K4C), which are 51.7 Å on the wide side (which normally faces the extracellular side of the bacterial membrane) and 29.2 Å on the narrow side (which normally faces the intracellular side of the bacterial membrane). Therefore, in the present model, disks of proportional sizes are used to represent the lipids and the channels in a particular orientation.

In order to illustrate how close two channels can be in a bilayer before their N-termini come into contact it is important to appreciate that the N-termini extend only from the narrow side of the channel, and so, depending on the orientations of two neighbouring channels, the minimum separation to keep the N-termini apart will vary. Figure 3.14 shows three possible situations that can occur, viewing the membrane from the top: two channels with their narrow ends facing the viewer (all the N-termini are located on the top surface of the bilayer), two channels with their wide ends facing the viewer's side of the bilayer (all the N-termini are located on the opposite side of the bilayer), and two channels with opposite orientations (the N-terminus of one of the channels is in one side and the N-terminus of the other channel is on the opposite side). It is important to note that the differences in diameters between the two sides of KcsA allows it to have one shell of lipid molecules on the narrow side that is hidden by the wider side when the viewer is seeing the channel from its wider side (see Figure 3.14A). Therefore, because the length of the N-terminus is very similar to that of three aligned phospholipid molecules, when two channels have their narrow sides facing the viewer, there will need to be at least three shells of lipid separating the proteins to avoid contact of their N-termini (which are on the viewers side) with the core of the neighbouring channels (Figure 3.14A). However, when two channels have their wide sides facing the viewer (so that the N-termini are on the opposite side of the bilayer, as shown in Figure 3.14B), there will only need to be a single shell of lipid molecules separating the channels on that side of the membrane to avoid contact of the N-termini with the core of the channels on the opposite side of the bilayer. Finally, when two channels have opposite orientations, three shells of lipid will be required to avoid contact of the core of the channels with the N-termini, as illustrated in Figure 3.14C.

Taking these considerations into account a geometrical model for the membrane can be drawn as shown in Figure 3.15. The models show 50 % of the channels in one orientation and 50 % in the opposite orientation. Packing is described by a regular repeating unit of two channels in each orientation, indicated by the black lines in Figure 3.15. The first model (Figure 3.15A) shows a bilayer with the minimum amount of lipids required to avoid contact of the N-termini of a given channel with the transmembrane body of its neighbouring channels. Such packing results in a lipid:channel molar ratio of 44:1; the model also implies that some lipids (shown in red) from the first shell of lipids around the channels with their wide side facing the viewer, and some lipids from the second shell of lipids around the channels with their narrow side facing the viewer are shared with a neighbouring channel. In the second model the shape of the geometric unit made up by the four channels has been modified to avoid sharing of the first and second shells of lipids around the wide and narrow sides of the channels respectively. This results in an increase in the spaces between the channels so that it is necessary to introduce more lipid molecules, resulting in a lipid:channel molar ratio of 53:1; these new lipid molecules that do not form part of the first and second shells of lipid around the wide and narrow sides of the channel, respectively, are coloured green in Figure 3.14B. Finally, in the third model (Figure 3.14C), the shape of the geometric unit has been changed to form a square, maintaining the minimum distance of three lipid shells between the channels at the sides of the square. This results in a further increase in the space between the channels with more lipid molecules (shown in green) being required, resulting in a lipid:channel molar ratio of 67:1.

As already described, with excess lipid in the system, the ESR results suggest that the number of lipid molecules in the first shell around the KcsA tetramer is ca. 31 (Table 3.3). The number of lipid molecules in the first shell around the KcsA tetramer, taking into account the different circumferences of the tetramer on the two sides of the membrane, is 33 (Figure 3.13). If, however, the N-terminal domains were rigidly fixed, a minimum number of ca. 44 lipid molecules per channel would be required to allow the channels to pack into the bilayer. However, there is no evidence to suggest that channels cannot incorporate fully into a lipid bilayer at molar ratios of lipid:channel below 44:1. In particular, the results of the sucrose gradient centrifugation experiments (Figure 3.3) suggest that at a 30:1 molar ratio of

lipid:channel the channel is fully incorporated. It therefore seems likely that the N-terminus of the channel is flexible and can bend and/or increase its tilt angle relative to the plane of the bilayer, allowing closer contact between the KcsA tetramers.

The function of the N-terminal domain of KcsA is unclear; functional assays of a KcsA mutant lacking residues 2-20 have not shown any significant difference with respect to the full length channel[58]. However, it has been reported that deletion of the N-terminus results in a dramatic decrease in the levels of expression of the channel, suggesting that it could be important for correct folding and targeting to the membrane. It has been proposed that the protrusion of the N-terminus away from the channel core, and the numerous positively charged residues found in the N-terminus, could help anchor the channel into the membrane[51].

Other groups have reported aggregation or formation of clusters of KcsA in artificial bilayers [79,80] and in *Streptomyces lividans* cells[94,95], but there is no clear agreement about the conditions under which aggregation occurs. Raja and Vales[80], based on electrophysiological studies, proposed that aggregation is triggered by the presence of 100 mM NaCl at a lipid:channel molar ratio of 200:1. In these studies membranes of three different lipid compositions were used: a 7:3 molar ratio of diphytanoyl PE to diphytanoyl PG, a 7:3 molar ratio of diphytanoyl PC to diphytanoyl PG and *E. coli* total lipid extract (where aggregation was suggested to take place in the presence of 100 mM NaCl). In the diphytanoyl mixtures no effects suggesting aggregation were observed, pointing to an important effect on the bilayer composition on protein aggregation. The experiments reported here were performed in the presence of KCl rather than NaCl, but aggregation was only observed at molar ratios of lipid:channel much lower than those used by Raja and Vales. The experiments performed by Molina *et al.*[79] involved fluorescence resonance energy transfer of labelled KcsA as well as electrophysiological studies, and were interpreted in terms of aggregation in the absence of NaCl and in the presence of 100 mM KCl at lipid:channel molar ratios higher than 100:1; the membranes were composed of asolectin, a complex mixture of lipids. Interestingly, the electrophysiological recordings performed by both groups[79,80] showed marked changes in the characteristic channel activity of KcsA, and such changes were suggested to be a consequence of channel aggregation. Hegermann *et al.*[94,95], using electron microscopy approaches,

reported clusters of KcsA in *S. lividans*, but at very low concentrations of KcsA in the membrane. Whether such clusters are physiologically relevant and represent aggregated channels with different conductance characteristics to non-aggregated channels is unknown.

In conclusion, the results of the ESR and fluorescence experiments reported here suggest that aggregation of KcsA occurs at lipid to channel molar ratios lower than ca. 88:1 due to favourable protein-protein interactions since random mixing would only result in protein-protein contacts below a lipid:channel molar ratio of ca. 30:1; these results therefore suggest that protein-protein contacts are more favourable than protein-lipid contacts. Aggregation of the channel is affected by the lipid composition. In DOPC bilayers, less favourable lipid-protein contacts allow more protein-protein interactions, whereas the stronger interaction between DOPG and KcsA results in aggregation being less favourable. Aggregation at low lipid:protein molar ratios implies that the N-termini in KcsA must distort to allow packing of the channel, but the aggregates are stably embedded in the lipid bilayer, as shown by the sucrose density gradient. In a typical membrane, the molar ratio of lipid:protein is ca. 100:1 so that random KcsA-KcsA contacts will be rare in the native membrane.

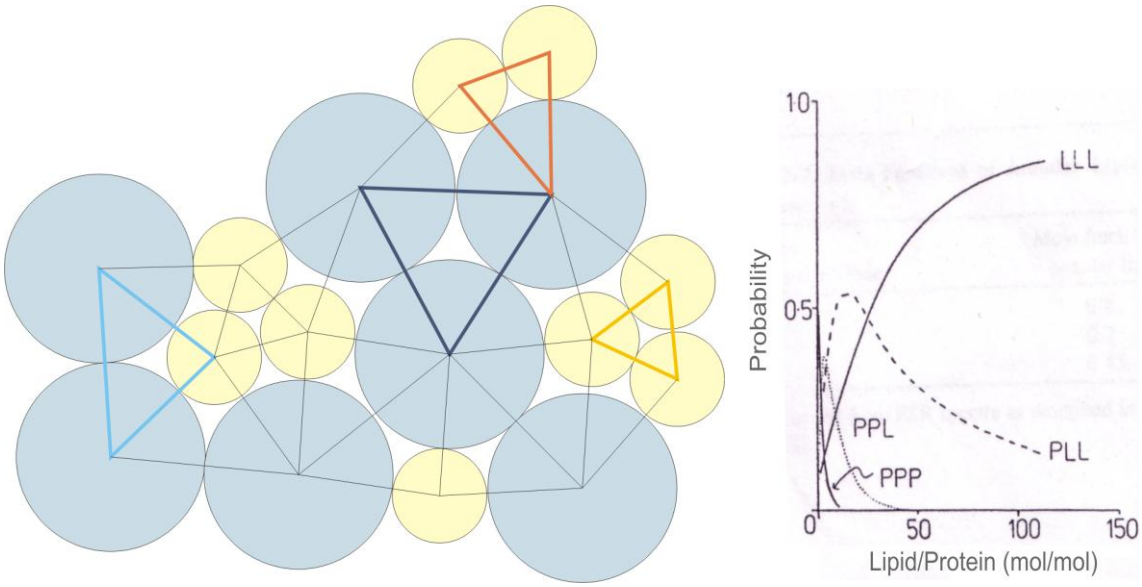

Figure 3.10 Model of a membrane used to estimate the probability of random contacts between lipids and proteins, as described by East *et al.*[86] Left, a diagram showing a membrane where the large disks represent the proteins and the small disks represent the phospholipids. The radii of the proteins were 4 times that of the phospholipids in the probability calculations, but for illustrative purposes in the diagram showed here the protein:lipid radii ratio used is smaller. The centres of each disc are connected to the neighbouring disks generating four types of triangles (examples are highlighted): PPP (dark blue), PPL (light blue), PLL (orange) and LLL (yellow), where P and L indicate protein and lipid molecules, respectively. On the right, is shown the probability of the occurrence of each type of triangle as a function of the lipid:protein molar ratio, assuming random mixing. The images were taken from East *et al.*[86]

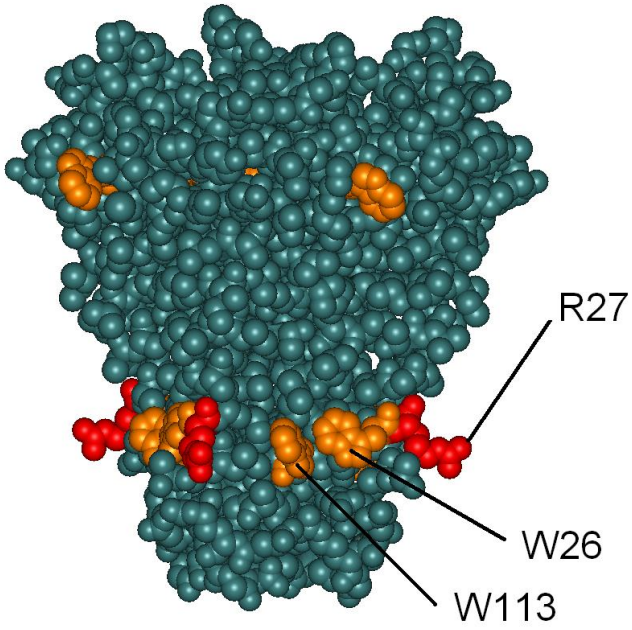

Figure 3.11 CPK representation of the crystal structure of KcsA highlighting the position of the Trp belts (orange) and Arg-27 (red). (PDB file 1K4C[53])

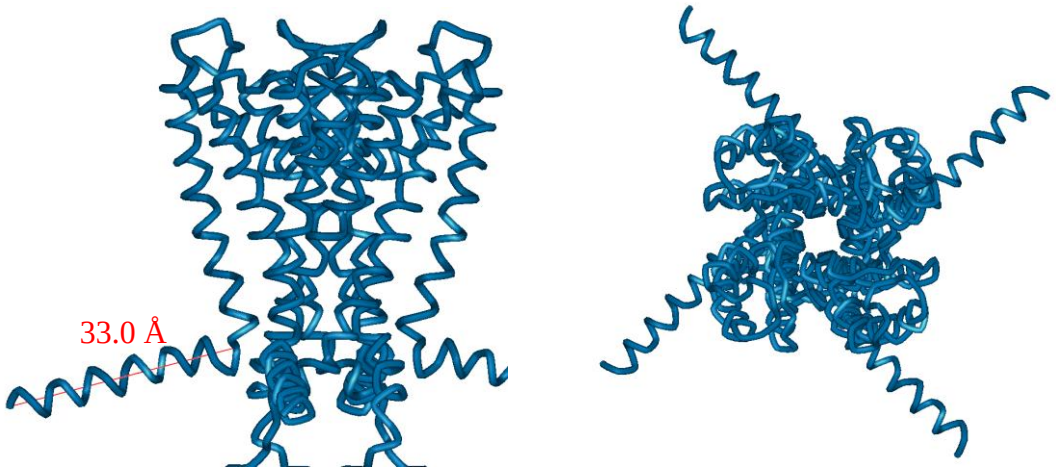

Figure 3.12 Detail of the structure of the peptide backbone of KcsA including the N-terminus. The transmembrane region (residues 23 to 119) is from the crystal structure of Doyle *et al*.[34] (PDB number 1BL8) and the N-termini (residues 5 to 22) correspond to the structure deduced from the ESR analysis of Cortes *et al*.[51] (PDB number 1F6G) Left: side view; right: top view.

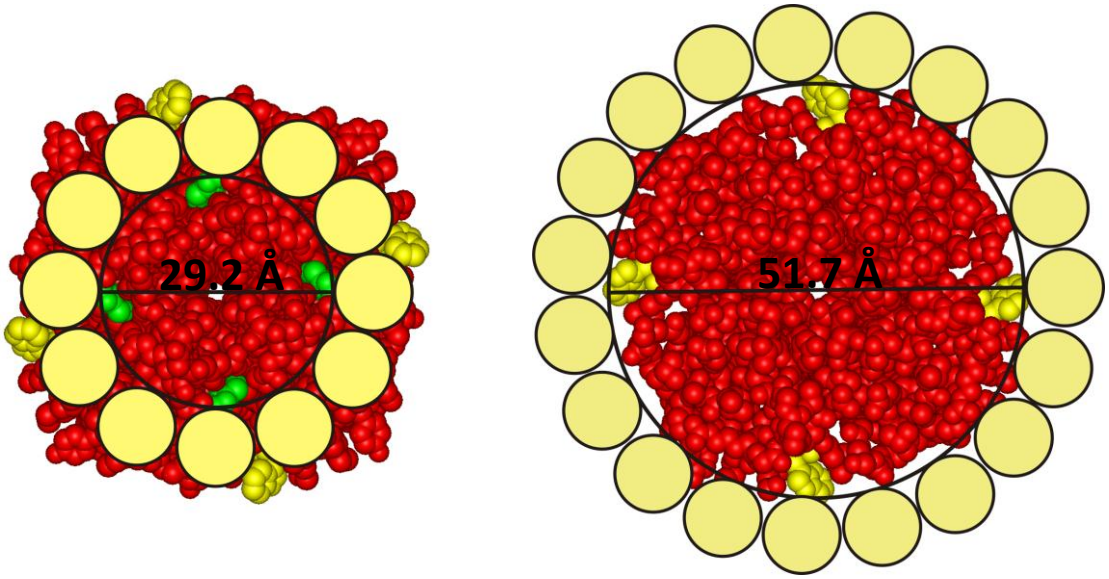

Figure 3.13 Diameter of the transmembrane region of KcsA on each side of the bilayer. Left: a view from the bottom of channel (the side that normally faces the intracellular side of the membrane). The distance between Trp-26 (green) of opposite monomers was used to estimate the diameter of the channel on its narrow side. Right: a view from the top of the channel (the side that normally faces the extracellular side of the membrane). The diameter was estimated measuring the distance between Trp-87 (yellow) of opposite monomers. In both cases (narrow side and wide side) the distances were measured between the carbons of the Trp side chains furthest apart in the crystal structure (PDB file 1K4C[53]). Lipid molecules of scaled diameter (9.6 Å) are shown as yellow circles around the protein. The total number of lipid molecules around both sides of the channel is 31, in agreement with the ESR data and the models built by Pali *et al*.[88]

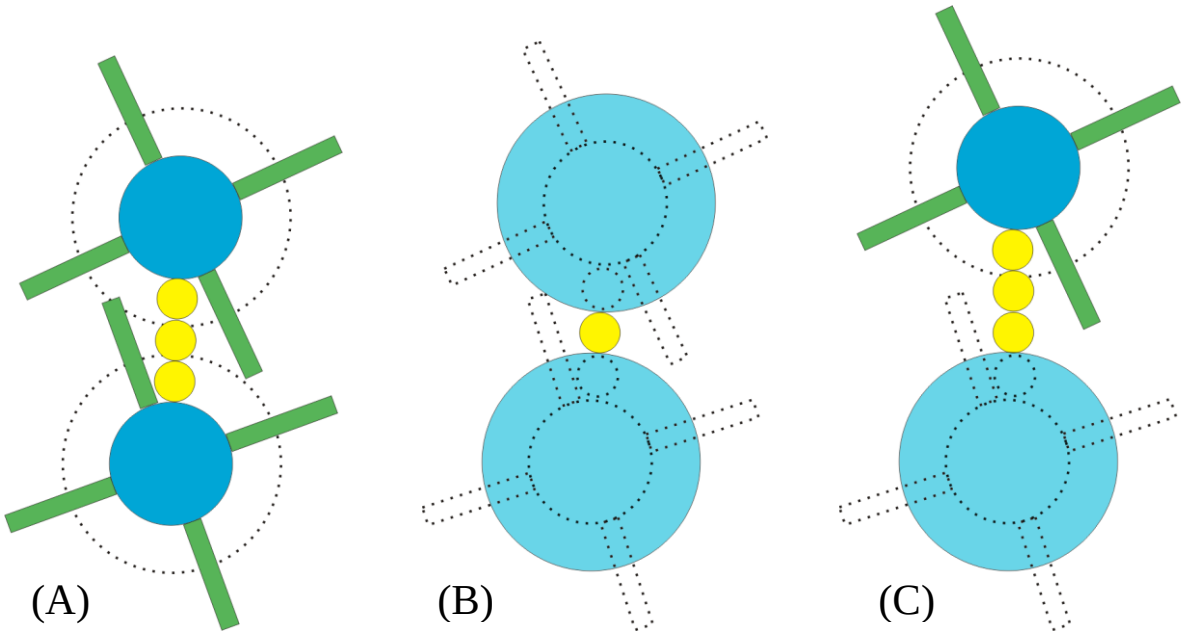

Figure 3.14 Three possible arrangements in the membrane for two channels close to each other. KcsA channels are represented by the large (wider side) and medium (narrower side) disks. The N-termini are represented as sticks protruding from the narrow side of the channel. The small yellow disks represent the lipids. All disks are scaled according to the measured diameters. The coloured elements face the viewer's side of the membrane, while the dotted lines represent the structures on the opposite side of the membrane.

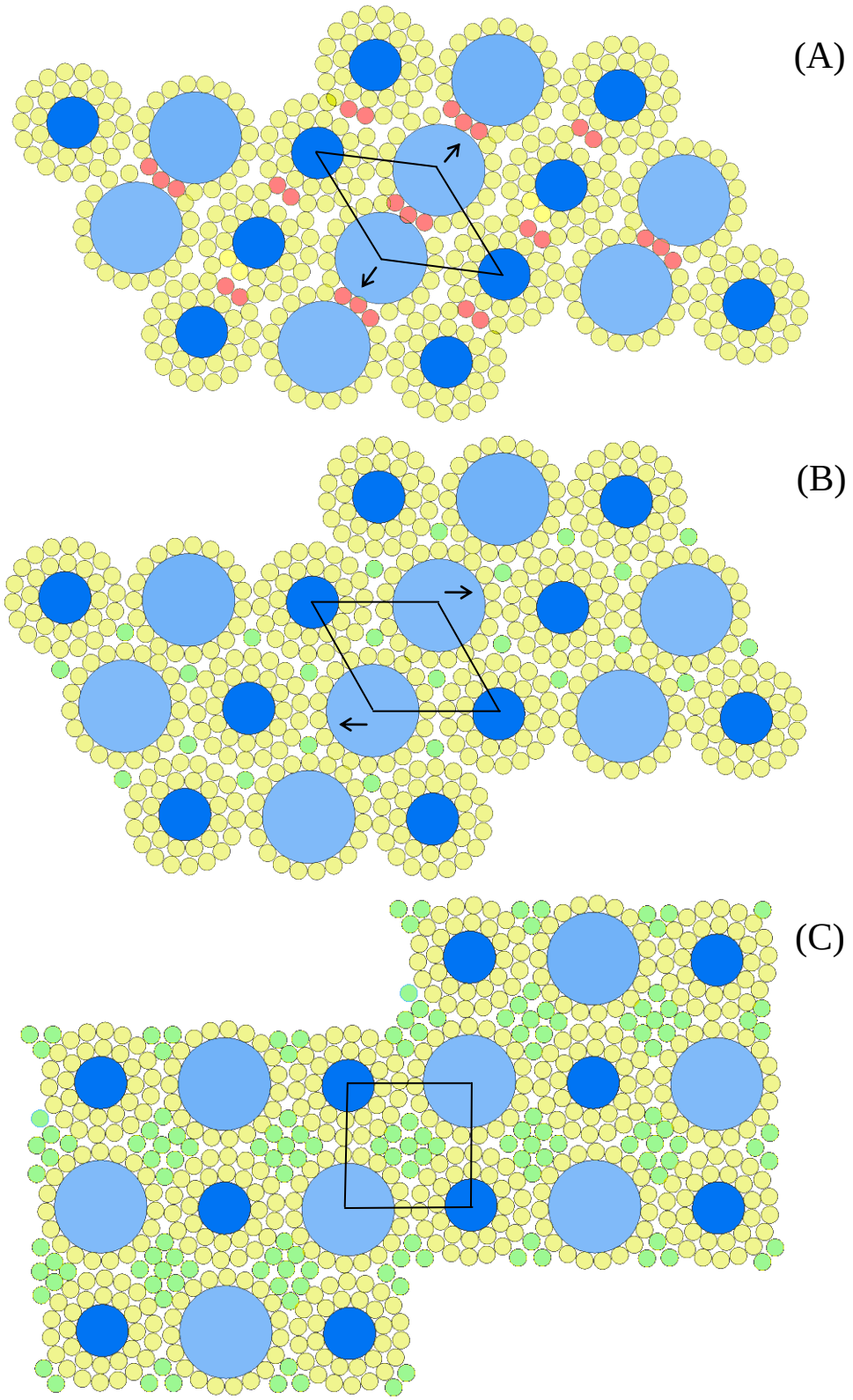

Figure 3.15 Geometrical models of lipid bilayers containing KcsA. (See figure legend on the following page.)

Figure 3.15 Geometrical models of lipid bilayers containing KcsA. The large, light blue disks represent the wide side of KcsA; the medium dark blue disks represent the narrow side of KcsA; the small yellow disks represent phospholipid molecules (in red, lipids from the first and second shells of lipid around the wide and narrow sides of the channels, respectively that are shared with neighbouring channels; in green, extra lipid molecules that do not belong to the first and second shells that are needed to fill in space in the bilayer. The black lines show a geometrical unit and the arrows indicate the changes in shape of the geometrical unit to give the model shown below. (A), (B) and (C) correspond to lipid:channel molar ratios of 44:1, 53:1 and 67:1, respectively, as described in the text.

Chapter 4: Interaction of fatty acids with KcsA: studies using fluorescence spectroscopy.

4.1 Introduction

Fatty acids, particularly polyunsaturated fatty acids, have been shown to modulate the activity of many types of potassium and other ion channels, but it is not yet certain how they act[43,44]. There are two main ways in which fatty acids could affect the activity of ion channels. One way is by changing the bulk physical properties of the membrane: the activity of membrane proteins can, for example, be affected by the fluidity or thickness of the lipid bilayer[4,22] and incorporation of fatty acids could affect such properties of the membrane and hence affect the activity of its proteins. However, this mechanism seems unlikely, because it would require large amounts of free fatty acid to be present in the lipid bilayer, and the proportion of free fatty acids in biological membranes is very low, often unmeasurable[11,96].

The second way in which fatty acids could affect ion channel activity is by direct binding to the channel. Fatty acids have been shown to be able to bind to annular sites on many membrane proteins using ESR[24,25] and fluorescence spectroscopy[97], and so these molecules could affect membrane protein function through direct interaction with the annular lipid binding sites. Less is known about the ability of fatty acids to interact with non-annular sites[32,97,98], located between the transmembrane α-helices or at protein-protein interfaces. Non-annular sites can be important for membrane protein function, and therefore it is of great interest to study interactions of fatty acids with these sites. A new type of site to which fatty acids have been recently suggested to be able to bind to regulate ion channel function is the hydrophobic inner cavity of the pore[45,46], where fatty acid molecules could block ion flux.

As described in Chapter 1, the potassium channel KcsA is an ideal model to study lipid interactions with both annular and non-annular sites. In this and the following chapter, interactions of fatty acids and uncharged fatty acid derivatives with

the different types of sites on KcsA are studied using fluorescence spectroscopy and ESR. The simple structure of fatty acids, consisting of a carboxylic acid with a long hydrocarbon chain, makes it easy to characterize their interactions with the protein. In the present chapter, fluorescence quenching of wild type KcsA and the mutant W67,68 are used to analyse the interaction of brominated fatty acids with the annular and non-annular sites of KcsA, respectively. The small R_o value of ca. 8 Å for the dibromo group[83,84] means that any binding of brominated fatty acids to the inner cavity will not result in fluorescence quenching because all the Trp residues in the channel are too distant from the cavity. Instead, binding of fatty acids to the cavity was analysed by ESR, as described in Chapter 5. The results described here for fatty acids binding at the annular and non-annular sites in KcsA will be later compared with those obtained with ESR in Chapter 5.

4.2 Methods

The samples for fluorescence quenching studies used in this chapter were prepared by mixing phospholipid and fatty acid or fatty acid derivative in organic solvent and then drying under a stream of N_2 as described in detail in Chapter 2, Section 2.2.3. In quenching curves involving mixtures of non-brominated fatty acid and DOPC (dioleoylphosphatidylcholine) and in mixtures of brominated fatty acid and DOPC, this method gave the same result as the titration method (see again Section 2.2.3), where small amounts of fatty acid are directly added to the reconstituted sample in the fluorescence cuvette. However, for quenching curves involving mixtures of non-brominated fatty acid, brominated fatty acid and DOPC the titration method was unreliable (data not shown), probably due to the large amounts of fatty acid that had to be added into the cuvette for these experiments. Details regarding protein production and purification are explained in Chapter 2, Sections 2.2.1 and 2.2.2, respectively. Tryptophan fluorescence was excited at 290 nm and the emission intensity was measured at 333 nm (see Appendix 1).

4.2.1 Analysis of partitioning of 9,10-dibromostearic acid into the lipid bilayer

Fatty acids have significant solubility in water, meaning that not all the fatty acid molecules in the system will incorporate into the lipid bilayer, some remaining in water. To study fatty acid interactions with KcsA it is necessary to know the proportion of the total fatty acid that is located in the lipid bilayer. This will depend on the concentration of the host lipid bilayer and can be described by a simple partition between water and the lipid bilayer[97]:

$$L + FA_w \rightleftharpoons L.FA \tag{4.1}$$

where L are the unoccupied binding sites in the host lipid bilayer, FA_w is the fatty acid free in water and $L.FA$ is the fatty acid incorporated into the host lipid bilayer. A dissociation constant K_d can be written for this equilibrium:

$$K_d = \frac{[L][FA_w]}{[L.FA]} \tag{4.2}$$

where the brackets denote concentrations. The meaning of K_d is complex, since partitioning of fatty acids into a lipid bilayer will introduce negative charge into the bilayer, this making the partitioning of further fatty acid into the bilayer less favourable, as a result of charge repulsion. However, these effects become small at high ionic strengths, and binding to the lipid bilayer can be defined by an effective K_d, applicable at the particular ionic strength and pH used in the experiment[97]. Considering that the total fatty acid (FA_t) is the sum of the fatty acid bound to the lipid bilayer ($L.FA$) and the free fatty acid in the aqueous media (FA_w), and assuming that the concentration of host lipid sites is in excess of the concentration of bound fatty acid, so that $[L] \approx [L_t]$, where $[L_t]$ is the total concentration of host lipid, the proportion of bound fatty acid can, from Eq. 4.2, be rewritten as:

$$\frac{[L.FA]}{[FA_t]} = \frac{[L_t]}{[L_t] + K_d} \tag{4.3}$$

From this equation it can be deduced that the higher the concentration of host lipid, the higher the proportion of fatty acid molecules partitioned into the lipid bilayer[97].

4.2.2 Analysis of fluorescence quenching with brominated lipids

How to describe binding at the annular sites.

The probability of fluorescence quenching for a membrane protein in a mixture of a lipid and its brominated form can be described in the simplest case of a protein with a single Trp residue that can be fully quenched (i.e. $F_{min} = 0$) by binding of a brominated lipid molecule close to it as follows[31,72,83]:

$$F/F_o = (1 - x_{Br})^n \tag{4.4}$$

where F_o is the fluorescence intensity in the non-brominated lipid, F is the fluorescence intensity in a given lipid mixture of brominated lipid and non-brominated lipid when the mole fraction of brominated lipid is x_{Br} and n is the number of lipid binding sites from which the fluorescence of the Trp residue can be quenched

(Figure 4.1). Depending on the structures of the lipid and the protein, the number of sites from which the brominated lipid can quench fluorescence will be different. Figure 4.2 shows the theoretical fluorescence quenching profiles for a protein in mixtures of brominated and non-brominated lipids, calculated from Eq. 4.4, as a function of the value of *n*. At a given mole fraction of brominated lipid, a higher *n* value results in stronger quenching, because the probability of a brominated molecule occupying one of the sites close enough to cause Trp quenching is high. Assuming that a brominated lipid and its non-brominated analogue have the same affinity for the lipid binding sites on the protein[31] the value of *n* can be determined by measuring the fluorescence intensity of the protein in mixtures of the brominated and non-brominated lipids and then fitting the experimental data to Eq. 4.4 to obtain *n*.

As described in Chapter 1, the annular lipid binding sites on a membrane protein are always occupied by lipid molecules that are in continuous exchange with the bulk of lipid molecules, acting like a solvent for the protein. Thus, binding of a lipid *A* and a lipid *B* at an annular site of a protein can be described in terms of a lipid exchange equilibrium (Figure 1.10). As a result, the model described above for fluorescence quenching can be extended to the case where a brominated lipid *A* and a non-brominated lipid *B* have different affinities for the annular sites in a protein[31,72,83]. In a membrane composed by the two different lipid molecules *A* and *B* an exchange equilibrium will be established at each lipid annular binding site (*P*):

$$PB + A \rightleftharpoons PA + B \tag{4.5}$$

A binding constant for the brominated lipid *A* relative to the non-brominated lipid *B* is given by:

$$K = \frac{[PA][B]}{[PB][A]} \tag{4.6}$$

from which:

$$[PA] = \frac{K[PB][A]}{[B]} \tag{4.7}$$

The fraction of sites occupied by the brominated lipid, f_{Br}, can be described as:

$$f_{Br} = \frac{[PA]}{[PA]+[PB]} = \frac{K[A]}{K[A]+[B]} \tag{4.8}$$

Because in the fluorescence experiments described here the numbers of molecules of brominated lipid *A* and non-brominated lipid *B* are much larger than the numbers of lipid binding sites, the concentration of unbound lipid *A* and *B* can be approximated by their total concentrations:

$$[A_t] = [PA] + [A] \approx [A] \tag{4.9}$$

$$[B_t] = [PB] + [B] \approx [B] \tag{4.10}$$

where $[A_t]$ and $[B_t]$ are the total concentrations of brominated lipid *A* and non-brominated lipid *B*, respectively, in the membrane. If then the concentrations are expressed in mole fraction units so that $[A_t] = x_{Br}$ and $[B_t] = (1\text{-}x_{Br})$ then Eq. 4.8 can be written as:

$$f_{Br} = \frac{[PA]}{[PA]+[PB]} = \frac{K \cdot x_{Br}}{K \cdot x_{Br} + (1 - x_{Br})} \tag{4.11}$$

Fluorescence quenching is then described by analogy with Eq. 4.4 as:

$$F / F_o = (1 - f_{Br})^n \tag{4.12}$$

The higher the binding constant *K* of the brominated lipid relative to the non-brominated lipid, the higher the probability that the brominated lipid will bind to the protein and cause quenching. Figure 4.3 shows the fluorescence quenching profiles for a protein in mixtures of brominated and non-brominated lipids calculated from Eq. 4.12 as a function of the value of *K*, with a fixed value of *n* of 1.69 (the average value of *n* for phospholipids interacting with KcsA[73]). When the *n* value for the brominated

lipid is known, it is possible to determine the relative affinities of lipids *A* and *B* for the protein by measuring tryptophan fluorescence intensities in mixtures of lipids *A* and *B* and then fitting to Eq. 4.12 to obtain *K*.

If the fluorescence of the Trp residue is not fully quenched by binding of brominated lipid, then the model needs to be modified by subtracting the residual fluorescence intensity of the protein in a membrane of fully brominated lipid (F_{min}) from the fluorescence values as follows:

$$\frac{F - F_{\min}}{F_o - F_{\min}} = (1 - f_{Br})^n \tag{4.13}$$

Rearranging terms gives the result:

$$F = F_{\min} + (F_o - F_{\min})(1 - f_{Br})^n \tag{4.14}$$

How to describe binding at the non-annular sites

There are two ways of describing binding of lipid molecules at the non-annular sites. One way is describing binding by a competitive model similar to that described above for the annular sites, where in a mixture of lipids *A* and *B*, the non-annular sites are occupied either lipid *A* or *B*. An alternative way to describe binding at the non-annular sites is by a simple binding model. If only one of the lipid species in the membrane is able to bind to the non-annular sites, for example lipid *A* (Figure 1.10), then:

$$P + A \rightleftharpoons PA \tag{4.15}$$

from which a binding constant K_b^* is described as:

$$K_b^* = \frac{[PA]}{[P][A]} \tag{4.16}$$

In such a situation, assuming again that [*A*] >>> [*PA*] the mole fraction of non-annular sites occupied by the brominated lipid *A* becomes:

$$f_{Br}^{*} = \frac{x_{Br}}{x_{Br} + \left(\frac{1}{K_b^{*}}\right)} \tag{4.17}$$

and fluorescence quenching is then defined by analogy with Eq. 4.14 as:

$$F = F_{\min} + (F_o - F_{\min})(1 - f_{Br}^{*})^n \tag{4.18}$$

Here, both Eq. 4.14 and Eq. 4.18 are applied to the experimental data obtained with the mutant W67,68, in mixtures of 9,10-dibromostearic acid and DOPC in order to compare the two models. A key difference between the two models is that in the competitive model the non-annular site will be always fully occupied, so that in a membrane containing only brominated lipid *A*, quenching will be maximum. This can be easily deduced from Eq. 4.11 as when the mole fraction of brominated lipid in the membrane, x_{Br}, is one, the fraction of brominated lipid bound at the site/s (f_{Br}) also becomes one, giving $F = F_{min}$ in Eq. 4.14. In contrast, in the simple binding model, if the affinity of the brominated lipid for the non-annular sites is not high enough (i.e. the K^{*}_{b} value is not much greater than 1 so that $1/K_b^{*} \approx 0$) then not all sites will be occupied in a membrane of brominated lipid (i.e. f^{*}_{Br} will be smaller than 1 even at $x_{Br} = 1$), and so the F_{min} value (which by definition predicts the fluorescence when the sites are fully occupied) will be smaller than the fluorescence value in bilayers at $x_{Br} = 1$. On the basis of these differences between the two models, it will be shown in the results section that fluorescence quenching with the mutant W67,68 follow a competitive binding model, and so the analysis for determination of the *n* value for fatty acids described below will be based on a competitive binding model when describing binding to both the non-annular and the annular sites.

Determination of the *n* value for fatty acids

The value of *n* for 9,10-dibromostearic acid cannot be determined from quenching of KcsA in mixtures of oleic acid and 9,10-dibromostearic acid alone

simply because fatty acids do not form bilayers on their own. Here, an alternative approach was used to determine the value of *n* for 9,10-dibromostearic acid for wild type KcsA and the W67,68 mutant.

First, the fluorescence intensity of KcsA (wild type and mutant W67,68) was measured in mixtures of oleic acid and 9,10-dibromostearic acid with DOPC containing a fixed molar ratio of total fatty acid to DOPC but varying the molar ratio of oleic acid to 9,10-dibromostearic acid. In these experiments, the fraction of sites occupied by 9,10-dibromostearic acid (f_{BrFA}) is then the product of the fraction of sites occupied by total fatty acid (oleic acid and 9,10-dibromostearic acid, f_{FA}) and the mole fraction of total fatty acid that is 9,10-dibromostearic acid (x_{BrFA}):

$$f_{\mathrm{BrFA}} = f_{FA} \cdot x_{BrFA} \tag{4.19}$$

In these experiments, by analogy with Eq. 4.11, f_{FA} is given by:

$$f_{FA} = \frac{K \cdot x_{FA}}{K \cdot x_{FA} + (1 - x_{FA})} \tag{4.20}$$

where x_{FA} is the mole fraction of total fatty acid in the membrane (which is constant) and K is the binding constant of fatty acid relative to DOPC. The measured fluorescence intensities in these type of experiments were then fitted for the KcsA mutant W67,68 to:

$$F = F_{\min} + (F_o - F_{\min})(1 - f_{FA} \cdot x_{BrFA})^n \tag{4.21}$$

For experiments with wild type KcsA, the equation used for fitting was more complex as described below (Eq. 4.25). To obtain *n* from Eq. 4.21 (or Eq. 25, see below) it is necessary to know *K*. These results were therefore combined with a second set of experiments.

In this second set of experiments, fluorescence quenching of KcsA (wild type and mutant W67,68) was measured in mixtures containing variable amounts of 9,10-

dibromostearic acid and DOPC. The data in these experiments could then be fitted to Eq. 4.14 for the mutant, and to Eq. 4.22 (again, see below) for wild type KcsA to give a value for *K* if the value for *n* was known.

Since in both sets of experiments *n* and *K* are unknown, an iterative fitting procedure was used. A starting value of *n* of 1 (a reasonable value within the range of *n* values normally observed) was taken to perform the first fit of the data for mixtures of 9,10-dibromostearic acid and DOPC to Eq. 4.14/4.22 (mutant W67,68/wild type KcsA), in order to obtain a first estimate of *K*. The obtained value of *K* was then used to calculate the fraction of sites occupied by brominated fatty acid from Eq. 4.20, and then this was used in Eq. 4.21/4.25 (mutant W67,68/wild type KcsA) to fit the data for mixtures of 9,10-dibromostearic acid, oleic acid and DOPC to obtain a value for *n*, which in turn was then used for a new fit to Eq. 4.14/4.22 to obtain a new value for *K* and so on, until successive iterations gave the same values of *n* and *K*.

Analysis of fluorescence quenching of wild type KcsA

Fluorescence quenching of wild type KcsA is more complex than for the mutant W67,68 (Eq. 4.14), because wild type KcsA contains five Trp residues in each monomer, of which four can be quenched by brominated lipids. As detailed in Chapter 1, Section 1.5.5, three of these Trp residues (W26, W87 and W113) are exposed to the lipid bilayer, and can be quenched by brominated lipid molecules binding to the annular sites, while the other two Trp (W67 and W68) are hidden within the structure of the channel with only W67 being quenched by binding of brominated lipid molecules at the non-annular sites (Figure 1.18). As a result, quenching of wild type KcsA is dominated by quenching of the lipid exposed Trp residues, but will also be affected by quenching of W67 by binding of brominated lipids at the non-annular sites. Assuming that all Trp residues have equal unquenched fluorescence intensities and that the three lipid-exposed Trp residues are equivalent[74], Eq. 4.14 can be modified to account for the different tryptophan residues as follows:

$$F = \frac{1 + 3F_{\min}^{A} + F_{\min}^{NA} + 3(1 - F_{\min}^{A})(1 - f_{Br}^{A})^{n_A} + (1 - F_{\min}^{NA})(1 - f_{Br}^{NA})^{n_{NA}}}{5} \qquad (4.22)$$

where $F^{A}_{\min}$ and $F^{NA}_{\min}$ are the residual fluorescence intensities for each of the three lipid exposed Trp residues and for W67, respectively, in a membrane of brominated lipid, f^{A}_{Br} and f^{NA}_{Br} are the fractions of annular and non-annular sites occupied by brominated phospholipid from which quenching of the lipid exposed tryptophans and W67 occurs, respectively, and n^{A} and n^{NA} are the number of annular and non-annular sites, respectively, from which the fluorescence of the respective Trp residues can be quenched. The value of n^{A} will be an average value for the three lipid exposed Trp residues. By analogy with Eq. 4.11, f^{A}_{Br} and f^{NA}_{Br} are described by:

$$f_{Br}^{A} = \frac{K^{A} \cdot x_{Br}}{K^{A} \cdot x_{Br} + (1 - x_{Br})} \tag{4.23}$$

$$f_{Br}^{NA} = \frac{K^{NA} \cdot x_{Br}}{K^{NA} \cdot x_{Br} + (1 - x_{Br})} \tag{4.24}$$

where K^{A} and K^{NA} are the relative lipid binding constants at the annular and non-annular sites, respectively. As for n^{A}, the value of K^{A} is an average for the sites corresponding to the three lipid exposed Trp residues.

Fluorescence quenching data obtained in mixtures of 9,10-dibromostearic acid and DOPC for wild type KcsA were therefore fitted to Eq. 4.22, using the values of n^{NA} and K^{NA} obtained with the mutant W67,68. A value of $F^{NA}_{\min} = 0$ was used as the experimental data showed quenching of W67 by 9,10-dibromostearic acid to be ca. 100 % efficient.

For experiments with varying amounts of oleic acid and 9,10-dibromostearic acid at a fixed molar ratio of total fatty acid to DOPC (see previous section) a similar model to that of Eq. 4.22 was used, with the relations described in Eq. 4.19 and 4.20 incorporated as follows:

$$F = \frac{1 + 3F^{A}_{\min} + F^{NA}_{\min} + 3(1 - F^{A}_{\min})(1 - f^{A}_{FA} \cdot x_{BrFA})^{n_A} + (1 - F^{NA}_{\min})(1 - f^{NA}_{FA} \cdot x_{BrFA})^{n_{NA}}}{5} \tag{4.25}$$

By analogy with Eq. 4.20, f^{A}_{FA} and f^{NA}_{FA}, are described by:

$$f_{FA}^{A} = \frac{K^{A} \cdot x_{FA}}{K^{A} \cdot x_{FA} + (1 - x_{FA})} \tag{4.26}$$

$$f_{FA}^{NA} = \frac{K^{NA} \cdot x_{FA}}{K^{NA} \cdot x_{FA} + (1 - x_{FA})} \tag{4.27}$$

where x_{FA} is the mole fraction of total fatty acid in the membrane (which is constant for each quenching curve) and K^{A} and K^{NA} are the fatty acid binding constants relative to DOPC at the annular and non-annular binding sites, respectively.

Alternative descriptions for binding of fatty acids and phospholipids to membrane proteins

As will be described in Section 4.3.2, data for 9,10-dibromostearic acid quenching at the non-annular sites fits to a value of *n* very close to one, as observed for brominated phosphatidylglycerol (BrPG)[13], consistent with either a single fatty acid or a single phospholipid molecule binding to the site. However, the *n* value determined for quenching at the annular sites is ca. 4 (Section 4.3.3), about double that for a phospholipid molecule (1.69)[73]. This suggests two fatty acids could bind at each phospholipid binding site in the annulus, consistent with the fact that the phospholipid molecule contains two acyl chains. In this case, it might be thought that competitive binding at the annular sites should be described as:

$$P.L \; + \; 2FA \; \rightleftharpoons \; P.FA_2 \; + \; L \tag{4.28}$$

where *FA* is the fatty acid, *L* the phospholipid and *P* the annular binding site, giving an exchange equilibrium:

$$K' = \frac{[P.FA_2][L]}{[P.L][FA]^2} \tag{4.29}$$

and the fraction of sites occupied by fatty acid would then be:

$$f_{FA}^{'} = \frac{[P.FA_2]}{[P.FA_2]+[P.L]} = \frac{K^{'} \cdot x^2}{(1-x)+K \cdot x^2} \tag{4.30}$$

where x is the mole fraction of fatty acid in the bilayer. However, the squared dependence on x would result in a cooperative quenching binding curve, which is clearly not observed in the experimental data (see Section 4.3.3). Indeed, binding of lipid molecules to the annular sites of a membrane protein is better described as an interaction of the lipid molecules with a general hydrophobic surface that needs to be solvated, and not as an interaction with a set of distinct and localised binding sites. Lipid molecules binding to a hydrophobic surface with non-localised sites could move along the surface from one site to another[99], allowing a single fatty acid molecule to bind and displace a phospholipid molecule located in a particular region of the surface without the need of two fatty acid molecules to displace the phospholipid molecule in that particular location. Hence, the fluorescence quenching experiments described here with fatty acids and phospholipids are analysed in terms of an exchange between single molecules (Eq. 4.5).

However, it could still be argued that because the phospholipid molecules that compose the lipid bilayer into which the fatty acid incorporates have two fatty acyl chains, the effective concentration of fatty acid molecules, which only have a single acyl chain, in a phospholipid bilayer, is smaller than that of phospholipid molecules, meaning that the probability of a phospholipid molecule coming into contact with the protein is greater than that of a fatty acid molecule. To account for this effect the concentrations of the two lipids could be expressed on an acyl chain basis[97,100]. And so, if each phospholipid molecule contributes two acyl chains, while a fatty acid molecule contributes only one acyl chain, the effective mole fraction of fatty acid in the membrane on a chain basis (x^c) would be:

$$x^c = \frac{[FA]}{[FA]+2[L]} \tag{4.31}$$

where [*FA*] is the concentration of fatty acid molecules and [*L*] is the concentration of phospholipid molecules. If then one considers that the mole fraction of fatty acid on a conventional molecular basis (x) is expressed as:

$$x = \frac{[FA]}{[FA]+[L]} \tag{4.32}$$

it can be deduced from Eq. 4.32 that, when considering mole fractions on a molecular basis:

$$[L] = [FA]\frac{(1-x)}{x} \tag{4.33}$$

and so substituting [*L*] from Eq. 4.33 (molecular basis) into Eq. 4.31 (chain basis), the mole fraction of fatty acid on a chain basis (x^c) can be related to the mole fraction of fatty acid on a molecular basis (x) as follows:

$$x^c = \frac{[FA]}{[FA]+2[FA]\frac{(1-x)}{x}} \tag{4.34}$$

The expression above can be rearranged to give:

$$x = \frac{2x^c}{1+x^c} \tag{4.35}$$

It is then possible to determine how expressing the concentration of fatty acid on a chain basis will affect the analysis of fluorescence quenching. Previously it had been shown that the fraction of sites occupied by brominated lipid (f_{Br}) could be described by Eq. 4.11 (when concentrations are expressed in mole fraction units, x_{Br}) as shown again here for clarity:

$$f_{Br} = \frac{[PA]}{[PA]+[PB]} = \frac{K \cdot x_{Br}}{K \cdot x_{Br} + (1-x_{Br})} \tag{4.11}$$

If the brominated molecule is a fatty acid and the mole fraction of brominated fatty acid (x_{Br}) is expressed on a chain basis then, using Eq. 4.35:

$$f_{Br} = \frac{K\left(\frac{2x^c_{Br}}{1+x^c_{Br}}\right)}{K\left(\frac{2x^c_{Br}}{1+x^c_{Br}}\right)+1-\left(\frac{2x^c_{Br}}{1+x^c_{Br}}\right)} = \frac{2K \cdot x^c_{Br}}{2K \cdot x^c_{Br} + (1-x^c_{Br})} \qquad (4.36)$$

where x^c_{Br} is the mole fraction of brominated fatty acid on a chain basis. It can be seen that the form and terms of Eq. 4.36 are equivalent to those of Eq. 4.11, the only difference being K in Eq. 4.11 is now replaced by $2K$. Hence, if the mole fraction of fatty acid in the membrane is expressed on a chain basis, the value of K obtained will be double the value obtained if the mole fraction is expressed on a conventional molecular basis.

In this chapter the fluorescence quenching data with 9,10-dibromostearic acid is analysed expressing the mole fraction of fatty acid on a conventional molecular basis. However, the consequences of expressing the mole fraction of fatty acid on a chain basis instead are discussed later.

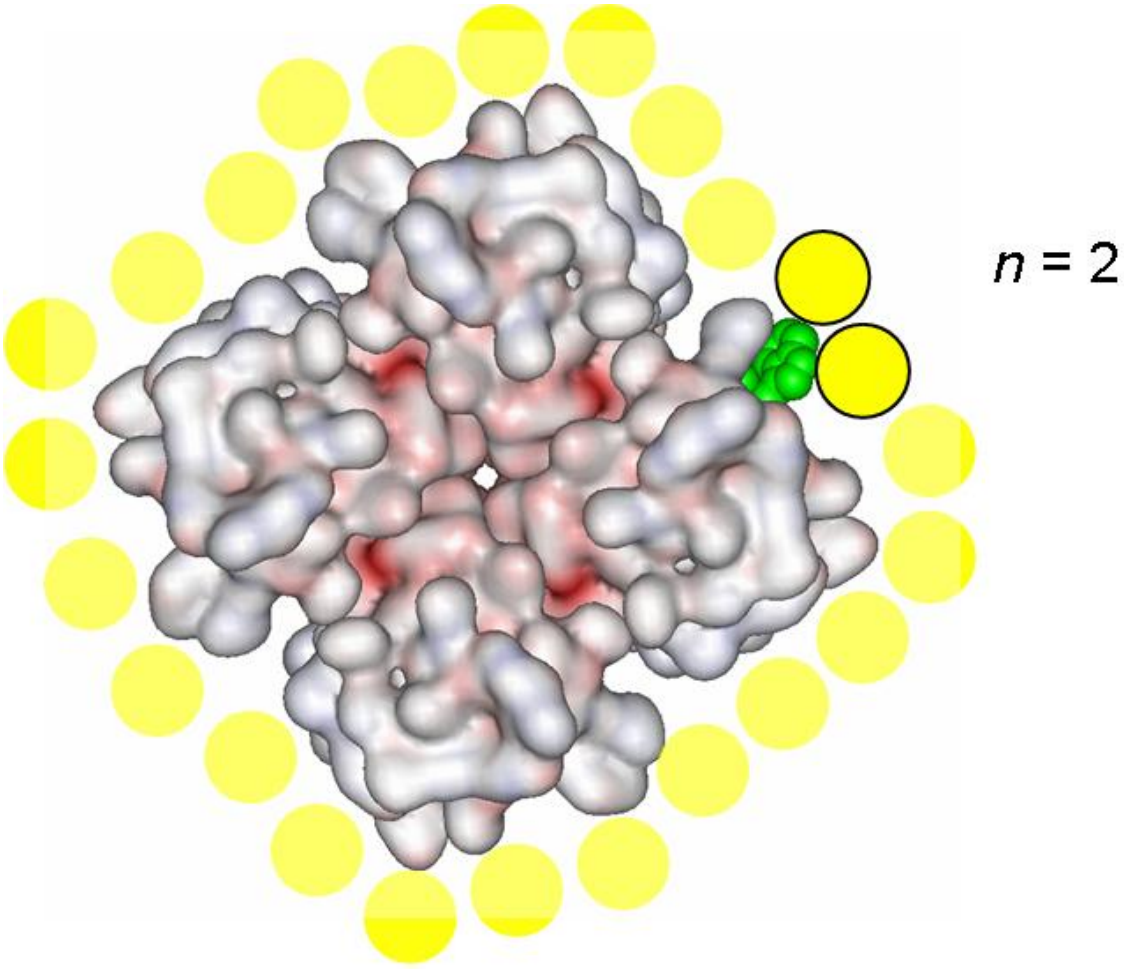

Figure 4.1 Example of lattice sites from which brominated lipids can cause quenching of Trp fluorescence in a protein. The image shows KcsA surrounded by lipids (yellow circles) viewed from the extracellular side of the membrane. A Trp residue is highlighted in green, in this case it is suggested that brominated lipid molecules can bind at two different positions (lipids highlighted in bright yellow with a black border) close enough to the Trp residue to cause fluorescence quenching. The *n* number in Eq. 4.4 indicates the number of sites that can be occupied by a brominated lipid close enough to a Trp residue to cause quenching; in this example $n = 2$.

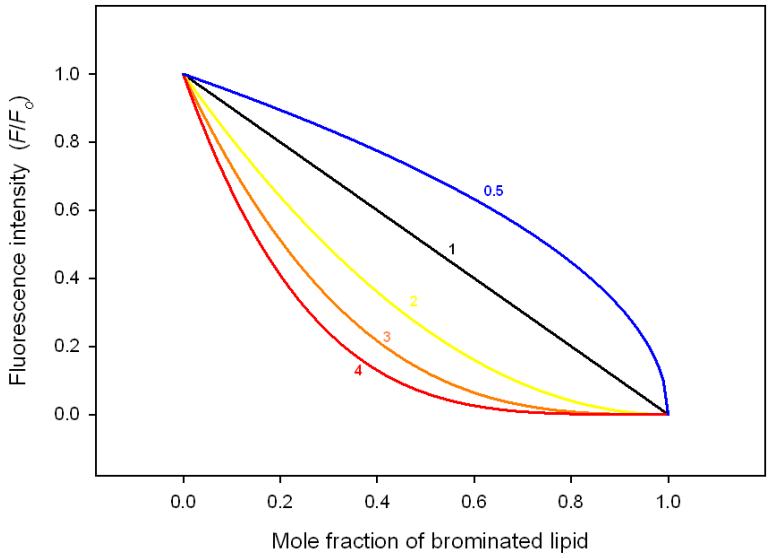

Figure 4.2 Theoretical curves for fluorescence quenching of a protein in mixtures of brominated and non brominated lipids as described by Eq. 4.4. Fluorescence intensities are plotted as a function of the mole fraction of brominated lipid. Each line represents a simulation of the fluorescence emission intensity with the value for *n* given above each curve and assuming Trp fluorescence is 100 % quenched in a bilayer of brominated lipid.

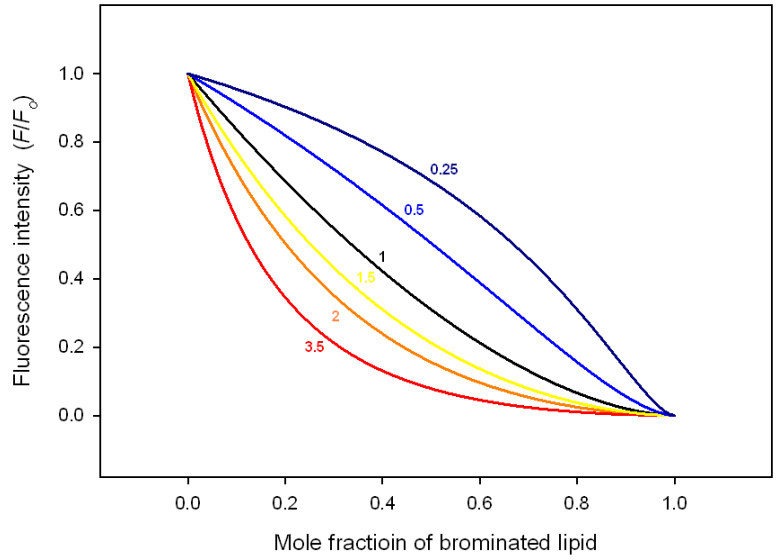

Figure 4.3 Theoretical curves for fluorescence quenching of a protein in mixtures of brominated and non brominated lipids as described by Eq. 4.12, at a fixed *n* value of 1.69. Fluorescence intensities are plotted as a function of the mole fraction of the brominated lipid. Each line represents a simulation of the fluorescence emission intensity with the given value for *K*, indicated on the respective curves and assuming Trp fluorescence is 100 % quenched in a bilayer of brominated lipid. The value for *n* was fixed at 1.69, which is the average value for a phospholipid molecule binding to KcsA[73].

4.3 Results

4.3.1 Partitioning of 9,10-dibromostearic acid into the lipid bilayer: studies of quenching of the fluorescence of wild type KcsA

As discussed in Section 4.2.1, fatty acids have a significant solubility in water, and so in order to study fatty acid interactions with KcsA using 9,10-dibromostearic acid, it is necessary to analyse the proportion of fatty acid that is being incorporated into the lipid bilayer. As explained in Section 4.2.1, the concentration of host lipid affects the proportion of fatty acid that incorporates into the bilayer, so that at low concentrations of host lipid, a significant fraction of the fatty acid present in the system may be in the aqueous phase, but at a sufficiently high concentration of host lipid, most of the fatty acid should be present in the lipid bilayer. Figure 4.4A shows fluorescence quenching curves for KcsA in DOPC with 9,10-dibromostearic acid at DOPC (host lipid) concentrations of 30 μM, 300 μM and 600 μM. The DOPC to KcsA tetramer ratio was 400:1 for the experiment at 30 μM DOPC and 4000:1 for the experiments at 300 μM and 600 μM DOPC. Fluorescence intensities are plotted as a function of the mole fraction of 9,10-dibromostearic acid. As shown, the level of quenching observed at a given mole fraction of 9,10-dibromostearic acid is less at 30 than at 300 μM lipid, but is the same at 300 and 600 μM. Thus at 30 μM lipid, a significant fraction of the 9,10-dibromostearic acid has not partitioned into the bilayer, but at 300 μM all the brominated fatty acid has partitioned into the bilayer, as shown by the fact that no additional quenching is observed when the lipid concentration is increased to 600 μM.

These results are consistent with the equation described in Section 4.2.1. An effective K_d value of 17 μM has been obtained experimentally for oleic acid in egg PC bilayers at pH 7.2 and a 100 mM NaCl concentration[97]; with this value for K_d, assuming that 9,10-dibromostearic acid has the same K_d as oleic acid, the estimated amount of 9,10-dibromostearic acid incorporated into the bilayer, when the host lipid concentration is 30 μM, is 64 %, while if the host lipid concentration is 300 μM and 600 μM the bound 9,10-dibromostearic acid is 95 % and 97 %, respectively. If this analysis is correct, then the quenching curve observed at 30 μM host lipid should be the same as that observed at 300 μM if account is taken of the fact that only 64 % of the added fatty acid is bound. Indeed, if the mole fraction of membrane bound fatty

acid is calculated at 30 μM lipid then the quenching profile becomes almost identical to that observed at 300 μM lipid (Figure 4.4B). This suggests that the K_d values for oleic acid and 9,10-dibromostearic acid are similar.

4.3.2 Binding to non-annular lipid binding sites on KcsA

Binding of 9,10-dibromostearic acid at the non-annular sites was first analysed in terms of a competitive binding model, where the annular sites are occupied either by fatty acid or DOPC. The *n* value and binding constant of 9,10-dibromostearic acid relative to DOPC at the non-annular sites were therefore determined for the mutant W67,68 as described in Section 4.2.2. Figure 4.5 shows the fluorescence quenching curve for mutant W67,68 in mixtures of 9,10-dibromostearic acid and DOPC. At increasing concentrations of 9,10-dibromostearic acid fluorescence quenching increases, demonstrating binding of the fatty acid at the non-annular sites. Figure 4.5 also shows the fluorescence intensity of the mutant in mixtures of oleic acid and DOPC. It can be seen that oleic acid also causes some quenching of fluorescence, although the level of quenching is less than that caused by the brominated fatty acid. Oleic acid has been shown previously to be a quencher of Trp fluorescence because of its carboxyl group[97]. In the experiments reported here, what is important is the quenching due to the bromine atoms in 9,10-dibromostearic and so the data were corrected by taking the ratio of the fluorescence in 9,10-dibromostearic acid to that in oleic acid at the same mole fraction of fatty acid. To calculate the *n* and *K* values for the fatty acid, the corrected version of the curve was fitted to Eq. 4.14 in the iterative process detailed in Section 4.2.2 along with fitting of the data from the experiments described below.

Fluorescence quenching in bilayers containing varying amounts of oleic acid and 9,10-dibromostearic acid in DOPC membranes at a fixed total fatty acid to DOPC molar ratio of 2:1 is shown in Figure 4.6A. In this case, fluorescence quenching by the carboxyl group did not need to be accounted for because the fraction of total fatty acid was the same in the different lipid mixtures and so changes in fluorescence intensity were due only to quenching by the bromine atoms. Iterative fittings of the data presented in Figure 4.6A to Eq. 4.21 along with the fitting of the corrected data in Figure 4.5 to Eq. 4.14, as described in Section 4.2.2, gave a value of $n = 0.94 \pm 0.19$

and K = 0.86 ± 0.08. The value of n is consistent with a single oleic acid molecule binding at a non-annular site to quench fluorescence of W67. The data for the 9,10-dibromostearic acid/DOPC mixtures gave an F_{min} value of 0.43 ± 0.03, indicating that in a hypothetical bilayer of 9,10-dibromostearic acid about 55 % of the total Trp fluorescence would be quenched. This value for F_{min} is consistent with the expected extensive quenching of W67 with little quenching of W68. Similarly, fitting of the 9,10-dibromostearic acid/oleic acid/DOPC data to Eq. 4.21 gave an F_{min} value of 0.61 ± 0.05, again suggesting extensive quenching of W67 with little quenching of W68.

Figure 4.6 also shows quenching curves for the mutant W67,68 with varying amounts of oleic acid and 9,10-dibromostearic acid at fixed total fatty acid to DOPC molar ratios of 1:1 (Figure 4.6B) and 0.5:1 (Figure 4.6C). In these cases, the amount of fatty acid in the membrane is smaller than in the previous example (total fatty acid to DOPC ratio of 2:1), giving lower levels of quenching resulting in less accurate determinations of the n and K values. For the quenching curve with a total fatty acid to DOPC ratio of 1:1, a free fit to Eq. 4.21 with a value of K of 0.86 (as determined above) gives an n value of 1.79 ± 0.18, approximately double the value of 0.94 ± 0.19 obtained previously, with an F_{min} value of 0.68 ± 0.02. However, fitting the data with fixed values of K = 0.86 and n = 0.94 also gives a good fit (red line), with a value of F_{min} of 0.50 ± 0.01 in better agreement with the expected value. For the quenching curve at a total fatty acid to DOPC molar ratio of 0.5 to 1, a free fit to Eq. 4.21 with K = 0.86 gives n = 0.57 ± 0.62 and F_{min} = 0.21 ± 0.77. The large errors for n and F_{min} highlight the problems of analysing data where the level of quenching is low. A fit of the data with fixed K = 0.86 and n = 0.94 (red line) shows a fit equally good as the free fit, with an F_{min} value of 0.49 ± 0.01, also in good agreement with the previous values. Thus the lower quenching values obtained at fatty acid to DOPC molar ratios of 1:1 and 0.5:1 make it difficult to obtain accurate n and K values, but the data are consistent with the n and K values obtained at the a 2:1 fatty acid to DOPC molar ratio.

The corrected fluorescence quenching data shown in Figure 4.5 in mixtures of 9,10-dibromostearic acid and DOPC was also fitted to the simple binding model proposed in Section 4.2.2 (Eq. 4.17 and 4.18) in which simple binding of the fatty acid to the non-annular sites was assumed, the site not being occupied by DOPC

(Figure 4.7). The experimental data did not give a good fit to this model, a free fit to Eq. 4.18 with a value for n = 0.94 (Figure 4.7, blue) gave a binding constant K_b^* = 0.03 ± 0.15 mole fraction^{-1}, which indicates a very low affinity of the fatty acid for the non-annular sites, with a physically impossible negative value for $F_{\min}$ of -17 ± 84. The low value of K_b^* implies that a large proportion of binding sites would be empty in a hypothetical membrane of 9,10-dibromostearic acid (e.g. at a mole fraction of 9,10-dibromostearic acid of one, the mole fraction of occupied sites would be only 0.03) and so the impossibly large negative value of $F_{\min}$ is necessary to fit the observed level of quenching. If the fitting is performed with the $F_{\min}$ value restricted to be equal to or above 0, then a value of K_b^* = 1.35 ± 1.12 mole fraction^{-1} with a value for $F_{\min}$ of 0.0 ± 0.6 are obtained, but clearly the fit is poor (Figure 4.7, red). Further, if the fit is performed with a fixed F_{min} value of 0.5, as expected for extensive quenching of W67 and weak quenching of W68, the fit becomes substantially poorer (Figure 4.7, green) giving K_b^* = 2.17 ± 2.12 mole fraction^{-1} and F_{min} = 0.5 ± 0.2.

Fluorescence quenching with the uncharged fatty acid analogues 9,10-dibromomethyl stearate and 9,10-dibromostearoyl alcohol was also studied. Quenching by oleyl alcohol was small, but significant (Figure 4.8) and fluorescence quenching by 9,10-dibromostearoyl alcohol, corrected for the quenching effect of oleyl alcohol, revealed very limited quenching attributable to the bromine atoms, as shown in Figure 4.8. The data suggests very little binding of 9,10-dibromostearoyl alcohol to the non-annular sites. Quenching by 9,10-dibromomethyl stearate was also very low, also suggesting poor binding of 9,10-dibromomethyl stearate to the non-annular sites (Figure 4.9). Figure 4.9 compares quenching with 9,10-dibromostearic acid, 9,10-dibromoleoyl alcohol and 9,10-dibromomethyl stearate.

4.3.3 Binding of fatty acids to annular lipid binding sites on KcsA

Binding to the annular sites on KcsA was studied with the wild type protein performing similar fluorescence quenching experiments to those described above. In this case, as explained in Section 4.2.2, the data from mixtures of 9,10-dibromostearic acid and DOPC were fitted to Eq. 4.22, the data being corrected for fluorescence quenching by oleic acid (Figure 4.10); the data from membranes containing varying amounts of oleic acid and 9,10-dibromostearic acid in a fixed total fatty acid to DOPC

molar ratio of 2:1 were fitted to Eq. 4.25 (Figure 4.11A). In both cases the parameters used for describing binding at the non-annular sites were those determined above (n^{NA} = 0.94, K^{NA} = 086 and F^{NA}_{min} = 0, as practically all fluorescence from W67 was being quenched). Iterative fittings of the data gave a binding constant for the fatty acid relative to DOPC at the annular sites of K^{A} = 0.73 ± 0.04, very similar to that at the non-annular sites; the resulting n value was n^{A} = 4.33 ± 0.20, slightly more than double that for a phospholipid molecule (n = 1.69)[73]; and a value of F^{A}_{min} = 0.27 ± 0.01 was obtained, indicating that about 70 % of the fluorescence from the lipid exposed tryptophan residues is effectively quenched by the brominated fatty acid.

Fluorescence quenching in membranes containing mixtures of oleic acid and 9,10-dibromostearic acid were also studied at fixed total fatty acid to DOPC molar ratios of 1:1 (Figure 4.11B) and 0.5:1 (Figure 4.11C). As for W67,68 the values for n^{A} and K^{A} determined at fatty acid to DOPC molar ratio of 2:1 fit well to the data at molar ratios of total fatty acid to DOPC of 1:1 and 0.5:1 (Figure 4.11, red lines).

Fluorescence quenching with the brominated uncharged fatty acid analogues was small (Figure 4.12), showing weak binding at the annular sites. Quenching by oleyl alcohol was insignificant, and so quenching by 9,10-dibromostearoyl alcohol did not need to be corrected. The fluorescence quenching data obtained with 9,10-dibromostearoyl alcohol was fitted to Eq. 4.22 (Figure 4.12): the value of n at the annular sites was expected to be the same as that for oleic acid, since quenching of the mutant W67,68 by 9,10-dibromostearoyl alcohol is insignificant, its relative binding constant at the non-annular sites must be low and so was set to zero. Thus the quenching data with 9,10-dibromostearoyl alcohol for wild type KcsA was fitted to Eq. 4.22 with K^{NA} = 0, and n^{A} = 4.33. The fit gives a relative binding constant for 9,10-dibromostearoyl alcohol of K^{A} = 0.34 ± 0.01, with an F^{A}_{min} value of 0.30 ± 0.11 in agreement with the value obtained previously for 9,10-dibromostearic acid.

Fluorescence quenching with 9,10-dibromomethyl stearate was very similar to that observed with brominated oleyl alcohol, up to a mole fraction of 9,10-dibromomethyl stearate of 0.33, suggesting that the relative binding constant for 9,10-dibromomethyl stearate is very similar to that of 9,10-dibromostearoyl alcohol (Figure 4.12). However, the levels of fluorescence quenching observed at mole fractions of

9,10-dibromomethyl stearate of 0.33, 0.5 and 0.67 are all very similar. This suggests that the lipid bilayer might be saturating with 9,10-dibromomethyl stearate so that at higher concentrations, the 9,10-dibromethyl stearate, rather than forming a homogeneous mixture with the phospholipid, could be forming a separate phase within the bilayer, or might not be incorporating into the lipid bilayer at all. Indeed, Smaby and Brockman[101] have reported a miscibility limit for methyl oleate in PC monolayers at a mole fraction of methyl oleate of 0.2. The data for 9,10-dibromomethyl stearate were not therefore fitted to Eq. 4.22, but the data shown in Figure 4.12 would suggest that the binding constant for 9,10-dibromomethyl stearate should be similar to that for 9,10-dibromostearoyl alcohol, and less than that for 9,10-dibromostearic acid.

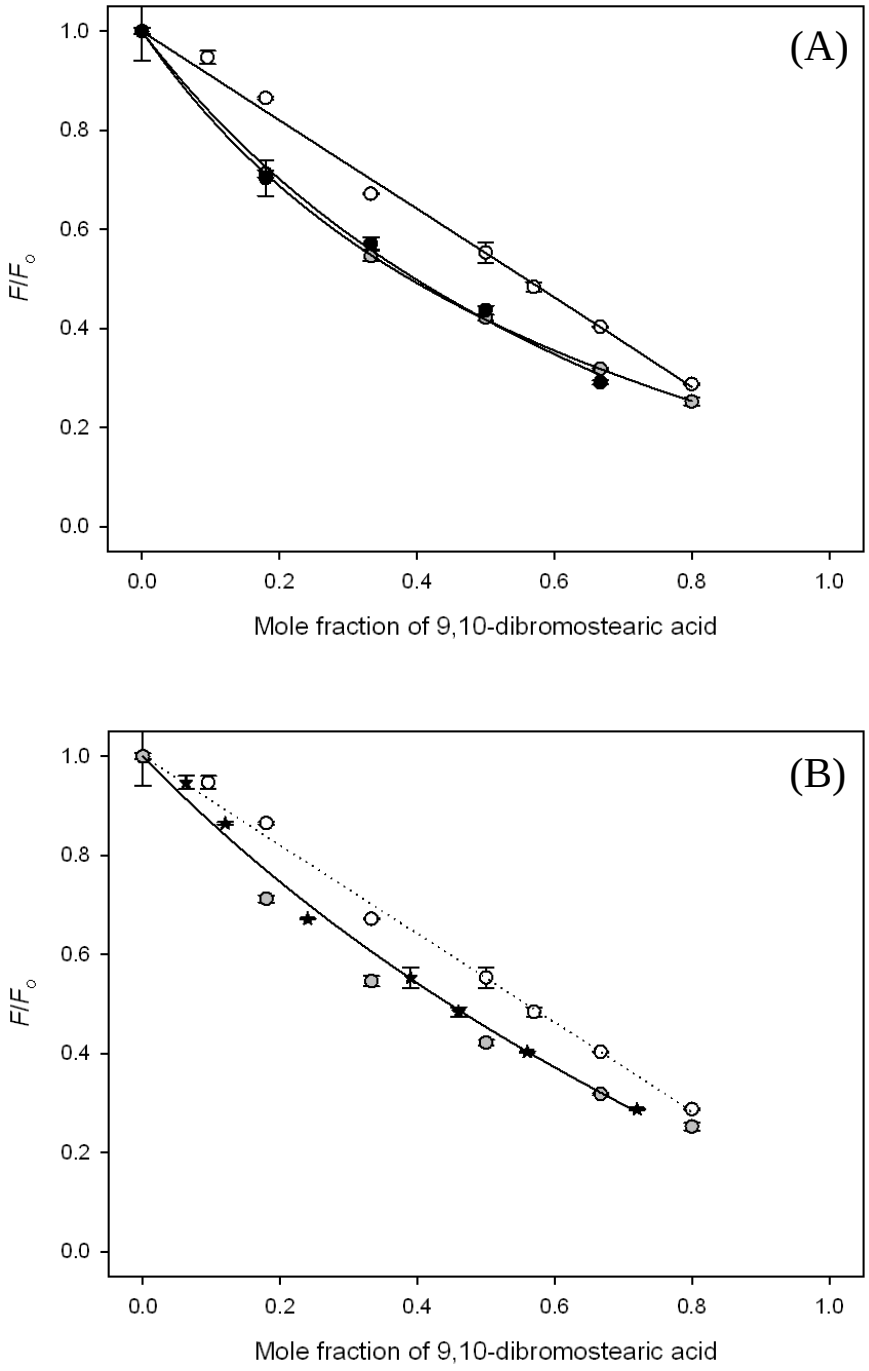

Figure 4.4 Effect of partitioning of 9,10-dibromostearic acid on fluorescence quenching of wild type KcsA reconstituted in DOPC bilayers. (A) Fluorescence intensities (F) measured relative to that in DOPC (F_o) are plotted as a function of the mole fraction of added fatty acid at lipid concentrations of 30 (○), 300 (◍) and 600 (●) µM DOPC. The lipid to KcsA tetramer molar ratio was 400:1 for the 30 µM DOPC samples, and 4000:1 for the 300 and 600 µM DOPC samples. The solid lines show fits to Eq. 4.14 with a value of n = 1.69. (B) The estimated mole fraction of fatty acid bound to the membrane for the samples with 30 µM DOPC (★) was calculated assuming 64 % of the total fatty acid had partitioned into the lipid bilayer. The data were fitted to Eq. 4.14 with a value of n = 1.69 (solid line). The data shown in (A) for 30 µM (○) and 300 µM (◍) DOPC are shown again for comparison. The data for 30 µM DOPC were fitted to Eq. 4.14 (dotted line) again for comparison. The buffer solution was 20 mM HEPES, pH 7.2 with 100 mM KCl.

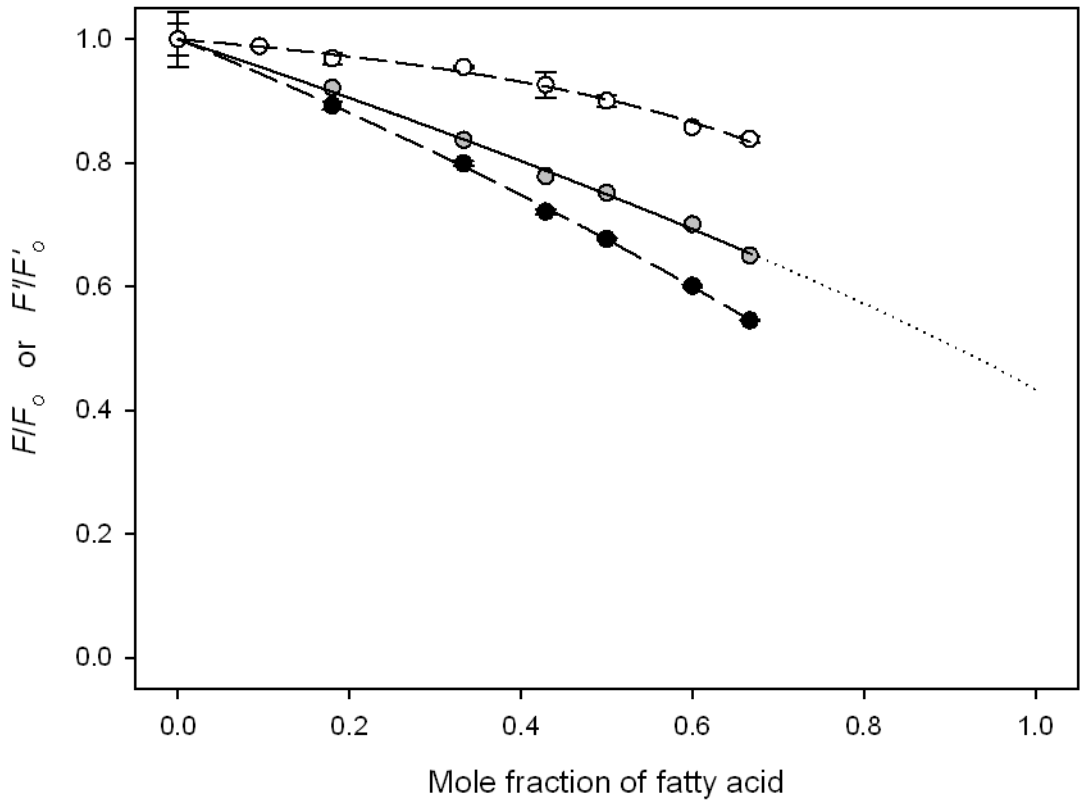

Figure 4.5 Quenching of fluorescence of the KcsA mutant W67,68 by oleic acid and 9,10-dibromostearic acid. The KcsA mutant W67,68 was reconstituted into mixtures of oleic acid and DOPC (○), and 9,10-dibromostearic acid and DOPC (●). For the data points (○,●) fluorescence intensities (*F*) are expressed as a fraction of the fluorescence of KcsA reconstituted in DOPC (F_o). Fluorescence intensities (F'/F'_o) in mixtures containing 9,10-dibromostearic acid were corrected for the fluorescence quenching observed on addition of oleic acid by taking the ratios of the fluorescence intensities in the presence of 9,10-dibromostearic acid to the fluorescence intensities in the presence of oleic acid at the corresponding mole fractions of fatty acid (●). Fluorescence intensities are plotted as a function of the mole fraction of fatty acid. The corrected data were fitted to Eq. 4.14 as described in the text (solid line). The dotted line shows an extrapolation of the fluorescence intensity for the corrected data up to a hypothetical membrane of 100 % 9,10-dibromostearic acid. The molar ratio of DOPC to KcsA tetramer was 2000:1, the concentration of DOPC being 300 μM and the concentration of KcsA tetramer being 0.15 μM.

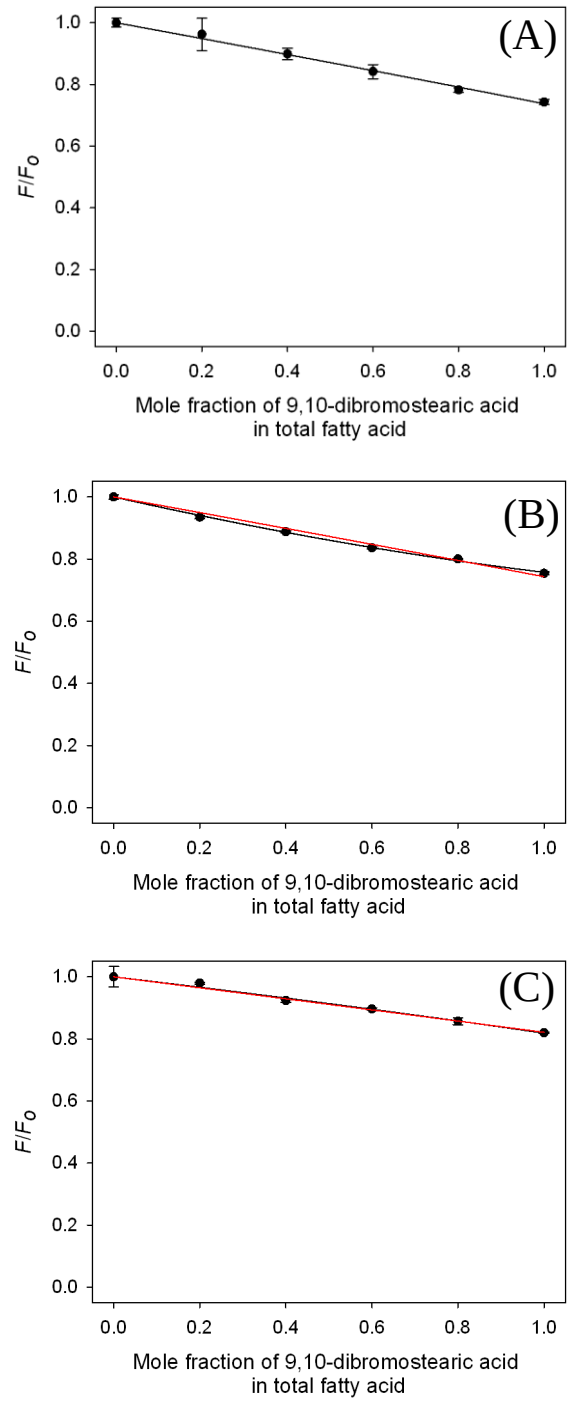

Figure 4.6 Fluorescence quenching of the KcsA mutant W67,68 in mixtures of oleic acid and 9,10-dibromostearic acid at fixed total molar ratios of fatty acid to DOPC. Fluorescence intensities (F) are expressed as a fraction of the fluorescence intensity at a mole fraction of 9,10-dibromostearic acid in the fatty acid mixture of zero (F_o), and are plotted as a function of the mole fraction of 9,10-dibromostearic acid in the total fatty acid mixture. Total fatty acid to DOPC molar ratios are 2:1 (A), 1:1 (B) and 0.5:1 (C). The black lines show free fits for K and F_{min} to Eq. 4.21 with n = 0.94. The red lines show fits to Eq. 4.21 with fixed K = 0.86 and n = 0.94. The experiments were performed with a DOPC concentration of 300 µM and a DOPC to KcsA tetramer molar ratio of 2000:1.

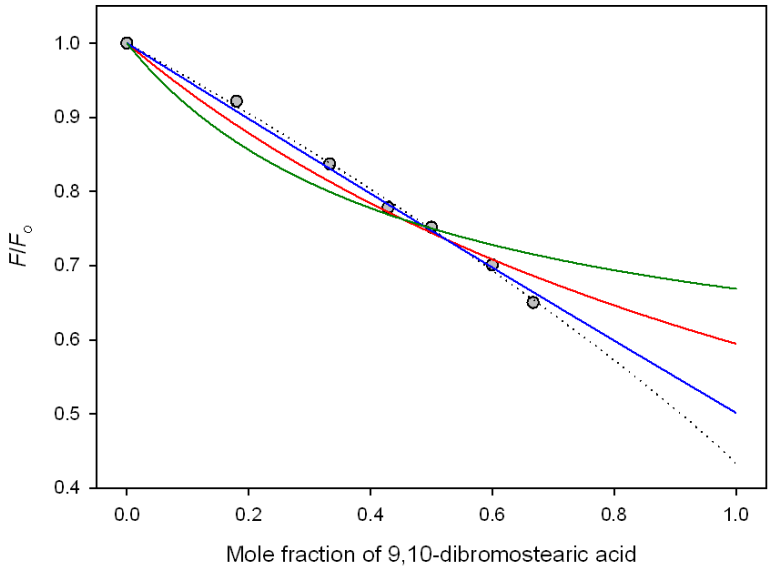

Figure 4.7 Alternative models to describe the binding of 9,10-dibromostearic acid to the non-annular sites on KcsA. The experimental data for the quenching of the KcsA mutant W67,68 in mixtures of 9,10-dibromostearic acid and DOPC corrected for quenching by oleic acid (●), as in Figure 4.5, are shown. The data were fitted to the simple binding model, Eq. 4.18, with n fixed at 0.94 (blue line) and the same fit again but now with F_{min} restricted to be greater than 0 (red line) or greater than 0.5 (green line), as described in the text. The dotted line shows fitting of the data to the competitive binding model (Eq. 4.14) as in Figure 4.5, for comparison.

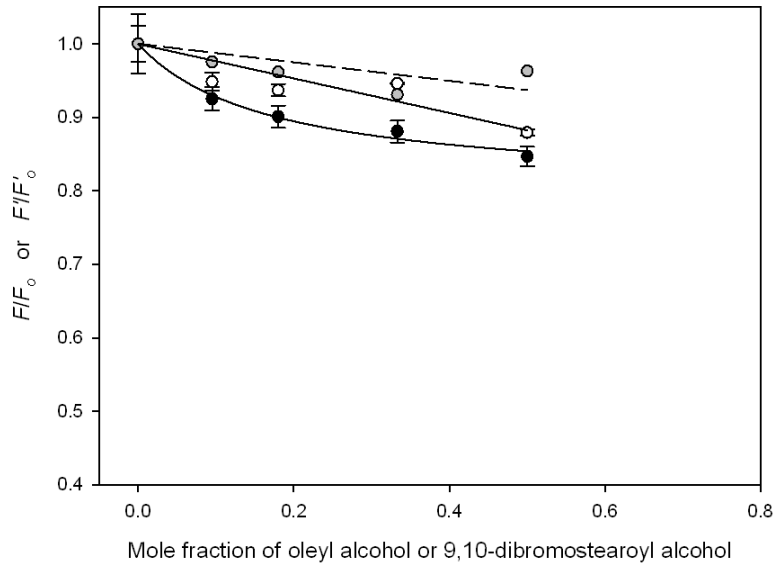

Figure 4.8 Fluorescence quenching of the KcsA mutant W67,68 in mixtures of oleyl alcohol (○) or 9,10-dibromostearoyl alcohol (●) and DOPC. Fluorescence intensities (F) are expressed as a fraction of the fluorescence intensity of the KcsA mutant in DOPC (F_o). The data for quenching by 9,10-dibromostearoyl alcohol were also corrected for quenching with oleyl alcohol (●), where F'/F'_o is the fluorescence intensity in 9,10-dibromostearoyl alcohol/DOPC mixtures at a given mole fraction divided by the fluorescence intensity in the corresponding oleyl alcohol/DOPC mixtures. The samples contained a DOPC concentration of 300 µM and a KcsA tetramer to DOPC molar ratio of 4000:1.

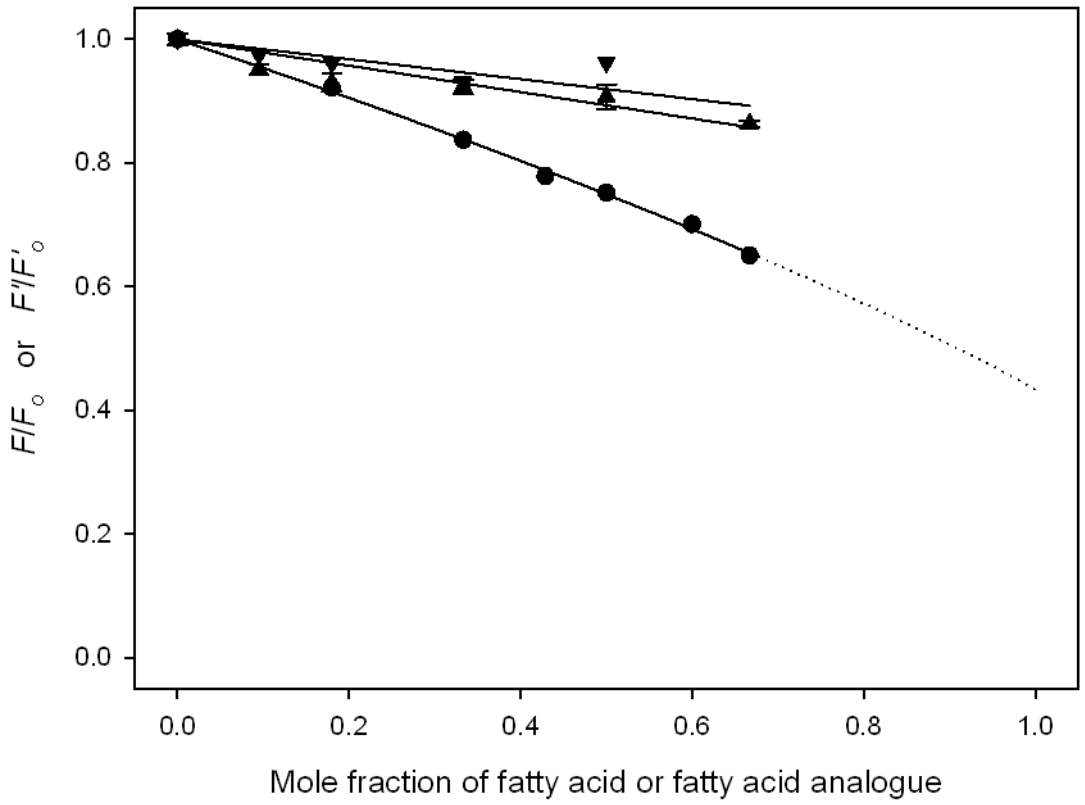

Figure 4.9 Comparison of fluorescence quenching of the KcsA mutant W67,68 with 9,10-dibromostearic acid (●), 9,10-dibromostearoyl alcohol (▼) and 9,10-dibromomethyl stearate (▲). Fluorescence intensities (F'/F'_o) for quenching with 9,10-dibromostearic acid and 9,10-dibromostearoyl alcohol have been corrected for quenching with the non brominated analogues as described in Figures 4.5 and 4.8, respectively. The concentration of DOPC was in all cases 300 μM, with a DOPC to KcsA tetramer molar ratio for the 9,10-dibromostearoyl alcohol and 9,10-dibromomethyl stearate samples of 4000:1, and a DOPC to KcsA tetramer molar ratio of 2000:1 for the 9,10-dibromostearic acid samples.

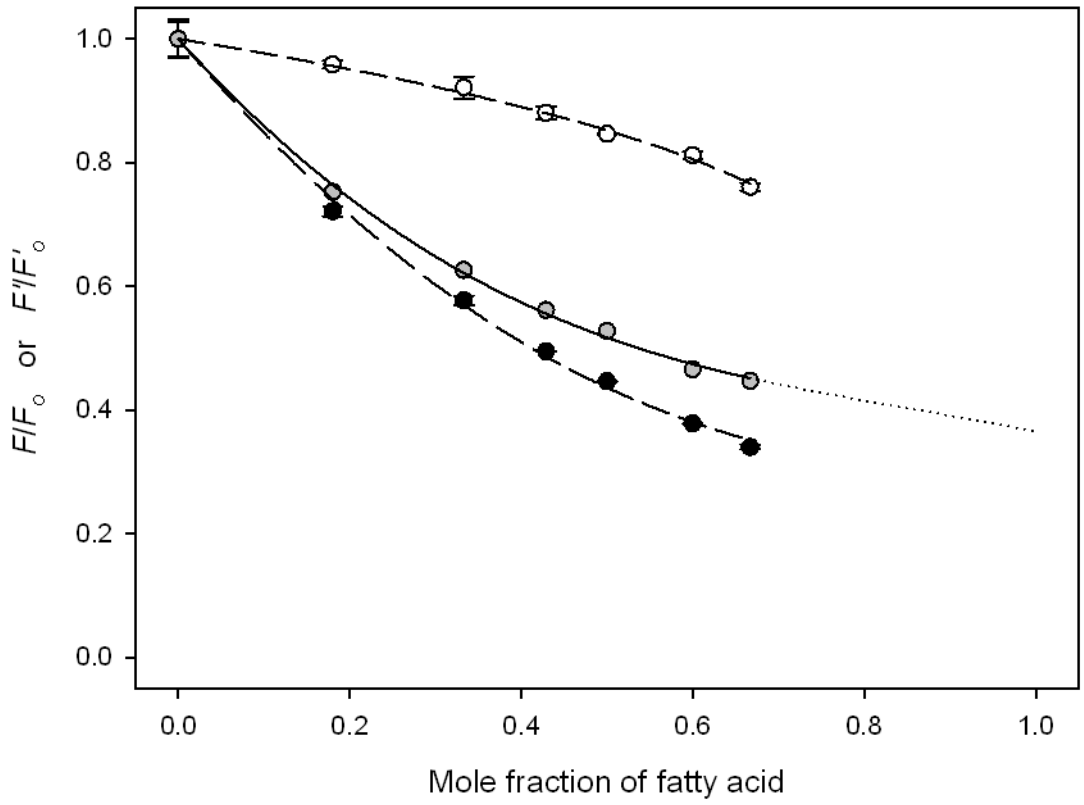

Figure 4.10 Quenching of fluorescence of wild type KcsA by oleic acid and 9,10-dibromostearic acid. Wild type KcsA was reconstituted into mixtures of oleic acid (○) or 9,10-dibromostearic acid (●) and DOPC. Fluorescence intensities (*F*) for data points (●,○) are expressed as a fraction of the fluorescence of KcsA reconstituted in DOPC alone (F_o). Fluorescence quenching with 9,10-dibromostearic acid was corrected for fluorescence quenching with oleic acid by calculating the ratio of the fluorescence intensity at a given mole fraction of 9,10-dibromostearic acid to the fluorescence intensity at the corresponding mole fraction of oleic acid (F'/F'_o, ◍). The solid line shows a fit of the data to Eq. 4.22, as described on the text. The dotted line shows extrapolation of the fluorescence intensity up to a hypothetical membrane of 100 % 9,10-dibromostearic acid.

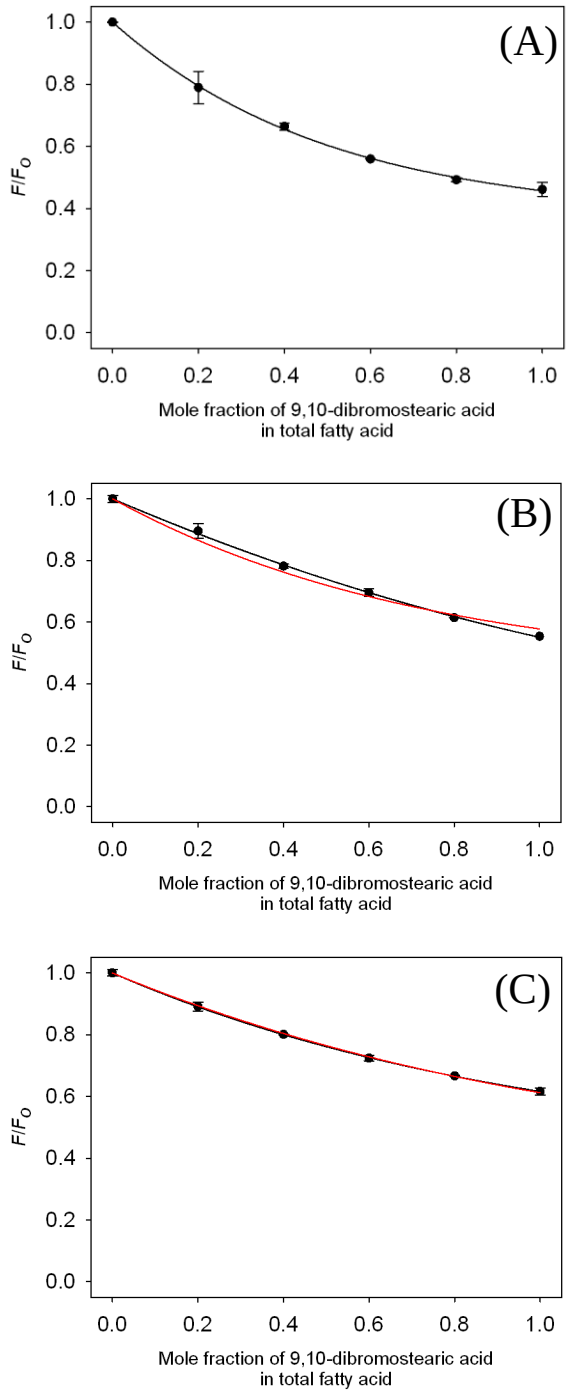

Figure 4.11 Fluorescence quenching of wild type KcsA in mixtures of oleic acid and 9,10-dibromostearic acid at fixed molar ratios of total fatty acid to DOPC. The molar ratios of fatty acid to DOPC shown are 2:1 (A), 1:1 (B) and 0.25:1 (C). Fluorescence intensities (F) are expressed as a fraction of the fluorescence intensity of KcsA at a mole fraction of 9,10-dibromostearic acid in the fatty acid mixture of zero (F_o) and are plotted as a function of the mole fraction of 9,10-dibromostearic acid in the total fatty acid mixture. The black lines show free fits of the data for to Eq. 4.25, as described in the text, while the red lines show fits with fixed n^A = 4.33 and K^A = 0.73. The experiments were performed with a DOPC concentration of 300 µM, with a DOPC to KcsA tetramer molar ratio of 2000:1.

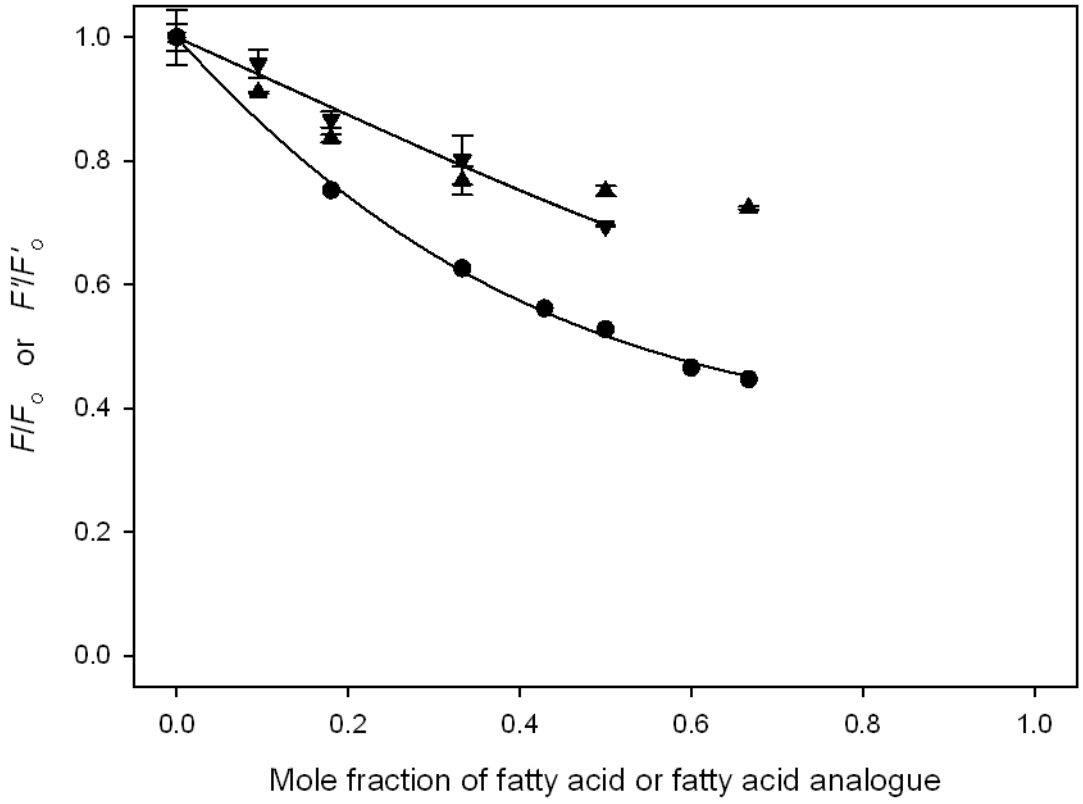

Figure 4.12 Comparison of fluorescence quenching of wild type KcsA by 9,10-dibromostearic acid (●), 9,10-dibromostearoyl alcohol (▼) and 9,10-dibromomethyl stearate (▲). Fluorescence intensities (F/F_o) for the samples with 9,10-dibromostearoyl alcohol and 9,10-dibromomethyl stearate are shown as a fraction of the fluorescence intensity of KcsA in DOPC. Fluorescence intensities (F'/F'_o) for the samples with 9,10-dibromostearic acid are corrected for fluorescence quenching by oleic acid as described in Figure 4.10. The 9,10-dibromostearic acid and 9,10-dibromostearoyl alcohol data were fitted to Eq. 4.22 as described in the text. The concentration of DOPC was in all cases 300 μM, with a DOPC to KcsA tetramer molar ratio for the 9,10-dibromostearoyl alcohol and 9,10-dibromomethyl stearate samples of 4000:1, and a DOPC to KcsA tetramer molar ratio of 2000:1 for the 9,10-dibromostearic acid samples.

4.4 Discussion

4.4.1 Binding of fatty acids to the annular sites of KcsA

The fluorescence quenching studies in the present chapter show that fatty acids are able to bind at both annular and non-annular sites on KcsA. As observed for other membrane proteins, interactions with the annular sites of KcsA show little specificity, with a binding constant K^A for oleic acid relative to DOPC of 0.73 ± 0.04, showing that the fatty acid has an affinity only slightly lower than that of DOPC for KcsA. Binding of phospholipids to the annulus of KcsA also shows little specificity (see Chapter 5) although there is a clear tendency for negatively charged phospholipids to show a slightly higher affinity than zwitterionic phospholipids. It might be expected then that a negatively charged fatty acid would also bind slightly better than DOPC to the annular sites on KcsA. One possible explanation for the slight weaker binding of oleic acid is the lack of a second fatty acyl chain. As described at the end of Section 4.2.2, an alternative way to analyse the fluorescence quenching data with fatty acids is by expressing the concentration of the fatty acid on a fatty acyl chain basis rather than on a molecular basis. The relative binding constant, K^C, calculated on a chain basis is double that calculated on a molecular basis, giving a value K^C of 1.46, similar to that of some of the negatively charged phospholipids (see Chapter 5). Another key factor is the protonation state of the fatty acid. The pK_a of a fatty acid in water is ca. 5, and so at physiological pH (7.2) the fatty acid in water will be fully deprotonated and hence negatively charged. However, the pK_a of oleic acid shifts to 7.4 as the fatty acid incorporates into the lipid bilayer because the uncharged form has a greater affinity for the bilayer than the charged form and because of the charge built up on the bilayer resulting from incorporation of the charged form, which further decreases the effective binding constant of the charged form[97]. As a result, at pH 7.2 ca. 60 % of the fatty acid will be protonated, and since the negative charge is important for interaction, as observed by the poor binding of the uncharged fatty acid analogues, this shift in pK_a upon incorporation into the lipid bilayer could contribute to the relatively low affinity measured for 9,10-dibromostearic acid.

Previous studies on KcsA by Alvis *et al.*[73] have shown that the number of lipid binding sites from which the fluorescence of an average Trp residue can be quenched

(the *n* value) is ca. 1.7 for the phospholipids PC, phosphatidylethanolamine (PE), phosphatidylglycerol (PG) and phosphatidylserine (PS), 2.5 for phosphatidic acid (PA) and 0.9 for cardiolipin (CL, a four acyl chain phospholipid). An *n* value of 1.7 for a two chain phospholipid would suggest about three acyl chains make contact with each lipid exposed Trp residues. The higher *n* value of 2.5 obtained for PA was attributed to the smaller headgroup of PA allowing acyl chains from neighbouring molecules to come closer together, so that PA is able to 'fit' more acyl chains around a Trp residue. The *n* value of 0.9 for CL, about half that for PG, would reflect the four acyl chain nature of the CL molecule. In the present studies, the value of *n* at the annular sites of KcsA for 9,10-dibromostearic acid was determined to be 4.33 ± 0.20, indicating that about four acyl chains can be accommodated around each lipid-exposed Trp residue, in good agreement with the phospholipid studies.

4.4.2 Binding of fatty acids to the non-annular sites

As described in Section 4.2.2 binding at the non-annular sites could be described in terms of a competitive binding model or a simple binding model. Figure 4.7 shows here that binding of the fatty acid to the non-annular sites can only be described in terms of a competitive binding model where the non-annular sites are always occupied, either by fatty acid or by DOPC. A simple binding model where DOPC cannot bind to the non-annular sites so that the non-annular sites are either empty or occupied by fatty acid does not fit the data due to the relatively low affinity of the fatty acid for the non-annular sites and the high levels of quenching observed at high concentrations of 9,10-dibromostearic acid. In previous experiments performed by Marius *et al.*[13] only a low level of quenching of W67 by brominated PC (BrPC) was observed, suggesting the zwitterionic phospholipid could not bind deep enough into the non-annular sites to quench W67. Marius *et al.*[13] also showed that, as opposed to BrPC, binding of brominated PG (BrPG) did result in extensive quenching of W67. These studies were interpreted as showing that the zwitterionic PC could not bind to the non-annular sites whereas the anionic PG could. In contrast, the experiments shown here with the fatty acid exclude the possibility of a simple binding model, suggesting that the low level of quenching by BrPC, if correct, results from a more peripheral binding of BrPC at the non-annular site, causing little quenching of W67, as illustrated in Figure 4.13, but still being competitive with fatty acid binding. The

binding constant for the fatty acid at the non-annular sites relative to PC, K^{NA}, has a value of 0.86 ± 0.08, indicating a slightly lower affinity for fatty acid than PC. Fitting the experimental data obtained by Marius *et al.*[13] to the competitive binding model gives a binding constant for PG relative to PC of 3.33 ± 0.35, which indicates that PG has a greater affinity for the non-annular sites than both the fatty acid and PC. Another observation is that the level of fluorescence quenching of W67 by 9,10-dibromostearic acid is higher than the level of quenching observed with BrPG[13]. This may be due to the fatty acid being able to access deeper in the non-annular sites thanks to its smaller headgroup compared to that of phospholipids.

As for the annular sites, it might have been expected that the negatively charged fatty acid would bind better than PC at the non-annular sites and it could again be argued that the lack of one of the acyl chains and other polar groups could be responsible for the weaker binding that is actually observed. Analysis of the data with the concentration of the fatty acid expressed as a mole fraction of fatty acyl chains in the membrane would again double the binding constant of the fatty acid at the non-annular sites giving a value of 1.72. Importantly, as discussed for the annular sites, the shift in pK_a upon incorporation of the fatty acid into the bilayer could be an important factor for the low affinity observed, as ca. 60 % of the fatty acid will be protonated. Preferential binding of anionic phospholipids to the non-annular sites has been proposed to be due to the presence of two arginine residues (R64 and R89) located at each side of the protein-protein interface that makes up the non-annular site, and molecular dynamic simulations have shown bound PG hydrogen bonding to these arginine residues[102]. However, recent experiments with the KcsA W67,68 mutant where these arginine residues are substituted by leucine, show that oleic acid can still bind equally well to the non-annular sites (unpublished data). This suggests that binding of the fatty acid is not due to direct interaction of the carboxyl group with these arginine residues and it could be another reason why the fatty acid binds weaker than DOPG at the non-annular sites. The diacylglycerol (DAG) moiety from the PG molecule bound at the non-annular site in the crystal structure of KcsA shows its *sn*-1 chain bound deeply into the groove between the adjacent monomers, while the *sn*-2 chain interacts less intimately with the channel[81] (Figure 4.14). Given the short range of Trp quenching by brominated molecules, quenching of W67 by BrPG probably occurs from the bromine atoms attached to the *sn*-1 chain, and so it would be expected

that quenching by 9,10-dibromostearic acid would be due to binding of the fatty acid at the non-annular site in a similar way to the *sn*-1 chain of PG. Indeed, in contrast to the *n* value obtained for fatty acid binding at the annular sites ($n^A = 4.33 \pm 0.20$), the *n* value at the non-annular sites is 0.94 ± 0.19, indicating that only one molecule of fatty acid can bind at a non-annular site to efficiently quench W67, in excellent agreement with the crystal structure of KcsA showing only one fatty acyl chain of the modelled PG molecule binding deep within the groove at the protein-protein interface the makes up the non-annular binding site[81] (Figure 4.14). If R64 and R89 are not directly involved in binding of the fatty acid, only the amide group from the protein backbone between T85 and L86 appears to be a potential hydrogen bond donor for the carboxyl moiety of the fatty acid binding at the non-annular sites, as shown in Figure 4.14.

A difference between the fluorescence quenching experiments performed by Marius *et al.*[13] and the experiments described in this chapter is the concentration of KCl in the sample buffer. In the experiments of Marius *et al*. the sample buffer did not contain KCl, giving a low ionic strength where the effects of the ionic interactions between the lipids and the protein would be maximised. In contrast, in the experiments reported here 100 mM KCl was included in the buffer to ensure good incorporation of the fatty acid into the lipid bilayer. The higher ionic strength in the experiments presented here could reduce any ionic interactions between the lipid and the protein. Moreover, it has been shown that the concentration of KCl can affect the conductance of the channel[103] and the structure of the selectivity filter[53] and it is possible that this could have some effect on binding of lipids at the non-annular sites.

4.4.3 Binding of uncharged fatty acid analogues to KcsA

Binding of uncharged fatty acid analogues to the annular sites is weak, with a binding constant for 9,10-dibromostearoyl alcohol relative to PC of 0.34 ± 0.01 (Figure 4.12). Even if the mole fraction of oleyl alcohol is expressed in terms of fatty acyl chain concentration the value of *K* only comes up to 0.68. The more limited miscibility of 9,10-dibromomethyl stearate in the lipid bilayer meant that its binding constant could not be efficiently determined, but the levels of quenching at low concentrations were similar to those obtained with 9,10-dibromostearoyl alcohol, suggesting a similar affinity for the annular sites (Figure 4.12). Binding of both of the

uncharged fatty acid analogues to the non-annular sites is insignificant, with almost no quenching of the fluorescence of W67. The weak binding of the uncharged fatty acid analogues at both annular and non-annular sites could be due to the weaker polar interactions that the uncharged analogues can establish with the channel. The ways in which these molecules interact with a lipid bilayer could also limit their interaction with the protein. These molecules have been shown to form tightly packed condensed complexes with PC in monolayers, with surface areas less than the sum of the surface areas of the two components[101]. If similar condensed complex formation occured in DOPC bilayers, weak binding of oleyl alcohol and methyl oleate to KcsA could in part be due to a strong interaction of these molecules with the lipid bilayer. Additionally, it has been suggested, for oleyl alcohol, that these condensed complexes could form separate domains within the membrane[104], and if that was the case and KcsA partitioned preferentially into the DOPC enriched domains, low levels of quenching by 9,10-dibromostearoyl alcohol would result.

Some of the studies showing fatty acid effects on ion channel function have shown that, in contrast, uncharged analogues like oleyl alcohol and methyl oleate do not have an affect on function[105-107]. However, for the Ca^{2+}-ATPase it has been shown, with fluorescence quenching studies of the kind described in this chapter, that 9,10-dibromostearoyl alcohol and 9,10-dibromomethyl stearate can interact with both annular and non-annular sites on the calcium pump[97], and moreover, the activity of the Ca^{2+}-ATPase is affected by binding of methyl oleate at the non-annular sites[108]. This then suggests that hydrophobic interactions can be important in interactions at non-annular sites and so the ability of uncharged molecules to bind to the non-annular sites of membrane proteins should not be ignored.

4.4.4 Conclusions

The fluorescence experiments presented here show that fatty acid molecules can interact with the transmembrane region of KcsA. As expected, interactions can take place with the annular sites of the channel, which are normally solvated by phospholipids. This has also been observed for numerous other membrane proteins using ESR[24,25]. Additionally, it is shown that fatty acid molecules can also interact with the non-annular sites of the channel. This is important because these type of sites,

located in clefts between transmembrane α-helices, are not accessible to all lipid molecules and are often important for membrane protein function. There are very few studies where the interaction of fatty acids with the non-annular sites of membrane proteins have been analysed[97,98,108]. As shown here for KcaA, Froud *et al*.[97] showed that for the Ca^{2+}-ATPase, fatty acids are able to interact with both annular and non-annular sites and, further, are able to affect the calcium pump activity[108]. This suggests that fatty acids can affect protein function by direct interactions with the annular and non-annular sites on a protein.

Another way in which fatty acids could influence membrane protein function is by increasing the negative charge on the bilayer surface: this could affect the local concentration of charged substrates and could also affect the membrane potential. Another way to influence protein function could be by altering the material properties of the lipid bilayer (thickness, fluidity, etc.) although it is likely that large concentrations of fatty acids would be required for this, and there is no direct evidence that suggests this kind of effect is an important mechanism to affect membrane protein function by fatty acids.

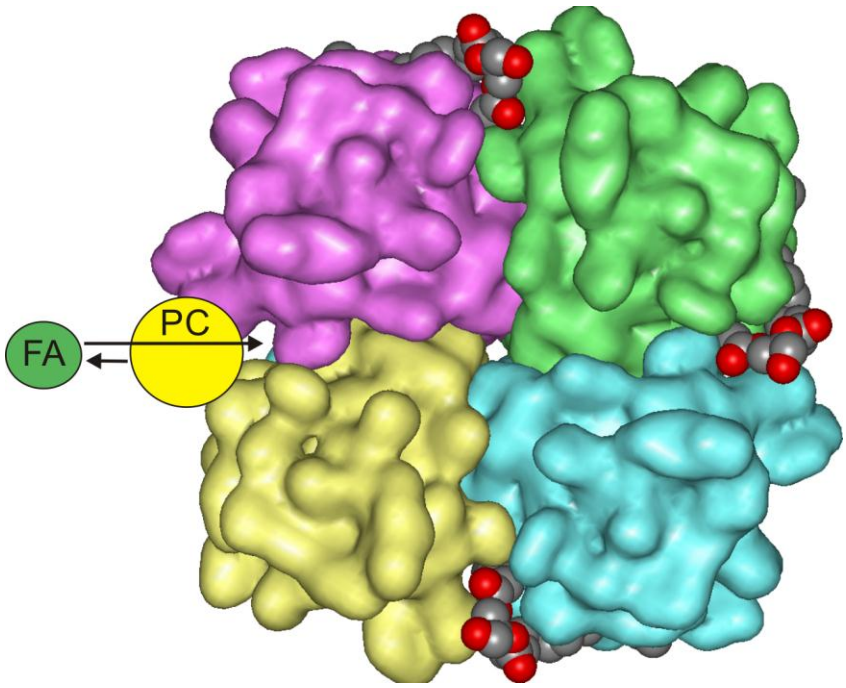

Figure 4.13 Competitive binding at the non-annular binding sites of KcsA. The image shows a view from the 'top' of the KcsA (the side of the channel facing the extracellular side of the bacterial membrane); the subunits are shown as the solvent accessible surface, each monomer with a different colour (PDB 1K4C)[53]. Three of the four diacylglycerol moieties from PG molecules modelled in the structure are shown in CPK representation. The low levels of fluorescence quenching with brominated DOPC suggest superficial binding of the zwitterionic phospholipid at the non-annular sites, as opposed to DOPG, which binds deep within the subunit-subunit interfaces, allowing it to cause quenching of W67. Binding of fatty acids at the non-annular sites will be competitive with binding of PC or other phospholipids.

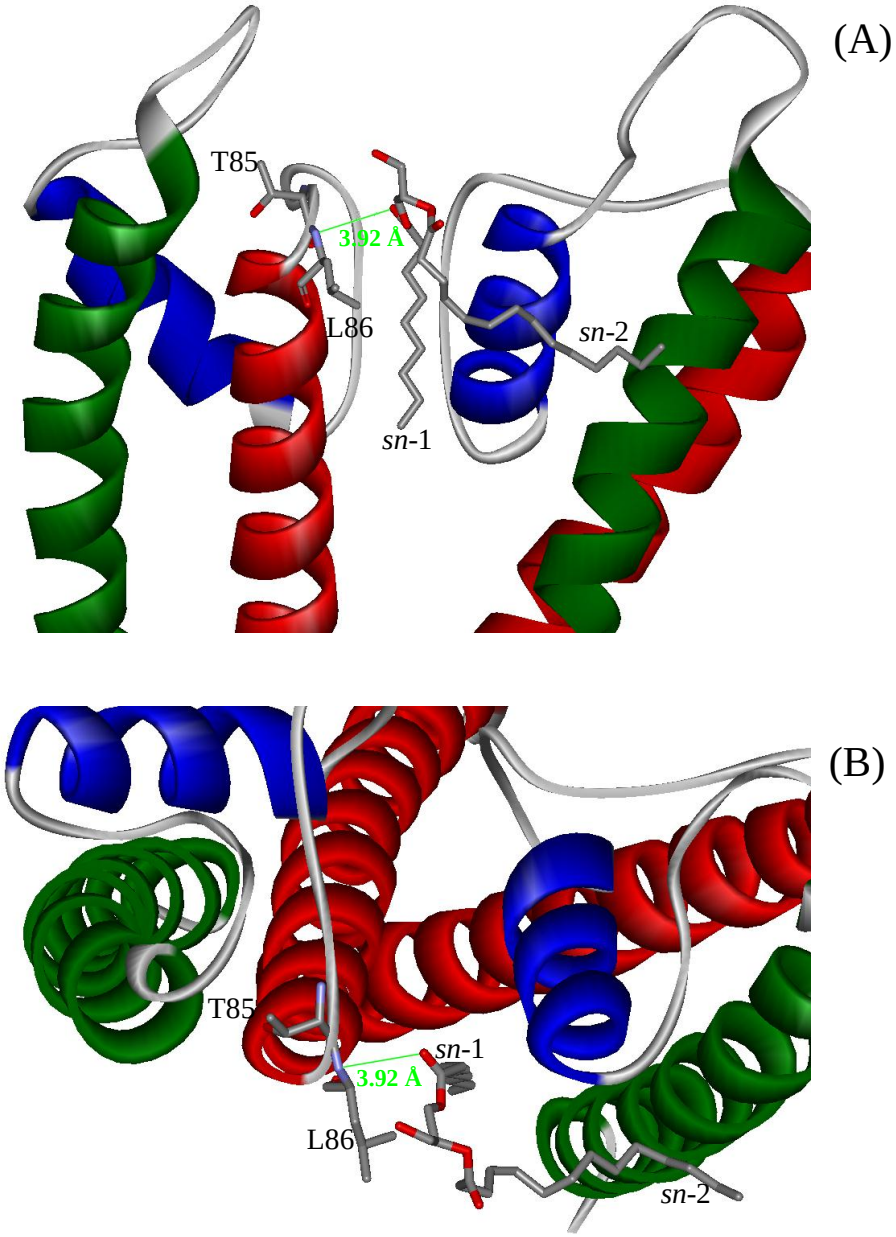

Figure 4.14 Polar groups that could be involved in binding of oleic acid at the non-annular sites on KcsA. Detail of two neighbouring monomers of the KcsA tetramer are shown in ribbon representation (PDB 1K4C)[53], with the inner transmembrane α-helix in red, the outer transmembrane α-helix in green and the pore α-helix in blue. The diacylglycerol moiety corresponding to a PG molecule bound at the non-annular site is shown in stick representation as are residues T85 and L86 (N atoms in blue, O atoms in red and C atoms in grey). The only hydrogen donor group (apart from R64 and R89) that appears to be close enough to interact with the carboxyl group of a fatty acid bound at the non-annular site is the NH group from the peptide bond between T85 and L86. Assuming that fatty acid molecules will bind in a similar way to the *sn*-1 chain of the DAG moiety in the crystal structure, the distance between the closest oxygen in the acyl chain and the nitrogen of the peptide bond is 3.92 Å. (A) shows a side view of the channel while (B) shows a view from the top (the side of the channel facing the extracellular side of the bacterial membrane).

Chapter 5: Interaction of fatty acids and phospholipids with KcsA: studies with ESR and spin labelled lipids

5.1 Introduction

Numerous studies have shown that fatty acids, particularly polyunsaturated fatty acids, can affect the activity of numerous ion channels, but it is yet uncertain how they act[43,44]. It is now clear that the lipids in the membrane can influence the activity of membrane proteins by direct interaction between the lipid and the protein[4,22], and therefore it is of interest to study the ability of fatty acids to interact with ion channels as a possible mechanism for ion channel function regulation. An important difference between fatty acids and phospholipids is the significant solubility of fatty acids in water; this property makes them attractive candidates for intervening in signalling and regulatory processes and could allow them to interact with regions on membrane proteins that are not in contact with the lipid bilayer. In 2003, Hamilton *et al.*[109], based on mutagenesis studies, suggested for the first time that arachidonic acid, a long chain polyunsaturated fatty acid, can inactivate calcium-activated potassium channels by binding at the wide inner cavity of the pore, blocking ion flux, much like numerous other channel pore blockers do. Further, in a more recent and extensive study published by Decher *et al.*[46], based again on mutagenesis experiments, it was shown that arachidonic acid and other polyunsaturated fatty acids can also bind to the pore of voltage-gated potassium channels to block ion flux, and, importantly, it was also shown that mRNA editing of a key hydrophobic residue lining the pore in just one of the four subunits making up the channel could hamper binding of the fatty acid to the pore, suggesting this as a mechanism for fine-tuning neuronal information.

The structure of the pore of potassium channels is highly conserved[34,48,49,53,54]; the short span at the entry of the pore from the extracellular side of the membrane that forms the selectivity filter is narrow and highly polar, with the carbonyl oxygen atoms of the signature sequence interacting with the bound potassium ions; the central cavity is, however, very hydrophobic and wider (Figures 1.13A and D) holding ca. 50 water

molecules. This hydrophobic water filled path allows potassium ions to pass rapidly across the membrane: the water molecules create the polar environment necessary for the ions to cross the hydrophobic core of the lipid bilayer, while the presence of the hydrophobic lining in the cavity means that the ions are not slowed down by strong interactions in their transit along the path. Due to the presence of such wide hydrophobic cavity potassium channels are easily blocked by hydrophobic cations, such as tetrabutylammonium (TBA), binding at the cavity impeding ion flux[67,70,71]. Further, long chain alkyl-triethylammonium cations bind with increasing affinity as their alkyl chain is elongated (up to twelve carbon atoms)[110-112], which highlights the importance of hydrophobic interactions for binding at the pore of potassium channels.

In contrast to the fluorescence quenching method used in the previous chapter, where the information comes from tryptophan residues located at particular positions in the KcsA channel, in the ESR experiments discussed in this chapter the information comes from spin labelled lipid molecules. Spin labelled lipid molecules interacting with a protein generate a broader ESR spectrum than spin labelled lipid molecules in the bulk lipid bilayer due to the more restricted mobility of the acyl chains to which the spin label probe is attached. In this way, interactions undetected by the fluorescence quenching method might, in principle, be observed with ESR. Importantly, the degree of broadening of the ESR spectra can reveal different types of lipid binding sites where the mobility of the acyl chain can be more or less restricted, depending on the type of binding site. Therefore, the ESR method might be useful for detecting binding of fatty acids at the inner cavity of KcsA. If, as proposed by the studies of Hamilton *et al.*[45] and Decher *et al.*[46], a fatty acid molecule can bind in the inner cavity of a potassium channel, the fluorescence quenching method is unlikely to be able to detect this in KcsA because all of the Trp residues are far away from the inner cavity. As explained in Chapter 1, Section 1.5.5 the efficiency of quenching tryptophan fluorescence by a pair of bromine atoms in the acyl chains of a brominated lipid molecule depends on the sixth power of the distance of separation between the Trp residue and the bromine atoms, as described by Eq 1.6, shown again here for clarity:

$$E = \frac{x \cdot R_o^6}{(d^6 + x \cdot R_o^6)} \qquad (1.6)$$

where E is the quenching efficiency, x is the number of brominated acyl chains causing quenching, d is the distance between the Trp residue and the bromine atoms and R_o is the distance at which quenching efficiency is 50 %, which in this case is ca. 8 Å[83,84]. Figure 5.1 shows the residues in KcsA that correspond to those shown to be involved in binding of arachidonic acid in the studies of Decher *et al*.[46] that are closest to Trp residues: A111 and I100. If, as proposed by Descher *et al*., only one fatty acid molecule binds in the inner cavity, using Eq. 1.6 with a value for x of 1, it is possible to estimate the quenching efficiency of a brominated fatty acid bound in the inner cavity with its pair of bromine atoms located next to each of the latter residues. It is not clear from where exactly on the Trp group the distance to the bromine atoms should be measured to apply Eq. 1.6, but experimental studies suggest that the best approach is to measure distances from the α-carbon of the Trp residue[85], and so the distances in Figure 5.1 have been measured in this way. For I100 the distances to all Trp residues are much greater than 8 Å, the smallest distance being of ca. 15 Å, between I100 and W68 in the same channel subunit; for a pair of bromine atoms right next to I100 the quenching efficiency of W68 in the same subunit would then only be 2 %. Distances to W68 in the other subunits are much greater, which would result in no quenching at all of those residues. A111, however, is close to W113 in the same subunit, being ca. 7 Å from its α-carbon. If the pair of bromine atoms were located next to A111, the quenching efficiency of W113 in that subunit would be 70 %. The distances to W133 in the neighbouring and opposite subunits are ca. 10 Å and 13 Å, respectively, and so their quenching efficiencies would be, respectively, 17 % and 5 %. The distance of A111 to the other closest tryptophan residue in the same subunit, W26, is ca. 12 Å, so that quenching efficiency for that particular Trp would be only 8 %. The distance to W26 in the other subunits is, even greater than 12 Å, and so their quenching efficiencies will be insignificant. Hence, if the bromine atoms were located next to A111, only one of the W113 in the channel would be efficiently quenched, which would result in quenching of about 5 % of the overall Trp fluorescence in KcsA, a very small change. This suggests that binding of a brominated fatty acid molecule to the inner cavity would not be detected by fluorescence quenching and, therefore,

using the ESR method could be a good way to study the possibility of fatty acids binding in the inner cavity of KcsA.

Using spin labelled lipids it is possible to calculate relative lipid binding constants which can then be compared with those obtained using fluorescence spectroscopy. However, it is important to note that the fluorescence results give an average relative binding constant over all the sites from which the fluorescence of the tryptophan residues can be quenched, whereas in the ESR experiments the relative binding constant obtained is a weighted average for all the sites to which the spin labelled molecule can bind. Because only low concentrations of spin labelled lipid are used in the ESR studies, lipid binding constants obtained by the ESR method could be dominated by a small number of binding sites of high affinity.

In this chapter it will be shown that ESR studies with spin labelled stearic acid, combined with the results obtained from fluorescence spectroscopy, suggest that fatty acids bind with high affinity to the inner cavity of KcsA and, for the first time, a dissociation constant for a fatty acid binding to the pore of an ion channel is determined.

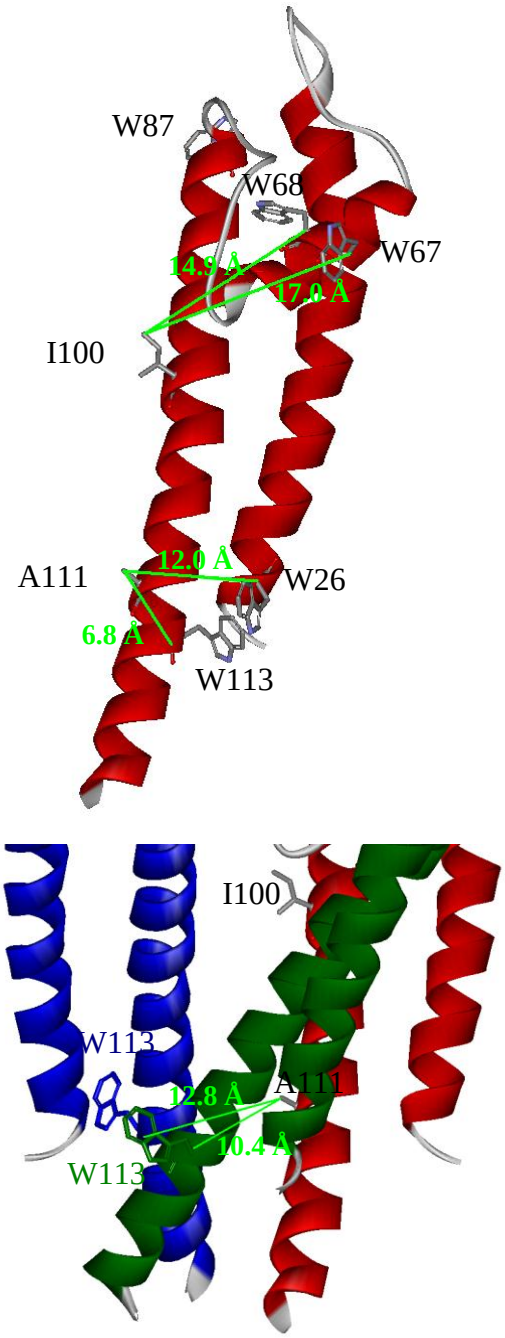

Figure 5.1 Residues in KcsA that correspond to residues involved in binding of arachidonic acid in voltage-gated potassium channels and that are located closest to Trp residues in KcsA. (A) shows one KcsA subunit with I100, A111 (which correspond to the location of residues involved in binding of arachidonic acid to the voltage-gated potassium channel from rat rKv1.5), and all the Trp residues in stick representation. (B) shows three KcsA subunits, each in a different colour. The subunit in red shows I100 and A111 in stick representation, the neighbouring subunit (green) and the opposite subunit (blue) show only W113 in order to illustrate the distances between residues of different subunits. In light green are shown the measured distances between the α-carbon of the Trp and the closest carbon atom of I100 or A111 facing the inner cavity. PDB file 1K4C[53].

5.2 Methods

Details about the protein production, purification and reconstitution of the samples for ESR measurements are described in Chapter 2.

5.2.1 Determination of relative phospholipid binding constants by ESR

To determine relative binding constants for phospholipids equivalent to those calculated from fluorescence quenching experiments, a preparation of KcsA reconstituted in dioleoylphosphatidylcholine (DOPC) at a DOPC:KcsA tetramer molar ratio of 60:1 was split into aliquots into which were incorporated, respectively, 1 mol % of spin labelled phosphatidylcholine (14-PCSL), phosphatidylethanolamine (14-PESL), phosphatidylglycerol (14-PGSL), phosphatidylserine (14-PSSL) or phosphatidic acid (14-PASL). Because all the samples came from the same initial preparation the resulting ESR spectra can be compared directly, the only difference between them being the incorporated spin labelled phospholipid. The differences between the proportions of spin labelled lipid in contact with the protein in each case depend on the different affinities of the lipids for the channel, and binding constants relative to DOPC (the unlabelled host lipid) can be calculated as described below.

Additionally, a preparation of KcsA reconstituted in dioleoylphosphatidylglycerol (DOPG) at a molar ratio of DOPG:channel of 60:1 was prepared in the same way and 14-PCSL was incorporated in order to measure the binding constant for PC relative to PG, to compare with that determined for PG relative to PC.

5.2.2 Determination of relative lipid binding constants from ESR spectra: combining information from two different spectra

Relative binding constants (K) for phospholipids, equivalent to those calculated from fluorescence quenching experiments, were determined using Eq. 3.13 derived from the lipid exchange equilibrium (Eq. 3.1) as described in Chapter 3, Section 3.2.4. Eq. 3.13 was rewritten to give:

$$\left(\frac{1-f}{f}\right)K+1=\frac{N_t}{N_b} \tag{5.1}$$

Because all the samples analysed have the same total lipid:channel molar ratio (N_t = 60) and assuming that the number of lipid binding sites is the same for all the phospholipids studied (N_b = 31 ± 3, see Chapter 3, Section 3.4), the term N_b/N_t will be the same for all samples. Assuming that a spin labelled phospholipid and its unlabelled form show the same binding affinity[24], the sample containing 14-PCSL in DOPC constitutes a reference spectrum, with a binding constant for 14-PCSL relative to DOPC of K_o = 1. The relative amount of immobile lipid in the 14-PCSL sample can then be compared with that in the sample with the second spin labelled phospholipid in DOPC to obtain the binding constant K of the second phospholipid relative to the host phospholipid DOPC:

$$\left(\frac{1-f}{f}\right)K+1=\frac{N_t}{N_b}=\left(\frac{1-f_o}{f_o}\right)K_o+1 \tag{5.2}$$

where f is the fraction of restricted component for the second spin labelled lipid, K is the affinity of the second spin labelled lipid relative to the host lipid (DOPC), f_o is the fraction of restricted component for the 14-PCSL sample and K_o = 1. Rearranging Eq. 5.2 gives:

$$K=\frac{f(1-f_o)}{f_o(1-f)} \tag{5.3}$$

which in fact simply reflects the lipid exchange equilibrium of Eq. 3.2.

5.2.3 Determination of relative lipid binding constants from the ESR spectra using the information in a single spectrum

Determination of relative lipid binding constants as described above has the advantage of combining information from two different ESR spectra, minimising the experimental error. Another advantage is that, as long as the two lipid species interact with the same number of binding sites, it is not necessary to know the number of sites.

However, if the two types of lipid interact with a different number of binding sites then this simple approach is no longer possible as it is then necessary to know the number of binding sites for each class of lipid. However, if the number of binding sites is known then individual spectra can be analysed to give the binding constant for the chosen lipid relative to the host lipid. Relative lipid binding constants can be calculated directly from Eq. 3.2, which is repeated here for convenience:

$$K = \frac{[PA][B]}{[PB][A]} \tag{3.2}$$

where the brackets indicate concentrations and *A* represents the spin labelled lipid, *B* the unlabelled host lipid, and *K* is the affinity of the site for *A* relative to *B*. All the terms can be calculated from the spectrum to obtain *K* as follows:

$$[A] = [A_t] \cdot (1\text{-}f) \tag{5.4}$$

$$[PA] = [A_t] \cdot f \tag{5.5}$$

$$[B] = [B_t] - [PB] \tag{5.6}$$

$$[PB] = [P_t] - [PA] \tag{5.7}$$

where $[A_t]$ is the total concentration of spin labelled lipid, f is the fraction of the restricted component in the ESR spectrum of the spin labelled lipid, $[B_t]$ is the total concentration of unlabelled host lipid, and $[P_t]$ is the concentration of binding sites involved in the exchange equilibrium.

5.2.4 Study of fatty acid interactions with KcsA by ESR

For the analysis of the interaction of 14-SASL with KcsA two different sets of samples of KcsA reconstituted in DOPC at lipid:channel molar ratios ranging from 30:1 to 100:1 were prepared as described in Chapter 2. As described in Section 3.2.1, each of these sets of samples were prepared in duplicate and one of the duplicates was labelled with 14-PCSL for the experiments discussed in Chapter 3 and the other duplicate was labelled with 14-SASL at a concentration of 0.5 mol % 14-SASL relative to the total lipid for the studies described in this chapter. The duplicates allowed a direct comparison of the samples labelled with 14-PCSL with the

corresponding samples labelled with 14-SASL: because the duplicates originated from the same preparation, the only difference between them is the spin labelled lipid incorporated.

Additionally, a sample of KcsA reconstituted in DOPG at a lipid:channel molar ratio of 88:1 prepared in the same way was also labelled with 0.5 mol % 14-SASL to allow analysis of binding of the fatty acid in a DOPG environment.

5.2.5 Analysis of binding of 14-SASL to KcsA.

As described below, ESR spectra for 14-SASL in the presence of KcsA are consistent with fatty acid binding to a single site in the central pore of KcsA. Again, as described below, the affinity of this site for 14-SASL appears much higher than that of the annular and non-annular sites so that over the concentration range in which the high affinity site becomes occupied by 14-SASL, there will be insignificant binding to the annular or non-annular sites on KcsA. Binding to the high affinity site can therefore be analysed in terms of 14-SASL in the aqueous medium, 14-SASL partitioned into the lipid bilayer and 14-SASL bound to the high affinity site (Figure 5.2).

The actual mechanism of binding of fatty acid to the central pore would not affect the measured equilibrium constants but probably involves binding from the aqueous pool of 14-SASL (Figure 5.2). The dissociation constant K_E describing the equilibrium between the fatty acid associated with the inner cavity and the fatty acid in the lipid bilayer is given by the product of the constant describing the dissociation of fatty acid from the inner cavity into the aqueous medium (K_w) and the constant describing the partition of the fatty acid from the aqueous medium into the lipid bilayer (K_p). The first step can be written as:

$$P.FA \rightleftharpoons FA_w + P \tag{5.8}$$

from which:

$$K_w = \frac{[FA_w][P]}{[P.FA]} \tag{5.9}$$

where FA_w is the free fatty acid in water, P is the unoccupied binding site in the inner cavity of KcsA and $P.FA$ is the fatty acid bound to the inner cavity. The second step can be written as:

$$FA_w + L \rightleftharpoons L.FA \tag{5.10}$$

from which:

$$K_p = \frac{[L.FA]}{[FA_w][L]} \tag{5.11}$$

where $L.FA$ is the fatty acid associated with the lipid bilayer and L is the host lipid. The equilibrium between fatty acid bound to protein and that bound to lipid can then be written as:

$$P.FA + L \rightleftharpoons FA_w + P + L \rightleftharpoons L.FA + P \tag{5.12}$$

The equilibrium constant for this process will be described by the dissociation constant K_E which is the product of the first two equilibrium constants:

$$K_E = K_w \cdot K_p \tag{5.13}$$

and so:

$$K_E = \frac{[FA_w][P]}{[P.FA]} \cdot \frac{[L.FA]}{[FA_w][L]} = \frac{[P][L.FA]}{[P.FA][L]} \tag{5.14}$$

which, of course, is the equilibrium defined by the two sides of the overall equilibrium described by Eq. 5.12. Eq. 5.14 can be transformed by substituting the following terms:

$$[P] = [P_t] - [P.FA] \tag{5.15}$$

$$[L.FA] = [FA_t] - [P.FA] - [FA_w] \approx [FA_t] - [P.FA] \quad (5.16)$$

$$[L] = [L_t] - [FA.L] \approx [L_t] \quad (5.17)$$

where $[P_t]$ is the total concentration of binding sites, $[FA_t]$ is the total fatty acid concentration and $[L_t]$ is the total concentration of host phospholipid. Eq. 5.16 is valid for the present ESR experiments because the samples are measured at very high concentration of host phospholipid (ca. 85000 μM), which results in almost all the fatty acid incorporating into the lipid bilayer, the amount free in water being insignificant in comparison. Eq. 5.17 is also true in the present experiments because $[FA_t] <<< [L_t]$ (the fatty acid being only 0.5 % mol of the total lipid content). Eq. 5.14 then becomes :

$$K_E = \frac{[P_t - P.FA][FA_t - P.FA]}{[P.FA][L_t]} \quad (5.18)$$

This equation was used to calculate a value for K_E for each individual sample labelled with 14-SASL: the deconvoluted spectra gave the fractions of immobilised fatty acid ($P.FA$) and the term $[P_t]$ was calculated, as discussed in the results section, by assuming that the number of binding sites per channel was one. Concentrations were expressed in mole fraction units as follows:

$$[FA_t] = \frac{0.005}{0.005 + 1 + \frac{1}{N_t}} \approx 0.005 \quad (5.19)$$

$$[P.FA] = f \cdot [FA_t] \quad (5.20)$$

$$[L_t] = \frac{1}{0.005 + 1 + \frac{1}{N_t}} \approx 1 \quad (5.21)$$

$$[P_t] = \frac{\frac{1}{N_t}}{0.005 + 1 + \frac{1}{N_t}} \approx \frac{1}{N_t} \quad (5.22)$$

where N_t is the molar ratio of host phospholipid:channel and f is the fraction of immobile 14-SASL. The latter approximations are true when the number of binding sites and total fatty acid molecules are much smaller than the number of host phospholipid molecules.

For the combined analysis of samples containing different molar ratios of lipid:channel, the terms in Eq. 5.18 can be rearranged to a quadratic giving the concentration of fatty acid bound to the inner cavity:

$$[P.FA] = \frac{\{[P_t] + [FA_t] + K_E \cdot [L_t]\} - \sqrt{\{[P_t] + [FA_t] + K_E \cdot [L_t]\}^2 - 4 \cdot [P_t] \cdot [FA_t]}}{2} \quad (5.23)$$

This equation was used to fit the data obtained for 14-SASL in samples with increasing DOPC:KcsA tetramer molar ratios in order to estimate a single K_E value. The data were represented using mole fraction units as described above, and plotted with the fatty acid bound to KcsA ($P.FA$ = y axis) as a function of the host phospholipid:channel molar ratio (N_t = x axis). The data were fitted using the non-linear least-square routine in SigmaPlot.

5.2.6 Estimation of a membrane partition coefficient for 14-SASL

As described in Chapter 4, due to the significant solubility of fatty acids in water, an effective dissociation constant (K_d, Eq. 4.2) needs to be estimated for fatty acids partitioning in the lipid bilayer[97]. The DOXYL moiety in the spin labelled fatty acid makes it more polar than stearic acid and oleic acid, so that it partitions less well into the lipid bilayer. Experimental data obtained for partitioning of 12-SASL into lipid bilayers by Rooney *et al.*[113] gives an effective K_d of 96 μM for 12-SASL in a medium of pH 7.2 and high ionic strength (0.1 M KCl) where the effects of charge repulsion are minimised. Blatt *et al.*[114] have shown that partition coefficients for spin labelled fatty acids with the spin label at positions between C10 and C16 are very similar, so that the effective K_d for 14-SASL has also been put at 96 μM.

5.2.7 Fluorescence quenching with 14-SASL

Fluorescence quenching experiments with wild type KcsA, the mutant W67,68 and with the hydrophobic tryptophan analogue NPTH (*N*-palmitoyl-L-tryptophan *n*-hexyl ester) in DOPC bilayers were performed as described in Chapter 2, Section 2.2.3 by titration with 14-SASL or 9,10-dibromostearic acid, allowing direct comparison of the quenching effects of the two fatty acids. Direct titration of 9,10-dibromostearic acid into the fluorescence cuvette was found to give the same result as when the fatty acid was dried together with the phospholipid prior to reconstitution, but since the titration method requires less fatty acid to be used in each set of measurements it was used for the present experiments with 14-SASL due to the limited availability of 14-SASL. For the NPTH samples, unlike with the KcsA samples, NPTH was directly dried from organic solvent together with the lipid and the use of detergent was unnecessary. All samples were prepared using 600 µM DOPC to ensure incorporation of the majority of the 14-SASL into the phospholipid bilayer; with a K_d = 96 µM, 86 % of the spin labelled fatty acid will partition into the lipid bilayer under these conditions. (For 9,10-dibromostearic acid, with a K_d = 17 µM, 97 % of the fatty acid will partition into the membrane.)

As described in Chapter 2, excitation of tryptophan fluorescence was performed at 290 nm and fluorescence intensities were measured at 333 nm (see also Appendix 1).

5.2.8 Simulation of the quenching curves expected for 9,10-dibromostearic acid

As described later, the ESR results suggest a high affinity binding site for fatty acids on KcsA. One possibility is that the high affinity site for fatty acids corresponds to the non-annular sites on KcsA or to some ‘hotspot’ for binding fatty acids in the lipid annulus. Binding of 9,10-dibromostearic acid to such a high affinity site would be expected to result in marked fluorescence quenching at low concentrations of 9,10-dibromostearic acid. Simulations were performed to determine the quenching profile expected from such binding, with the mutant W67,68 reporting on binding to just the non-annular sites or with the wild type KcsA being sensitive to binding to a ‘hotspot’ in the lipid annulus of each subunit.

Simulations of quenching resulting from binding at the non-annular site in the mutant W67,68 used Eq. 4.14 with an n value of 0.94, an F_{min} value of 0.43 as determined experimentally in Chapter 4, and the chosen value for K.

Two models were used to describe the effect expected from binding in the lipid annulus. In the first it was assumed that binding of the fatty acid is similar at all annular sites. Quenching was then calculated using Eq. 4.22 with the following parameters: $n^A = 4.3$, $n^{NA} = 0.94$, $F^A_{min} = 0.27$, $F^{NA}_{min} = 0$, $K^{NA} = 0.86$, as determined experimentally (Chapter 4) and the chosen value for K^A.

The second model assumed strong binding of the fatty acid at a single 'hotspot' in the annulus of each subunit, the site being close enough to one of the lipid exposed tryptophan residues to result in quenching. Eq. 4.22 was therefore modified to give:

$$F = [1 + F^{HA}_{min} + 2F^{A}_{min} + F^{NA}_{min} + (1 - F^{HA}_{min})(1-f^{HA}_{Br})^{nHA} + 2(1 - F^{A}_{min})(1-f^{A}_{Br})^{nA} + (1 - F^{NA}_{min})(1-f^{NA}_{Br})^{nNA}]/5 \quad (5.24)$$

where F^{HA}_{min} is the minimum fluorescence intensity for the lipid exposed tryptophan residue quenched by the fatty acid binding at the 'hotspot' in a hypothetical membrane of 100 % brominated fatty acid, n^{HA} is the number of high affinity binding sites from which fluorescence of one of the lipid exposed tryptophan residues can be quenched, which is assumed to have a value of 1, and f^{HA}_{Br} is the fractional occupancy of the 'hotspot' by brominated fatty acid, described, by analogy to Eq. 4.11, as follows:

$$f^{HA}_{Br} = \frac{K^{HA} \cdot x_{Br}}{K^{HA} \cdot x_{Br} + (1 - x_{Br})} \quad (5.25)$$

where K^{HA} is the relative binding constant of the fatty acid at the annular 'hotspot'. The values of K^{NA}, n^{NA}, F^A_{min}, F^{NA}_{min}, n^A were the same as in the previous simulation with a $K^A = 0.73$, as determined experimentally in the previous chapter. The value of

F^{HA}_{min} was fixed at 0.27, the same determined for the other annular sites, with $n^{HA} = 1$, and the chosen value for K^{HA}.

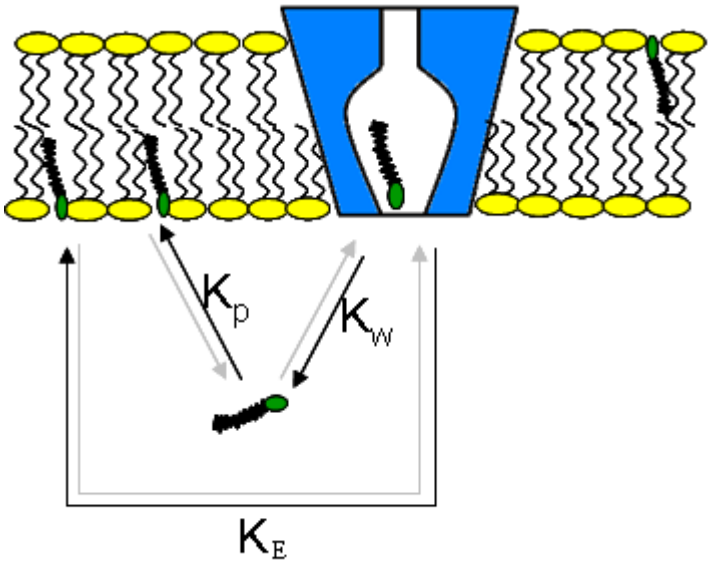

Figure 5.2 Schematic model for fatty acid binding to the inner cavity of KcsA. The solubility of the fatty acid in water would allow it to access the inner cavity when the channel is open, as illustrated in the diagram. Dissociation of the fatty acid from the inner cavity into water is described by the dissociation constant K_w, and partitioning of the fatty acid into the phospholipid bilayer is described by K_p. The overall equilibrium between fatty bound to the inner cavity and fatty acid incorporated into the lipid bilayer is described by the dissociation constant K_E, given by $K_E = K_w \cdot K_p$.

5.3 Results

5.3.1 Interaction of phospholipids with KcsA: studies with ESR

In order to compare the relative affinities of different phospholipids for KcsA by ESR, the channel was reconstituted in DOPC bilayers at a DOPC:KcsA tetramer molar ratio of 60:1. 14-PCSL, 14-PESL, 14-PGSL, 14-PSSL and 14-PASL were added to aliquots of the same reconstituted KcsA sample. Spectra are shown in Figure 5.3, normalised to equal area. All the spectra measured at 30 ˚C and shown in Figure 5.3 were successfully deconvoluted, but only some of the spectra recorded at 25 ˚C or 35 ˚C could be successfully fitted. Appendix 2 contains the details of all the deconvolutions; spectral deconvolution of the same sample measured at different temperatures did not show any significant differences in the fraction of immobile and mobile components.

Table 5.1 summarizes the proportion of the immobile component for each sample at 30 ˚C together with the lipid binding constants relative to PC calculated using Eq. 5.3, as described in section 5.2.2.

Figure 5.3 also shows the normalised ESR spectra for 14-PGSL and 14-PCSL for KcsA reconstituted in DOPG at a DOPG:channel molar ratio of 60:1 (blue), and Table 5.2 gives the fraction of the immobile component for each spectrum, and the corresponding lipid binding constants relative to DOPG. PC shows a lower affinity for KcsA than DOPG, with a binding constant relative to DOPG of 0.62 ± 0.26; the inverse of the latter value gives the binding constant of DOPG relative to PC, with a value of 1.61, in excellent agreement with the value of 1.76 ± 0.22 obtained for KcsA reconstituted in DOPC. The ESR spectra for both 14-PGSL and 14-PCSL in DOPG show slightly greater maximum splittings than those seen in DOPC membranes (Figure 5.3), as also observed in Chapter 3 (Figure 3.7). The reason for this difference is not known, but the fact that the splitting for all the different phospholipids in DOPC are similar, and the splitting for 14-PGSL and 14-PCSL in DOPG are also similar, suggests that the observed differences in splitting are due to the unlabelled host phospholipid and not the spin labelled species.

5.3.2 Interaction of fatty acids with KcsA: studies with ESR

Interaction of 14-SASL with KcsA in a DOPC background

The interaction of spin labelled stearic acid (14-SASL) with KcsA was studied in the same way as described for the phospholipids in the previous section. Figure 5.4 shows the ESR spectrum of 14-SASL in DOPC bilayers containing KcsA at a 60:1 molar ratio of DOPC:channel and compares it with the spectrum of a similar sample containing 14-PCSL. Two important features stand out in the 14-SASL spectrum. First, it can be seen that for 14-SASL the proportion of the immobile component is markedly higher than for 14-PCSL (Figure 5.4) or for the other spin labelled phospholipids (Figure 5.3); this suggests that 14-SASL has a much higher affinity for KcsA than the spin labelled phospholipids. Second, the maximum splitting for the immobile component with 14-SASL (64.6 Gauss) is markedly larger than that observed for 14-PCSL (ca. 60.7 Gauss), indicating that the fatty acyl chain of 14-SASL is much more restricted in motion when bound to KcsA than is the spin-labelled chain of 14-PCSL. In fact, the spectrum of 14-SASL bound to KcsA resembles the spectrum of 14-SASL bound to BSA (Figure 5.4 in light green), suggesting that the interaction of the fatty acid with the channel is significantly different from that normally observed with the annulus of a transmembrane protein.

The very high fraction of the immobile component observed for 14-SASL in the presence of KcsA is unexpected since the fluorescence quenching results with brominated fatty acids described in the previous chapter suggest that the affinity of the annular and non-annular sites for fatty acid and phospholipids are rather similar. One difference between the fluorescence and ESR studies is that the fluorescence studies were performed at a molar ratio of lipid:channel of 400:1 or higher where aggregation of KcsA does not occur whereas the ESR studies shown in Figure 5.4 were performed at a molar ratio of lipid:KcsA of 60:1 where some aggregation is possible, as described in Chapter 3. Effects of lipid:channel molar ratio on the interaction between 14-SASL and KcsA were therefore studied. As in the experiments described in Chapter 3 with 14-PCSL, two different sets of samples were analysed. Figures 5.5 and 5.6 show the normalised spectra of each of the set of samples. It is clear that in both sets of samples at all lipid:channel molar ratios the proportion of immobile component is very markedly higher than with the phospholipids (compare with Figures 3.4, 3.5

and 3.6) and the maximum splitting remains the same. Many of the spectra could not be deconvoluted adequately but Table 5.3 summarizes the fraction of immobile component from those spectra successfully deconvoluted; details of the analysis of these can be found in Appendix 2.

Interaction of 14-SASL with KcsA in a DOPG background

Binding of 14-SASL to KcsA was also studied with DOPG as the background lipid, for a sample at a molar ratio of DOPG:channel of 88:1. Figure 5.7 compares the ESR spectrum with that obtained with DOPC as the background lipid at the same lipid:channel molar ratio. It can be seen that the spectra are practically identical, the sample in DOPG only having a slightly smaller maximum splitting (63.5 Gauss). Deconvolution of the spectra give a fraction of 14-SASL interacting with KcsA of 0.788 ± 0.013, the same as in the DOPC sample (0.781 ± 0.07, Table 5.3).

Effect of pH upon interaction of 14-SASL with KcsA

The effect of changing the pH on the interaction of 14-SASL with KcsA was studied. At physiological pH (7.2) all the fatty acid in the aqueous medium will be deprotonated as the pK_a of a fatty acid in water is ≈ 5. The pK_a will, however, change as it incorporates into the DOPC bilayer shifting to 7.4[97], so that ca. 40 % of the bound fatty acid will remain negatively charged. This change in pK_a upon incorporation into the lipid bilayer is due to stronger binding of the uncharged form of the fatty acid than of the charged form, and is also affected by the charge build up on the bilayer resulting from the binding of the charged form of the fatty acid, further decreasing the effective binding constant for the charged form[97]. Here the importance of charge on 14-SASL binding to KcsA was determined by studying binding at pH 3.9 where all the fatty acid will be protonated, both in aqueous solution and bound to the lipid bilayer.

Figure 5.8 compares the ESR spectrum of 14-SASL in the sample containing a DOPC:KcsA tetramer molar ratio of 60:1 at pH 7.2 with that at pH 3.9. The ESR spectrum at pH 3.9 shows that most of the 14-SASL is no longer interacting with the channel, suggesting that the negative charge is important for the interaction. Importantly, the maximum splitting of the small immobile component present at pH 3.9 remains the same as in the sample of pH 7.2, indicating that the fraction of fatty

acid that is still interacting with the channel is doing so in a similar way as at pH 7.2. A small third component can be observed inbetween the other two (low magnetic field peaks) that becomes more apparent when measured at 15 ˚C. This indicates that a small fraction of the spin labelled fatty acid has a mobility different to those observed previously.

The effect of decreasing the pH was also studied for KcsA in DOPG at a molar ratio of DOPG:channel of 88:1 (Figure 5.9). In this case, the entire immobile component present at pH 7.2 has disappeared at pH 3.9. When measured at 15 ˚C, another immobile component different to the one at pH 7.2 again becomes obvious, with a splitting very similar to that of the third component observed in the DOPC sample at pH 3.9. At first sight, the spectrum at pH 3.9 measured at 25 ˚C may look like a single component spectrum, but in fact the spectrum measured at 25 ˚C does not fit to a single mobile component (Figure 5.10, green) because there is a new immobile component of smaller splitting, as clearly seen when the spectrum is measured at 15 ˚C; deconvolution of the spectra at 25 ˚C (see the fitted spectra in red in Figure 5.10) revealed a fraction of immobile component of 0.407 ± 0.044.

5.3.3 Fluorescence quenching with 14-SASL

One possible explanation for the high affinity binding of 14-SASL observed with the ESR experiments is that the DOXYL group present in 14-SASL results in much stronger binding to the annular or non-annular sites on KcsA than observed with 9,10-dibromostearic acid. This idea was tested making use of the fact that the DOXYL group, like the dibromo group, is a quencher of tryptophan fluorescence.

The spin labelled group in 14-SASL has been shown to cause static quenching of tryptophan fluorescence in lipid bilayers, and the critical distance from which efficient quenching occurs has been estimated to be 11 Å, so that for a spin labelled lipid to cause significant quenching of a Trp residue in a protein the lipid will need to be in contact with the protein[115]. However, because of its ability to cause efficient quenching from a longer distance than bromine (ca. R = 8 Å, as detailed in Chapter 2), quenching with 14-SASL would be expected to be slightly more efficient than with 9,10-dibromostearic acid. This is confirmed in Figure 5.11A showing the quenching of the hydrophobic tryptophan analogue NPTH with the two fatty acids; the acyl

chains attached to the tryptophan in NPTH makes it incorporate fully into the lipid bilayer[97]. It can be seen that the level of quenching with 14-SASL is slightly greater than with 9,10-dibromostearic acid, but with a similar concentration dependence. This shows therefore that, as expected, the fluorescence quenching properties of 14-SASL and 9,10-dibromostearic acid are very similar.

Figure 5.11 also shows that quenching of wild type KcsA with 9,10-dibromostearic acid and with 14-SASL are also very similar, the only difference being a slightly higher degree of quenching with the spin labelled fatty acid. The same is also true with the mutant W67,68. These experiments therefore show that the affinity of 14-SASL for the annular and non-annular sites in KcsA must be very similar to that of 9,10-dibromostearic acid, and so the high affinity site observed in the ESR experiments is unlikely to correspond to binding to the annular or non-annular sites.

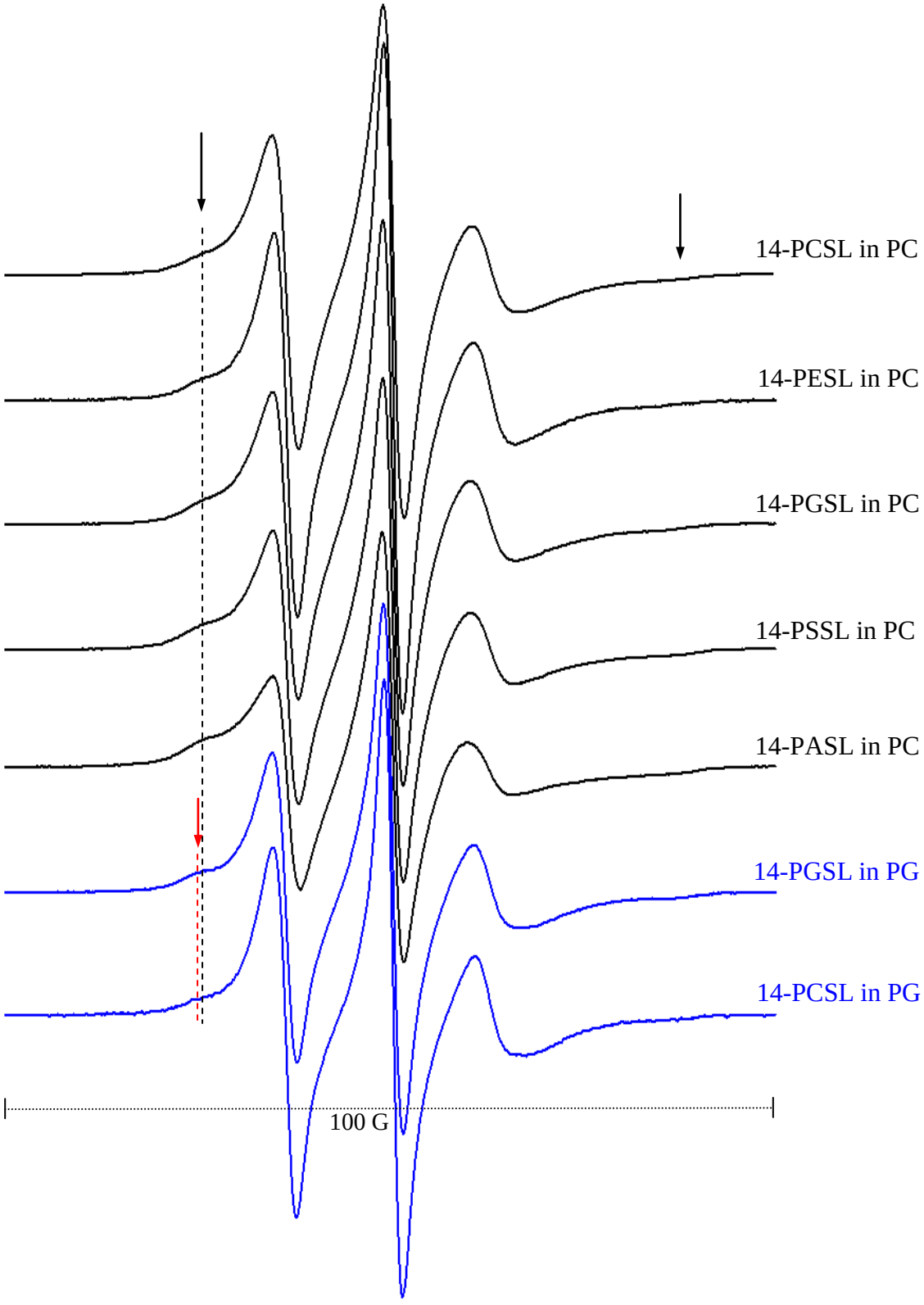

Figure 5.3 Normalised ESR spectra for spin labelled phospholipids in DOPC (black) or DOPG (blue) membranes at a lipid:channel molar ratio of 60:1, measured at 30 ˚C. The outer peaks from the component arising from spin labelled phospholipid in contact with the protein are marked by the black arrows. The low field peak arising from the immobilised component is in the same position for all the spin labelled phospholipids in DOPC, as marked by the black dashed line, but for samples in DOPG the peak is at a slightly lower field, as shown by the red arrow and dashed line. The total scan width is 100 gauss.

Spin labelled lipid	Fraction of immobile component	Binding constant *K* relative to PC	Binding constant *K* relative to PC obtained by fluorescence quenching[73]
PC	0.291 ± 0.066	1	1
PE	0.432 ± 0.007	1.85 ± 0.05	0.69 ± 0.10
PG	0.419 ± 0.032	1.76 ± 0.24	1.66 ± 0.20
PS	0.525 ± 0.013	2.69 ± 0.14	2.16 ± 0.17
PA	0.600 ± 0.025	3.65 ± 0.41	1.95 ± 0.22

Table 5.1 Fraction of the immobile component and the lipid binding constants relative to DOPC derived from the ESR spectra in membranes containing a DOPC:channel molar ratio of 60:1, measured at 30 ˚C. Details of the deconvolution analysis are shown in Appendix 2. The relative binding constants obtained from the ESR measurements were calculated from Eq. 5.3 and are compared with those determined by fluorescence quenching measurements by Alvis *et al*[73].

Spin labelled lipid	Fraction of immobile component	Binding constant *K* relative to 14-PGSL
14-PGSL	0.360 ± 0.066	1
14-PCSL	0.259 ± 0.072	0.62 ± 0.26

Table 5.2 Fraction of the immobile component and the lipid binding constants relative to DOPG derived from the ESR spectra of 14-PGSL and 14-PCSL in membranes containing a DOPG:KcsA tetramer molar ratio of 60:1, measured at 30 ˚C. Details of the deconvolution analysis are shown in Appendix 2. As in Table 5.1, the relative binding constants were obtained from Eq. 5.3.

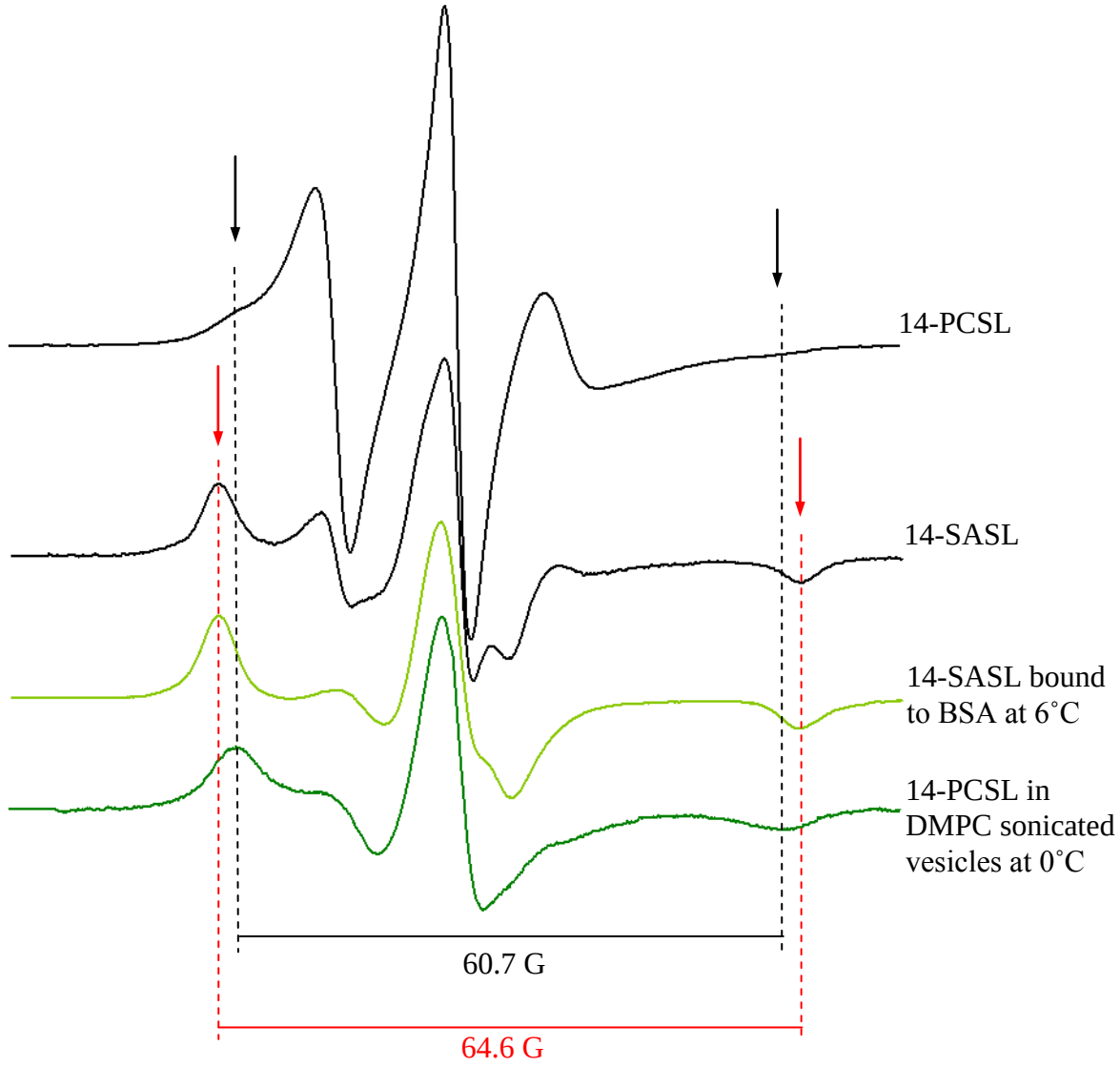

Figure 5.4 Comparison of normalised ESR spectra for 14-SASL and 14-PCSL in membranes containing a DOPC:channel molar ratio of 60:1, measured at 25 ˚C. The spectra are also compared with the single restricted component spectra used for deconvolution of the composite spectra, in order to highlight the location of the outer peaks. The black arrows and dashed lines indicate the location of the outer peaks in the 14-PCSL composite spectrum, which match that of the single restricted component spectrum of 14-PCSL in sonicated vesicles of DMPC at 0˚C (dark green). The red arrows and dashed lines mark the outer peaks in the 14-SASL composite spectrum, which in turn match that of the spectrum of 14-SASL bound to BSA at 6˚C (light green). The total scan width is 100 gauss.

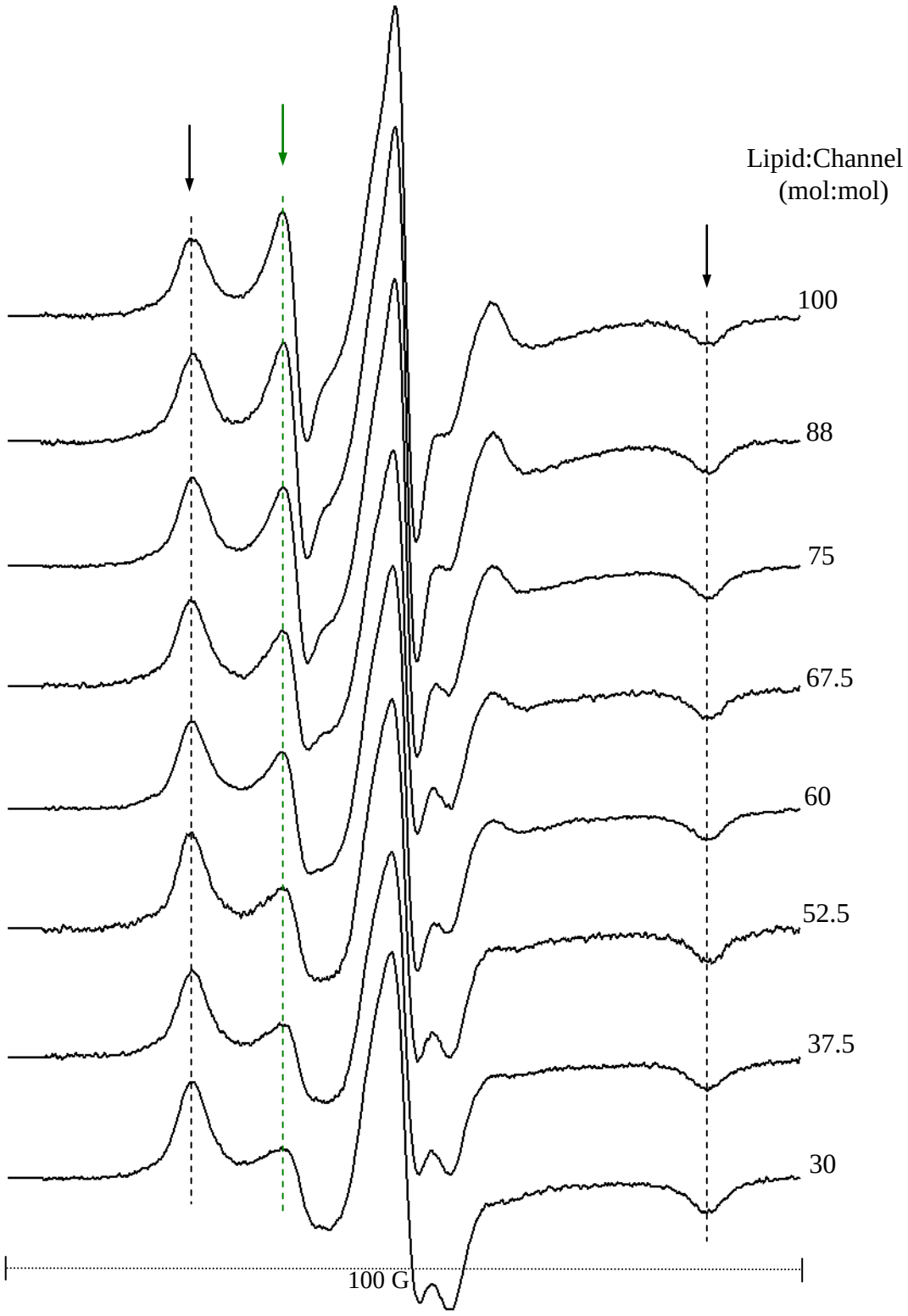

Figure 5.5 Normalised ESR spectra for 14-SASL in DOPC membranes containing KcsA as a function of DOPC:channel molar ratio, recorded at 25 ˚C. The set of samples in this figure originated from the same preparation as that used to obtain the spectra shown in Figure 3.4. Here, the component arising from 14-SASL in contact with KcsA (restricted component) dominates the spectra (black arrows), with small amounts of a mobile component (compare with Figures 3.4, 3.5 and 3.6). The low field peak of the mobile component is indicated by the green arrow and green dashed line. Total scan with is 100 gauss.

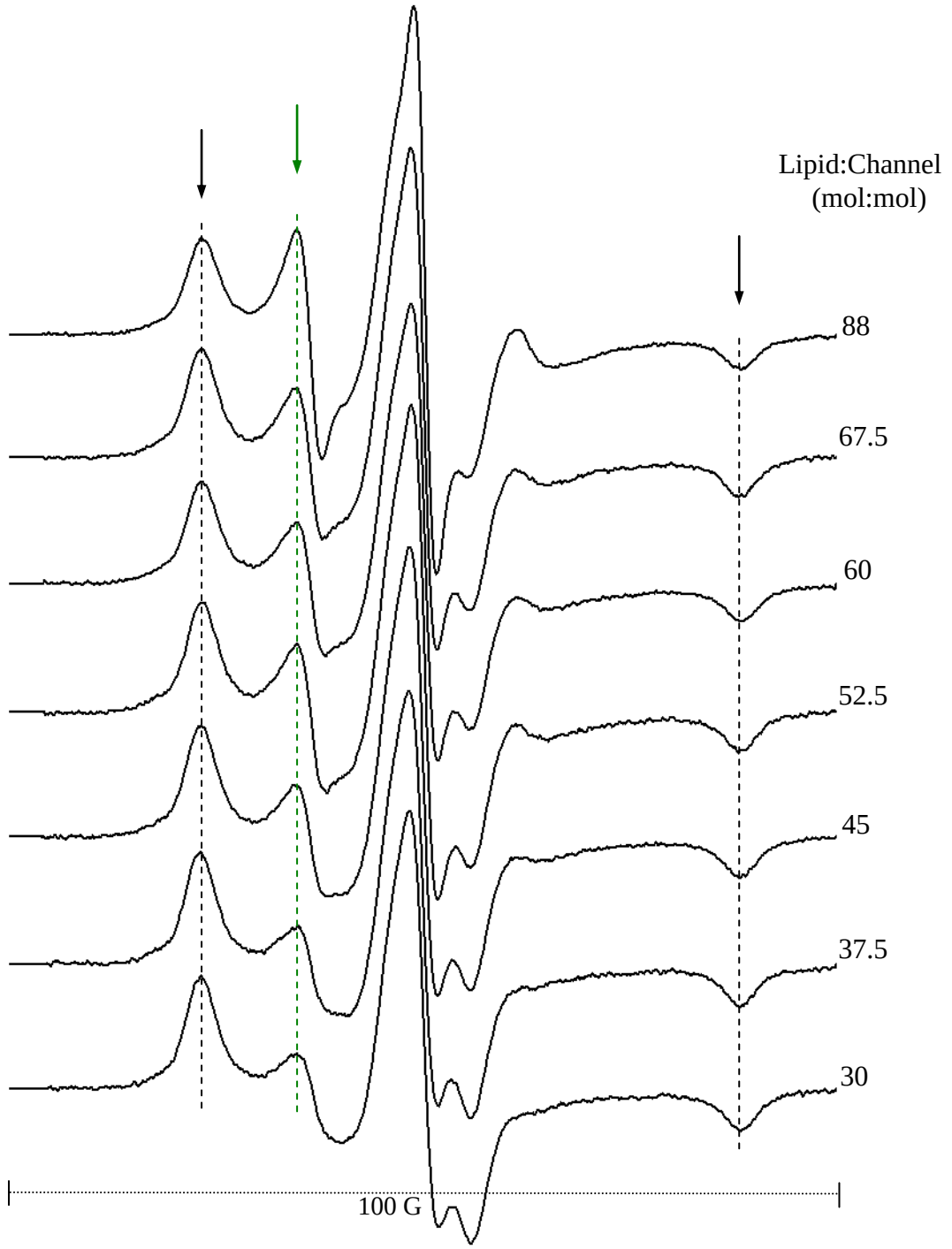

Figure 5.6 Normalised ESR spectra of a second set of samples of 14-SASL in DOPC membranes containing KcsA as a function of DOPC:channel molar ratio, recorded at 25˚C. This set of samples originated from the same preparation used to obtain the spectra shown in Figure 3.5. Details are as in figure legend 5.5.

DOPC/KcsA tetramer molar ratio	Fraction of immobile component in the 14-SASL spectra (*f*)	Fraction of immobile component in the 14-PCSL spectra (f_o)	Relative binding constant if 14-SASL and 14-PCSL bind to the same sites	Relative binding constant if 14-SASL binds only at a 'hotspot' in the annulus or at the non-annular sites
30 (2nd)	0.900 ± 0.020	0.294 ± 0.037	21.61 ± 6.00	61.20 ± 17.08
37.5 (2nd)	0.900 ± 0.025	0.286 ± 0.042	22.47 ± 8.32	79.53 ± 29.62
60 (2nd)	0.837 ± 0.012	0.240 ± 0.010	16.26 ± 1.54	77.45 ± 7.45
67.5 (1st)	0.837 ± 0.013	0.275 ± 0.038	13.54 ± 1.40	88.56 ± 9.30
88 (2nd)	0.781 ± 0.07	*0.369 ± 0.044	6.01 ± 0.26	82.67 ± 3.58
100 (1st)	0.738 ± 0.012	0.319 ± 0.037	6.01 ± 0.39	75.12 ± 5.03

Table 5.3 Fraction of the immobile component of 14-SASL in DOPC membranes containing KcsA (*f*) at the given lipid:channel molar ratios, and relative 14-SASL binding constants calculated as described in the text. Details of the deconvolution analysis are shown in Appendix 2. Only the spectra that were accurately deconvoluted are shown here; next to the lipid:channel molar ratio, in parenthesis, is given the set of samples to which each particular deconvoluted spectrum belongs. The fraction of the immobile component of the corresponding samples labelled with 14-PCSL (f_o) is also listed. The relative binding constant for 14-SASL calculated assuming that 14-SASL and 14-PCSL bind to the same sites was calculated from Eq. 5.3. Relative binding constants for 14-SASL were also calculated as described in Section 5.2.3 assuming that 14-SASL binds just to a 'hotspot' in the annulus of a KcsA monomer or at the non-annular binding sites; in both cases four binding sites were assumed per KcsA channel. All spectra were recorded at 25˚C.

*The fraction of the immobile component for 14-PCSL at a lipid:channel molar ratio 88:1 shown here corresponds to that obtained from the 1st set of samples.

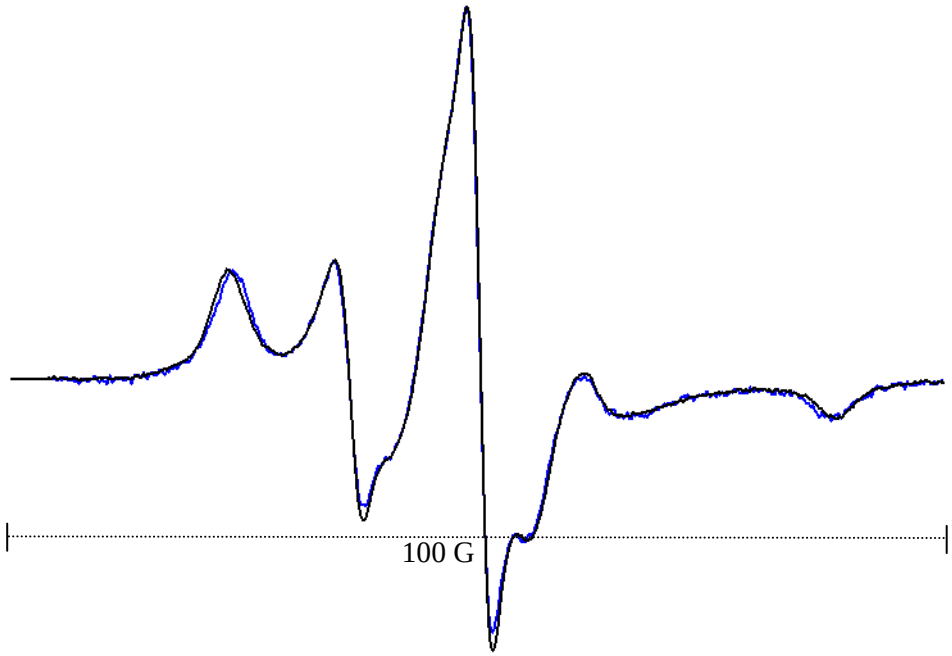

Figure 5.7 Comparison of the normalised ESR spectra for 14-SASL in DOPG (blue) and DOPC (black) containing KcsA at a lipid:channel molar ratio of 88:1, measured at 25˚C. The two spectra are almost identical, the sample in DOPG having only a slightly smaller maximum splitting. The scan width is 100 gauss.

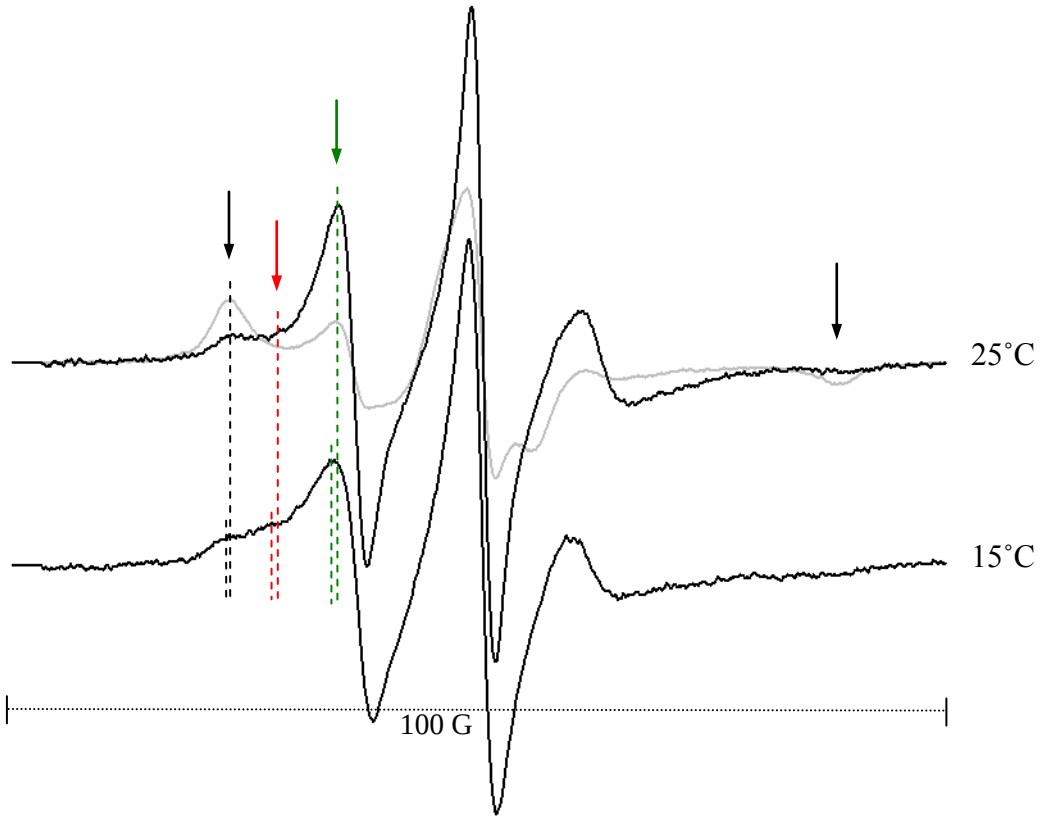

Figure 5.8 Normalised ESR spectra for 14-SASL in DOPC membranes containing KcsA at a DOPC:channel molar ratio of 60:1 at pH 3.9 (black) and pH 7.2 (grey). At the lower pH, a large proportion of the strongly immobilised component disappears, as indicated by the black arrows. The green arrow marks the low field peak from the mobile component and a possible low field peak arising from a third component is indicated by the red arrow. The spectra recorded at 25 ˚C are compared with the spectrum at pH 3.9 and 15 ˚C. At the lower temperature the possible third component becomes more apparent, and as expected, the maximum splitting of each of the components increases, as reflected by the shift of the low field peaks towards the left of the spectra, indicated by the dashed lines. The scan width is 100 gauss.

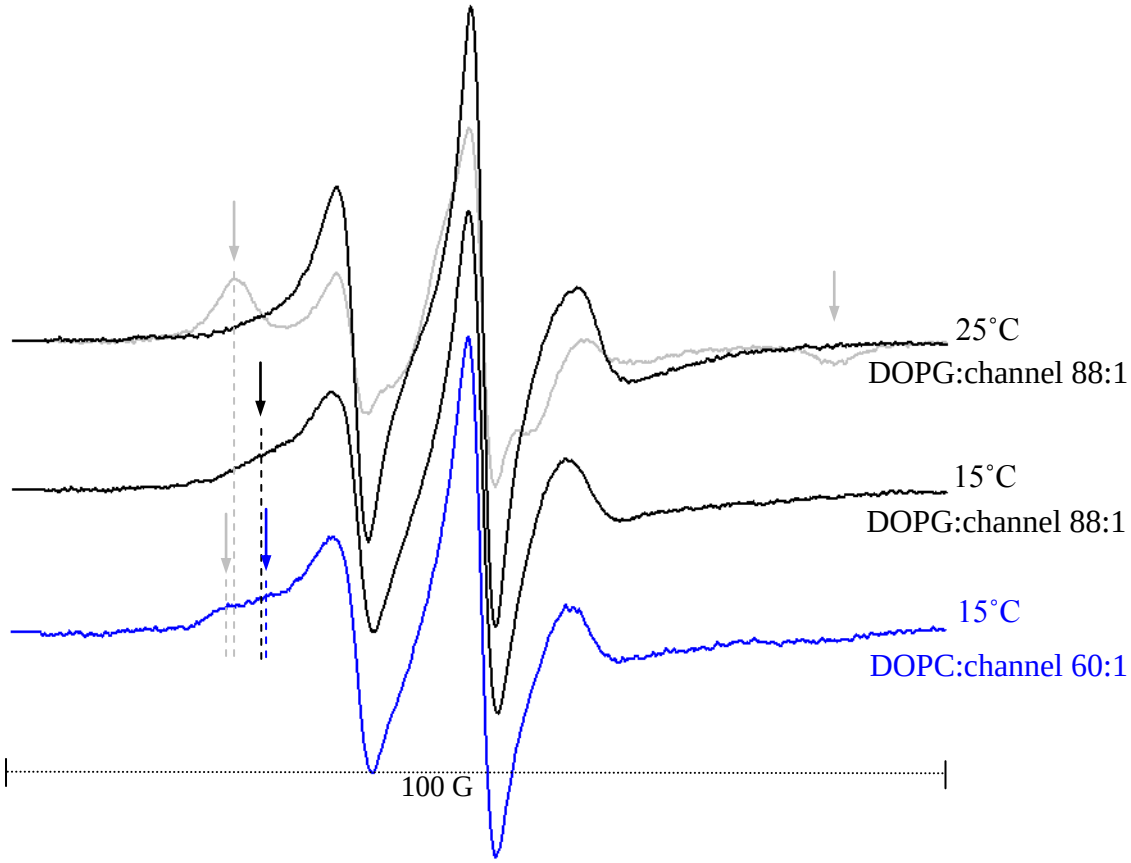

Figure 5.9 Normalised ESR spectra for 14-SASL in DOPG membranes containing KcsA at a DOPG:channel molar ratio 88:1, at pH 3.9 (black) and pH 7.2 (grey). In DOPG membranes, at the lower pH and 25 ˚C all the strongly immobilised component has disappeared, as indicated by the grey arrows, and signs of a third component are not evident. However, at 15 ˚C an immobile component can be observed (black arrow), with a position close to that of the third component (blue arrow) observed in the sample shown in Figure 5.8, here shown in blue. The scan width is 100 gauss.

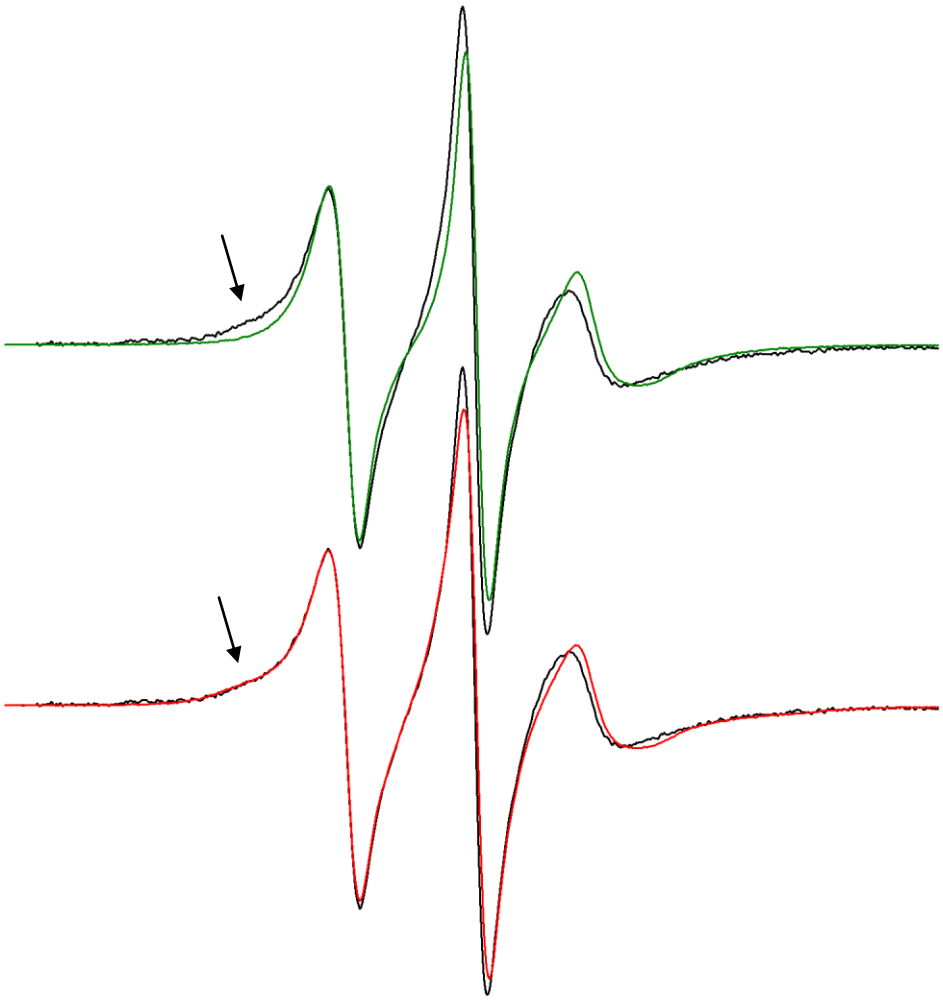

Figure 5.10 Analysis of the spectra for 14-SASL in DOPG membranes containing a DOPG:channel molar ratio of 88:1 at pH 3.9. The experimental spectrum is the same as in Figure 5.9 and is shown in black. When fitting the experimental spectrum to a single mobile component (green), the mismatch of the peak at low magnetic field clearly shows that an immobile component is also present in the experimental spectrum, as indicated by the arrow. When the experimental spectrum is fitted to two components (immobile and mobile), the low magnetic field peaks fit well in the fitted spectrum (red), as indicated by the arrow. It can also be seen that the rest of the spectrum fits better when using two components than when using a single mobile component.

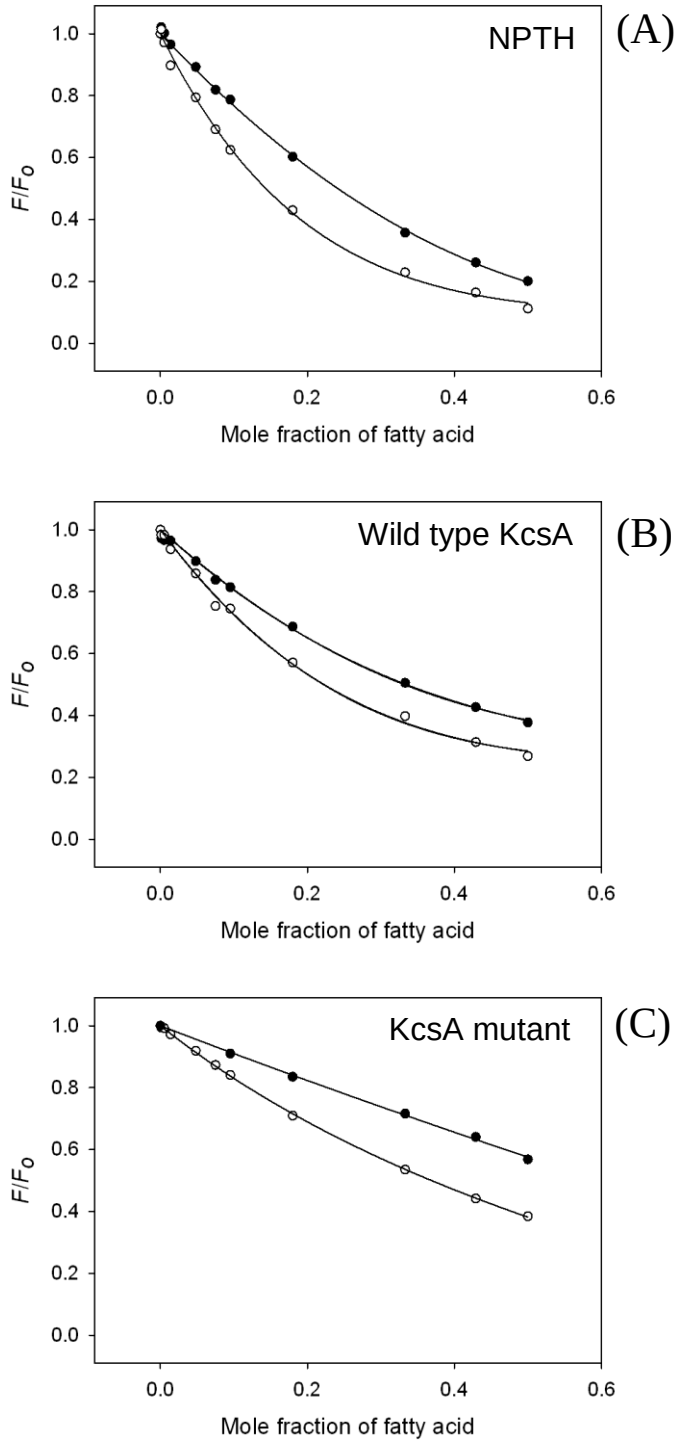

Figure 5.11 Fluorescence quenching with 9,10-dibromostearic acid and 14-SASL. Fluorescence quenching is compared for the hydrophobic tryptophan analogue NPTH (A), wild type KcsA (B) and the KcsA mutant W67,68 (C). Experiments were performed by direct titration with 9,10-dibromostearic acid (●) or 14-SASL (○) at a DOPC to NPTH molar ratio of 300:1, and at a DOPC to KcsA tetramer molar ratio of 4000:1 for wild type KcsA and 1600:1 for the mutant W67,68. The DOPC concentration was in all cases 600 µM.

5.4 Discussion

5.4.1 Interaction of phospholipids with KcsA: studies with ESR

All phospholipids, including PE, showed a slightly greater affinity for KcsA than PC ranking as follows: PC < PE ≈ PG < PS< PA (Table 5.1). The range of relative lipid binding constants (*K* values) observed are similar to those observed for other membrane proteins obtained with ESR[24] and fluorescence spectroscopy[14,31,73,83,116,117], effects of lipid headgroup structure being rather small with *K* values lower than 5. Only in a few cases have larger relative binding constants been reported, as in the mechanosensitive channel MscL, where, using fluorescence quenching studies, a cluster of three positively charged residues was shown to bind phosphatidic acid with a binding constant relative to PC of ca. 8.5 [14].

The relative binding constants for KcsA obtained from fluorescence studies with brominated phospholipids[73] are not the same as those obtained here with ESR. Table 5.1 compares the two sets of binding constants. Both ESR and fluorescence spectroscopy methods report a higher binding constant for anionic lipid that for DOPC, although with ESR the estimated binding constant for PA is greater than that estimated from the fluorescence data. Another difference between the two sets of data is that the ESR results show a binding constant for PE greater than for PC, whereas the fluorescence data suggest a binding constant for PE less than that for PC.

There are a number of possible explanations for the differences between the two sets of results. One possibility is that a small number of sites on KcsA show a high affinity for PE and PA and the ESR results will be dominated by this high affinity binding (the resulting *K* values being a weighted average in favour of the high affinity binding sites) whereas the fluorescence results give a binding constant more equally averaged over all the binding sites. This is likely to be particularly important for anionic lipids which can bind to non-annular as well as annular sites.

An additional complication is that the ESR experiments were performed at a molar ratio of DOPC:KcsA tetramer of 60:1, conditions under which KcsA shows

some aggregation, as discussed in Chapter 3, whereas the fluorescence experiments were performed at a molar ratio of lipid:channel ratio of 400:1, conditions under which there is no aggregation; aggregation of KcsA could affect the way lipids interact with the protein.

Another difference between the two approaches is that in the ESR approach the lipid composition of the membrane remains essentially constant, being predominantly the host lipid DOPC in all experiments, whereas in the fluorescence approach the lipid composition varies from 100 % DOPC to 100 % of the second lipid, and it is possible that lipid binding to the protein is affected by the nature of the lipid in the bilayer. For example, it is known that water molecules interact differently with the headgroups of PC and PE[118]. Since hydrogen bonding of a PE molecule to KcsA will be in competition with hydrogen bonding of that PE molecule with water, it is possible that the affinity of PE for KcsA will be different in backgrounds of PC and PE. For the charged lipids, relative binding constants for PG and PS are very similar for the ESR and fluorescence determinations (Table 5.1). The large difference in the relative binding constant for PA determined by the two different methods could again be related to the differences in the background lipid. It has been suggested that the phosphomonoester headgroup of PA has unique properties with respect to its ionisation behaviour, because it is strongly influenced by the background lipid composition and the interaction with positively charged residues (Figure 5.12)[119,120]. One of the hydroxyl groups of the phosphomonoester headgroup has a low pK_{a1} of 3.2 in a PC background bilayer that causes it to be fully deprotonated at physiological pH, while the other hydroxyl group has a pK_{a2} of 7.92, also in a PC background, which is strongly influenced by its environment. In their studies, Kooijman *et al.*[119] propose that this second hydroxyl group is held in a protonated state due to the formation of a hydrogen bond with the negatively charged oxygen atom from the other deprotonated hydroxyl group, this interaction being responsible for the pK_{a2} of 7.92 that keeps most of the PA with only one negative charge at the physiological pH. They also showed that interaction with positively charged lysine or arginine residues located at the membrane interface of transmembrane peptides destabilises this interaction by formation of a hydrogen bond between the amine group in the side chains and the negatively charged oxygen, which results in deprotonation of the second hydroxyl group (Figure 5.12); this then causes an increase in the negative charge on PA which

could result in stronger interaction between PA and the positively charged residues in the peptides[120]. It is possible that this effect explains the strong interaction observed with ESR but in the fluorescence quenching experiments the effect could be lost due to the increasing PA content of the samples. As the PA content increases, so does the negative charge on the membrane, attracting protons to the surface and decreasing the interfacial pH, favouring the protonated state of the second hydroxyl group of PA, which would prevent the more favourable interaction with the positively charged residues described above. Indeed Kooijman *et al.*[119] also showed that the presence of the negatively charged PS in the membrane could affect the ionisation state of PA in this way.

5.4.2 Interaction of fatty acids with KcsA: studies with ESR

The results with spin labelled phospholipids suggest, in agreement with the fluorescence quenching results[73] that binding of phospholipids to annular sites around KcsA is relatively non-specific. This is also consistent with the fluorescence quenching results with 9,10-dibromostearic acid that show that fatty acids can bind at these annular sites (Chapter 4, Section 4.3.3). Binding of fatty acids at annular sites around a variety of membrane proteins has also been studied using spin labelled lipids, giving binding constants for 14-SASL generally similar to those obtained with 14-PASL[24]. ESR spectra for the immobilised 14-SASL component in the presence of transmembrane proteins are also comparable to those for the immobilised 14-PASL component[24,25], consistent with fatty acid binding to the same sites on a membrane protein as phospholipids. However, the results obtained with 14-SASL binding to KcsA are very different. First, the fraction of immobile component for the 14-SASL spectra is much greater than that for the spin labelled phospholipids (compare Figures 5.5 and 5.6 with Figures 5.3, 3.4, 3.5 and 3.6), indicating that the fatty acid has a much greater affinity for the protein than do the phospholipids. Second, the maximum splitting of 14-SASL is larger than that of the spin labelled phospholipids (see Figure 5.4), resembling the spectra of the fatty acid bound to BSA. This indicates that the acyl chain of the fatty acid is strongly immobilised, in a similar way as to when it is bound to the hydrophobic pockets of BSA[121,122].

Binding of 14-SASL to KcsA can be analysed in a number of possible ways. Deconvolution of the fatty acid spectrum in the sample at a lipid:channel molar ratio of 60:1 (Figure 5.4) shows that the fraction of immobile component is 0.837 ± 0.012. If 14-SASL binds to KcsA at the same sites as the spin labelled phospholipids, the binding constant for fatty acid relative to PC can be determined from Eq. 5.3 by comparison with the ESR spectra for 14-PCSL recorded under the same conditions, as previously done with phospholipids (Tables 5.1 and 5.2). From Eq. 5.3, using an f_o value for 14-PCSL of 0.240 (Table 3.3), the resulting K value for 14-SASL is 16.26 ± 2.56, much higher than the value obtained by fluorescence quenching (0.73 ± 0.04) with brominated fatty acid and wild type KcsA (see Chapter 4, Section 4.4.1). To see what fluorescence quenching would be expected if 9,10-dibromostearic acid bound to the annular binding sites with a K_A value of 16.26, with binding to the non-annular sites described by a K^{NA} value of 0.87, as determined from the fluorescence quenching experiments, the expected fluorescence quenching curve was calculated using Eq. 4.22 and, as shown in Figure 5.13A (blue), predicts marked quenching at very low concentration of 9,10-dibromostearic acid, totally inconsistent with the experimental data.

Another possibility is that the ESR results with 14-SASL are dominated by binding to a particular 'hotspot' on KcsA. If such a hotspot existed amongst the annular sites on KcsA, and if the ESR spectrum was due solely to binding of fatty acid to the hotspot, then the relative binding constant calculated as described in Section 5.2.3, would be K^{HA} = 77.45 ± 7.45. The result of such binding on the fluorescence intensity would depend on the location of the proposed hotspot relative to the Trp residues in KcsA. With three lipid-exposed Trp residues per monomer, binding to an annular site would locate the fatty acid close enough to at least one residue to result in quenching. If binding at a hotspot resulted in quenching of fluorescence of just one of the lipid-exposed tryptophan residues in wild type KcsA, a hypothetical quenching curve for 9,10-dibromostearic acid and wild type KcsA could be calculated for K^{HA} = 77.45, the other binding constants taking the values already determined, as described in Section 5.2.8, using Eq. 5.24. As can be seen (Figure 5.13A, red), with such a high relative binding constant for a particular annular site, the fluorescence quenching curve shows a steep decrease in fluorescence at the start of the curve, at mole fractions of fatty acid below 0.2 (as marked by the red arrow). The

fluorescence quenching curve of wild type KcsA shown in Figure 5.11B with 9,10-dibromostearic acid does not show any such marked quenching at small mole fractions of fatty acid, suggesting that the presence of a hotspot with high affinity in the annular sites is unlikely.

Another possibility is that 14-SASL binds preferentially to the non-annular sites on KcsA with a high affinity. It is possible that binding to such sites would give a more restricted mobility for the chain, as shown by the increased splitting in the ESR spectrum. It might seem that this would be inconsistent with the fact that spin labelled PG in the presence of KcsA gives a splitting similar to that of spin labelled PC (Figure 5.3) even though PG binds with higher affinity to the non-annular sites than does PC. However, the X-ray diffraction study of KcsA shows that only one of the two chains of PG penetrates deeply into the non-annular site and this is the *sn*-1 chain[81] (Figure 1.17 in Chapter1), whereas the spin label in spin labelled PG is on the *sn*-2 chain (Figures 2.2 in Chapter 2 and 4.14 in Chapter 4) and so it is likely that its mobility is more like that of the lipids interacting with the annular sites. If it is assumed that 14-SASL is binding only to the non-annular sites on KcsA then using the equations described in Section 5.2.3 with four binding sites per tetramer, the observed fraction of immobile 14-SASL (0.837) gives a binding constant for 14-SASL relative to PC at the non-annular sites of 77.45 ± 7.45, a very high value. Again this is inconsistent with the results obtained from fluorescence quenching studies with brominated fatty acid where, from studies with the W67,68 mutant, a relative binding constant of 0.86 ± 0.08 was obtained. The expected quenching curve for the mutant if the brominated fatty acid had a relative affinity of 77.45 was calculated (Eq. 4.14) and again is inconsistent with the experimental data (Figure 5.13B).

Thus it seems that binding of 9,10-dibromostearic acid to KcsA at either the annular or non-annular sites with an affinity required to match the ESR results with 14-SASL would result in fluorescence quenching curves inconsistent with the experimental data. Of course, a remaining possibility is that the different chemical structures of 9,10-dibromostearic acid and 14-SASL results in their binding to KcsA at annular or non-annular sites with very different affinities. However, this can be tested, using the ability of the nitroxide spin label to quench tryptophan fluorescence. As shown in Figure 5.11, fluorescence quenching curves observed with 9,10-

dibromostearic acid or 14-SASL are very similar for both wild type KcsA and W67,68, and, in particular, there is no suggestion of the marked quenching at low concentration of 14-SASL that would be expected from the high affinity 14-SASL binding detected in the ESR spectrum.

Another possibility is that the very high level of immobilized fatty acid observed in the ESR spectra (Figure 5.4) is related in some way to aggregation of KcsA; the fluorescence studies were recorded at a molar ratio of lipid:channel of 400:1 or higher, where aggregation of KcsA does not occur whereas the ESR studies shown in Figure 5.4 were performed at a molar ratio of lipid:KcsA of 60:1 where some aggregation is possible, as described in Chapter 3. However, in studies of 14-SASL binding to KcsA as a function of the molar ratio of lipid:channel, high levels of immobilization of 14-SASL were observed even at high molar ratios of lipid:channel (100:1) where no aggregation of KcsA is expected (Figure 5.5, Figure 5.6 and Table 5.3). It is also observed that the maximum splitting is constant at all lipid:channel molar ratios (Figures 5.5 and 5.6), suggesting that the spectra do not arise from interaction of the fatty acid with channel aggregates.

The remaining possibility is that the binding site detected in the ESR experiments is a site different from the annular and non-annular sites detected in the fluorescence quenching experiments. Indeed, the ESR data seem to be inconsistent with competitive binding at the annular binding sites. If a binding constant for 14-SASL relative to PC is calculated from Eq. 5.3 using the spectra of 14-SASL and 14-PCSL at a DOPC:KcsA tetramer molar ratio of 100:1 (for the first set of samples: f = 0.738 and f_o = 0.319, respectively) a K value of 6.01 ± 1.63 is obtained, much lower than the value of 16.26 ± 2.56 obtained from the samples at a molar ratio of 60:1, although still much higher than that obtained from the fluorescence analysis. Again, as shown in Figure 5.13A (green), the expected fluorescence quenching curve with a value for K of 6.01 is also inconsistent with the experimental quenching data. When relative binding constants for 14-SASL were calculated in the same way for the other molar ratios of lipid:channel (Table 5.3), it was found that the resulting relative binding constants increase with decreasing molar ratio of lipid:channel from 6.0 to 21.6. This implies that the spectra from 14-SASL and 14-PCSL originate from interactions with different sites in the protein, as the proportion of 14-SASL and 14-

PCSL bound to the channel varies differently when the lipid:channel molar ratio is changed.

5.4.3 14-SASL binds to the inner cavity of KcsA with great affinity

If 14-SASL is not binding to the annular or non-annular sites, it must be binding to some alternative site (or sites) on KcsA. If these sites were distant from the Trp residues in KcsA then binding of either 14-SASL or brominated fatty acid to the new sites would not result in fluorescence quenching, and the fluorescence quenching experiments would detect only binding to the annular and non-annular sites. Binding of 14-SASL to the new sites would have to result in marked immobilization of the chain to explain the large increase in maximum splitting observed in the ESR spectra on binding. Binding would also have to be of very high affinity to explain the experimental results, so that, under the conditions of the ESR spectra where the concentration of 14-SASL in the membrane is just 0.5 mol %, the new sites would essentially be the only sites on KcsA to which 14-SASL would bind. The presence of just such a site has been suggested by two studies: one on calcium-gated potassium channels[45] and the other on voltage-gated potassium channels (Kv)[46]. In both studies, block of potassium channel current by the polyunsaturated fatty acid arachidonic acid (C20:4) was analysed in mutagenesis experiments which suggested that the fatty acid bound to the hydrophobic lining of the central aqueous cavity of the pore. Binding of a brominated or spin-labelled fatty acid to such a site in KcsA would indeed be too distant from the Trp residues in KcsA to result in fluorescence quenching.

The mutagenesis studies performed by the two groups are summarised in the aligned sequences shown in Figure 5.14. In the studies performed by Hamilton *et al.*[45] two calcium-activated potassium channels were analysed, hIK1 (from human), whose current is blocked by arachidonic acid, and rSK2 (from rat), which is not blocked by arachidonic acid. In the experiments, chosen residues predicted to face the pore of the hIK1 channel were mutated to residues of rSK2 at the corresponding positions. It was found that the mutations T250S and V275A abolished current inhibition by arachidonic acid in hIK1 (Figure 5.14, residues in red in the hIK1 sequence). These residues correspond to T75 and I100 in KcsA, respectively (Figure 5.14). Importantly, the reverse mutations in rSK2 (that is S359T and A384V) allowed current block with

arachidonic acid in rSK2, giving strong evidence for the two residues being responsible of binding arachidonic acid in the pore of the channel. Mutation of other residues in hIK1 that did not affect current block by arachidonic acid are highlighted in green in the hIK1 sequence. In the studies performed by Decher *et al.*[46], residues in the pore region of a voltage-gated potassium channel from rat, rKv1.5, were mutated to Ala. Among other new mutations, the authors found that mutation V494A (which corresponds to the V275 that was identified in hIK1) would also abolish current block by arachidonic acid in rKv1.5; however, mutation T469A (which corresponds to the T250 identified in hIK1) did not have any effect on channel block by arachidonic acid. An explanation for this apparent contradiction could lay on the nature of the mutations performed in the different experiments. As shown in Figure 5.15, in the KcsA structure T75 points its CH_3 and OH groups towards the inner cavity, suggesting both groups could be involved in binding of arachidonic acid in hIK1 and rKv1.5. In the hIK1 study, mutation of the Thr to Ser would only leave an OH group available for interaction with the fatty acid, but in the rKv1.5 study, mutation of the Thr to Ala would leave a CH_3 group available instead. This then suggests that a hydrophobic interaction between the CH_3 group of the Thr and the fatty acid could take place in the pore of both channels, which would explain why channel block was abolished in hIK1 but not in rKv1.5 in the mutagenesis experiments.

Three of the mutated residues that abolished current block by arachidonic acid in rKv1.5 (including V494) are in the same position as residues in KcsA (Figure 5.14, residues in blue in the KcsA sequence) shown to be important for binding of hydrophobic cation pore blockers like tetraethylammonium (TEA) and tetrabutylammonium (TBA)[67,70,71]. These same residues have also been shown to be important for binding of pore blocking β subunits (peripheral subunits that can associate to some voltage-gated potassium channels)[67,68,123,124] in other potassium channels. Figure 5.15 shows the position of these residues in the KcsA structure and details of how the TBA molecule binds in the inner cavity.

The studies performed by Decher *et al.*[46] showed the particular importance of the Ile residue (I497 in rKv1.5, see note in Figure 5.14 with respect to the residues numbering in rKv1.5), because this residue is highly conserved in Kv channels and can be changed naturally to Val by mRNA editing in human Kv1.1 (hKv1.1, see the

sequence in Figure 5.14 where I400 is highlighted in red), as well as in mouse and rat Kv1.1. hKv1.1 is also sensitive to current inhibition by arachidonic acid and the change of the particular Ile residue to Ala also abolished current inhibition; the same change had the same effect in other Kv channels as well. The study further showed that mutation of this Ile to Ala in just one of the four subunits of a channel was enough to avoid current inhibition by arachidonic acid, suggesting a single binding site for the fatty acid in the pore of the channel.

Alignment of the sequences of KcsA, Kv and calcium-activated (hIK1 and rSK2) potassium channels show that, even though the positions of the residues involved in binding arachidonic acid or hydrophobic cations such as TBA are the same in the different channels, the particular type of residue can vary from one type of channel to another (Figure 5.14). For example, for the position of I100 in KcsA, a Val is present in the other channels; for F103 in KcsA, an Ile is present in Kv channels and a Thr in calcium-activated channels, etc. This suggests that binding of hydrophobic molecules in the pore of potassium channels involve interactions with hydrophobic residues lining the pore, but the specificity of the residue-ligand interaction may vary according to the particular properties of the inner cavity of each channel. The importance of hydrophobic interactions for binding at the pore of potassium channels has been further highlighted by experiments performed with long chain alkyl-triethylammonium pore blockers[110-112], where blockers with longer alkyl chains (alkyl chains of up to twelve carbon atoms) had greater affinity for the pore. Figure 5.14 summarises mutagenesis studies performed by Choi *et al.*[112] comparing binding of TEA and long chain alkyl-triethylammonium ions in *Shaker*, a voltage-gated potassium channel from *Drosophila melanogaster*. Mutation of residues closest to the selectivity filter, just in the upper region of the inner cavity, (M440I and T441S in *Shaker*, shown in yellow in the *Shaker* sequence) reduced the binding affinity for TEA, but had little effect upon binding of C_{10}-TEA, while mutation of a polar residue located lower in the inner cavity to a hydrophobic residue (T469A, T469I and T469V) increased the affinity for C_8-TEA and C_{10}-TEA but had little effect on the affinity for TEA. Thr-469 does not face the inner cavity in the crystal structure solved for the mammalian version of the *Shaker* channel[125], but it is located right next to the conserved isoleucine residue in Kv channels (I497 in rKv1.5) shown to be essential for binding of arachidonic acid (Figure 5.14), suggesting that mutations of Thr-469

favoured the hydrophobic interaction with the conserved isoleucine rather than affecting interaction with the alkyl chain directly. In any case, the studies highlight the importance of the hydrophobic interaction of the alkyl chain for binding to the inner cavity.

The information shown in the wide range of studies on large hydrophobic molecules binding to the inner cavity of the pore of potassium channels suggests that the strong binding of the fatty acid observed here by ESR for KcsA could occur at the pore of the channel. Indeed, the immobile component in the ESR spectra of 14-SASL resembles that of the fatty acid bound to BSA, and since fatty acids bind in deep hydrophobic pockets in serum albumin[122] it is likely that 14-SASL is binding to a hydrophobic cavity in KcsA such as that in the pore. A recent study revealing the crystal structure of KcsA in its opened state[50] showed how the helical bundle beneath the inner cavity opens widely, so that the diameter of the permeation pathway to the inner cavity is ca. 32 Å at its widest point and ca. 14 Å at its narrowest (Figure 5.16). With a diameter of ca. 4.8 Å for an all-*trans* fatty acyl chain there would be plenty of space to allow a fatty acid molecule to enter the inner cavity of KcsA.

As mentioned above, the positions of three of the residues shown to be important for channel block with arachidonic acid are also important for binding of TBA in KcsA (Ile-100, Phe-103 and Thr-107, highlighted in blue in the KcsA sequence, Figure 5.14)[67,70,71]. These three residues are proposed to establish hydrophobic interactions with TBA (see the location of the residues in the KcsA structure in Figure 5.15) and therefore could also allow binding of a fatty acid molecule. However, it is not obvious where the negatively charged headgroup would be located within the pore of the channel. Neither of the two articles that propose arachidonic acid binding to the pore of a potassium channel to block ion flux discuss how the negatively charged head group of the fatty acid can be accommodated in the hydrophobic pore of a channel that transports positively charged ions. Surprisingly, the studies published by Decher *et al.*[46] showed a model of the rKv1.5 channel based on the crystal structure of the open rat Kv1.2 channel to which a molecule of N-arachidonylethanolamide (AEA or anandamide, which also causes current block, but has no charge) was docked, but no models with binding of arachidonic acid are shown or discussed. Nevertheless, the docking models with anandamide showed numerous

possibilities, with the flexible acyl chain of anandamide (C20:4) folding in a number of different ways to bind to the cavity of the channel. The ethanolamide headgroup was in most cases located towards the selectivity filter, next to the Thr residues in its entrance, but, as indicated by the authors, interacting mainly with non-polar residues. This idea would be in agreement with the possibility of T250 in hIK1 being important for establishing hydrophobic interactions with arachidonic acid, as discussed above. But, where could the negatively charged head group of the fatty acid be localised in the pore of the potassium channel? One possibility is, of course, that the bound fatty acid is fully protonated, avoiding the problem of a negatively charged group in a hydrophobic environment (the effect of pH on binding is discussed later). Alternatively, if the head group remained negatively charged, it would be expected that the charged group would be stabilised in such environment through some polar interactions. As just mentioned, T250 identified in hIK1[45] (corresponding to T75 in KcsA, Figure 5.15) appeared to be a good candidate for establishing a hydrogen bond with the fatty acid head group, but the mutagenesis experiments performed by Hamilton *et al.*[45] and Decher *et al.*[46] suggest that this Thr is not involved in polar interactions. An alternative candidate could be T107 in KcsA, but this residue is not conserved and corresponds to a Val in all the other potassium channels shown in Figure 5.14, suggesting that T107 in KcsA is involved only in hydrophobic interactions, as suggested also from its interaction with TBA (Figure 5.15). The next polar residue in the sequence, T112 in KcsA, has its OH group pointing towards the neighbouring transmembrane helix, practically inaccessible from the pore cavity; moreover, a Ser residue that appears in its place in the Kv channels (Figure 5.14), did not affect binding of arachidonic acid in rKv1.5 when mutated to Ala. In short, looking at the KcsA structure there appears not to be any obvious residues that could interact with a negatively charged carboxyl group, consistent with fact that uncharged AEA can block current in Kv channels just like arachidonic acid. It could then be possible that the headgroup simply remains hydrated and/or protonated in the cavity.

The various binding equilibria for a fatty acid molecule binding in the inner cavity of KcsA are shown in Figure 5.2 and, as already described, there are a number of equivalent ways in which binding can be described. Binding to the central pore could be described in terms of partitioning of fatty acid into the lipid bilayer followed by equilibration between the lipid bilayer and the pore. Alternatively, binding to the

pore could be described in terms of the equilibrium between pore bound and aqueous fatty acid, with partitioning of the fatty acid into the lipid bilayer simply depleting the pool of fatty acid available to bind to the pore. It is important to note that these two descriptions are equally valid in thermodynamic terms, and it is not possible to distinguish between them on the basis of thermodynamic measurements alone. It might seem more plausible to suggest that fatty acid binds directly to the pore from the aqueous medium rather than penetrating from the lipid bilayer into the pore through gaps between the transmembrane α-helices. However, entry directly into the pore would probably require that the channel be open. Indeed, in the experiments performed by Decher *et al*.[46] current inhibition of Kv channels by arachidonic acid showed use-dependence, i.e. the channels needed to be opened for inhibition to take place, suggesting the fatty acids access the inner cavity from the aqueous medium through the open pore. Further, their study also showed that the fatty acid competed with the pore blocker TEA for Kv current inhibition and, since TEA is known to require potassium channels to be open to access the inner cavity, this result suggests a similar mechanism for fatty acid binding. With respect to KcsA in particular, binding of TBA to KcsA has been shown to have an *on-rate* (ca. 10^{10} $M^{-1}s^{-1}$) substantially higher than that measured for eukaryotic channels (10^{3}-10^{7} $M^{-1}s^{-1}$), which results in a very low dissociation constant of TBA for KcsA (10 nM)[71], in contrast to that for eukaryotic channels (ca. 20 μM)[126]. It has been proposed that this effect is due to the greater accessibility of the inner cavity of KcsA, whose C-terminal domain has a simpler structure than those of the eukaryotic counterparts, resulting in an apparent higher affinity of TBA for KcsA[71]. It therefore seems likely that fatty acids will easily access the inner cavity of KcsA from the aqueous medium.

For ease of comparison with the binding data for phospholipids, fatty acid binding to the inner cavity will be described here by the dissociation constant K_E relating the concentration of pore-bound fatty acid to that present in the lipid bilayer (Figure 5.2), with no implied implication as to mechanism. As detailed in Section 5.2.5, since K_E describes binding of the fatty acid in the membrane to the inner cavity, the product of K_w, which describes dissociation of the fatty acid from the inner cavity into the aqueous medium, and K_p, which describes incorporation of the fatty acid into the bilayer from the aqueous medium, will give K_E. To calculate K_E from the ESR spectra it is necessary to know the number of binding sites. The model proposed by

Decher *et al.*[46] suggests that this is one. If more than one 14-SASL were to bind to each pore in KcsA it is likely that spin-spin interactions would result in broadening of the ESR spectra, and this was not observed, although the low molar ratio of 14-SASL to KcsA tetramer would any way have made multi-occupancy rare. The ESR spectra were therefore analysed assuming a single fatty acid binding site per channel. Eq. 5.18 was then used to calculate the value of K_E for each of the deconvoluted spectra (Table 5.4). Also, as described in Section 5.2.6, with a K_p value of (1/96) μM^{-1} for 14-SASL, K_w can be calculated using Eq. 5.13, giving the values listed in Table 5.4. Binding constants at all lipid-channel ratios between 100:1 and 37.5:1 are in good agreement, although values determined at a molar ratio of lipid:channel of 30:1 are slightly higher, possibly related to the extensive aggregation of KcsA expected at this molar ratio of lipid:channel.

A more accurate estimate of K_E was obtained by fitting all the experimental data on the levels of immobilized (bound) fatty acid to the quadratic equation (Eq. 5.23) derived from the binding equilibrium as described in Section 5.2.5, again considering that only one fatty acid molecule bound per cavity. As shown in Figure 5.17, the data (Table 5.3, black) fitted well to Eq. 5.23 giving a $K_E = 0.0023 \pm 0.0001$, a value similar to those obtained previously for each individual samples (Table 5.4). From the latter K_E value, K_w can again be calculated with Eq 5.13 giving a value of 0.221 ± 0.010 μM. The high fraction of bound 14-SASL means that it is not possible to determine accurately the number of binding sites per channel (N_b value), since when most of the 14-SASL is bound the ratio $K_E/N_b = 0.0023$ is a constant independent of N_b. For example, the data shown in Figure 5.17 fit equally well with a number of binding sites per channel of 4, with a K_E value of 0.012 ($K_E /N_b = 0.003$; blue line).

An alternative procedure to analyse binding of the fatty acid to KcsA would be as a hypothetical lipid exchange equilibrium (Eq. 3.2), in which case, Eq. 3.13 could be used to fit the data from Table 5.3. A free fit to Eq. 3.13 for N_b and K gives a number of binding sites per channel (N_b value) of 3.3 ± 6.4 and a binding constant of 14-SASL relative to DOPC of 89 ± 184; the large errors on both N_b and K suggest that the values for these two parameters are highly correlated. Indeed, fits to the data with N_b fixed at values of 1, 5, 10 and 15 gave good agreement with the experimental data

(Figure 5.18A and B) and only with values of N_b as high as 20 and 30 was the experimental data clearly in disagreement with the fits (Figure 5.18 C and D). Thus, as with the previous analysis, it is not possible to obtain accurate values of both N_b and K from the ESR data. Obtaining an N_b value would require experiments at much higher molar ratios of 14-SASL to KcsA tetramer, so that a higher proportion of 14-SASL was not bound to the protein, but high concentrations of 14-SASL could result in problems with spin-broadening of spectra for lipid-bound 14-SASL and for KcsA bound 14-SASL if more than one molecule of 14-SASL could bind per channel.

5.4.4 Effect of pH upon interaction of 14-SASL with KcsA

The intensity of the immobile component present in the ESR spectrum of 14-SASL in the DOPC:channel system at pH 7.2 decreased markedly at pH 3.9 with an increase in the mobile component (Figure 5.8). There are several possible explanations. One possibility is that both the immobile and mobile signal come from fatty acid binding to the cavity, the immobile component being charged fatty acid and the mobile being protonated fatty acid. However, exchange of protons between the charged and uncharged forms would be expected to be fast on the ESR time scale and an averaged spectrum would have been expected rather than the observed sum of two distinct components. Moreover, it would have to be assumed that the mobility of the protonated fatty acid in the inner cavity is like the mobility of the fatty acid in the lipid bilayer, extremely unlikely. More likely is that at low pH a large fraction of protonated fatty acid leaves the cavity binding site and partitions into the lipid bilayer. Indeed, the maximum splitting of the immobile component that remains at pH 3.9 is the same as in the sample at pH 7.2 (Figure 5.8), suggesting that a small amount of 14-SASL is still binding at the inner cavity of the channel giving raise to the immobile component whilst the mobile component is lipid bound fatty acid.

The latter explanation seems very plausible, however, as discussed in Section 5.4.3, there are no residues in the inner cavity of KcsA that are likely to interact with the negatively charged head group of the fatty acid, and the wide range of studies that analyse binding of molecules to the pore of potassium channels show that hydrophobic interactions appear to be most important. This suggests that the negative charge in 14-SASL may not be important for interacting with the inner cavity of KcsA,

and the effect observed upon changing the pH to 3.9 could be due to an increased affinity of the uncharged fatty acid for the lipid bilayer rather than a reduced affinity for the inner cavity. The protonated form of a fatty acid will bind more strongly to a lipid bilayer than the ionised form because the chain can penetrate further into the lipid bilayer in the absence of a charged headgroup: the difference in binding constant of a charged and uncharged form was estimated to be ca. 250 fold[97]. If the reduced fraction of fatty acid bound to the cavity of KcsA upon the change in pH was due solely to an increase in the affinity of the fatty acid for the lipid bilayer, then the value of K_E of 0.0023 obtained for the fatty acid at pH 7.2 would become 0.57 at a pH 3.9. If the strongly immobilised component that remains at pH 3.9 in the DOPC sample (Figure 5.8) reflects protonated fatty acid binding to the inner cavity, an approximate deconvolution of the spectrum giving a fraction of protonated fatty acid bound to the cavity of 0.356 (see a comment with respect deconvolution below) allows then to calculate the dissociation constant for the protonated fatty acid K_E as described in Section 5.2.5, giving K_E = 0.027, about ten times that obtained for pH 7.2 (Table 5.4). As already described, it is not known if the fatty acid is protonated or deprotonated when bound to the inner cavity but it is likely that the protonated form could bind to the cavity with greater affinity than the charged form. This idea would be in agreement with the estimated K_E value of 0.027 for the protonated fatty acid because the increased affinity of the fatty acid for the inner cavity could have partially compensated the higher K_E value of 0.57 expected due to the increased affinity of the protonated fatty acid for the lipid bilayer. Uncharged anandamide (C20:4) showed a greater current block effect on Kv1.1 than arachidonic acid (C20:4)[46], suggesting the negative charge in arachidonic acid makes the interaction with the Kv1.1 less favourable. Because anandamide has four double bonds, despite being uncharged it will not partition into the bilayer greatly[127], this allowing it to interact better with Kv1.1 than negatively charged arachidonic acid. However, protonated 14-SASL (which lacks double bonds) will have a much greater affinity for the bilayer than its charged form, this reducing the number of fatty acid molecules bound to KcsA.

It can also be seen in the low field region of the spectrum (Figure 5.8) that in-between the two main peaks there appears to be a small third peak, which could correspond to a third component. This could represent a small fraction of the 14-SASL binding to the annulus of KcsA. When the spectrum is recorded at 15 ˚C, this

third component is more apparent, thanks to the reduced mobility of the acyl chains, which results in a decrease of intensity of the mobile component (Figure 5.8). It can also be seen that at the lower temperature the reduced mobility of the fatty acid chains causes the maximum splitting of the different components to increase slightly, with the peaks at low magnetic field shifting slightly to the left. If the change in pH had freed a large proportion of the fatty acid from the high affinity binding site, it would be reasonable that a small fraction of such freed fatty acid could be interacting now with the transmembranous region of KcsA. Unfortunately, the sample signal intensity was not high enough to allow meaningful analysis in terms of three components, particularly when one of the components would only be present in small amount. An approximate deconvolution was therefore performed in terms of just two components ignoring the possible small third component, giving an immobile component fraction of 0.356 at pH 3.9 (25 ˚C), compared to the value of 0.837 obtained at pH 7.2, (Table 5.3), suggesting that about 43 % of the fatty acid immobilised at pH 7.2 left the cavity by changing the pH to 3.9. Details of the deconvolution can be found in Appendix 2.

Decreasing the pH to 3.9 for 14-SASL in KcsA in DOPG also had a marked effect upon interaction of the fatty acid with KcsA. In this case, the entire immobile component present at pH 7.2 disappeared, and a new immobile component similar to that observed in the DOPC sample at pH 3.9 appeared instead (Figure 5.9). Deconvolution of the spectrum of the sample in DOPG at 25 ˚C reveals a fraction of this new immobile component of 0.407 ± 0.044. If this immobile component represented the protonated fatty acid freed from the inner cavity now interacting with the annular sites of KcsA, a binding constant of the protonated fatty acid relative to PG could be calculated using Eq. 5.3 and the f_o of 0.331 obtained from 14-PGSL in the sample of DOPG:channel molar ratio of 88:1 (Table 3.3, Chapter 3). The resulting K value of 1.39 ± 0.27 would suggest that the uncharged fatty acid has slightly higher affinity for KcsA than DOPG. This contrasts with the fluorescence experiments described in Chapter 4 that showed that uncharged forms of the fatty acid bind weakly to the annulus of KcsA. As described above for PE binding to KcsA, a possibility is that a small number of annular sites on KcsA showing high affinity for the uncharged fatty acid could dominate the ESR spectrum (discussed further in the next paragraph), while in the fluorescence quenching experiments, the presence of three lipid exposed tryptophans per monomer means that only molecules binding to many annular sites

will result in a significant decrease in fluorescence intensity. Also, the difference in membrane composition in the two methods could influence interaction of the protein with the lipids. As mentioned in Chapter 4, Section 4.4.3, the miscibility of the uncharged fatty acid analogues is limited[101]; since in the ESR experiments only 0.5 mol % of the lipid molecules correspond to the spin labelled fatty acid and in the fluorescence experiments the uncharged fatty acid analogues reach concentrations of up to 66 mol %, it is possible that in the ESR experiments the small concentration of protonated fatty acid means that it is fully miscible with the lipid bilayer.

Uncharged hydrophobic molecules have been observed for some membrane proteins bound tightly to a small number of sites in the transmembrane region of the protein. One example is the hydrophobic inhibitor of the calcium ATPase, thapsigargin, which binds to a site located between transmembrane helices 3 and 7[22,128]. Another example is that of squalene binding to a groove in the transmembrane region of bacteriorhodopsin, where the long hydrocarbon chain is bent into an 'S' shape located within the hydrophobic core of the bilayer[22,129]. A third example has been published recently for the cytochrome c oxidase complex in which three triglyceride molecules appear bound in deep cavities within the transmembrane region (Figure 5.19). The shapes of these cavities do not allow interactions with the headgroups of phospholipid molecules, and the smaller number of polar interactions seems to be compensated for by a large number of hydrophobic interactions[130]. Hence, the possibility of strong binding of a protonated fatty acid molecule to a small number of sites in the transmembranous region of KcsA cannot be ignored.

If, as discussed above, the strongly immobilised component that remains at pH 3.9 in the DOPC sample (Figure 5.8) reflects protonated fatty acid binding to the inner cavity with a K_E = 0.027, with a dissociation constant of this magnitude, some binding to the cavity would also be expected in the DOPG sample but, at 25 ˚C no strongly immobilised component is seen (Figure 5.9). The DOPG sample was recorded at a molar ratio lipid:channel of 88:1, compared to a lipid:channel molar ratio of 60:1 for the DOPC sample. The reduced protein content in the DOPG sample would result in reduced binding, but, with a K_E of 0.027, the immobile component would be expected to be 0.27, easily observable. One possible explanation could be that the high negative charge of a DOPG bilayer results in a lower local pH close to the membrane surface

and so a larger proportion of the fatty acid is in the protonated form, with a consequent reduced amount of binding in the cavity.

5.4.5 Biological relevance

Despite the large variety of potassium channels, their structure is highly conserved, and the prokaryotic channel KcsA has served as a reference model for understanding their properties[34,48,67]. Fatty acids, especially polyunsaturated fatty acids, have been shown to influence the activities of numerous potassium channels and many other ion channels[43,44]. Generally, the effects are inhibitory, but there are cases where fatty acids can act as activators, like in some two-pore domain potassium channels, suggesting that fatty acids interact differently in different channels.

Binding of fatty acids to the cavity of potassium channels could be a mechanism to block ion flux *in vivo*. The inhibitory effects described in the literature are generally caused by polyunsaturated fatty acids, which are of particular interest due to the already known bioactive properties of arachidonic acid (C20:4) and its derivatives; monounsaturated fatty acids and saturated fatty acids, when they have been studied, have sometimes been found to have only a small or no effect[43,44]. However, some potassium channels are blocked by non-polyunsaturated fatty acids. For example the calcium-activated potassium channel hIK1[45,131] is blocked by arachidonic acid, but also by linoleic acid (C18:2) and myristic acid (C14:0) at the same concentrations of fatty acid (3 μM). As discussed in the previous section, the inhibitory action of fatty acids on this channel in particular has been proposed to consist of blocking of the pore by binding at its hydrophobic inner cavity, suggesting that polyunsaturation of the fatty acid chain is not essential for binding. The experiments performed with saturated long chain alkyl-triethylammonium pore blockers[110-112] (see Section 5.4.3) also show that a saturated alkyl chain of at least twelve carbon atoms in length can interact strongly with the pore of potassium channels.

It is not clear why in some cases only polyunsaturated fatty acids block ion channel activity. An important property of polyunsaturated hydrocarbon chains is that the presence of *cis* double bonds separated by a single bond confers great flexibility to

the hydrocarbon chain because the energy barriers between the different conformers generated by rotation about the C-C bonds in-between the double bonds are very low[132,133]. It might simply be that, given the variability of the residues that line the hydrophobic inner cavity of the different potassium channels, some may only be able to accommodate polyunsaturated chains in their pore because these are better able to adapt their conformation for interaction. Molecular dynamic simulations with rhodopsin (the light sensitive G-protein-coupled receptor) have shown that the chains of polyunsaturated lipids can flex and penetrate deeply into the core of the protein, affecting helix-helix interactions that have been proposed to induce transition to its active form[134]; hence, it is possible that the flexibility of polyunsaturated chains may facilitate interactions with the pore and other parts of ion channels. Also, as mentioned in Section 5.4.3, it has been proposed that the apparent greater affinity of TBA (10 nM)[71] for KcsA than for its eukaryotic counterparts (20 μM)[126] is due to the simpler structure of the intracellular domains in KcsA, which allow greater accessibility to its pore, the much bulkier cytoplasmic C-terminal domains of the other potassium channels acting as kinetic barriers that decrease the on-rate of molecules binding to the pore. If binding of large molecules like fatty acids to the cavities of potassium channels occurs from the aqueous medium, their access to the cavity could be greatly limited by these cytoplasmic domains, and the flexibility of the polyunsaturated chains could allow them to fold and reach the pore of the channels more easily; Figure 5.20 shows representative conformations from dynamic simulations of docosahexaenoic acid (DHA, C22:6)[132] to illustrate the degree of flexibility of polyunsaturated fatty acids.

Studies with voltage-gated sodium channels suggest that a kinetic barrier effect could be important. Sodium channels have a very similar architecture to that of potassium channels, but the four subunits making up the channel core being fused in one polypeptide[135]. The main polypeptide that constitutes the channel pore and voltage sensor is called the α-subunit, but other polypeptides (β-subunits) can associate with the channel on the cytoplasmic side to modulate channel function. In studies of the inhibition of the human voltage-gated sodium channel hH1 Xiao *et al.*[136] showed that polyunsaturated fatty acids as well as monounsaturated oleic acid and saturated stearic acid were able to block sodium currents when the α-subunit was expressed on its own, but only polyunsaturated fatty acids could cause current block if

the β-subunits were coexpressed with the α-subunits. Although there are no extensive studies proving binding of fatty acids to the cavity of the hH1 sodium channel, another study performed by Xiao *et al.*[137] found that a point mutation in one of the transmembrane α-helices that making up the pore in the α-subunit (helix D1-S6) of hH1 strongly reduces current block by all fatty acids. Further, local anaesthetics like lidocaine and etidocaine are known to inhibit sodium channel current by occluding the pore of the channels, and fatty acids affect sodium channels in a very similar way to local anaesthetics[137]. However, determination of the binding site of the fatty acids in the sodium channel is complex, because the mutation identified by Xiao *et al.*[137] does not affect binding of local anaesthetics, but affects binding of batrachotoxin, a toxin found in South American frogs that maintains the channel open. Nevertheless the binding sites for batrachotoxin and local anaesthetics are believed to be very close[138]. In summary, the results obtained by Xiao *et al.* suggest that fatty acids are acting by blocking the pore of hH1, but when β-subunits associate to the cytoplasmic side of the channel these act as kinetic barriers that hamper block by the less flexible saturated and monounsaturated fatty acids. Another factor that may reduce channel block by monounsaturated and saturated fatty acids could be their more limited solubility in water compared with that of the polyunsaturated forms[127], so that monounsaturated and saturated fatty acids will remain mostly sequestered by the lipid bilayer not being able to access the channel pore. Such effect would be complex and difficult to evaluate, as it is strongly influenced by the ionic strength, local pH and lipid/fatty acid concentrations[97].

Numerous studies suggest that regulation of ion channel function by fatty acids occur in living organisms[43,139]. In the experiments discussed in this chapter a value of K_E of 0.0023 combined with a partition coefficient K_p of 96 μM, gives a dissociation constant K_d (Eq. 5.13) for 14-SASL binding at a single site in the cavity of KcsA of 0.22 μM, a dissociation constant in-between that of the pore blockers TBA (10 nM)[71] and TEA (75 mM)[69]. The concentrations of fatty acid required to observe effects in eukaryotic channels are larger, ranging from ca. 1 and 30 μM, which, as mentioned above, may be due to numerous factors such as differences in the structures of the channels, kinetic impediment from cytoplasmic domains/subunits, fatty acid partitioning into the bilayer and the particular methodology applied in the study. For example, numerous studies overexpress cloned channels in *Xenopus*

oocytes in which current measurements are performed[43]. With a total phospholipid content of ca. 35 nmol in a single oocyte[140], then for an oocyte in an aqueous chamber of 1 ml capacity the lipid concentration will be ca. 35 µM. Assuming that all the phospholipid is in membranes into which the fatty acid can partition, then for oleic acid with an effective K_d of 17 µM[97], ca. 65 % of the oleic acid will partition into the oocyte membrane, and so application of 20 µM oleic acid would result in ca. 7 µM fatty acid in the aqueous media. It has also been suggested that the concentrations necessary to observe the effects of fatty acids in eukaryotic channels are physiologically relevant because those values are close to the values of K_m of arachidonic acid for the cyclooxygenase (5 µM) and lipooxygenase (3.4-28 µM) enzymes[141], both known to metabolise arachidonic acid *in vivo*[142].

Concentrations of free fatty acids in resting cells are generally very low, but esterified fatty acids can be enzymatically cleaved from membrane phospholipids upon stimulating signals from neurotransmitters, neurotrophic factors and cytokines, making them available for regulation of biological processes, as already known for arachidonic acid and anandamide[43]. Phospholipids with polyunsaturated acyl chains are particularly abundant in neuronal membranes, and the large number of studies suggests that fatty acids released from phospholipids could directly influence neuronal activity through regulation of ion channel function. The experiments performed by Decher *et al.*[46] have further shown that mRNA editing of Kv1.1 channels (change of an Ile residue facing the pore to Ala) occurs to different degrees, in physiologically significant levels, in different human tissues; such editing in just one of the subunits of the Kv1.1 channel was shown to be enough to abolish current block by arachidonic acid, and further, combination of a single Kv1.1 subunit with other Kv1.x subunits would also hinder current block by arachidonic acid in heteromeric channels. The authors proposed that fatty acid molecules together with mRNA editing can serve as mechanism for fine regulation of the nervous system. Indeed, mRNA editing of several proteins involved in electrical and chemical neurotransmission has been identified[143] and a recent study suggests that mRNA editing may be more common than initially expected[144]. In fact, some glutamate receptor ion channels (far relatives of potassium channels involved in excitatory neurotransmission[145]) have been shown also to undergo mRNA editing at a site which, surprisingly, also affects inhibition by fatty acids[146,147]. Finally, the effects of fatty acids on ion channels have also been

proposed to be important in cardiac muscle. Numerous studies have shown that polyunsaturated fatty acids have antiarrhythmic effects in cultured cells and in animals. Blockage of sodium channels by polyunsaturated fatty acids to stop action potentials together with blockage of voltage-gated calcium channels in the sarcoplasmic reticulum to stop intracellular calcium overload has been proposed as mechanisms by which fatty acids could generate their antiarrhythmic action[139].

5.4.6 Summary

The experiments with spin labelled phospholipids and 14-SASL presented in this chapter show that there is a marked difference between the immobile component of the ESR spectra of the phospholipids and the fatty acid arising from their interaction with KcsA. The ESR spectra of the phospholipids reveal relative affinities for KcsA that are similar to those reported for other membrane proteins. However, the spectra of 14-SASL reveals that the mobility of the chain of the fatty acid is much more restricted than that of the phospholipids, resembling that of the fatty acid bound to BSA, and the proportion of fatty acid in contact with the channel is much greater than that of the phospholipids. Together with the results obtained in Chapter 4, the data suggest that 14-SASL binds with high affinity at the hydrophobic inner cavity of the pore of KcsA. Two other studies have already proposed that binding of fatty acids to the cavities of potassium channels can cause current block[45,46], suggesting this as a mechanism for fine regulation of cellular responses *in vivo*.

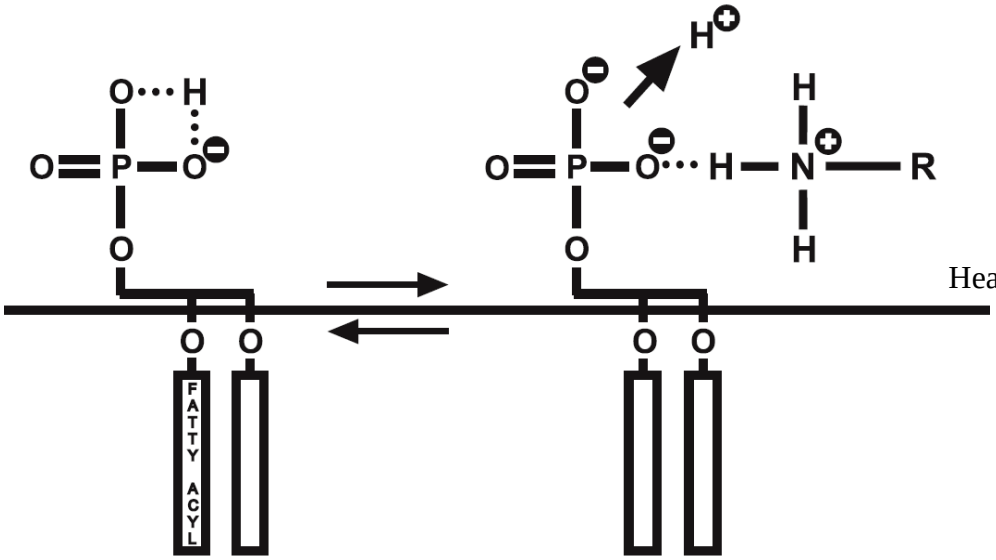

Figure 5.12 Electrostatic/hydrogen bond switch in phosphatidic acid proposed by Kooijman *et al.*[120] The OH group in PA is stabilised by hydrogen bonding with the negatively charged phosphate oxygen. When the lipid interacts with a positively charged amino acid, the negatively charged phosphate oxygen hydrogen bonds with the amine group of the amino acid, the OH group in PA then deprotonating. The increase in negative charge could strengthen the lipid-protein interaction. Taken from Kooijman *et al.*[120]

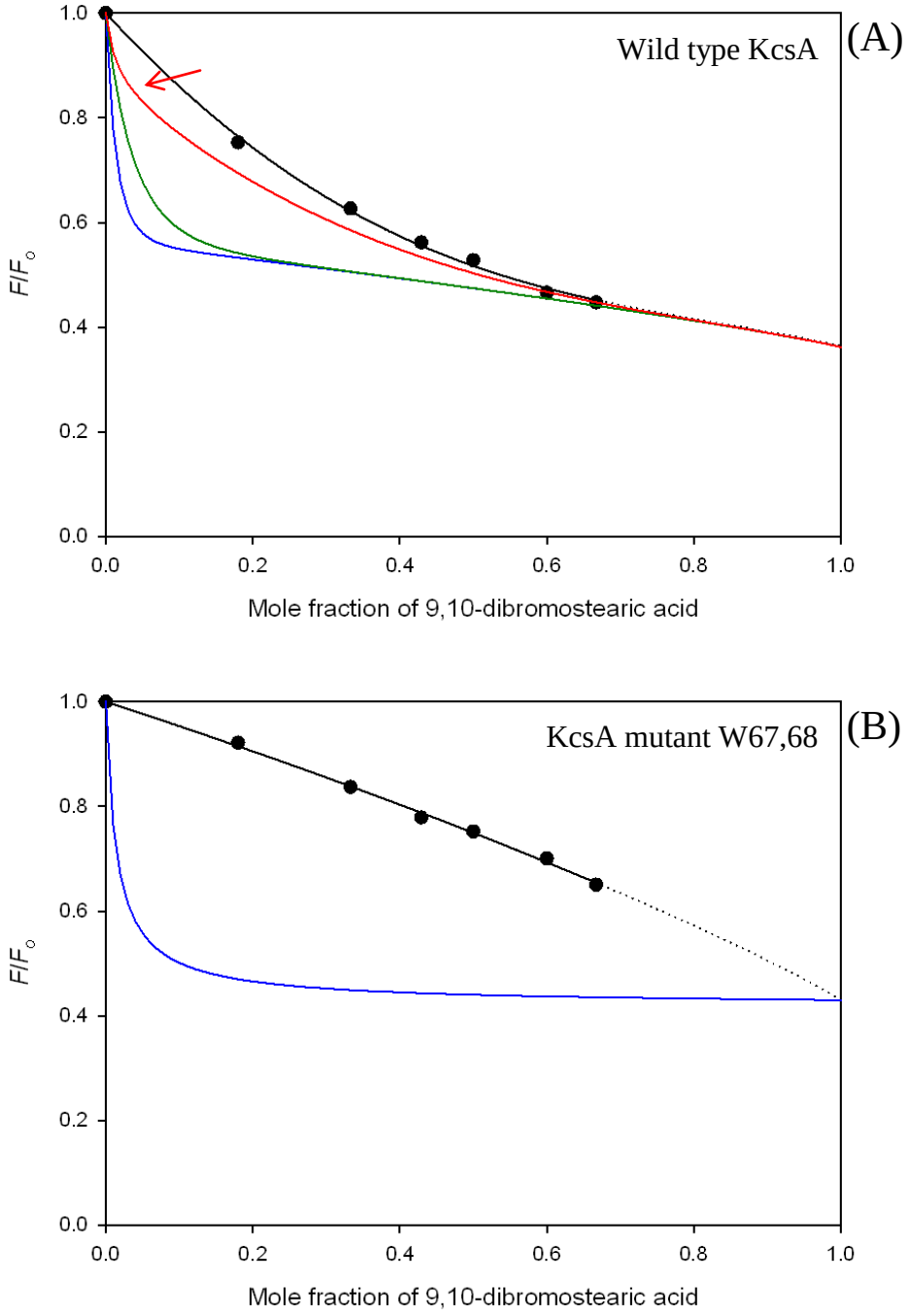

Figure 5.13 Simulated fluorescence quenching curves for brominated fatty acid, for wild type KcsA (A) and the mutant W67,68 (B). The experimental data (black dots) are from Figures 4.12 (A) and 4.9 (B) and the black lines show the best fit to Eq. 4.22 (A) and 4.14 (B), respectively, extrapolated to a mole fraction of 1 for the fatty acid (dotted line). (A), in blue and green are the predicted quenching curves for K^A = 16.26 and K^A = 6.01, respectively, calculated using Eq. 4.22 (averaged binding at the annular sites) with n^A = 4.6, n^{NA} = 0.92, F^A_{min} = 0.27, F^{NA}_{min} = 0 and K^{NA} = 0.86; in red is the predicted curve for K^{HA} = 77.45 using Eq. 5.24 (binding at a 'hotspot' in the annulus) with the same values for n^A, n^{NA}, F^A_{min} and F^{NA}_{min} as previously and K^A = 0.73, F^{HA}_{min} = 0.27 and n^{HA} = 1. (B), in blue is the predicted curve for K^{NA} = 77.45 using Eq. 4.14 (binding at the non-annular sites) with n^{NA} = 0.94 and F_{min} = 0.43.

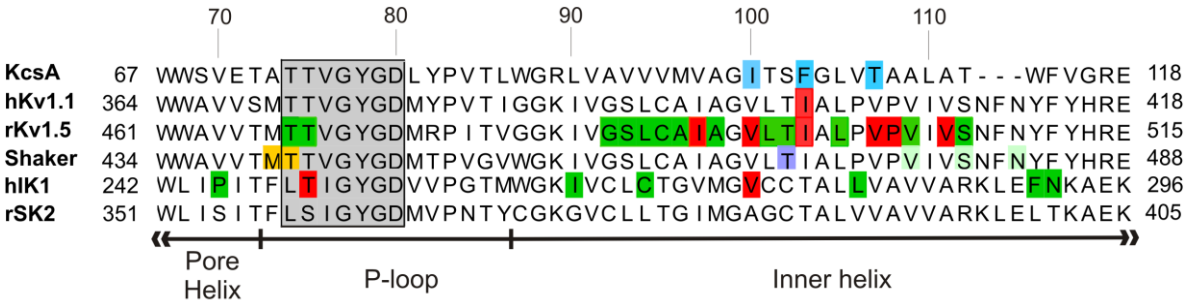

Figure 5.14 Sequence alignment of the pore region of representative potassium channels. In the KcsA sequence residues implicated in binding of the hydrophobic pore blocker TBA[70,71] are highlighted in blue. In the hKv1.1 sequence Ile-400, necessary for binding of arachidonic acid is highlighted in red. Ile-400 in hKv1.1 can be substituted by a valine via mRNA editing which hinders binding of arachidonic acid[46]. For the rKv1.5 sequence, residues for which alanine scanning mutagenesis was performed by Decher *et al.*[46] are highlighted in green when the change to alanine did not affect blocking by arachidonic acid and in red when the mutation prevented blocking. The mutagenesis studies performed in *Shaker* by Choi *et al.*[112] are summarised in the sequence as follows: Thr-469, for which mutation affected binding of long chain alkyl-TEA blockers but did not affect binding of TEA, is highlighted in purple; residues where mutation had no effect on binding of the blockers are in light green; and residues whose mutation affected binding of TEA but not binding of long chain alkyl-TEA blockers are in yellow. Finally, the experiments performed by Hamilton *et al.*[45] where residues in the arachidonic acid sensitive calcium-activated channel hIK1 were mutated to the corresponding residues in the arachidonic acid insensitive calcium-activated channel rSK2 are summarised in the hIK1 sequence: in red are the residues whose mutagenesis hampered current block by arachidonic acid in hIK1 and in green those which had no effect. The rSK2 sequence is also shown. For all sequences the signature sequence that forms the selectivity filter is boxed in grey. The numbering at the top corresponds to the KcsA sequence. Sequences were obtained from the following accession numbers (version number indicated in parenthesis) from the NCBI (National Centre for Biotechnology Information) website: KcsA, P0A334(.1); hKv1.1, Q09470(.2); rKv1.5, NP_037104(.1); Shaker, CAA29917(.1); hIK1, AAC23541(.1); rSK2, AAB09563(.1).

Note: for unknown reasons, the sequence numbering of rKv1.5 in the articles from Decher *et al.*[46] does not correspond to that of the accession number sequence indicated in their studies. Here the numbering corresponding to that accession number has been used.

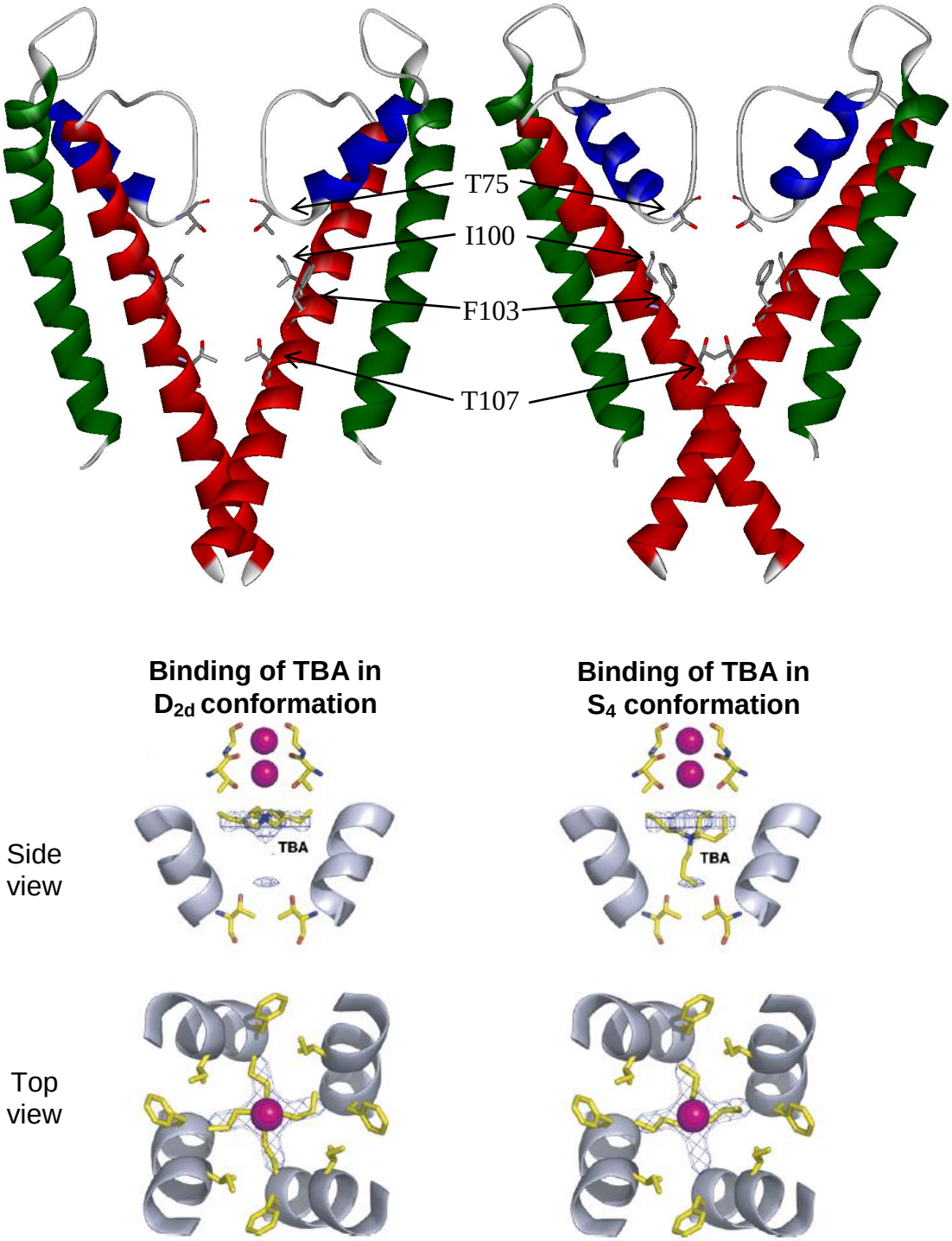

Figure 5.15 Residues in KcsA implicated in binding of the hydrophobic cation pore blocker TBA[70,71]. Top: two images of two monomers of KcsA (PDB 1K4C) slightly rotated along the pore axis showing the three residues implicated in binding TBA (I100, F103, T107) and also T75, which corresponds to T250 in hIK1, shown to be necessary for current block by arachidonic acid in the hIK1 channel[45]. Bottom: detail of the crystal structure of KcsA showing the electron density map for the bound TBA[71]. The TBA molecule is modelled into the electron density in two different conformations, D_{2d} (left) and S_4 (right). I100 and P103 form a ring of hydrophobic and aromatic contacts that provide favourable van der Waals interactions with TBA; additionally, when the molecule binds in its S_4 conformation it contacts the hydrophobic group of T107. The bottom images were taken from Faraldo-Gómez *et al.*[71]

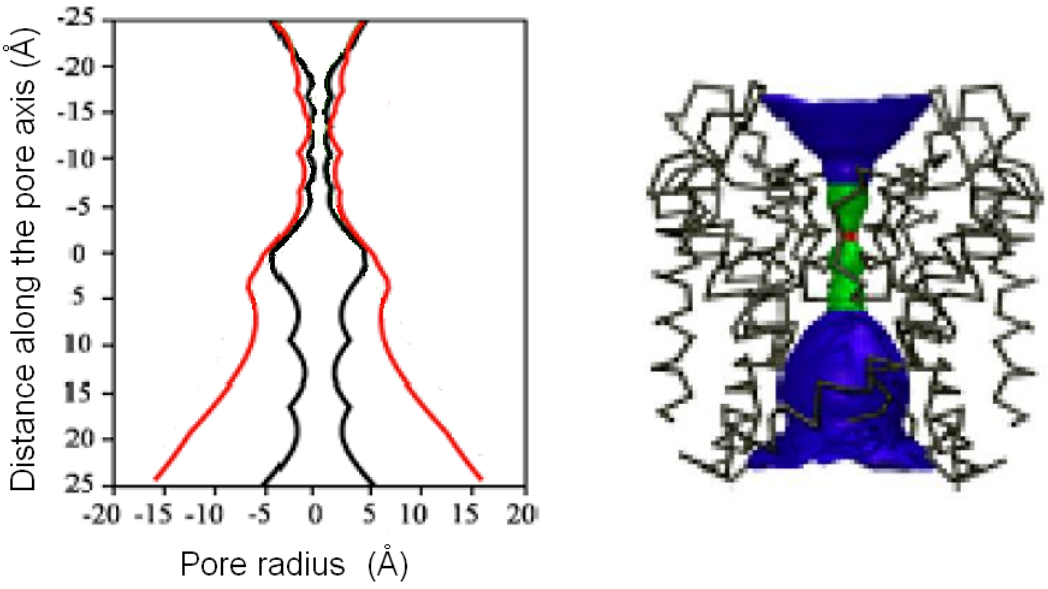

Figure 5.16 The permeation pathway in the open KcsA channel[50]. Left, radius profile along the pore axis of opened (red) and closed KcsA (black). The maximum opening in the open structure is ca. 32 Å in diameter near residue Thr-112; the pathway narrows to ca. 14 Å before reaching the internal cavity. Right, volume representation of the permeation pathway in the open structure of KcsA: in orange are coloured regions of pore radius less than 2 Å, in green regions between 2-3 Å and in blue are regions with radius greater than 3 Å. Images taken from Cuello *et al*.[50]

DOPC/KcsA tetramer molar ratio	K_E (adimensional)	K_w (μM)
30 (2nd)	0.0032 ± 0.0007	0.308 ± 0.071
37.5 (2nd)	0.0025 ± 0.0007	0.236 ± 0.069
60 (2nd)	0.0024 ± 0.0003	0.233 ± 0.022
67.5 (1st)	0.0021 ± 0.0002	0.199 ± 0.021
88 (2nd)	0.0021 ± 0.0001	0.201 ± 0.009
100 (1st)	0.0022 ± 0.0002	0.215 ± 0.016
Averaged value	0.0024 ± 0.0008	0.232 ± 0.076

Table 5.4 Dissociation constants for fatty acid binding to the inner cavity of KcsA. The dissociation constant K_E for each sample was calculated using the respective fractions of the immobile component of 14-SASL listed in Table 5.3 as described in Section 5.2.5, with Eq. 5.18. The dissociation constant K_w was determined from Eq. 5.13 assuming $K_p = (1/96)\ \mu M^{-1}$.

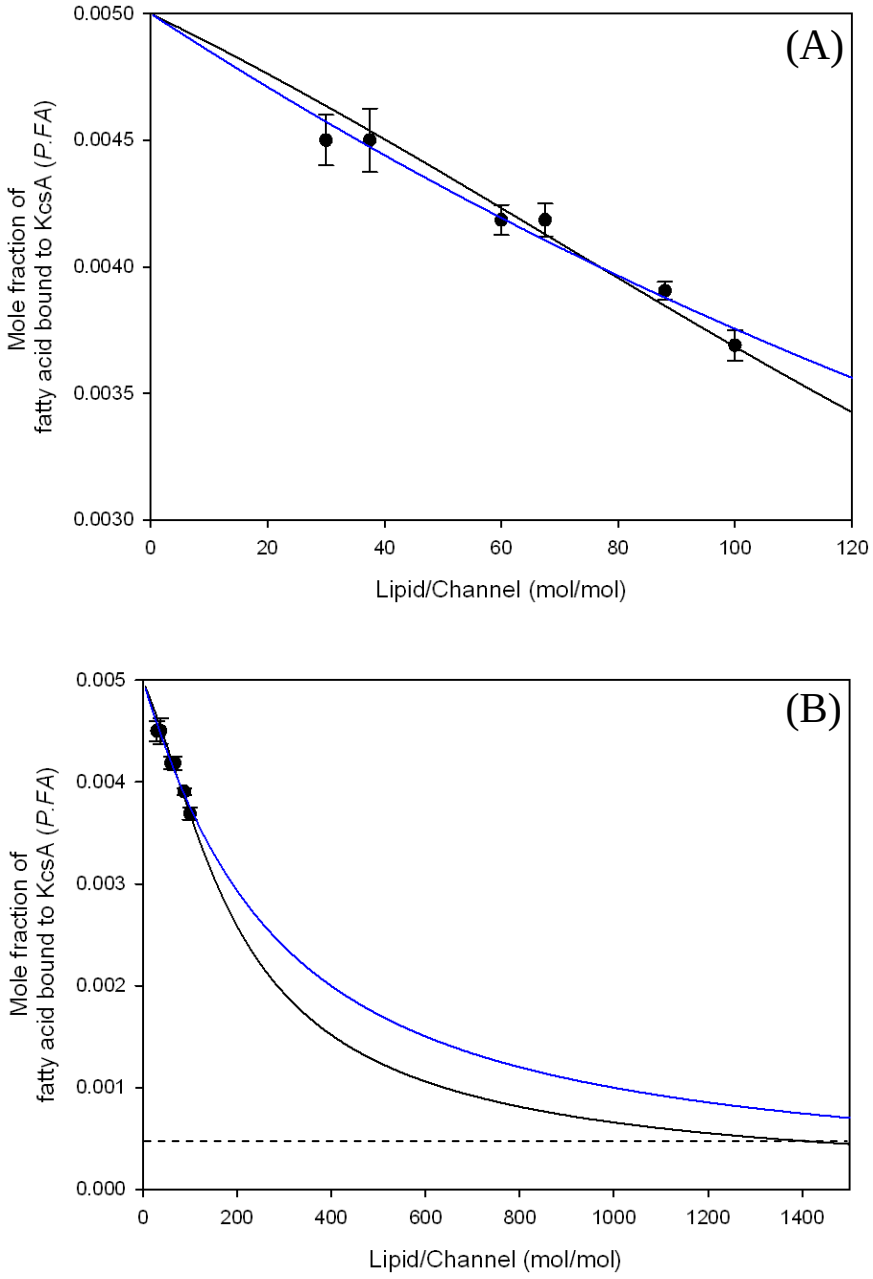

Figure 5.17 Mole fraction of 14-SASL bound to the inner cavity of KcsA as a function of lipid:channel molar ratio. (A) The experimental data (●) from the 14-SASL spectra listed in Table 5.3 were fitted to Eq. 5.23 as described in Section 5.2.5 with a fixed N_b value of 1 (black line), giving a dissociation constant K_E = 0.0023 ± 0.0001, in close agreement with the individual K_E values listed in Table 5.4. The blue line shows a fit to Eq. 5.23 with a fixed N_b value of 4. In (B) the data (●) are plotted on an expanded scale showing that when the proportion of bound fatty acid is very high it is not possible to distinguish between 1 or 4 binding sites per channel. Below the dotted line more than 90 % of the fatty acid would be expected not to be bound to the channel assuming one site per channel (black line). For all data points the mole fraction of total 14-SASL was 0.005.

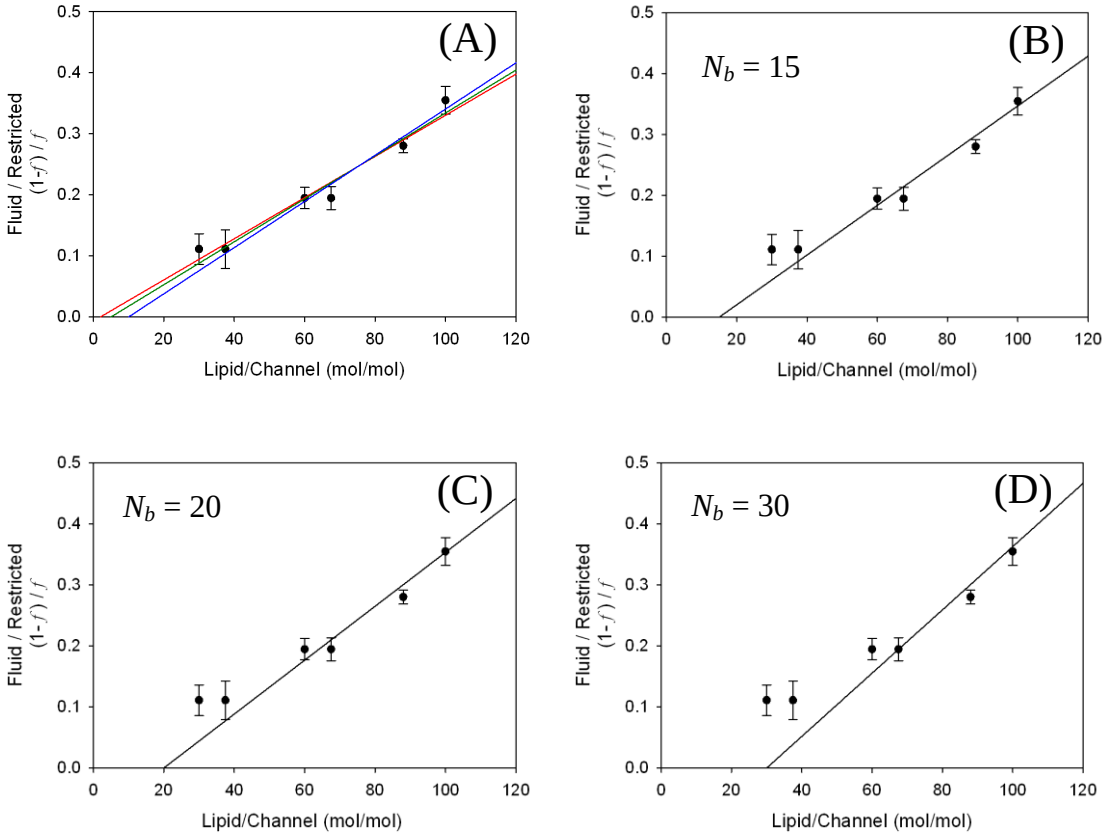

Figure 5.18 Fits of the 14-SASL data to a 'hypothetical' lipid exchange equilibrium. The ratios of fluid to restricted component in the deconvoluted ESR spectra for 14-SASL (Table 5.3) are plotted as a function of lipid:channel molar ratio. The data were fitted to a model with the fatty acid in an exchange equilibrium with the host lipid (DOPC) as described by Eq. 3.13. The different fits result from varying the number of lipid binding sites (N_b). In (A) N_b was fixed as follows: 2, red; 5, green; 10, blue. A reasonable fit to the data was obtained for all these N_b values. In plots (B), (C) and (D) N_b was 15, 20 and 30 respectively. For plots C and D the fits were judged to be poor.

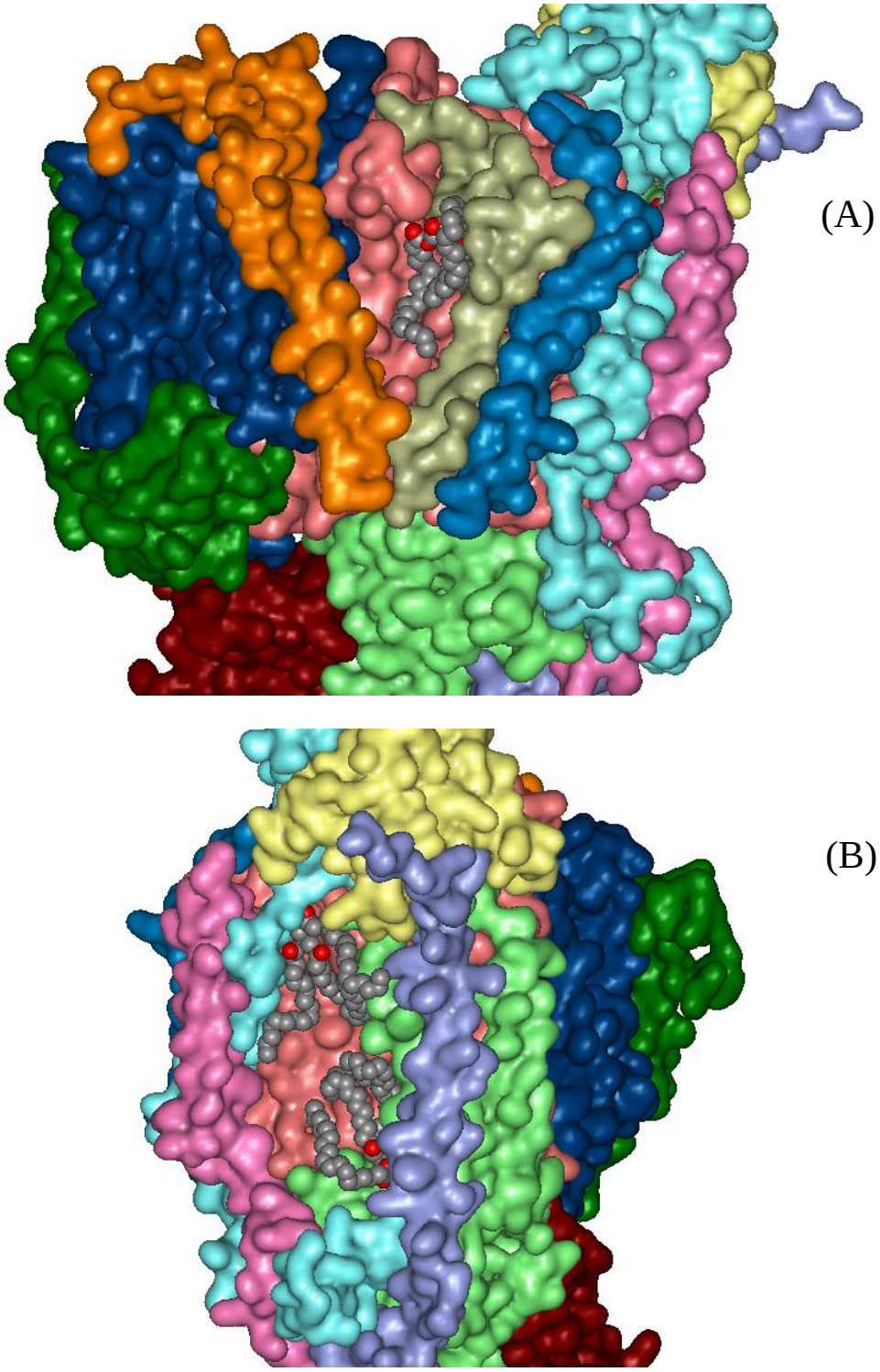

Figure 5.19 Three triglyceride molecules in the crystal structure of the cytochrome c oxidase obtained by Shinzawa-Itoh *et al*.[130] The regions where the uncharged lipids bind are shown. The three triglyceride molecules, shown in space-fill representation, bind in deep cavities within the multimeric complex that cannot accommodate phospholipid headgroups. The two images show cytochrome c oxidase rotated around the normal to the plane of the bilayer, with one of the triglyceride molecules on (A) and the other two on (B). The subunits are shown as solvent accessible surfaces, each with a different colour. PDB accession number 2DYR.

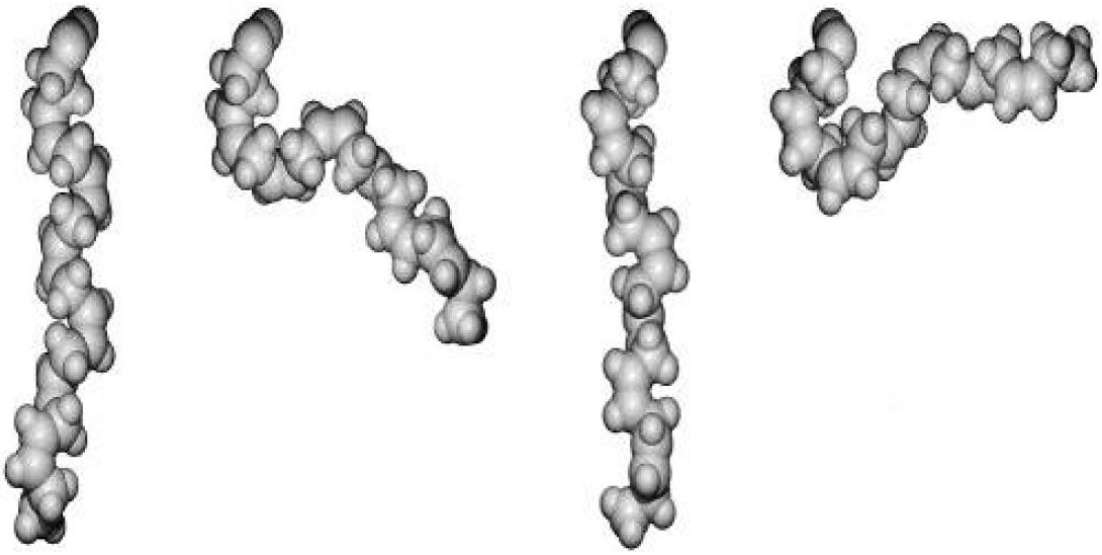

Figure 5.20 Representative conformations of the polyunsaturated fatty acid docosahexaenoic acid (DHA) from molecular dynamic simulations performed by Feller *et al.*[132]

Chapter 6: Final discussion.

The interaction of membrane proteins with lipid molecules can influence their structure, oligomeric state and activity[4,22], and thus there is great interest in understanding how lipids exert their effects on membrane proteins. Some of the first studies revealing lipid molecules interacting with membrane proteins came from ESR analysis with spin labelled lipids, in which a population of lipids with restricted mobility revealed a spectrum different from that of the bulk lipid[148]. These observations suggested that a shell of lipid molecules (annular lipids) around the transmembrane region of a membrane protein solvated the protein in a similar way to the shell of water molecules that solvate a water soluble protein[12]. Fluorescence spectroscopy studies with brominated lipids then further suggested the existence of an additional set of lipid binding sites, referred to as non-annular lipid binding sites, located between transmembrane α-helices or at protein-protein contacts[32]. Numerous X-ray and electron diffraction studies have now shown some of these lipid molecules bound to membrane proteins (mainly non-annular lipid molecules), giving structural detail on the nature of their interaction with the membrane proteins[4,22,23].

However, in many cases it is still not known how lipid molecules mediate their effects. Two main types of explanations have been used to address the question of how lipids affect membrane protein function[12]. One type of explanation refers to the bulk physical properties of the bilayer (fluidity, tension, curvature stress), while the other type of explanation focuses on the molecular detail of individual lipid-protein interactions. Obviously, this last type of analysis is difficult because it requires detailed knowledge of the atomic structures of the proteins, and will be different for different proteins. In some cases the bulk physical properties of the bilayer might explain some of the effects observed in membrane proteins, but in numerous cases specific lipid-protein interactions will occur and affect membrane protein function without any direct relation to the bulk physical properties of the bilayer. For example, KcsA requires the presence of negatively charged phospholipids in the bilayer to increase its open probability[13] and these effects of negatively charged lipids on KcsA

follow from their specific interaction with the non-annular sites on the channel (acting like cofactors), rather than from any change in the physical properties of the bilayer. Sometimes effects on membrane protein activity show a correlation with a change in the physical properties of the bilayer, but this need not point to the real cause of the change in protein activity. For example, it is known that an excess in membrane tension is responsible for opening of the mechanosensitive channel of large conductance MscL, and the sensitivity of the channel to membrane tension is different in different lipid bilayers[4]. It was first shown, with the use of single channel patch clamping techniques, that in bilayers rich in phosphatidylethanolamine (PE) McsL required more membrane tension to open than in bilayers rich in phosphatidylcholine (PC), and this was suggested to be due to the curvature stress of the membrane rich in PE since PE has a tendency to form the H_{II} phase[149]. However, later studies of MscL in vesicles of phosphatidylcholine (PC), PE, phosphatidylethanolamine-*N*-methyl (Me-DOPE) and phosphatidylethanolamine-*N*,*N*-dimethyl (Me_2-DOPE) showed that Me_2-DOPE, Me-DOPE and PE all had similar effect on MscL despite their different spontaneous curvature and suggested that what was important was the presence of a hydrogen bond donor group in the lipid headgroup capable of interacting with the MscL channel[150]. This example highlights the importance of understanding the molecular detail of the various possible lipid-protein interactions, and their effects on membrane protein structure, oligomeric state and function.

The studies presented in this thesis have focused on the potassium channel KcsA and an analysis of lipid binding at both annular and non-annular sites on the channel (Chapter 3 and Chapter 4), and at an additional binding site for fatty acids in the pore of the channel (Chapter 5). Ion channels constitute a large and important group of membrane proteins that, by regulating ion flux across the lipid bilayer, are involved in numerous physiological processes[8]. For instance they control the cell volume and maintain the resting membrane potential, but thanks to their ability to respond to a great variety of stimuli (electrical, mechanical and chemical) they are able to regulate many different cellular processes, from muscle contraction and neuronal integration[8] to cell proliferation[151] and apoptosis[152]. As a consequence ion channels are involved in numerous diseases including neurological, cardiovascular and muscular diseases[153], diabetes[154] and cancer[155], and so it is not surprising that ion channels are the target of numerous drugs used today[156].

Much of the structural knowledge of ion channels comes from studies of potassium channels. In the late 1990s sequencing of prokaryote genomes allowed identification of numerous potassium channels that could be easily cloned and overexpressed in *E. coli*[157], and this allowed the first atomic structure of a potassium channel (KcsA) to be obtained by MacKinnon and co-workers in 1998[34]. KcsA has since become a fundamental model in potassium channel research as it has been shown to be a representative member of the large potassium channel family[48,49]. The structures of a mammalian voltage gated potassium channel[125] and other prokaryotic potassium channels[38] have confirmed the structural similarities, validating KcsA as a good research model. As discussed in Chapter 1, KcsA is also ideal for studying lipid-protein interactions, which is why KcsA was chosen here for a thorough analysis of lipid-protein interactions at the various lipid binding sites.

Chapter 3 described studies of the influence that the annular shell of lipids can have on protein-protein contacts. There is increasing interest in exploring the ability of membrane proteins to oligomerise, as this can have important functional consequences. A good example is the Ryanodine receptor, a calcium channel that is present in numerous copies in the sarcoplasmic reticulum of skeletal muscle. Structural studies with electron microscopy and computational modelling propose that the channels pack orderly by specific domain-domain interactions to drive direct physical coupling between the channels in contact; this would allow coordinated opening of a given group of channels and could well explain experimental observations of the excitation-contraction coupling in the skeletal muscle[19]. More recently, clusters of the bacterial mechanosensitive channel MscL in reconstituted systems have also been observed using confocal and atomic force microscopy, and changes in channel activity in patch clamp recordings have been attributed to channel-channel contacts[158]. Also, as discussed in Chapter 3, aggregation of KcsA has been previously reported and as for MscL, it has been suggested that changes in channel activity could arise from channel-channel contacts[79,80]. The biological relevance of these observations in MscL and KcsA are, however, unknown, but there is growing interest on the potential role that protein-protein contacts can have in such type of protein clusters[20].

Clustering of other channels like the acetylcholine receptor[159] and the inwardly rectifying potassium channel Kir4.1[17] have been known (for a long time) to rely on anchoring proteins, but little is known about the role of the lipid bilayer on protein clustering. Most studies looking at the influence of the lipid bilayer on protein aggregation have focused on the effects of hydrophobic mismatch between lipids and proteins, showing that this hydrophobic mismatch can trigger protein aggregation[21,160]. A recent study using molecular dynamic coarse-grained simulations has also suggested that membrane curvature and the orientation of the protein in the membrane can also affect membrane protein aggregation[161]. The study compared simulations of simplified model membrane proteins of conical shape incorporated into planar lipid bilayers and into vesicles of ca. 32 nm diameter (comparable to synaptic vesicles). In planar bilayers, hydrophobic mismatch would promote aggregation of the protein, but in the vesicle system aggregation was only promoted when the orientation of the protein was such that the cone shape of the protein did not match the curved shape of the vesicle. The experiments discussed in Chapter 3 explored the influence of the lipid bilayer on KcsA aggregation. The experiments showed that protein aggregation was influenced by two factors: the lipid:protein molar ratio and the lipid headgroup of the lipids composing the bilayer. For a membrane protein like KcsA or the Ca^{2+}-ATPase, whose annulus is solvated by ca. 30 lipid molecules, random protein-protein contacts are only expected to be significant below lipid:protein molar ratios of ca. 30:1[86]. The ESR and fluorescence experiments showed that in PC bilayers KcsA aggregated below lipid:channel molar ratios of ca. 90:1 and therefore the data indicate that protein-protein contacts in KcsA are significantly more favourable than lipid-protein contacts. This is unusual as for many membrane proteins protein-protein interactions are not significant until the lipid:protein molar ratio drops below that required to form a complete annular shell around the protein[24]. A factor that could influence protein aggregation is the shape of the protein; for example, the transmembrane domains of proteins with large cytoplasmic domains will not be able to come into contact due to stearic hindrance. The experiments also showed that aggregation of KcsA was reduced in bilayers of negatively charged phosphatidylglycerol (PG), which has greater affinity for KcsA than PC, suggesting that the affinities of the lipids composing the membrane are an important factor for determining protein aggregation. From a physiological perspective, biological membranes have on average a

lipid:protein molar ratio of about 100:1 and therefore it would not be expected that KcsA aggregated in the average biological membrane.

Chapters 4 and 5 discussed studies of fatty acids and their potential sites of action on potassium channels. For more than 16 years numerous studies have reported the influence of fatty acids on ion channel function, but it is still not known how these lipids carry out their effects at the molecular level[43,44]. Two studies, based on mutagenesis experiments, have given strong evidence for regulation of potassium channels by fatty acids by blocking the hydrophobic inner cavity of the pore[45,46]. For the first time here, biophysical techniques have been applied to prove direct binding of fatty acids to annular and non-annular sites and to the inner cavity of a potassium channel, obtaining binding constants. In Chapter 4, quenching of tryptophan fluorescence with brominated fatty acids showed that fatty acids are able to bind at the annular and non-annular sites. The ability of fatty acids to interact with the non-annular sites is particularly important, as binding of phospholipids to this type of site often affects protein function. In fact, binding of negatively charged phospholipids at these sites in KcsA is necessary for activity, and it would be of great interest to see if binding of fatty acids at these sites also allowed channel activity. The difficulty is that activation of KcsA requires a low pH, and at low pH the fatty acid would protonate and lose its negative charge; as shown in Chapter 4, the negative charge of the carboxyl group is important for binding, uncharged fatty acid analogues binding weakly to the annular sites and being unable to bind at the non-annular sites.

ESR experiments performed in Chapter 5 suggested binding of the fatty acid to the hydrophobic inner cavity of KcsA, and a strong binding constant of ca. 220 nM was estimated, assuming a single binding site in the cavity. This strong affinity is comparable to the K_m values of arachidonic acid for enzymes that are known to metabolize the fatty acid *in vivo*, suggesting binding of fatty acids at the inner cavity of potassium channels to block ion flux could indeed occur in living organisms[141]. It will be of great interest to confirm binding of the fatty acid in the cavity of KcsA through other biophysical techniques, like for example, solid state NMR, where binding of spin labelled fatty acid to reconstituted KcsA would be expected to alter the spectrum of isotopically labelled residues in the channel. This method could also allow identify particular residues involved in binding of the fatty acid. It will also be

important to confirm the binding stoichiometry. The cavity is probably big enough to hold two fatty acid molecules, if tightly packed (as mentioned by Decher *et al.*[46] in their published answers to referees reports on their paper). Binding of one fatty acid molecule may allow the inner bundle of the channel to close, as when it binds TBA, but binding of two fatty acid molecules could prevent closing of the inner helix bundle. Experiments performed by Smithers *et al.* (unpublished data) using a fatty acid containing the dansyl fluorescent probe[162] may indicate that, as assumed in Chapter 5, only one fatty acid molecule binds in the cavity.

Also in Chapter 5, experiments analysing binding of fatty acid at low pH showed a marked decrease in fatty acid binding to the cavity. As discussed in Chapter 5, less binding of the protonated fatty acid to the cavity could follow from an increased affinity for the lipid bilayer or a decreased affinity for the inner cavity. There are no obvious residues in the inner cavity of KcsA that could be potential binding sites for the negatively charged carboxyl group, and it would be of great interest to determine whether the negative charge in the fatty acid is actually necessary for strong binding to the cavity.

6.1 Final remarks

The increasing importance and complexity that is being revealed in biological membranes since Singer and Nicolson proposed their fluid mosaic model in 1972 indicate that to fully understand these systems it is necessary to understand their molecular detail. The studies presented in this thesis have used a biophysical approach to explore, at the molecular level, the properties of lipid-protein interactions. Conveniently simplified models have been used to address key questions in the field. Much work is still needed both in model and biological systems, and it is hoped that the experiments presented here will lead to further studies for the understanding of the importance of lipid-protein interactions in biological systems.

Appendices

Appendix 1: Purification, absorbance and fluorescence emission spectra of KcsA

KcsA was purified as described in Section 2.2.2. From 12 l of bacterial culture approximately 15-20 g of wet cell pellet were obtained and used for purification. Collected fractions were always checked by SDS-PAGE to confirm purity, oligomerisation and approximate concentration. Figure A1.1 shows SDS-PAGEs from wild type KcsA and the mutant W67,68. The presence of Trp residues may be important for the stability of the protein, acting as 'floats' that help anchor the protein in the membrane and Trp residues could have a similar effect in stabilizing the protein in detergent micelles. Despite elimination of the three lipid-exposed Trp residues in W67,68, the protein is still stable in the presence of 0.5 % SDS. The majority of the protein runs as a tetramer, and the SDS-PAGE analysis does not show significant differences between wild type KcsA and W67,68. The molecular weight of the tetrameric fusion protein is 70.4 KDa, but in both cases the protein runs just below the 66 KDa standard, which could be due to the compact tetrameric form of the protein.

Fractions with the highest amount of tetramer were chosen and mixed together. The concentration was then determined by absorption spectroscopy (Figure A1.2). Approximately 2 ml at 4-9 mg/ml of protein were obtained from each purification (i.e. 0.6-1.5 mg of protein per litre of bacterial culture).

The fluorescence emission spectra of wild type KcsA and the mutant W67,68 reconstituted into DOPC is shown in Figure A1.3. Both spectra are similar, with the fluorescence emission maxima located between 331-333 nm, consistent with the data obtained by Marius *et al.*[74]. This is consistent with a location for the Trp residues within a hydrophobic environment, at the glycerol backbone region of the lipid bilayer for the lipid exposed tryptophan residues and an environment of similar polarity for the non-lipid exposed Trp residues. To optimally detect any changes in fluorescence

intensity, all quenching experiments were carried out measuring KcsA fluorescence emission at 333 nm.

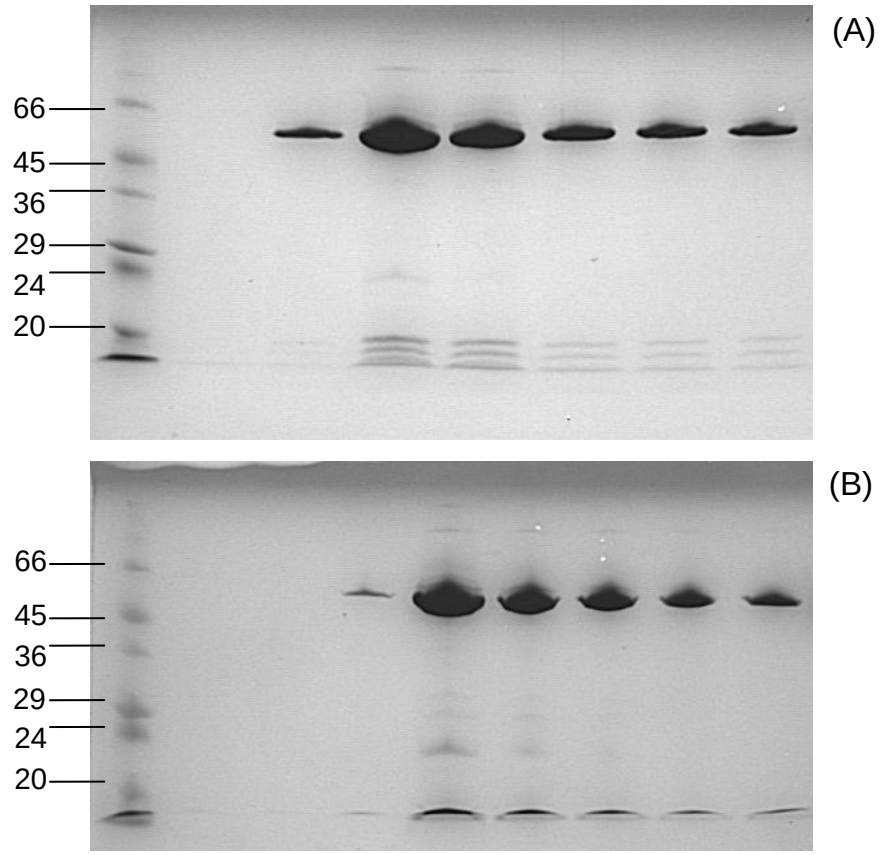

Figure A1.1. Coomassie stained SDS-PAGE from fractions collected in the purification of wild type KcsA (A) and mutant W67,68 (B). In both cases, the majority of the protein runs as a tetramer (70.4KDa fusion protein). On the left, are shown molecular weight markers with the respective weights in KDa.

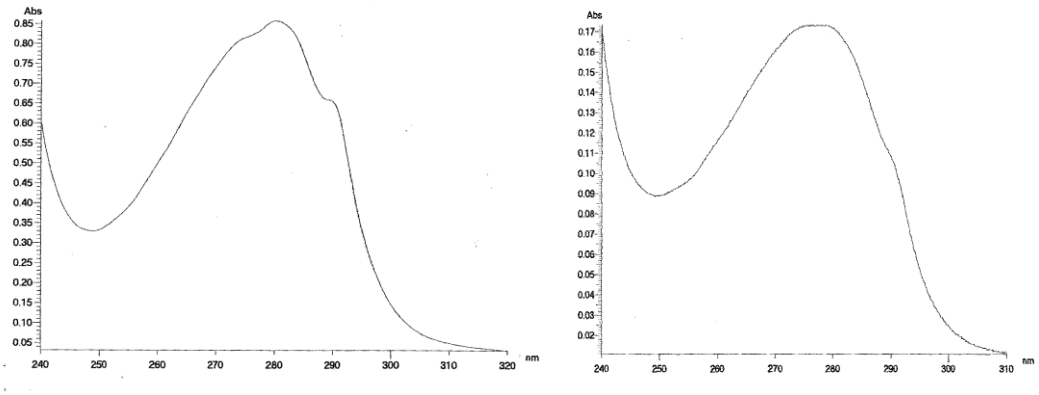

Figure A1.2 Absorption spectra of purified wild type KcsA (left) and the mutant W67,68 (right) in 1 % SDS.

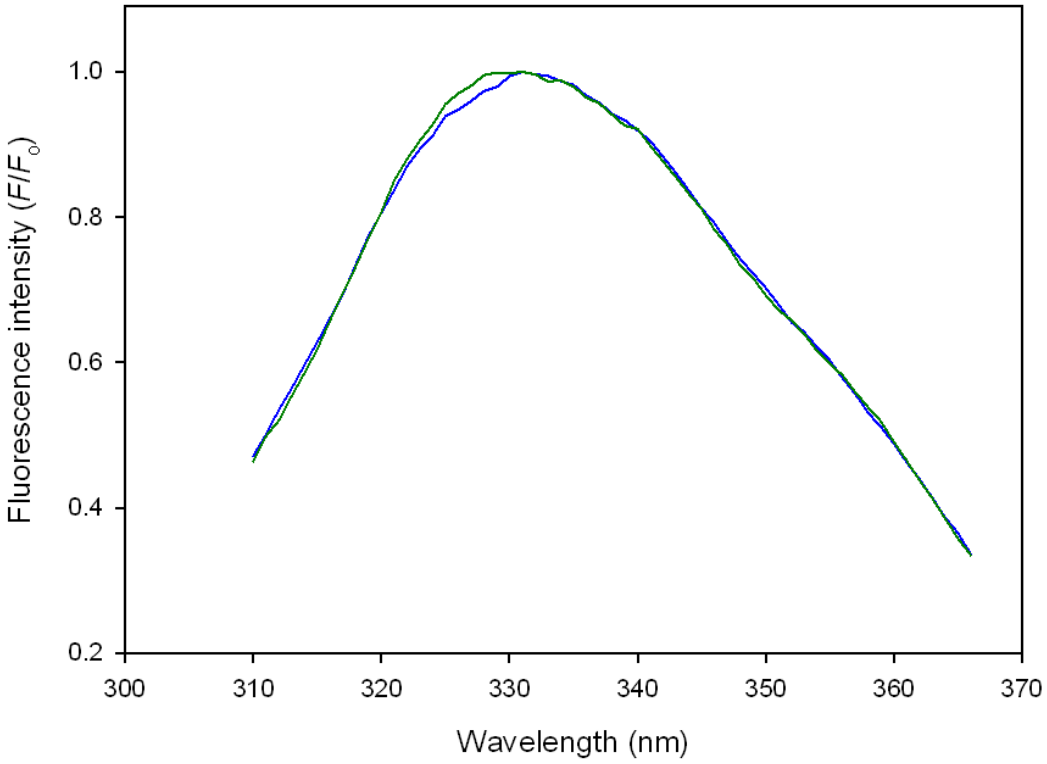

Figure A1.3 Fluorescence emission spectra of wild type KcsA (blue) and the mutant W67,68 (green) reconstituted in DOPC. Fluorescence intensities are expressed as the fraction of the maximum fluorescence intensity from the respective spectra (F_o, fluorescence at 333 nm). The concentration of KcsA monomer was 0.3 μM and the molar ratio of lipid:KcsA monomer was 100:1; the buffer was 20 mM Hepes containing 1 mM EGTA and 100 mM KCl, pH 7.2.

Appendix 2: ESR spectral deconvolution.

The ESR spectra were deconvoluted as described in Chapter 2, Section 2.2.6. Here a summary of the analysis of the spectra is presented. Tables A2.1 to A2.6 gather together the immobile fraction of spin label lipid estimated in each spectral analysis and other relevant information. As explained in Section 2.2.6, two single component spectra were combined to fit the composite spectrum. For each composite spectrum analysed the best fits are shown in Figures A2.1 to A2.5 along with the subtraction of each fitted spectrum from the experimental spectrum to help evaluate the goodness of the fit; also a 'noise' value corresponding to the sum of the absolute values of the differences between the experimental and the fitted spectra over the region chosen to fit the spectrum (generally the low magnetic field region of the spectrum, see Figure 2.4) is given in the respective tables. An error for the fraction of immobile component determined by the fitting analysis was estimated by taking the range between the best fit and a second fit with low noise found to not reproduce the features of the experimental spectrum as well as the best fit (case A). In numerous occasions more than one combination of single component spectra gave a good fit for the same composite spectrum; in this case (case B) the immobile component was taken as the average of the immobile components determined by the different best fits, and the error was taken as the largest range between those immobile components determined from the fits. Error bars for the estimation of the number of the lipid binding sites per channel (N_b values, Chapter 3, Table 3.3) and the relative lipid binding constants (K values Chapter 5, Table 5.1, Table 5.2 and Table 5.3) were determined by calculating the difference between the N_b or K values estimated and the N_b or K values that would be obtained if the immobile components were taken as the estimated error limits (i.e. if an immobile component was estimated to be 0.278 ± 0.022, the error for the calculated N_b value would be taken as the difference between the calculated N_b value and the N_b value obtained with an immobile component of 0.278 + 0.022 = 0.300 or 0.278 - 0.022 = 0.256, the value most different being the one chosen to calculate the error).

It is important to note that that for those samples where the spectra are analysed as a function of the lipid:protein molar ratio (Tables A2.1, A2.2, A2.3 and

A2.6) the measuring temperatures of the single mobile components used for the fits increase as the lipid:protein molar ratio increases. This is because the fluidity of the bulk lipid in the membrane is slightly affected by the protein content, becoming more fluid as the protein content decreases. As explained in the introduction, as the mobility of the acyl chain increases, the ESR spectrum narrows and its intensity increases (i.e. the spectra 'sharpens'). Indeed, it can be seen in the experimental spectrum how the mobile component becomes sharper (i.e. more mobile) as the lipid:protein molar ratio increases (see normalised spectra in Chapter 3 and Chapter 5). Therefore it is important to note that, in many cases, the increase in the intensity of the mobile peak is the result of only a more fluid bilayer and not a higher fraction of mobile component, as revealed by deconvolution of the spectra.

			Components used in fit		Shift		Case A		Case B	
N_t	f	Noise	DMPC	DOPC	DMPC	DOPC	Final f	Error	Final f	Error
30	0.300	811	0 ˚C	6˚C	R10	L2			0.278	0.022
	0.256	838	0 ˚C	5˚C	R8	L2				
37.5	0.300	1013	0 ˚C	8˚C	R8	L2	0.300	0.019		
	0.319	871	0 ˚C	8˚C	R8	L4				
45	0.225	1031	0 ˚C	12˚C	R4	L1	0.225	0.012		
	0.237	932	0 ˚C	12˚C	R4	L2				
52.5	0.275	1049	0 ˚C	10˚C	R8	L1			0.281	0.006
	0.287	926	0 ˚C	10˚C	R8	L2				
60	0.269	951	0 ˚C	10˚C	R6	L2			0.278	0.009
	0.287	1034	0 ˚C	11˚C	R8	L2				
67.5	0.275	2098	0 ˚C	19˚C	L4	L2	0.275	0.038		
	0.237	1686	0 ˚C	17˚C	L4	L2				
75	0.244	1445	0 ˚C	20˚C	R0	L0			0.263	0.019
	0.281	1496	0 ˚C	21˚C	R0	L0				
88	0.369	1004	0 ˚C	23˚C	L8	L0	0.369	0.044		
	0.325	1047	0 ˚C	21˚C	L8	L0				
100	0.306	955	0 ˚C	21˚C	L6	L0			0.319	0.037
	0.294	1129	0 ˚C	22˚C	L0	L0				
	0.356	1129	0 ˚C	23˚C	L2	L0				

Table A2.1 Summary of spectral analysis for the first set of samples of 14-PCSL in DOPC bilayers containing KcsA as a function of DOPC:channel molar ratio, recorded at 25 ˚C. The data correspond to those in Chapter 3: Figure 3.4 and Table 3.3. N_t is the DOPC:KcsA tetramer molar ratio in the sample; f is the fraction of immobile component determined by a particular fit, while the 'final f' refers to the fraction of immobile component considered most appropriate from the different fits according to the two different cases observed in the analysis (case A and B), as explained in the text (the poorer fits chosen to estimate error bars in case A are highlighted in grey); the 'noise' is the sum of the absolute values obtained from the subtraction of the fitted spectrum from the experimental spectrum over the region of the spectrum chosen for the fit (low field region, see Figure 2.4); as explained in the Chapter 2, Section 2.2.6, the single spectra chosen for the fits correspond, in this case, to 14-PCSL in DMPC sonicated vesicles (immobile component) and in DOPC vesicles (mobile component), and the temperature at which the single component was measured are indicated in the table; 'shift' refers to the shift along the x-axis of the single component spectrum with respect to the composite spectrum required for a particular fit, where R*n* indicates a shift to the right (i.e. towards high magnetic field) of *n* units (a unit corresponding to 0.1 G) and L*n* indicates a shift to the left (i.e. towards low magnetic field).

			Components used in fit		Shift		Case A		Case B	
N_t	f	Noise	DMPC	DOPC	DMPC	DOPC	Final f	Error	Final f	Error
30	0.281	1269	0 ˚C	8 ˚C	R8	L2			0.294	0.037
	0.331	1398	0 ˚C	10 ˚C	R10	L2				
	0.269	1445	0 ˚C	8 ˚C	R8	L1				
37.5	0.300	1076	0 ˚C	10 ˚C	R8	L1			0.286	0.042
	0.313	923	0 ˚C	10 ˚C	R8	L2				
	0.244	1126	0 ˚C	8 ˚C	R6	L0				
45	0.256	976	0 ˚C	12 ˚C	R8	L0			0.262	0.007
	0.262	982	0 ˚C	13 ˚C	R10	L1				
	0.269	869	0 ˚C	13 ˚C	R10	L2				
52.5	0.250	1433	0 ˚C	15 ˚C	R2	L1			0.275	0.025
	0.300	1410	0 ˚C	16 ˚C	R2	L1				
60	0.231	1456	0 ˚C	14 ˚C	R4	L1			0.240	0.010
	0.250	1436	0 ˚C	15 ˚C	R6	L2				
67.5	0.219	1389	0 ˚C	15 ˚C	R8	L2			0.231	0.044
	0.200	1415	0 ˚C	14 ˚C	R4	L1				
	0.275	1363	0 ˚C	16 ˚C	R6	L2				
75	0.325	1170	0 ˚C	18 ˚C	L2	L0	0.325	0.019		
	0.306	1486	0 ˚C	19 ˚C	L4	L1				
100	0.325	1753	0 ˚C	18 ˚C	L6	L0	0.325	0.031		
	0.356	1474	0 ˚C	18 ˚C	L6	L2				

Table A2.2 Summary of spectral analysis for the second set of samples of 14-PCSL in DOPC bilayers containing KcsA as a function of DOPC:channel molar ratio, recorded at 25 ˚C. The data correspond to those in Chapter 3: Figure 3.5 and Table 3.3. Details are as in the legend to Table A2.1.

			Components used in fit		Shift		Case A		Case B	
N_t	f	Noise	DMPC	DOPC	DMPC	DOPC	Final f	Error	Final f	Error
30	0.450	612	0 ˚C	12 ˚C	R10	L2			0.413	0.038
	0.375	621	0 ˚C	10 ˚C	R8	L2				
37.5	0.381	724	0 ˚C	10 ˚C	R6	L2			0.384	0.003
	0.387	756	0 ˚C	11 ˚C	R6	L2				
45	0.369	660	0 ˚C	12 ˚C	R6	L0			0.369	0.006
	0.363	695	0 ˚C	12 ˚C	R4	L0				
	0.375	680	0 ˚C	12 ˚C	R8	L0				
52.5	0.363	699	0 ˚C	12 ˚C	R4	L2	0.363	0.007		
	0.356	767	0 ˚C	13 ˚C	R4	L2				
60	0.331	564	0 ˚C	12 ˚C	R4	R1			0.335	0.004
	0.338	566	0 ˚C	13 ˚C	R4	L0				
75	0.269	450	0 ˚C	13 ˚C	R6	R1			0.310	0.041
	0.350	513	3 ˚C	15 ˚C	R4	L0				
88	0.356	548	3 ˚C	16 ˚C	R6	R2			0.331	0.025
	0.306	575	3 ˚C	14 ˚C	R2	R2				
100	0.250	523	0 ˚C	15 ˚C	R8	L0			0.285	0.035
	0.319	531	3 ˚C	16 ˚C	R2	L0				

Table A2.3 Summary of the spectral analysis of 14-PGSL in DOPG bilayers containing KcsA as a function of DOPG:channel molar ratio, recorded at 25 ˚C. The data correspond to those in Chapter 3, Figure 3.6 and Table 3.3. Details are as in the legend to Table A2.1.

				Components used in fit		Shift		Case A		Case B	
Spin label	Temp.	*f*	Noise	DMPC	DOPC	DMPC	DOPC	Final *f*	Error	Final *f*	Error
PA	35 ˚C	0.575	1127	11 ˚C	19 ˚C	L2	L0	0.575	0.038		
		0.613	912	11 ˚C	19 ˚C	L2	L2				
	30 ˚C	0.600	1125	9 ˚C	15 ˚C	L2	L0	0.600	0.025		
		0.575	1031	9 ˚C	13 ˚C	L2	L0				
PS	35 ˚C	0.525	852	11 ˚C	23 ˚C	L6	L0	0.525	0.037		
		0.488	1123	11 ˚C	23 ˚C	L6	R1				
	30 ˚C	0.525	1122	9 ˚C	20 ˚C	L2	L0	0.525	0.013		
		0.512	909	9 ˚C	18 ˚C	L4	L0				
	25 ˚C	0.500	1133	5 ˚C	12 ˚C	L0	L0			0.553	0.060
		0.613	986	9 ˚C	16 ˚C	L2	L0				
		0.587	942	9 ˚C	15 ˚C	L4	L0				
PG	30 ˚C	0.425	1299	9 ˚C	18 ˚C	L4	L0			0.419	0.032
		0.425	1413	9 ˚C	18 ˚C	R2	L0				
		0.387	1167	9 ˚C	16 ˚C	R0	L0				
		0.438	980	9 ˚C	16 ˚C	R0	L2				
	25 ˚C	0.438	1358	3 ˚C	12 ˚C	R4	L0			0.357	0.082
		0.275	1165	0 ˚C	8 ˚C	R6	L0				
PE	30 ˚C	0.425	950	9 ˚C	23 ˚C	L2	L0			0.432	0.007
		0.438	911	11 ˚C	23 ˚C	L2	L0				
	25 ˚C	0.425	1249	3 ˚C	17 ˚C	R6	L0			0.396	0.046
		0.412	1414	3 ˚C	17 ˚C	R6	R1				
		0.350	1070	0 ˚C	15 ˚C	R12	L0				
PC	35˚C	0.306	797	13 ˚C	21 ˚C	L16	L0	0.306	0.019		
		0.325	905	13 ˚C	21 ˚C	L10	L0				
	30 ˚C	0.325	1016	9 ˚C	17 ˚C	L6	L0			0.291	0.066
		0.325	1049	9 ˚C	17 ˚C	L4	L0				
		0.225	1046	0 ˚C	14 ˚C	R6	L0				
	25 ˚C	0.269	951	0 ˚C	10 ˚C	R6	L2			0.278	0.009
		0.287	1034	0 ˚C	11 ˚C	R8	L2				

Table A2.4 Summary of the spectral analysis of spin labelled phospholipids in DOPC bilayers containing KcsA at a lipid:channel molar ratio of 60:1, recorded at 25, 30 and 35 ˚C. The data correspond to those presented in Chapter 5, Figure 5.3 and Table 5.1. The details are as in the legend to Table A2.1.

				Components used in fit		Shift		Case A		Case B	
Spin label	Temp	*f*	Noise	DMPC	DOPC	DMPC	DOPC	Final *f*	Error	Final *f*	Error
PG	30 ˚C	0.425	507	9 ˚C	20 ˚C	L6	R0			0.360	0.066
		0.294	490	0 ˚C	17 ˚C	R8	R1				
	25 ˚C	0.338	566	0 ˚C	13 ˚C	R4	L0			0.375	0.037
		0.412	565	3 ˚C	14 ˚C	R0	L0				
PC	30 ˚C	0.237	504	0 ˚C	19 ˚C	R8	R1			0.259	0.072
		0.200	405	0 ˚C	18 ˚C	R4	L2				
		0.331	566	9 ˚C	21 ˚C	L6	R1				
		0.269	445	9 ˚C	20 ˚C	L8	R2				
	25 ˚C	0.319	619	3 ˚C	15 ˚C	R0	R1	0.319	0.012		
		0.307	618	3 ˚C	15 ˚C	R0	R2				

Table A2.5 Summary of spectral analysis for spin labelled phospholipids in DOPG bilayers containing KcsA at a lipid:channel molar ratio of 60:1, measured at 25 and 30 ˚C. The data correspond to those presented in Chapter 5, Figure 5.3 and Table 5.2. The details are as in the legend to Table A2.1.

			Components used in fit		Shift		Case A		Case B	
N_t	f	Noise	SA-BSA	DOPC	SA-BSA	DOPC	Final f	Error	Final f	Error
30 (2^{nd})	0.900	1418	6 ˚C	10˚C	R5	L2	0.900	0.020		
	0.920	1588	6 ˚C	12˚C	R5	R1				
37.5 (2^{nd})	0.900	1219	6 ˚C	10˚C	R5	L2	0.900	0.025		
	0.925	1617	6 ˚C	14˚C	R5	L0				
60 (2^{nd})	0.837	1917	6 ˚C	14˚C	R7	L0	0.837	0.012		
	0.825	2026	6 ˚C	12 ˚C	R6	R0				
67.5 (1^{st})	0.850	1972	6 ˚C	18 ˚C	R6	R0			0.837	0.013
	0.837	1832	6 ˚C	14 ˚C	R6	R2				
	0.837	2049	10 ˚C	15 ˚C	R4	R0				
	0.825	1950	6 ˚C	13 ˚C	R6	R2				
88 (2^{nd})	0.788	1588	10 ˚C	19 ˚C	R6	L0			0.781	0.007
	0.775	1610	10 ˚C	18 ˚C	R6	R2				
100 (1^{st})	0.738	1524	10 ˚C	19 ˚C	R6	R2	0.738	0.012		
	0.750	1545	6 ˚C	19 ˚C	R8	R0				
*88	0.788	1288	16 ˚C	19 ˚C	R6	R0	0.788	0.013		
	0.775	1221	16 ˚C	17 ˚C	R6	R2				
†60 (1^{st})	0.356	1431	6 ˚C	16 ˚C	R10	R4			0.356	0.007
	0.363	1625	6 ˚C	16 ˚C	R7	R3				
	0.350	1550	10 ˚C	16 ˚C	R6	R4				
	0.356	1432	13 ˚C	16 ˚C	R10	R4				
*†88	0.363	1034	9 ˚C	17 ˚C	R2	R2			0.407	0.044
	0.450	1019	13 ˚C	19 ˚C	L4	R2				

Table A2.6 Summary for the spectral analysis for 14-SASL in DOPC or DOPG (*) membranes containing KcsA at the given lipid:channel molar ratios. The data correspond to those described in Chapter 5, Figures 5.5 (first set of data for samples in DOPC: as indicated in parenthesis in the N_t column in this Table), 5.6 (second set of data for samples in DOPC: also indicated in parenthesis in the N_t column here), 5.7 (in DOPG bilayers), 5.8 (pH 3.9 in DOPC bilayers), 5.9 (pH 3.9 in DOPG bilayers) and Table 5.3. In this case, the single component spectra chosen for the fits were taken from a library of 14-SASL bound to BSA (immobile component) and 14-PCSL in DOPC bilayers (mobile component) at the shown temperatures, as described in the text. Samples reconstituted in DOPG are marked with (*) and samples at pH 3.9 are indicated by (†). The details are as in the legend to Table A2.1.

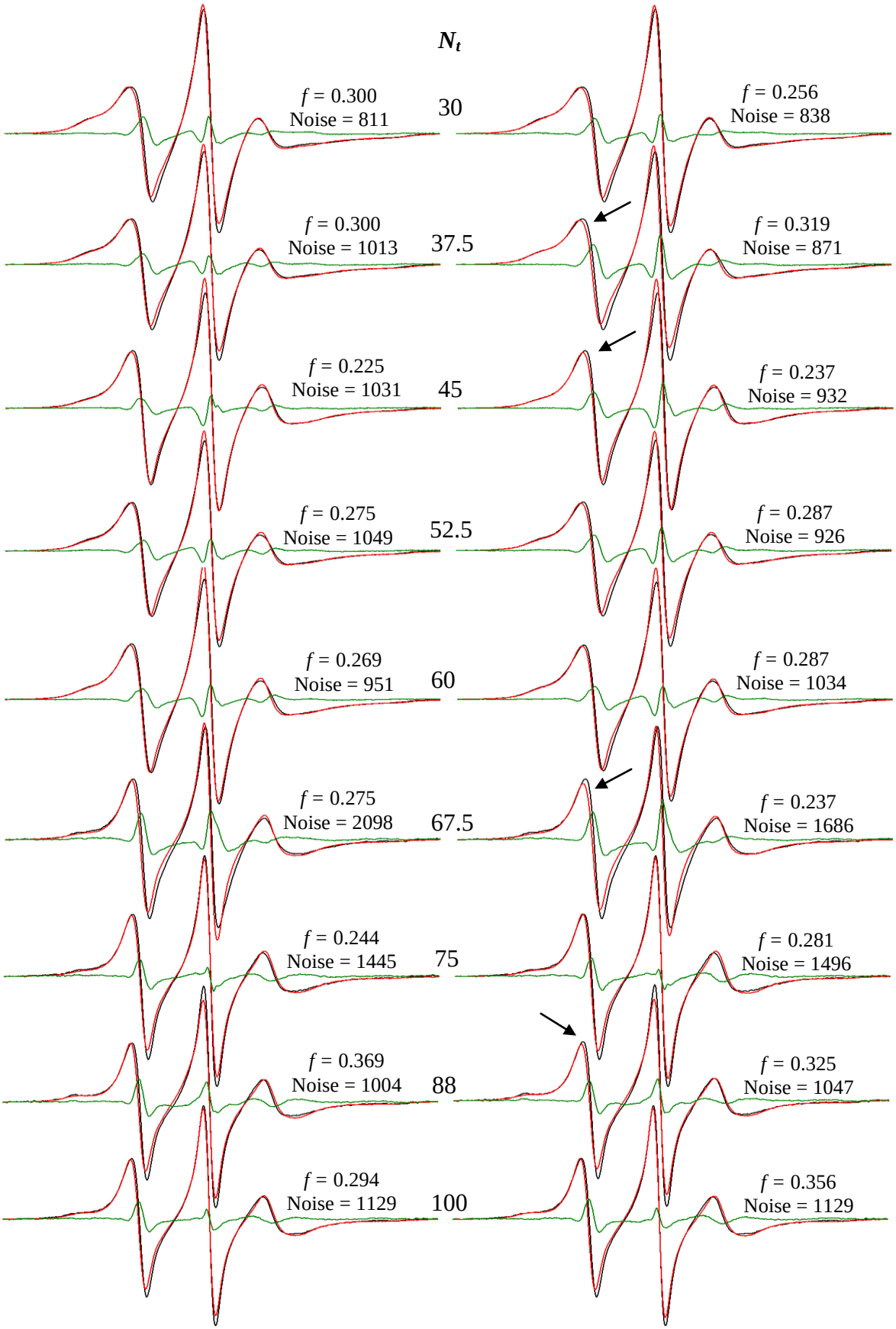

Figure A2.1 Spectral analysis for 14-PCSL (1st set of samples, 25 ˚C) in DOPC bilayers containing KcsA at the given molar ratios of lipid:channel. (See figure legend on p. 232.)

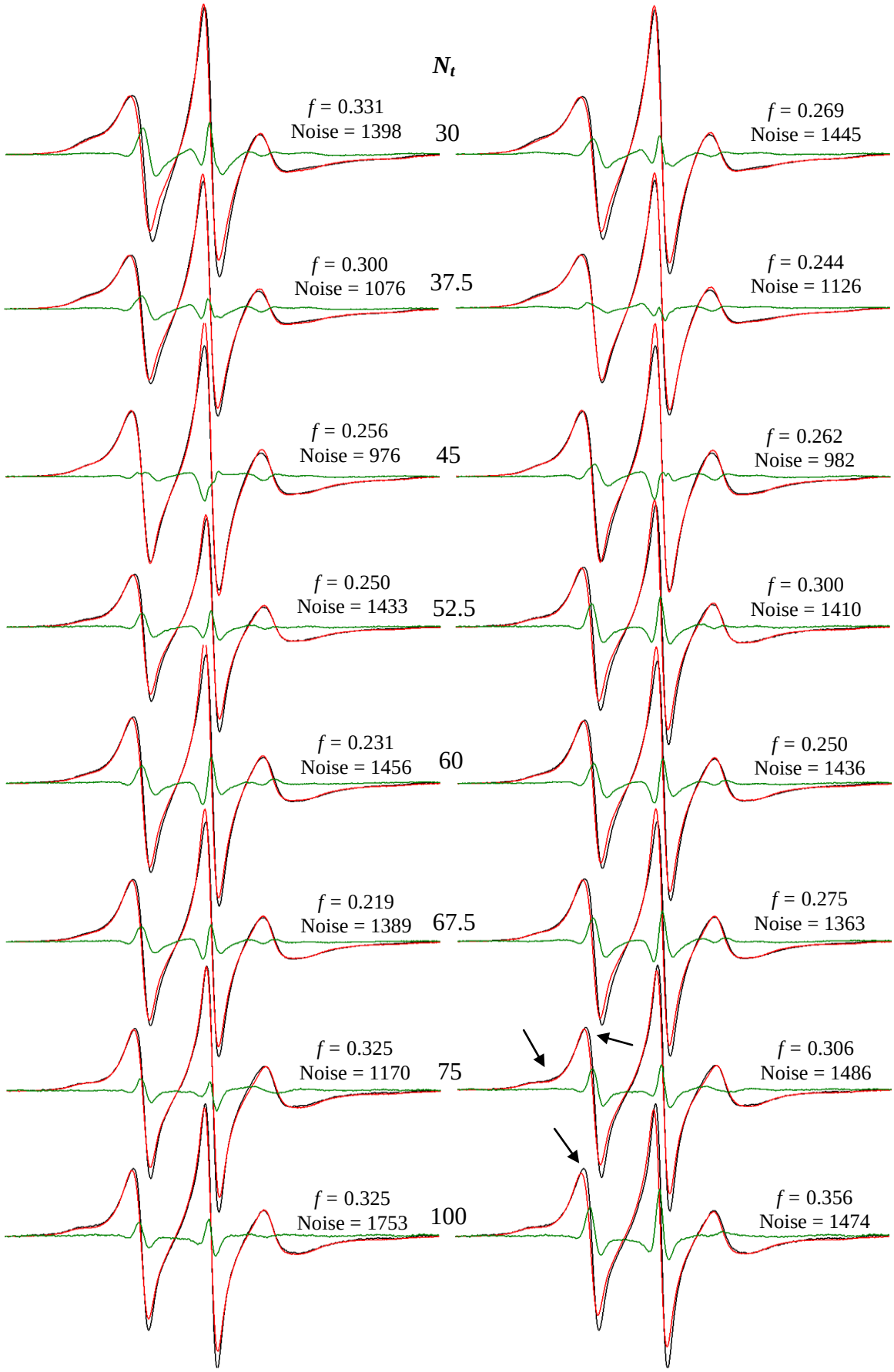

Figure A2.2 Spectral analysis for 14-PCSL (2nd set of samples, 25 ˚C) in DOPC bilayers containing KcsA at the given molar ratios of lipid:channel. (See figure legend on p. 232.)

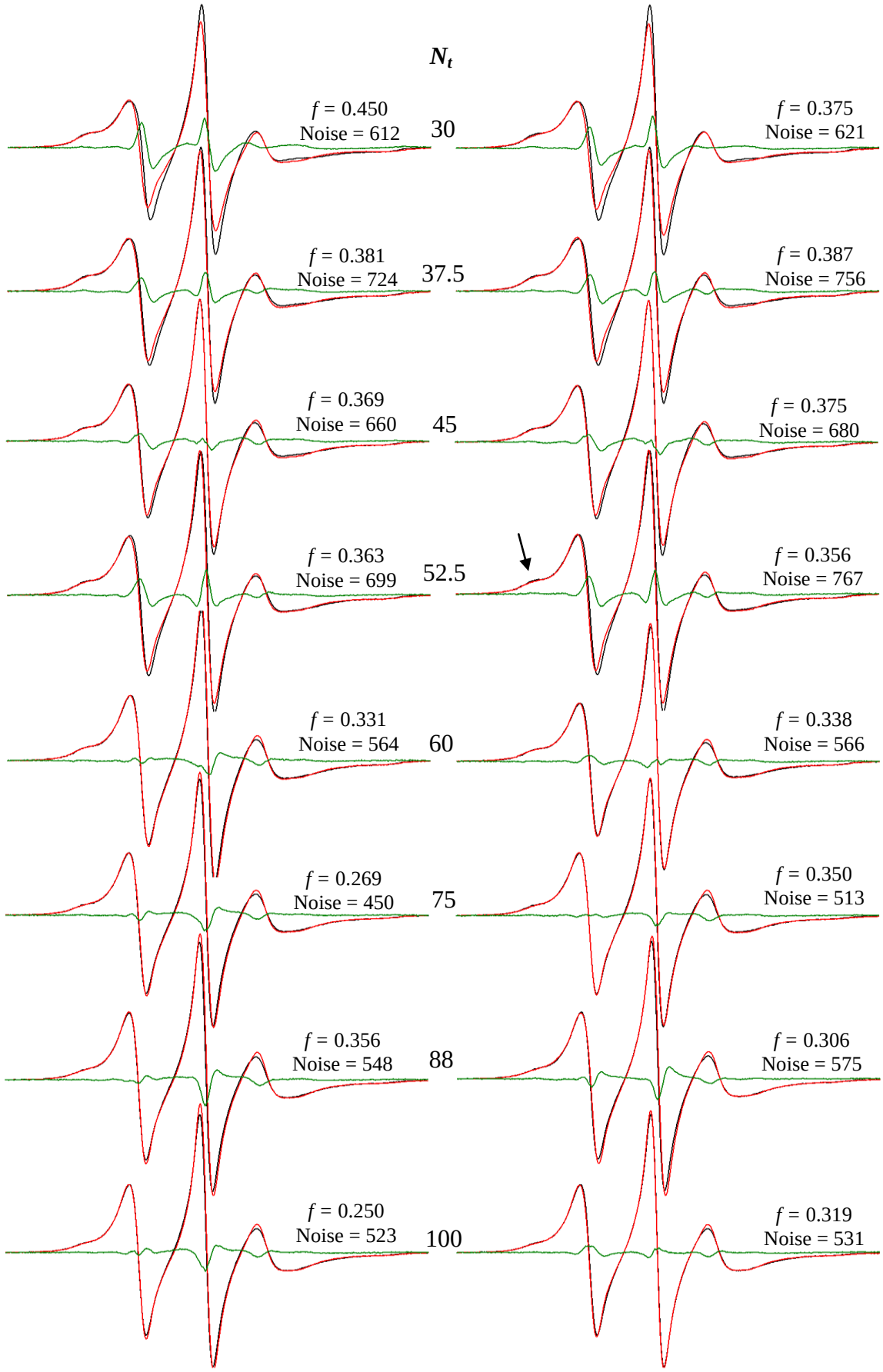

Figure A2.3 Spectral analysis for 14-PGSL (25 ˚C) in bilayers of DOPG containing KcsA at the given lipid:channel molar ratios. (See figure legend on p. 232.)

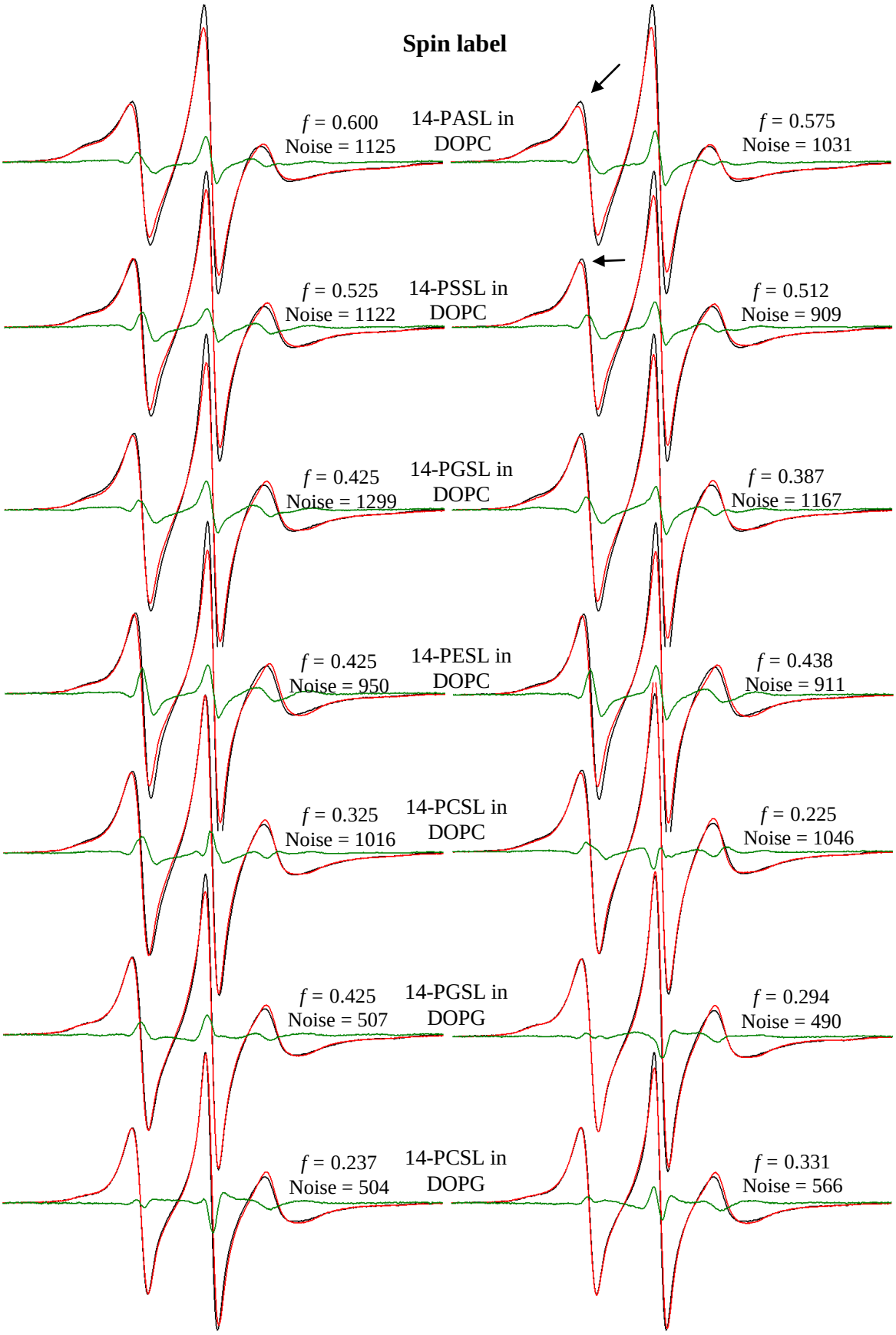

Figure A2.4 Analysis of the ESR spectra of spin labelled phospholipids in DOPC or DOPG bilayers containing KcsA at a molar ratio of lipid:channel of 60:1, measured at 30 ˚C. (See figure legend on p. 232.)

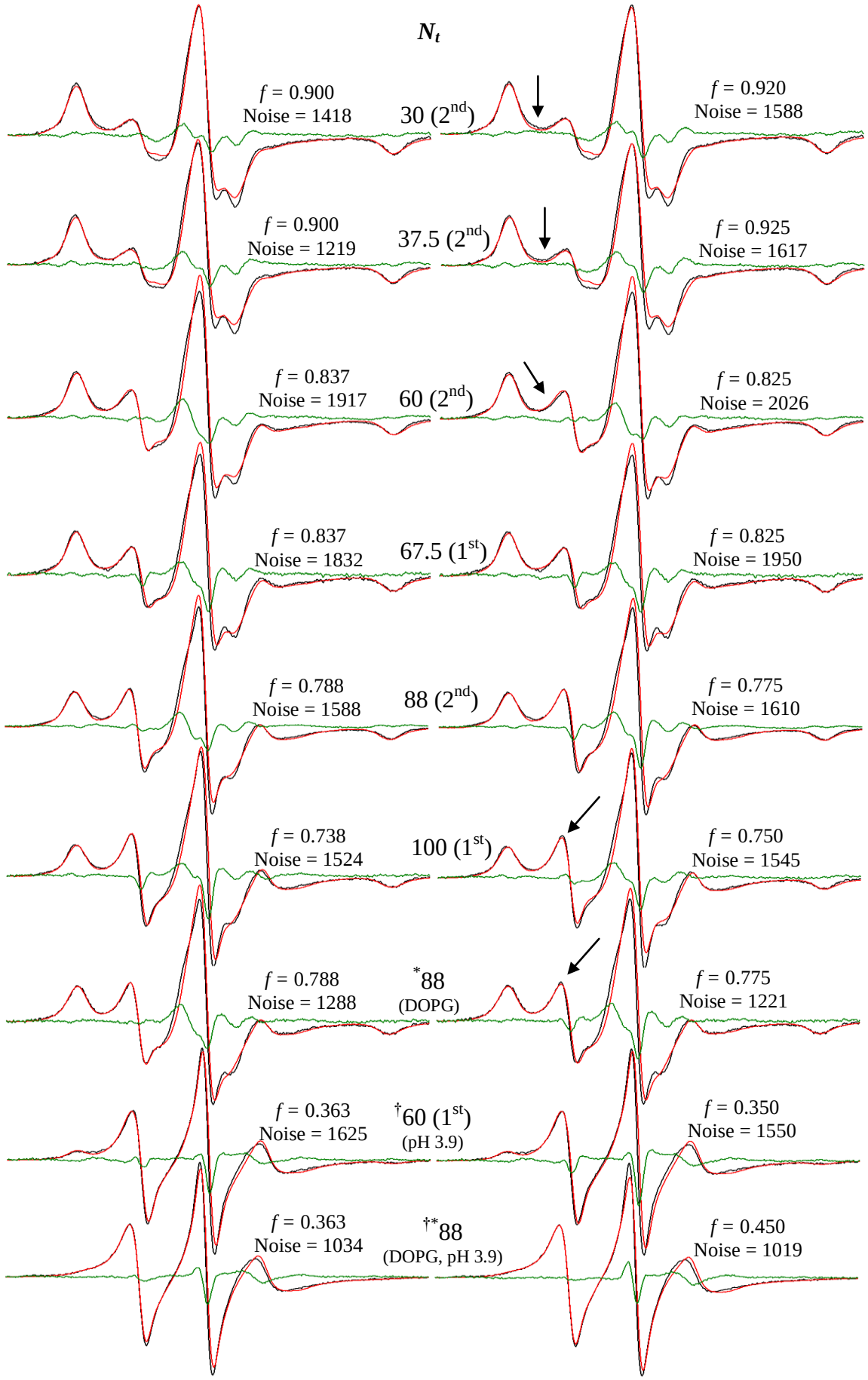

Figure A2.5 ESR spectral analysis for 14-SASL. (See figure legend on p. 232.)

Figure A2.1 Spectral analysis for 14-PCSL (1st set of samples, 25 ˚C) in DOPC bilayers containing KcsA at the given molar ratios of lipid:channel. The spectra are those from Chapter 3, Figure 3.4. The spectra were analysed as described in the text; detailed information about the analysis is gathered in Table A2.1. In black are the experimental spectra, in red are the fitted spectra and in green are the subtractions of the fitted spectra from the experimental spectra. Two fits are shown for each experimental spectrum (which correspond to those in Table A2.1) and the lipid to channel molar ratio (N_t) of the sample is indicated in-between the two fits. The fraction of immobilised spin labelled lipid (*f*) and the noise for each fit are also indicated for each fit. Fits of low noise but clearly poorer than the other fits due to failure to reproduce particular features of the spectra (case B, see text) are indicated by an arrow which points to the region of the spectra poorly fitted and correspond to those fits highlighted in grey in Table A2.1. Note that for the samples of lipid:channel molar ratios of 37.5:1, 45:1 and 67.5:1 the noise of the poorer fit (highlighted with the arrow), is markedly lower than for the better fit. This is simply because the noise was measured in the region to the left (low field) of the highest point of the low field peak of the mobile component (see Figure 2.4 in Chapter 2) and so the very poor fit to the high field side of the peak is not accounted for in the noise. The high field side of the low field mobile peak was not considered for the fittings due to its sharpness, as it was found that small differences in this region would dominate fitting of the spectra, undermining the other features.

*Note: the spectra for the different lipid to protein ratios shown here are not normalised relative to each other, as the purpose of the figure is to illustrate the fitting procedure. The normalised spectra are shown in Chapter 3, Figure 3.4.

Figure A2.2 Spectral analysis for 14-PCSL (2nd set of samples, 25 ˚C) in DOPC bilayers containing KcsA at the given molar ratios of lipid:channel. The spectra are those from Chapter 3, Figure 3.5. Details are given in the legend to Figure A2.1. Other detailed information about the analysis can be found in Table A2.2.

Figure A2.3 Spectral analysis for 14-PGSL (25 ˚C) in bilayers of DOPG containing KcsA at the given lipid:channel molar ratios. The spectra are those shown in Chapter 3, Figure 3.6. Details are given in the legend to Figure A2.1. Other detailed information about the analysis can be found in Table A2.3.

Figure A2.4 Analysis of the ESR spectra of spin labelled phospholipids in DOPC or DOPG bilayers containing KcsA at a molar ratio of lipid:channel of 60:1, measured at 30 ˚C. The spectra correspond to those shown in Chapter 5, Figure 5.3. Details are given in the legend to Figure A2.1. Other detailed information about the analysis can be found in Tables A2.4 and A2.5.

Figure A2.5 ESR spectral analysis for 14-SASL. The spectra for 14-SASL measured at 25 ˚C in DOPC or DOPG (*) bilayers containing KcsA at the given lipid:channel molar ratios (N_t) correspond to those in Chapter 5, Figures 5.5, 5.6, 5.7, 5.8 and 5.9. As in all the other samples, the pH was 7.2, except for the samples marked with (†) whose pH was 3.9. In parenthesis is indicated the set of samples to which each spectrum belongs. The rest of samples could not be deconvoluted adequately. Note that deconvolution of the sample in DOPC at pH 3.9 has been approximated in terms of only two components, despite there being three components (see Section 5.4.4). Details are the same as in the legend to Figure A2.1 Other detailed information about the analysis is gathered in Table A2.6.

References

1. Luckey L. Membrane structural biology: with biochemical and biophysical foundations.; 1st ed.; Cambridge University Press: Cambridge, 2008.

2. Berg, J. M., Tymoczko, J. L. and Stryer, L. Biochemistry; 5th ed.; W. H. Freeman and Company: New York, 2002.

3. Zhong-Can, O., Ji-Xing, L. and Yu-Zhang, X. Geometric methods in the elastic theory of membranes in liquid crystal phases; World Scientific: Singapore, 1999.

4. Lee, A. G. (2004) How lipids affect the activities of integral membrane proteins. *Biochim. Biophys. Acta* 1666, 62-87.

5. Vance, D. E. and Vance, J. E. Biochemistry of lipids, lipoproteins, and membranes; 3rd ed.; Elsevier Science: 1996.

6. Brown, D. A., London, E. (1997) Structure of detergent-resistant membrane domains: does phase separation occur in biological membranes? *Biochem. Biophys. Res. Commun.* 240, 1-7.

7. Garrett, R. H. and Grisham, C. M. Biochemistry; international ed.; Saunders College: 1995.

8. Alberts, B., Johnson, A., Lewis, J., Raff, M., Roberts, K. and Walter, P. Molecular biology of the cell; 4th ed.; Garland Science: New York, 2002.

9. Lee, A. G. (2005) How lipids and proteins interact in a membrane: a molecular approach. *Mol. Biosyst.* 1, 203-212.

10. Singer, S. J., Nicolson, G. L. (1972) The fluid mosaic model of the structure of cell membranes. *Science* 175, 720-731.

11. Escriba, P. V., Gonzalez-Ros, J. M., Goni, F. M., Kinnunen, P. K. J., Vigh, L., Sanchez-Magraner, L., Fernandez, A. M., Busquets, X., Horvath, I. and Barcelo-Coblijn, G. (2008) Membranes: a meeting point for lipids, proteins and therapies. *J. Cell. Mol. Med.* 12, 829-875.

12. Lee, A. G. (2011) Biological membranes: the importance of molecular detail. *Trends. Biochem. Sci.* 36, 493-500.

13. Marius, P., Zagnoni, M., Sandison, M. E., East, J. M., Morgan, H. and Lee, A. G. (2008) Binding of anionic lipids to at least three nonannular sites on the potassium channel KcsA is required for channel opening. *Biophys. J.* 94, 1689-1698.

14. Powl, A. M., East, J. M. and Lee, A. G. (2005) Heterogeneity in the binding of lipid molecules to the surface of a membrane protein: hot spots for anionic lipids on the mechanosensitive channel of large conductance MscL and effects on conformation. *Biochemistry* 44, 5873-5883.

15. Fung, J. J., Deupi, X., Pardo, L., Yao, X. J., Velez-Ruiz, G. A., DeVree, B. T., Sunahara, R. K. and Kobilka, B. K. (2009) Ligand-regulated oligomerization of β_2-adrenoceptors in a model lipid bilayer. *EMBO J.* 28, 3315-3328.

16. Pin, J. P., Kniazeff, J., Liu, J., Binet, V., Goudet, C., Rondard, P. and Prézeau, L. (2005) Allosteric functioning of dimeric class C G-protein-coupled receptors. *FEBS J.* 272, 2947-2955.

17. Horio, Y., Hibino, H., Inanobe, A., Yamada, M., Ishii, M., Tada, Y., Satoh, E., Hata, Y., Takai, Y. and Kurachi, Y. (1997) Clustering and enhanced activity of an inwardly rectifying potassium channel, Kir4.1, by an anchoring protein, PSD-95/SAP90. *J. Biol. Chem.* 272, 12885-12888.

18. Misonou, H., Mohapatra, D. P., Park, E. W., Leung, V., Zhen, D., Misonou, K., Anderson, A. E. and Trimmer, J. S. (2004) Regulation of ion channel localization and phosphorylation by neuronal activity. *Nat. Neurosci.* 7, 711-718.

19. Yin, C. C., Blayney, L. M. and Anthony Lai, F. (2005) Physical coupling between ryanodine receptor-calcium release channels. *J. Mol. Biol.* 349, 538-546.

20. Bray, D., Duke, T. (2004) Conformational spread: the propagation of allosteric states in large multiprotein complexes. *Annu. Rev. Biophys. Biomol. Struct.* 33, 53-73.

21. Killian, J. A. (1998) Hydrophobic mismatch between proteins and lipids in membranes. *Biochim. Biophys. Acta* 1376, 401-415.

22. Lee, A. G. (2003) Lipid-protein interactions in biological membranes: a structural perspective. *Biochim. Biophys. Acta* 1612, 1-40.

23. Marsh, D., Páli, T. (2006) Lipid conformation in crystalline bilayers and in crystals of transmembrane proteins. *Chem. Phys. Lipids.* 141, 48-65.

24. Marsh, D. (2008) Electron spin resonance in membrane research: protein-lipid interactions. *Methods* 46, 83-96.

25. Marsh, D., Horvath, L. I. (1998) Structure, dynamics and composition of the lipid-protein interface. Perspectives from spin-labelling. *Biochim. Biophys. Acta* 1376, 267-296.

26. Hubbell, W. L., Gross, A., Langen, R. and Lietzow, M. A. (1998) Recent advances in site-directed spin labeling of proteins. *Curr. Opin. Struct. Biol.* 8, 649-656.

27. Lakowicz, J. R. Principles of fluorescence spectroscopy; 3rd ed.; Springer: New York, 2006.

28. Powl, A. M., Carney, J., Marius, P., East, J. M. and Lee, A. G. (2005) Lipid interactions with bacterial channels: fluorescence studies. *Biochem. Soc. Trans.* 33, 905-909.

29. Powl, A. M., Wright, J. N., East, J. M. and Lee, A. G. (2005) Identification of the hydrophobic thickness of a membrane protein using fluorescence spectroscopy: studies with the mechanosensitive channel MscL. *Biochemistry* 44, 5713-5721.

30. Bolen, E. J., Holloway, P. W. (1990) Quenching of tryptophan fluorescence by brominated phospholipid. *Biochemistry* 29, 9638-9643.

31. East, J. M., Lee, A. G. (1982) Lipid selectivity of the calcium and magnesium ion dependent adenosine triphosphatase, studied with fluorescence quenching by a brominated phospholipid. *Biochemistry* 21, 4144-4151.

32. Simmonds, A. C., East, J. M., Jones, O. T., Rooney, E. K., Mcwhirter, J. and Lee, A. G. (1982) Annular and non-annular binding-sites on the (Ca^{2+} + Mg^{2+})-ATPase. *Biochim. Biophys. Acta* 693, 398-406.

33. MacKinnon, R. (2003) Potassium channels. *FEBS Lett.* 555, 62-65.

34. Doyle, D. A., Cabral, J., Pfuetzner, R. A., Kuo, A., Gulbis, J. M., Cohen, S. L., Chait, B. T. and MacKinnon, R. (1998) The structure of the potassium channel: molecular basis of K^+ conduction and selectivity. *Science* 280, 69-77.

35. Korn, S. J., Trapani, J. G. (2005) Potassium channels. *IEEE Trans. Nanobioscience.* 4, 21-33.

36. Lesage, F., Terrenoire, C., Romey, G. and Lazdunski, M. (2000) Human TREK2, a 2P domain mechano-sensitive K^+ channel with multiple regulations by polyunsaturated fatty acids, lysophospholipids, and G_s, G_i, and G_q protein-coupled receptors. *J. Biol. Chem.* 275, 28398-28405.

37. Yellen, G. (2002) The voltage-gated potassium channels and their relatives. *Nature* 419, 35-42.

38. Kuo, M. M. C., Haynes, W. J., Loukin, S. H., Kung, C. and Saimi, Y. (2005) Prokaryotic K^+ channels: from crystal structures to diversity. *FEMS Microbiol. Rev.* 29, 961-985.

39. Schmidt, D., Jiang, Q. X. and MacKinnon, R. (2006) Phospholipids and the origin of cationic gating charges in voltage sensors. *Nature* 444, 775-779.

40. Zheng, H., Liu, W., Anderson, L. Y. and Jiang, Q. X. (2011) Lipid-dependent gating of a voltage-gated potassium channel. *Nat. Commun.* 2, 250.

41. Tucker, S. J., Baukrowitz, T. (2008) How highly charged anionic lipids bind and regulate ion channels. *J. Gen. Physiol.* 131, 431-438.

42. Logothetis, D. E., Lupyan, D. and Rosenhouse-Dantsker, A. (2007) Diverse Kir modulators act in close proximity to residues implicated in phosphoinositide binding. *J. Physiol.* 582, 953-965.

43. Boland, L., Drzewiecki, M. (2008) Polyunsaturated fatty acid modulation of voltage-gated ion channels. *Cell. Biochem. Biophys.* 52, 59-84.

44. Meves, H. (2008) Arachidonic acid and ion channels: an update. *Br. J. Pharmacol.* 155, 4-16.

45. Hamilton, K. L., Syme, C. A. and Devor, D. C. (2003) Molecular localization of the inhibitory arachidonic acid binding site to the pore of hIK1. *J. Biol. Chem.* 278, 16690-16697.

46. Decher, N., Streit, A. K., Rapedius, M., Netter, M. F., Marzian, S., Ehling, P., Schlichthorl, G., Craan, T., Renigunta, V., Kohler, A., Dodel, R. C., Navarro-Polanco, R. A., Preisig-Muller, R., Klebe, G., Budde, T., Baukrowitz, T. and Daut, J. (2010) RNA editing modulates the binding of drugs and highly unsaturated fatty acids to the open pore of Kv potassium channels. *EMBO J.* 29, 2101-2113.

47. Schrempf, H., Schmidt, O., Kummerlen, R., Hinnah, S., Muller, D., Betzler, M., Steinkamp, T. and Wagner, R. (1995) A prokaryotic potassium-ion channel with two predicted transmembrane segments from *Streptomyces lividans*. *EMBO J.* 14, 5170-5178.

48. MacKinnon, R., Cohen, S. L., Kuo, A., Lee, A. and Chait, B. T. (1998) Structural conservation in prokaryotic and eukaryotic potassium channels. *Science* 280, 106-109.

49. Lu, Z., Klem, A. M. and Ramu, Y. (2001) Ion conduction pore is conserved among potassium channels. *Nature* 413, 809-813.

50. Cuello, L. G., Jogini, V., Cortes, D. M. and Perozo, E. (2010) Structural mechanism of C-type inactivation in K^+ channels. *Nature* 466, 203-208.

51. Cortes, D. M., Cuello, L. G. and Perozo, E. (2001) Molecular architecture of full-length KcsA: role of cytoplasmic domains in ion permeation and activation gating. *J. Gen. Physiol.* 117, 165-180.

52. Uysal, S., Vásquez, V., Tereshko, V., Esaki, K., Fellouse, F. A., Sidhu, S. S., Koide, S., Perozo, E. and Kossiakoff, A. (2009) Crystal structure of full-length KcsA in its closed conformation. *Proc. Natl. Acad. Sci. USA* 106, 6644-6649.

53. Zhou, Y. F., Morais-Cabral, J. H., Kaufman, A. and MacKinnon, R. (2001) Chemistry of ion coordination and hydration revealed by a K^+ channel-Fab complex at 2.0 angstrom resolution. *Nature* 414, 43-48.

54. Roux, B., MacKinnon, R. (1999) The cavity and pore helices in the KcsA K^+ channel: electrostatic stabilization of monovalent cations. *Science* 285, 100-102.

55. Heginbotham, L., LeMasurier, M., Kolmakova-Partensky, L. and Miller, C. (1999) Single *Streptomyces lividans* K^+ channels. *J. Gen. Physiol.* 114, 551-560.

56. Thompson, A. N., Posson, D. J., Parsa, P. V. and Nimigean, C. M. (2008) Molecular mechanism of pH sensing in KcsA potassium channels. *Proc. Natl. Acad. Sci. USA* 105, 6900-6905.

57. Perozo, E., Cortes, D. M. and Cuello, L. G. (1998) Three-dimensional architecture and gating mechanism of a K^+ channel studied by EPR spectroscopy. *Nat. Struct. Mol. Biol.* 5, 459-469.

58. Perozo, E., Marien, D., Cortes and Cuello, L. G. (1999) Structural rearrangements underlying K^+-channel activation gating. *Science* 285, 73-78.

59. Baker, K. A., Tzitzilonis, C., Kwiatkowski, W., Choe, S. and Riek, R. (2007) Conformational dynamics of the KcsA potassium channel governs gating properties. *Nat. Struct. Mol. Biol.* 14, 1089-1095.

60. Shimizu, H., Iwamoto, M., Konno, T., Nihei, A., Sasaki, Y. C. and Oiki, S. (2008) Global twisting motion of single molecular KcsA potassium channel upon gating. *Cell* 132, 67-78.

61. Jiang, Y., Lee, A., Chen, J., Cadene, M., Chait, B. T. and MacKinnon, R. (2002) Crystal structure and mechanism of a calcium-gated potassium channel. *Nature* 417, 515-522.

62. Blunck, R., Cordero-Morales, J. F., Cuello, L. G., Perozo, E. and Bezanilla, F. (2006) Detection of the opening of the bundle crossing in KcsA with fluorescence lifetime spectroscopy reveals the existence of two gates for ion conduction. *J. Gen. Physiol.* 128, 569-581.

63. Cordero-Morales, J. F., Cuello, L. G., Zhao, Y., Jogini, V., Cortes, D. M., Roux, B. and Perozo, E. (2006) Molecular determinants of gating at the potassium-channel selectivity filter. *Nat. Struct. Mol. Biol.* 13, 311-318.

64. Cordero-Morales, J. F., Jogini, V., Lewis, A., Vasquez, V., Cortes, D. M., Roux, B. and Perozo, E. (2007) Molecular driving forces determining potassium channel slow inactivation. *Nat. Struct. Mol. Biol.* 14, 1062-1069.

65. Cuello, L. G., Jogini, V., Cortes, D. M., Pan, A. C., Gagnon, D. G., Dalmas, O., Cordero-Morales, J. F., Chakrapani, S., Roux, B. and Perozo, E. (2010) Structural basis for the coupling between activation and inactivation gates in K^+ channels. *Nature* 466, 272-275.

66. Yellen, G. (1998) The moving parts of voltage-gated ion channels. *Q. Rev. Biophys.* 31, 239-295.

67. Zhou, M., Morais-Cabral, J. H., Mann, S. and MacKinnon, R. (2001) Potassium channel receptor site for the inactivation gate and quaternary amine inhibitors. *Nature* 411, 657-661.

68. Decher, N., Gonzalez, T., Streit, A. K., Sachse, F. B., Renigunta, V., Soom, M., Heinemann, S. H., Daut, J. and Sanguinetti, M. C. (2008) Structural determinants of $Kv_{\beta}1.3$-induced channel inactivation: a hairpin modulated by PIP_2. *EMBO J.* 27, 3164-3174.

69. Kutluay, E., Roux, B. and Heginbotham, L. (2005) Rapid intracellular TEA block of the KcsA potassium channel. *Biophys. J.* 88, 1018-1029.

70. Lenaeus, M. J., Vamvouka, M., Focia, P. J. and Gross, A. (2005) Structural basis of TEA blockade in a model potassium channel. *Nat. Struct. Mol. Biol.* 12, 454-459.

71. Faraldo-Gomez, J. D., Kutluay, E., Jogini, V., Zhao, Y., Heginbotham, L. and Roux, B. (2007) Mechanism of intracellular block of the KcsA K^+ channel by tetrabutylammonium: insights from X-ray crystallography, electrophysiology and replica-exchange molecular synamics simulations. *J. Mol. Biol.* 365, 649-662.

72. Williamson, I. M., Alvis, S. J., East, J. M. and Lee, A. G. (2002) Interactions of phospholipids with the potassium channel KcsA. *Biophys. J.* 83, 2026-2038.

73. Alvis, S. J., Williamson, I. M., East, J. M. and Lee, A. G. (2003) Interactions of anionic phospholipids and phosphatidylethanolamine with the potassium channel KcsA. *Biophys. J.* 85, 3828-3838.

74. Marius, P., Alvis, S. J., East, J. M. and Lee, A. G. (2005) The interfacial lipid binding site on the potassium channel KcsA is specific for anionic phospholipids. *Biophys. J.* 89, 4081-4089.

75. Cortes, D. M., Perozo, E. (1997) Structural dynamics of the *Streptomyces lividans* K^+ channel (SKC1): oligomeric stoichiometry and stability. *Biochemistry* 36, 10343-10352.

76. Heginbotham, L., Odessey, E. and Miller, C. (1997) Tetrameric stoichiometry of a prokaryotic K^+ channel. *Biochemistry* 36, 10335-10342.

77. Krishnan, M. N., Bingham, J. P., Lee, S. H., Trombley, P. and Moczydlowski, E. (2005) Functional role and affinity of inorganic cations in stabilizing the tetrameric structure of the KcsA K^+ channel. *J. Gen. Physiol.* 126, 271-283.

78. Zimmer, J., Doyle, D. A. and Grossmann, J. G. (2006) Structural characterization and pH-induced conformational transition of full-length KcsA. *Biophys. J.* 90, 1752-1766.

79. Molina, M. L., Barrera, F. N., Fernandez, A. M., Poveda, J. A., Renart, M. L., Encinar, J. A., Riquelme, G. and Gonzalez-Ros, J. M. (2006) Clustering and coupled gating modulate the activity in KcsA, a potassium channel model. *J. Biol. Chem.* 281, 18837-18848.

80. Raja, M., Vales, E. (2009) Effects of sodium chloride on membrane fusion and on the formation of aggregates of potassium channel KcsA in *Escherichia coli* membrane. *Biophys. Chem.* 142, 46-54.

81. Valiyaveetil, F. I., Zhou, Y. and MacKinnon, R. (2002) Lipids in the structure, folding, and function of the KcsA K^+ channel. *Biochemistry* 41, 10771-10777.

82. Heginbotham, L., Kolmakova-Partensky, L. and Miller, C. (1998) Functional reconstitution of a prokaryotic K^+ channel. *J. Gen. Physiol.* 111, 741-749.

83. Powl, A. M., East, J. M. and Lee, A. G. (2003) Lipid-Protein Interactions studied by introduction of a tryptophan residue: the mechanosensitive channel MscL. *Biochemistry* 42, 14306-14317.

84. Mall, S., Broadbridge, R., Sharma, R., East, J. M. and Lee, A. G. (2001) Self-association of model transmembrane α-elices is modulated by lipid structure. *Biochemistry* 40, 12379-12386.

85. Carney, J., East, J. M. and Lee, A. G. (2007) Penetration of lipid chains into transmembrane surfaces of membrane proteins: studies with MscL. *Biophys. J.* 92, 3556-3563.

86. East, J. M., Melville, D. and Lee, A. G. (1985) Exchange rates and numbers of annular lipids for the calcium and magnesium ion dependent adenosine triphosphatase. *Biochemistry* 24, 2615-2623.

87. Marsh, D., Pali, T. (2004) The protein-lipid interface: perspectives from magnetic resonance and crystal structures. *Biochim. Biophys. Acta* 1666, 118-141.

88. Pali, T., Bashtovyy, D. and Marsh, D. (2006) Stoichiometry of lipid interactions with transmembrane proteins - Deduced from the 3D structures. *Protein Sci.* 15, 1153-1161.

89. Marsh, D. (2003) Lipid-binding proteins: structure of the phospholipid ligands. *Protein Sci.* 12, 2109-2117.

90. Brotherus, J. R., Griffith, O. H., Brotherus, M. O., Jost, P. C., Silvius, J. R. and Hokin, L. E. (1981) Lipid-protein multiple binding equilibriums in membranes. *Biochemistry* 20, 5261-5267.

91. Huang, C. H., Charlton, J. P. (1971) Studies on phosphatidylcholine vesicles. *J. Biol. Chem.* 246, 2555-2560.

92. Matthews, B. W. (1968) Solvent content of protein crystals. *J. Mol. Biol.* 33, 491-497.

93. Chambers, J. A. A. and Rickwood, D. Biochemistry Labfax; 1st ed.; BIOS Scientific Publishers: Oxford, 1993.

94. Hegermann, J., Overbeck, J. and Schrempf, H. (2006) *In vivo* monitoring of the potassium channel KcsA in *Streptomyces lividans* hyphae using immuno-electron microscopy and energy-filtering transmission electron microscopy. *Microbiology* 152, 2831-2841.

95. Hegermann, J., Lunsdorf, H., Overbeck, J. and Schrempf, H. (2008) Polyphosphate at the *Streptomyces lividans* cytoplasmic membrane is enhanced in the presence of the potassium channel KcsA. *J. Microsc.* 229, 174-182.

96. van Meer, G., Voelker, D. R. and Feigenson, G. W. (2008) Membrane lipids: where they are and how they behave. *Nat. Rev. Mol. Cell Biol.* 9, 112-124.

97. Froud, R. J., East, J. M., Rooney, E. K. and Lee, A. G. (1986) Binding of long-chain alkyl derivatives to lipid bilayers and to (Ca^2+-Mg^2+)-ATPase. *Biochemistry* 25, 7535-7544.

98. Rooney, E. K., Gore, M. G. and Lee, A. G. (1987) Two classes of binding site for hydrophobic molecules on bacterioopsin. *Biochemistry* 26, 3688-3697.

99. Aveyard, R. and Haydon, D. A. An introduction to the principles of surface chemistry; 1st ed.; Cambridge University Press: Cambridge, 1973.

100. Lee, A. G. (1983) An overlapping site model for the lipid annulae of membrane proteins. *FEBS Lett.* 151, 297-302.

101. Smaby, J. M., Brockman, H. L. (1985) Miscibility, chain packing, and hydration of 1-palmitoyl-2-oleoyl phosphatidylcholine and other lipids in surface phases. *Biophys. J.* 48, 701-707.

102. Deol, S. S., Domene, C., Bond, P. J. and Sansom, M. S. P. (2006) Anionic phospholipid interactions with the potassium channel KcsA: simulation studies. *Biophys. J.* 90, 822-830.

103. LeMasurier, M., Heginbotham, L. and Miller, C. (2001) KcsA: it's a potassium channel. *J. Gen. Physiol.* 118, 303-314.

104. Grunze, M., Haest, C. W. M. and Deuticke, B. (1982) Lateral segregation of membrane lipids and formation of stable rod-shaped membrane projections in erythrocytes treated with long-chain alcohols. *Biochim. Biophys. Acta* 693, 237-245.

105. Fink, M., Lesage, F., Duprat, F., Heurteaux, C., Reyes, R., Fosset, M. and Lazdunski, M. (1998) A neuronal two P domain K^+ channel stimulated by arachidonic acid and polyunsaturated fatty acids. *EMBO J.* 17, 3297-3308.

106. Chemin, J., Nargeot, J. and Lory, P. (2007) Chemical determinants involved in anandamide-induced inhibition of T-type calcium channels. *J. Biol. Chem.* 282, 2314-2323.

107. Börjesson, S. I., Parkkari, T., Hammarström, S. and Elinder, F. (2010) Electrostatic tuning of cellular excitability. *Biophys. J.* 98, 396-403.

108. Froud, R. J., East, J. M., Jones, O. T. and Lee, A. G. (1986) Effects of lipids and long-chain alkyl derivatives on the activity of calcium-magnesium ATPase. *Biochemistry* 25, 7544-7552.

109. Hamilton, J. A., Cistola, D. P. (1986) Transfer of oleic-acid between albumin and phospholipid-vesicles. *Proc. Natl. Acad. Sci. USA* 83, 82-86.

110. Armstron, C. M. (1969) Inactivation of potassium conductance and related phenomena caused by quaternary ammonium ion injection in squid axons. *J. Gen. Physiol.* 54, 553-&.

111. Armstron, C. M. (1971) Interaction of tetraethylammonium ion derivatives with potassium channels of giant axons. *J. Gen. Physiol.* 58, 413-&.

112. Choi, K. L., Mossman, C., Aubé, J. and Yellen, G. (1993) The internal quaternary ammonium receptor site of *Shaker* potassium channels. *Neuron* 10, 533-541.

113. Rooney, E. K., East, J. M., Jones, O. T., Mcwhirter, J., Simmonds, A. C. and Lee, A. G. (1983) Interaction of fatty acids with lipid bilayers. *Biochim. Biophys. Acta* 728, 159-170.

114. Blatt, E., Chatelier, R. C. and Sawyer, W. H. (1984) Partition and binding constants in micelles and vesicles from fluorescence quenching data. *Chem. Phys. Lett.* 108, 397-400.

115. London, E., Feigenson, G. W. (1981) Fluorescence quenching in model membranes. 1. Characterization of quenching caused by a spin-labeled phospholipid. *Biochemistry* 20, 1932-1938.

116. O'Keeffe, A. H., East, J. M. and Lee, A. G. (2000) Selectivity in lipid binding to the bacterial outer membrane protein OmpF. *Biophys. J.* 79, 2066-2074.

117. Powl, A. M., East, J. M. and Lee, A. G. (2007) Different effects of lipid chain length on the two sides of a membrane and the lipid annulus of MscL. *Biophys. J.* 93, 113-122.

118. Milhaud, J. (2004) New insights into water-phospholipid model membrane interactions. *Biochim. Biophys. Acta* 1663, 19-51.

119. Kooijman, E. E., Carter, K. M., van Laar, E. G., Chupin, V., Burger, K. N. J. and de Kruijff, B. (2005) What makes the bioactive lipids phosphatidic acid and lysophosphatidic acid so special? *Biochemistry* 44, 17007-17015.

120. Kooijman, E. E., Tieleman, D. P., Testerink, C., Munnik, T., Rijkers, D. T. S., Burger, K. N. J. and de Kruijff, B. (2007) An electrostatic/hydrogen bond switch as the basis for the specific interaction of phosphatidic acid with proteins. *J. Biol. Chem.* 282, 11356-11364.

121. Morrisett, J. D., Pownall, H. J. and Gotto, A. M. (1975) Bovine serum-albumin - study of fatty-acid and steroid binding-sites using spin-labeled lipids. *J. Biol. Chem.* 250, 2487-2494.

122. Bhattacharya, A. A., Grüne, T. and Curry, S. (2000) Crystallographic analysis reveals common modes of binding of medium and long-chain fatty acids to human serum albumin. *J. Mol. Biol.* 303, 721-732.

123. Bhalla, T., Rosenthal, J. J. C., Holmgren, M. and Reenan, R. (2004) Control of human potassium channel inactivation by editing of a small mRNA hairpin. *Nat. Struct. Mol. Biol.* 11, 950-956.

124. Decher, N., Kumar, P., Gonzalez, T., Renigunta, V. and Sanguinetti, M. C. (2005) Structural basis for competition between drug binding and $Kv_{\beta}1.3$ accessory subunit-induced N-type inactivation of Kv1.5 channels. *Mol. Pharmacol.* 68, 995-1005.

125. Long, S. B., Campbell, E. B. and MacKinnon, R. (2005) Crystal structure of a mammalian voltage-dependent *Shaker* family K^+ channel. *Science* 309, 897-903.

126. French, R. J., Shoukimas, J. J. (1981) Blockage of squid axon potassium conductance by internal tetra-N-alkylammonium ions of various sizes. *Biophys. J.* 34, 271-291.

127. Anel, A., Richieri, G. V. and Kleinfeld, A. M. (1993) Membrane partition of fatty acids and inhibition of T cell function. *Biochemistry* 32, 530-536.

128. Toyoshima, C., Nomura, H. (2002) Structural changes in the calcium pump accompanying the dissociation of calcium. *Nature* 418, 605-611.

129. Luecke, H., Schobert, B., Richter, H. T., Cartailler, J. P. and Lanyi, J. K. (1999) Structure of bacteriorhodopsin at 1.55 Å resolution. *J. Mol. Biol.* 291, 899-911.

130. Shinzawa-Itoh, K., Aoyama, H., Muramoto, K., Terada, H., Kurauchi, T., Tadehara, Y., Yamasaki, A., Sugimura, T., Kurono, S., Tsujimoto, K., Mizushima, T., Yamashita, E., Tsukihara, T. and Yoshikawa, S. (2007) Structures and physiological roles of 13 integral lipids of bovine heart cytochrome c oxidase. *EMBO J.* 26, 1713-1725.

131. Devor, D. C., Frizzell, R. A. (1998) Modulation of K^+ channels by arachidonic acid in T84 cells. I. Inhibition of the Ca^2+-dependent K^+ channel. *Am. J. Physiol. Cell. Physiol.* 274, C138-C148.

132. Feller, S. E., Gawrisch, K. and MacKerell, A. D. (2002) Polyunsaturated fatty acids in lipid bilayers: intrinsic and environmental contributions to their unique physical properties. *J. Am. Chem. Soc.* 124, 318-326.

133. Feller, S. E. (2008) Acyl chain conformations in phospholipid bilayers: a comparative study of docosahexaenoic acid and saturated fatty acids. *Chem. Phys. Lipids.* 153, 76-80.

134. Grossfield, A., Feller, S. E. and Pitman, M. C. (2006) A role for direct interactions in the modulation of rhodopsin by w-3 polyunsaturated lipids. *Proc. Natl. Acad. Sci. USA* 103, 4888-4893.

135. Marban, E., Yamagishi, T. and Tomaselli, G. F. (1998) Structure and function of voltage-gated sodium channels. *J. Physiol.* 508, 647-657.

136. Xiao, Y. F., Wright, S. N., Wang, G. K., Morgan, J. P. and Leaf, A. (2000) Coexpression with β_1-subunit modifies the kinetics and fatty acid block of $hH1_\alpha$ Na^+ channels. *Am. J. Physiol. Heart. Circ. Physiol.* 279, H35-H46.

137. Xiao, Y. F., Ke, Q., Wang, S. Y., Auktor, K., Yang, Y., Wang, G. K., Morgan, J. P. and Leaf, A. (2001) Single point mutations affect fatty acid block of human myocardial sodium channel α subunit Na^+ channels. *Proc. Natl. Acad. Sci. USA* 98, 3606-3611.

138. Linford, N. J., Cantrell, A. R., Qu, Y., Scheuer, T. and Catterall, W. A. (1998) Interaction of batrachotoxin with the local anesthetic receptor site in transmembrane segment IVS6 of the voltage-gated sodium channel. *Proc. Natl. Acad. Sci. USA* 95, 13947-13952.

139. Xiao, Y. F., Sigg, D. C. and Leaf, A. (2005) The antiarrhythmic effect of n-3 polyunsaturated fatty acids: modulation of cardiac ion channels as a potential mechanism. *J. Membr. Biol.* 206, 141-154.

140. Petcoff, D. W., Holland, W. L. and Stith, B. J. (2008) Lipid levels in sperm, eggs, and during fertilization in *Xenopus laevis*. *J. Lipid Res.* 49, 2365-2378.

141. Anderson, M. P., Welsh, M. J. (1990) Fatty acids inhibit apical membrane chloride channels in airway epithelia. *Proc. Natl. Acad. Sci. USA* 87, 7334-7338.

142. Brash, A. R. (2001) Arachidonic acid as a bioactive molecule. *J. Clin. Invest.* 107, 1339-1345.

143. Hoopengardner, B., Bhalla, T., Staber, C. and Reenan, R. (2003) Nervous system targets of RNA editing identified by comparative genomics. *Science* 301, 832-836.

144. Li, M., Wang, I. X., Li, Y., Bruzel, A., Richards, A. L., Toung, J. M. and Cheung, V. G. (2011) Widespread RNA and DNA sequence differences in the human transcriptome. *Science*.

145. Wollmuth, L. P., Sobolevsky, A. I. (2004) Structure and gating of the glutamate receptor ion channel. *Trends. Neurosci.* 27, 321-328.

146. Wilding, T. J., Zhou, Y. and Huettner, J. E. (2005) Q/R site editing controls kainate receptor inhibition by membrane fatty acids. *J. Neurosci.* 25, 9470-9478.

147. Wilding, T. J., Fulling, E., Zhou, Y. and Huettner, J. E. (2008) Amino acid substitutions in the pore helix of GluR6 control inhibition by membrane fatty acids. *J. Gen. Physiol.* 132, 85-99.

148. Marsh, D. (2010) Electron spin resonance in membrane research: protein-lipid interactions from challenging beginnings to state of the art. *Eur. Biophys. J.* 39, 513-525.

149. Moe, P., Blount, P. (2005) Assessment of potential stimuli for mechano-dependent gating of MscL: effects of pressure, tension, and lipid headgroups. *Biochemistry* 44, 12239-12244.

150. Powl, A. M., East, J. M. and Lee, A. G. (2008) Importance of direct interactions with lipids for the function of the mechanosensitive channel MscL. *Biochemistry* 47, 12175-12184.

151. Wonderlin, W. F., Strobl, J. S. (1996) Potassium channels, proliferation and G1 progression. *J. Membr. Biol.* 154, 91-107.

152. Ryu, S. Y., Peixoto, P. M., Teijido, O., Dejean, L. M. and Kinnally, K. W. (2010) Role of mitochondrial ion channels in cell death. *BioFactors* 36, 255-263.

153. Felix, R. (2000) Channelopathies: ion channel defects linked to heritable clinical disorders. *J. Med. Genet.* 37, 729-740.

154. Rolim, A. L., Lindsey, S. C., Kunii, I. S., Fujikawa, A. M., Soares, F. A., Chiamolera, M. I., Maciel, R. M. B. and Silva, M. R. D. (2010) Ion channelopathies in endocrinology: recent genetic findings and pathophysiological insights. *Arq. Bras. Endocrinol. Metabol.* 54, 673-681.

155. Sontheimer, H. (2008) An unexpected role for ion channels in brain tumor metastasis. *Exp. Biol. Med.* 233, 779-791.

156. Camerino, D., Tricarico, D. and Desaphy, J. F. (2007) Ion channel pharmacology. *Neurotherapeutics* 4, 184-198.

157. MacKinnon, R., Doyle, D. A. (1997) Prokaryotes offer hope for potassium channel structural studies. *Nat. Struct. Mol. Biol.* 4, 877-879.

158. Grage, S. L., Keleshian, A. M., Turdzeladze, T., Battle, A. R., Tay, W. C., May, R., Holt, S. A., Contera, S. A., Haertlein, M., Moulin, M., Pal, P., Rohde, P. R., Forsyth, V. T., Watts, A., Huang, K. C., Ulrich, A. and Martinac, B. (2011) Bilayer-mediated clustering and functional interaction of MscL channels. *Biophys. J.* 100, 1252-1260.

159. Colledge, M., Froehner, S. C. (1998) To muster a cluster: anchoring neurotransmitter receptors at synapses. *Proc. Natl. Acad. Sci. USA* 95, 3341-3343.

160. Gil, T., Ipsen, J. H., Mouritsen, O. G., Sabra, M. C., Sperotto, M. M. and Zuckermann, M. J. (1998) Theoretical analysis of protein organization in lipid membranes. *Biochim. Biophys. Acta* 1376, 245-266.

161. Parton, D., Klingelhoefer, J. and Sansom, M. (2011) Aggregation of model membrane proteins, modulated by hydrophobic mismatch, membrane curvature, and protein class. *Biophys. J.* 101, 691-699.

162. Lee, A. G., East, J. M., Jones, O. T., Mcwhirter, J., Rooney, E. K. and Simmonds, A. C. (1982) Interaction of fatty acids with the calcium-magnesium dependent adenosine triphosphatase from sarcoplasmic reticulum. *Biochemistry* 21, 6441-6446.